The University Of Sheffield.

Department Of Mechanical Engineering

ON THE STABILITY OF VARIABLE HELIX MILLING TOOLS

by

Mr. **Luis Ureña**

Submitted in fulfilment of the degree of Doctor of Philosophy

August 2020

Supervisors: Prof. Neil Sims
Dr. Erdem Ozturk

SUMMARY

One of the main aims of the manufacturing industry has been to maximise the material removal rate of machining processes. However, this goal can be restricted by the appearance of regenerative chatter vibrations. In milling, one approach for regenerative chatter suppression is the implementation of variable-helix cutters. However, these tools can lead to isolated unstable regions in the stability diagram. Currently, variable-helix unstable islands have not been extensively researched in the literature. Therefore, the current thesis focuses on studying and experimentally validating these islands.

For the validation, an experimental setup that scaled not only the structural dynamics but also the cutting force coefficients was proposed. Therefore, it was possible to attain larger axial depths of cut while assuming linear dynamics. The variable-helix process stability was modelled using the semi-discretization method and the multi-frequency approach. It was found that the variable helix tools can further stabilise a larger width of cut due to the distributed time delays that are a product of the tool geometry.

Subsequently, a numerical study about the impact of structural damping on the variable-helix stability diagram revealed a strong relationship between the damping level and instability islands. The findings were validated by performing trials on the experimental setup, modified with constrained layer damping to recreate the simulated conditions. Additionally, a convergence analysis using the semi-discretization method (SDM) and the multi-frequency approach (MFA) revealed that these islands are sensitive to model convergence aspects. The analysis shows that the MFA provided converged solutions with a steep convergence rate, while the SDM struggled to converge.

In this work, it is demonstrated that variable-helix instability islands only emerge at relatively high levels of structural damping and that they are particularly susceptible to model convergence effects. Meanwhile, the model predictions are compared to and validated against detailed experimental data that uses a specially designed configuration to minimise experimental error. To the authors' knowledge, this provides the first experimentally validated study of unstable islands in variable helix milling, while also demonstrating the importance of accurate damping estimates and convergence studies within the stability predictions.

ACKNOWLEDGEMENTS

I would like first to thank God for blessing, guiding, and strengthen me throughout this journey called life. He is my refuge and my fortress, my God, in whom I trust.

I also would like to express my deep appreciation to the people who have supported me along the course of my studies. First of all, I would like to thank my first supervisor professor Neil Sims for all the insightful guidance, support, encouragement, and patience toward complete my PhD studies. Neil's experience, passion and dedication to research guided and motivated me every weekly meeting to tackle the different challenges I faced during my project. This experience further shaped me to be a better researcher. Additionally, I would also like to thank my second supervisor Dr Erdem Ozturk for sharing with me all his experience during my experimental tests. Thanks to his technical guidance and support throughout my test I could have access to the training and most of the equipment I required for my trials.

Furthermore, I would like to thank IFARHU and the Technological University of Panama for sponsoring my PhD studies.

Last but not least, I would like to thank my family in Panama, especially to my mother Trinidad Mendieta for always being with me in the distance. Also, I would like to thanks my small family, yes you Marta, you have been a really important and special person for me these years. You introduced me to mindfulness to better manage the stress and encouraged me to be healthier. These two things deeply impacted my life for good. Thanks for all the love.

CONTENTS

List of Figures

List of Tables

1. Introduction

1.1. Background

Machining is a set of manufacturing processes that mechanically transform raw materials into desired shapes by controlled material removal [1]. The machining group encompasses processes such as boring, drilling, milling, and turning. In particular, one of the most versatile machining processes is milling. It comprises removing material from a workpiece by feeding it to a rotatory cutter with one or many teeth. Its versatility means that with milling it is possible to make many other machining processes, such as drilling, boring, gear cutting, and slotting.

Depending on the orientation between the cutter-rotation axis and the workpiece machined face, milling can be classified as peripheral or face milling. In face milling, the cutter-rotation axis is perpendicular to the workpiece machined face, as shown in Figure 1.1 a). In peripheral milling, the cutter-rotation axis is parallel to the workpiece machined face (Figure 1.1 b)).

Peripheral milling, that is the subject of this thesis, can further be classified as up- and down-milling depending on the relationship between the cutting and workpiece feed velocities (Figure 1.2). In up-milling, the cutting velocity at the start angle of the cutter teeth is opposite to the workpiece feed velocity, as shown in Figure 1.2 a). In down milling, the teeth cutting velocity at the exit angle is parallel to the feed velocity, as illustrated in Figure 1.2 b). In Figure 1.2 a) and b), the amount of material removed by every tooth (known as a chip and shown in dashed lines), subsequently

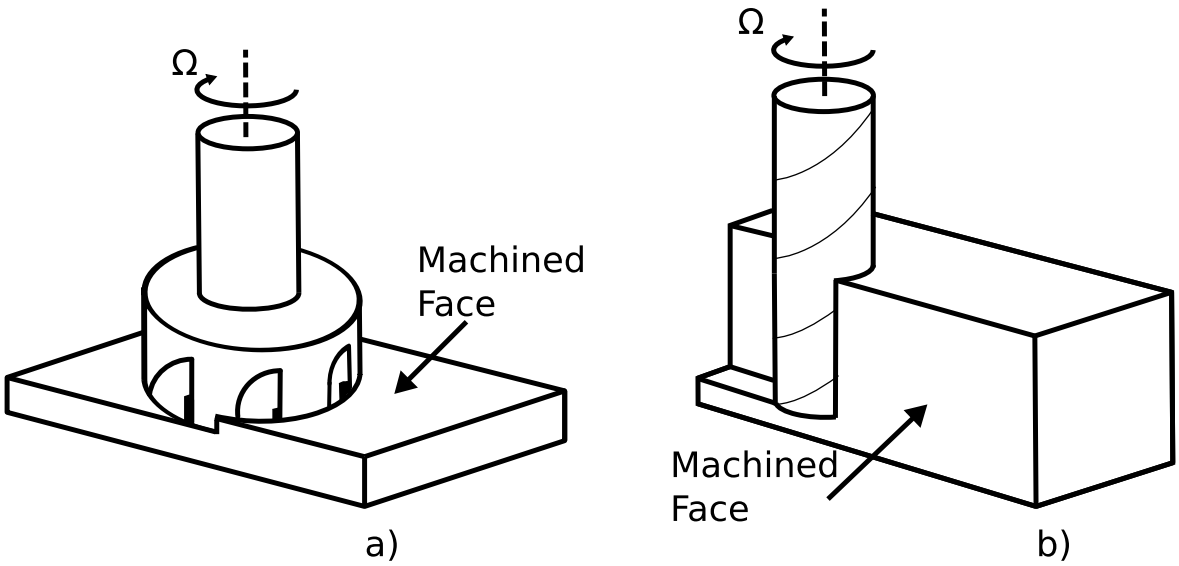

Figure 1.1.: a) Face milling process, b) Peripheral milling process

increase or decrease for the up- or down-milling when the teeth travel along the cutting region. Furthermore, the mechanistic cutting force model implemented in most of the milling cases assumes that the forces are proportional to the chip cross-sectional area. Consequently, in up-milling, the teeth leave the cutting region with maximum cutting forces, while in down-milling they do it with forces almost null. As a result, down-milling is recommended for tight-tolerance requirements as finishing, while the up-milling for roughing tasks that require larger-material removal. However, down-milling should be avoided in screw-feed type machine tools without backlash compensation, because it may cause unsteady cutting-table motions leading to high magnitude impact forces [2, 3].

In industry, one of the main aims is to maximise the productivity of machining by increasing material removal rates. In milling, this is achieved by increasing the cutting speeds and depths of the cut. However, one of the main obstacles that emerge by increasing these parameters is unwanted and unstable vibrations known as chatter. Chatter vibrations are detrimental for the integrity of the workpiece, cutter, and machine tool [4]. Chatter may reduce the tool life because of the excessive high-

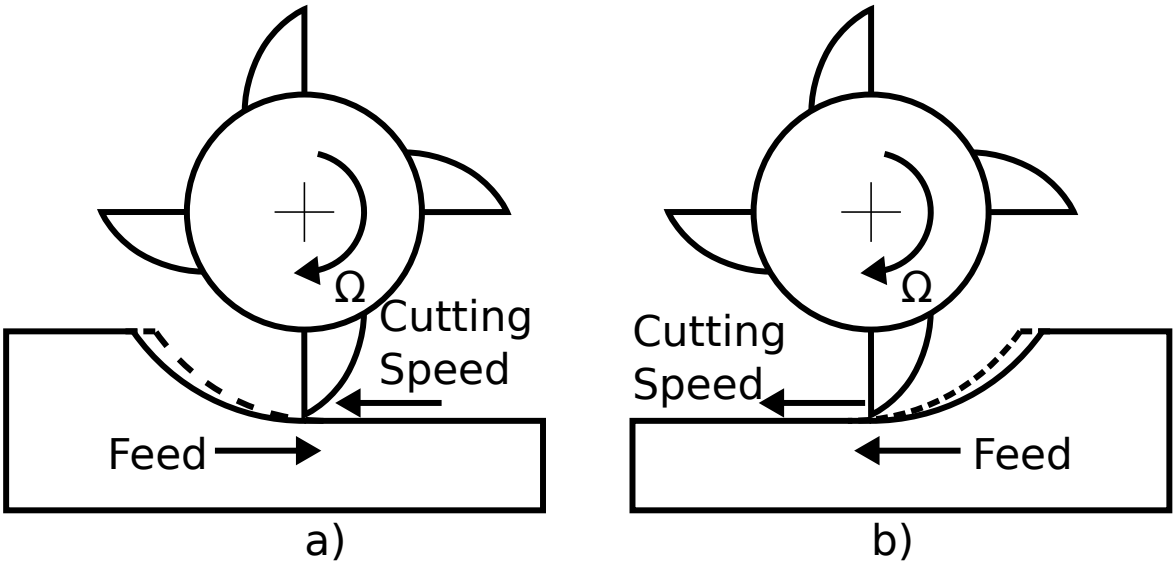

Figure 1.2.: a) Up-milling process, b) Down-milling process

amplitude vibrations along with a temperature increment that promotes tool wear. These vibrations stimulate the impact of the cutter with the workpiece, resulting in poor surface roughness and undesirable marks on the final component. For example, A thin-walled workpiece may experience considerable large distortions from the desired shapes [5,6]. Also, the continuous impact of the tool with the workpiece may aggravate residual stresses conditions of the machined surface product of the non-uniform plastic deformation. Furthermore, it may experience a localised thermal expansion and phase transformation caused by the high-temperature gradient [7]. Therefore, chatter vibrations have turned into one of the primary manufacturing challenges to boost productivity.

The vibrations experienced in milling operation are forced and self-excited chatter vibrations. The former type of vibration is produced whenever the fundamental frequency component of the periodic cutting force, or any of its harmonics, is near the system's natural frequencies. On the other hand, self-excited chatter vibrations can be produced by mode-coupling and/or regeneration of the chip thickness. First, mode-coupling chatter vibration occurs when the vibration in one direction of the cutting

plane excites vibrations in the other direction of the same plane. As a result, the mode-coupling chatter frequency can reach values near the system's natural frequencies, resulting in an unstable cutting process. Regenerative chatter in milling occurs whenever the waviness printed on the workpiece surface by one tooth, is out of phase with the waviness left by the previous tooth. Hence, the chip thickness, and therefore the forces, may grow exponentially resulting in a poor surface finish, tool wear, and catastrophic damage to the machine.

Comparing the forced and self-excited chatter vibrations, forced vibrations can be simply predicted by applying the process force model to the transfer function model of the machine tool. The resulting vibrations can be obtained by numerical integration. On the other hand, self-excited chatter vibrations are harder to predict and may be more detrimental for machining operations because of the above-mentioned instability.

In terms of self-excited vibrations, in most cases, regenerative chatter vibration appears at a lower depth of cut than mode-coupling as described by Stone [8]. Therefore, it is first necessary to suppress regenerative chatter to attain the depths of cut where mode coupling vibration emerges. Hence, there has been a substantial amount of research studying the regenerative chatter problem.

In the late 1950s, the machine chatter theory was first developed by Tobias and Fishwick [9,10]. Many researchers for more than a century have contributed to regenerative chatter theory development, including Altintas and Budak [11, 12], Merritt [13], and Tlusty [14, 15]. The authors implemented Nyquist and Bode plots to show the connection between the cutting forces and the dynamic chip thickness that leads to a relationship between the critical chip depth of the cut and the spindle speed. This relationship is embodied into a stability lobe diagram (Figure 1.3), which makes it possible to select the parameters for a cutting process with the highest achievable material remove rate.

However, these methodologies have slowly rooted in the industry sector, in which, for example, most of the small and medium enterprises still nowadays avoid chatter by reducing the machining parameters. One reason for the slow acceptance of these methods is the high complexity of these techniques and the necessity of further test with specialised equipment (e.g. tap testing kit, dynamometer) to fine-tune the chatter models. Therefore, this also requires having trained personnel to define adequate procedures and to interpret the results.

Nowadays, these constrain have softened with the appearance of software packages such as CutPro and Metalmax, which facilitates the milling process optimisation [16, 17]. Most of these software require as an input the cutting conditions, the frequency response function of the machine tool and workpiece, and the cutting-force coefficients that characterise the machining system. Subsequently, they implement integrated solver engines based on chatter prediction techniques such as the MFA or the SDM to determine chatter-free cutting conditions. After, these process requirements can be used in computer-aided manufacturing (CAM) environment, to generate the numerical control (NC) program of the higher level milling task such as pocketing and trochoidal milling [18, 19].

More advanced software such as MACHpro allows virtual machining, in which the NC programs are further simulated taking into account the three-dimensional tool-workpiece engagement along complex cutting trajectories [20,21]. The software's engine predicts chatter at discrete steps of these trajectories, optimising the cutting process and updating the NC codes.

One limitation of these software is the lack of packages for analytical chatter stability prediction with irregular milling cutters (e.g. variable helix and harmonically varied cutters), relying mainly on milling simulations to characterise unstable processes. This may be linked to the fact that analytical methodologies to study irregular milling cutters have developed at a slower rate than conventional milling tools because of

their higher dynamic complexity [22, 23]. Also, implementing these cutters requires geometrical optimisation to achieve the desired chatter performance, otherwise, they may lead to unwanted results. Therefore, these tools are generally implemented in specialised sectors (e.g. aerospace industry), for applications where conventional tools underperform. As a result, there are still phenomenons that occur in the stability charts of non-conventional milling cutters that have not been analytical and experimentally studied. Conditions such as stable and unstable islands have not been profoundly studied and validated yet, so there is no record of the method's accuracy capturing these conditions.

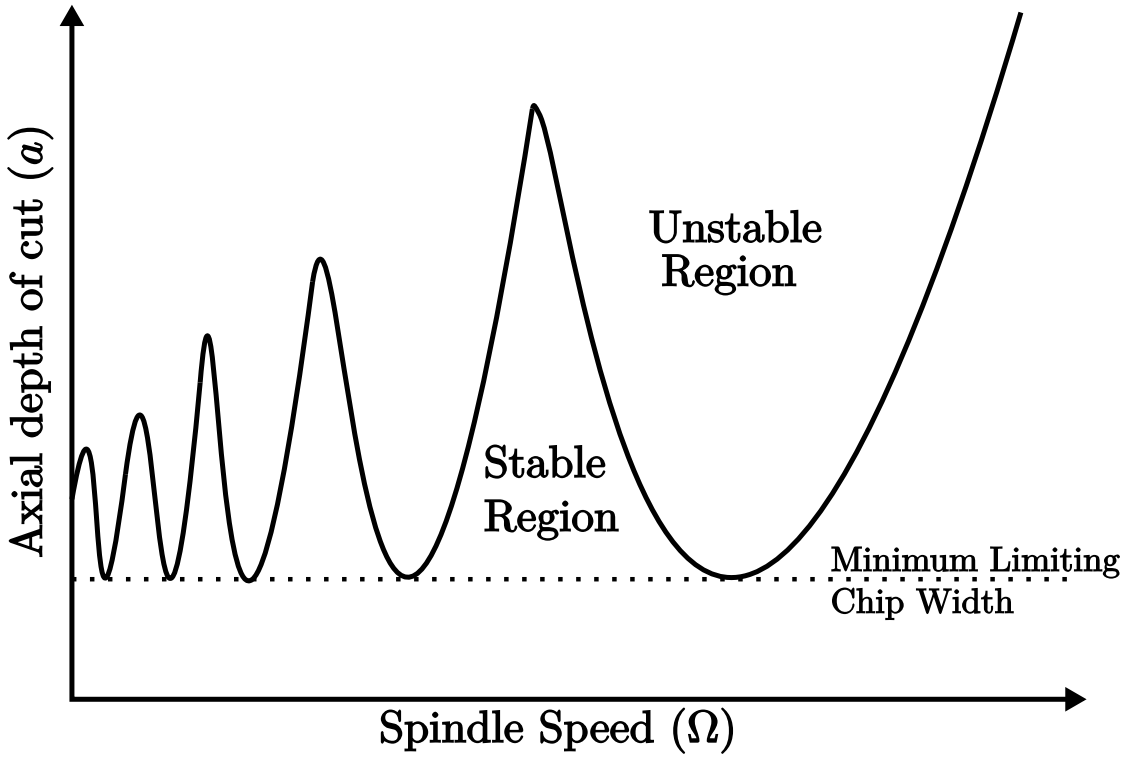

Figure 1.3.: Stability lobe diagram.

For applications that require cutting conditions beyond stability boundaries, unavoidable chatter vibrations can be suppressed by using active and/or passive approaches.

Active approaches monitor process state variables using sensors, and feed the sensor signals to a controller that changes cutting parameters (e.g. spindle speed), or suppress the vibration using actuators. Alternatively, regenerative chatter can also be passively suppressed or avoided by an adequate machine tool system design. This approach includes implementing devices to increase the structural stiffness and/or damping levels, that lead to higher feasible material removal rates.

In milling, another promising approach for regenerative chatter disruption is the use of milling tools with irregular shapes. The concept behind this approach relies on the fact that consecutive wavinesses printed on the workpiece surface by conventional cutters are characterised by a constant time delay. With irregular milling tools, this value is broken into multiple or distributed time delays, leading to alterations in the regenerative-chatter stability. These alterations may be beneficial or detrimental for the process stability, therefore these tools require an adequate optimisation for particular cases [24].

Some of the most implemented designs in the literature are shown in Figure 1.4. Figure 1.4 a) shows a conventional milling tool for comparison purposes. Figure 1.4 b) presents a variable-pitch milling tool that is characterised by having non-equal pitches on the tip of the tool and equal helix angles. Therefore, the pitches, and consequently the time delays, vary between flutes but not throughout the axis of the tool. On the contrary, variable-helix milling tools (Figure 1.4 c)) possess equal pitches on the tooltip, but non-equal helix angles on the flutes. Thus, the pitches change throughout the tool, having distributed time delays. Further, milling tools with variable helix and pitch (Figure 1.4 d)), combine both concepts implementing non-equal pitches and helix angles. In more complex tool configurations, such as the harmonically varied helix milling tools (Figure 1.4 e)), the flute helix angles are varied along the tool following periodic functions. In contrast, in serrated milling tools (Figure 1.4 f)) the tool diameter changes throughout the cutter following a periodic function.

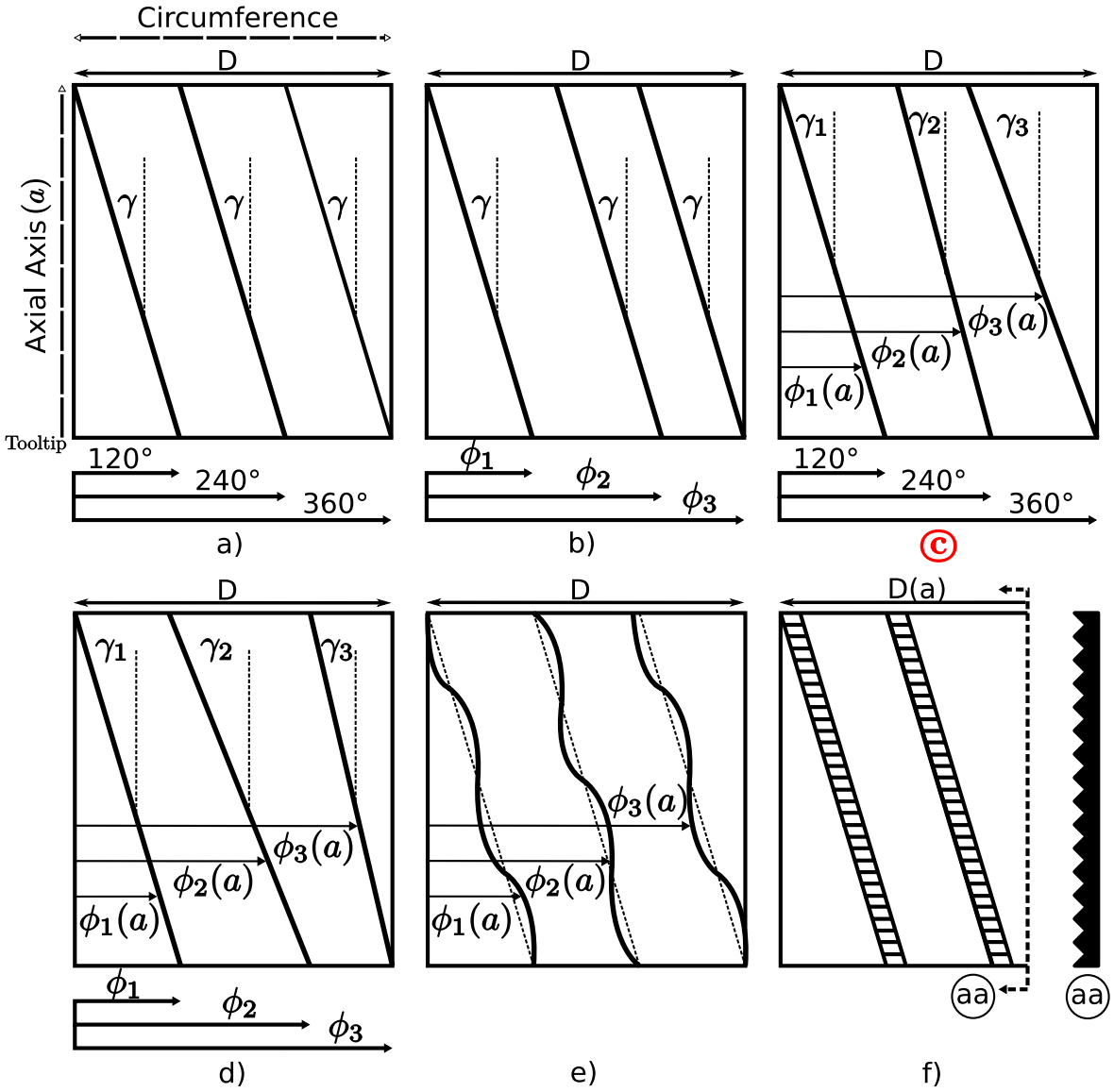

Figure 1.4.: Circumferential view of milling tool geometry. a) Conventional milling tool, b) Variable-pitch milling tool, c) Variable-helix milling tool (Tool implemented in the current project), d) Variable pitch and helix milling tool, e) Harmonically varied milling tool, f) Serrated milling tool (Cross section (aa) shows the tool's serration).

While several works have documented outstanding chatter stability using these tools, some of them have reported the appearance in simulations of isolated unstable regions in the stability diagram [25–27]. These unstable regions emerge due to the delay

alteration induced by the tool geometry. For variable-helix milling tools, that is the subject of this thesis, Figure 1.5 shows a schematic illustrating an oversimplification of the island occurrence mechanism. While the island appearance is indeed more complex, this schematic illustrates how the tool geometry can lead to these isolated unstable regions. As it is shown in Figure 1.4 c), these tools possess equally spaced pitches at the tooltip as conventional milling tools. Therefore, the stability lobe diagram for both tools at lower axial depths of cut is similar, as illustrated in Figure 1.5. However, while increasing the axial depths of cut, the regenerative effect experience by the variable-helix milling process may be disrupted as a result of the teeth pitch variations caused by the non-equal helix angles. This behaviour may lead to unstable isolated regions in the stability diagram.

While this phenomenon was explained using the lower region of a lobe, it may occur in any region of the stability diagram because of the strong relationship between the delays and the process stability condition [25, 27]. However, although variable-helix milling tools can lead to these isolated unstable conditions, their capability to stabilise at higher axial depths of cut allows increasing considerably the material removal rate. Consequently, it is fundamental to understand, predict and avoid these conditions to increase the variable-helix milling productivity.

To the best knowledge of the author, variable-helix instability islands have not been rigorously studied in the literature, other than through simulation studies. Therefore, the present thesis seeks to address this shortfall.

1.2. Aim and objectives

The main aim of the current research is to experimentally validate isolated unstable regions that emerge in the stability lobe diagram using variable-helix milling tools. To achieve this aim, the primary objectives are:

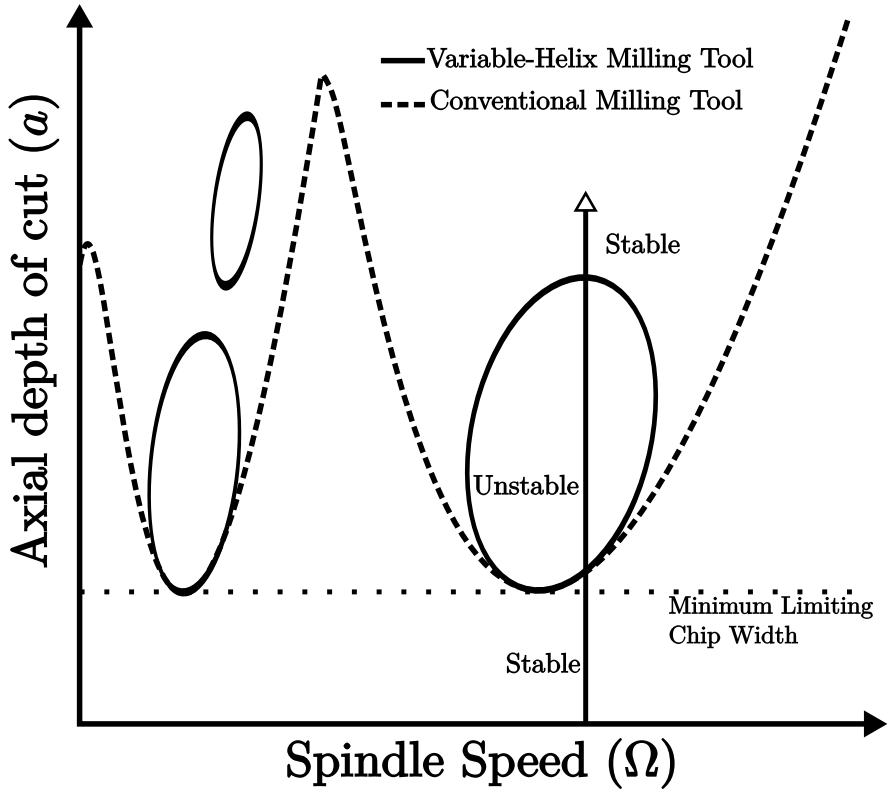

Figure 1.5.: Simplified schematic describing the variable-helix instability island mechanism. These islands appear in the stability diagram due to the further stabilization at higher axial depths of cut induced by the non-equal helix angles on the tool.

1. To perform an extensive literature review about variable-helix instability islands.

2. To develop a one-degree-of-freedom scaled experiment for validation of the variable-helix stability diagram at larger depths of cut.

3. To investigate the tool-geometrical factors and structural-dynamic conditions that lead to the variable-helix instability island occurrence.

4. To study the model convergence of the multi-frequency approach and semi-discretization method around a variable-helix instability island.

5. To validate the variable-helix unstable islands with the tuned experimental setup.

1.2.1. Thesis outline

The rest of the thesis structure organisation is as follows:

Chapter 2 presents the literature review of the thesis, beginning with some of the most important chatter prediction research. Next, chatter detection techniques are addressed, revising the different sensors implemented for chatter detection, and the different signal processing for this purpose. After discussing the different active and passive chatter suppression techniques, the literature reviewed is focused on the main topic of the research that is unstable islands found with variable-helix milling tools.

Afterwards, Chapter 3 presents the theoretical background for regenerative chatter modelling. It starts with regenerative chatter modelling for a single-point cutting process. Later, the two analytical methods implemented in the research are presented, these being the multi-frequency approach (MFA) and the semi-discretization method (SDM). Finally, Chapter 3 assesses the MFA and SDM programs implemented in the investigation using a case study found in the literature.

Next, Chapter 4 presents the one-degree-of-freedom scaled experimental setup implemented for the analysis and validation of the variable-helix instability islands. This section first presents the flexure device, workpiece material, and the custom variable-helix milling tool used in the project. Later, Chapter 4 analyses the helix angle influence on the cutting force coefficients, and therefore on the stability lobe diagram. Finally, a particular region of the stability diagram with a potential instability island is validated using the experimental configuration.

Chapter 5 demonstrates in simulations the effect of structural damping on the presence of variable-helix instability islands. Later, a convergence analysis using the MFA and SDM is performed around an island. Next, the structural damping of the original experimental configuration is increased using constraint-layer damping to recreate the

simulated conditions. Finally, the instability island is validated with the modified experimental setup.

Chapter 6 finally presents the conclusions reached throughout the project and the potential future works.

2. Literature Review

2.1. Introduction

Since early times, machinists have dealt with the fundamental task of defining the optimal parameters for maximum machining productivity. In most situations, the operator executes this through a cumbersome and ineffective set of trial-and-error tests. Aware of this, Taylor F., chair of the American society of mechanical engineers (ASME), conducted a secretive and extensive experimental investigation about it. Taylor later summarised the results gathered from over twenty-six years in the report 'On the art of cutting metals' [28]. Taylor stated in this work that 'probably no rules or formulae can be devised which will accurately guide the machinist in taking maximum cuts and speeds possible without producing chatter.' The machining community took this statement as a challenge, and have tried over the years to prove it inaccurate. Nowadays, with over a century of investigation, the community has revealed many key aspects about the nature of chatter. Therefore, this understanding has led to the development of tools to guide the machinist to achieve productive machining processes.

For instance, H. Ernst first presented the shear-plane concept of chip formation in 1938 [29]. This idea prompted Merchant in [30, 31] to establish the static orthogonal cutting model. This model relates the tool geometry, material properties and process conditions to the cutting forces. Afterwards, Arnold [32, 33] studied the vibration mechanism in steel. These studies then worked as a backbone for Tobias and Fishwick's [9, 10, 34, 35] and Tlusty and Polacek's [14, 36–38] regenerative chatter models. Several authors later deepened the regenerative effect knowledge implementing many control

theory techniques. Then, authors such as Altintas [39], Insperger [40], and Ding [41] developed analytical chatter stability predictions such as the Multi-frequency approach, Semi-discretization Method and the Fully Discretized Method.

With the current computer developments, these methods have been powerful tools for machine-tool system optimisation. Furthermore, it even allows the monitoring and suppression of chatter in real-time using different sensors and chatter detection techniques. Sensors such as accelerometers, microphones, and dynamometers have been broadly implemented in the literature, along with different chatter related signal statistics for chatter detection. The chatter prediction and real-time detection have led to active and/or passive chatter suppression approaches that allow to even further expand the capabilities machine tools. In summary, despite early pessimist conjectures about machining chatter, many of the key features behind its physics can now be explained. Though new challenges have appeared, tools have been developed that provide the means to maximise industrial machining productivity.

The following sections present the thesis's literature review. First, section 2.2 presents the chatter prediction approaches. Later, sections 2.4, and 2.5 deal with chatter detection, active, and passive chatter suppression techniques. Finally, section 2.6 presents a review on milling with irregular-shape tools. This section in particular introduces the focus of this thesis, which is the instability island that appears in the stability diagram while using variable-helix milling cutters.

2.2. Chatter Prediction

After Taylor's investigation, Ernst [29] and Merchant [30, 31] studied chip formation, leading to the static orthogonal cutting theory that relates the cutting forces to the tool geometry and process parameters. Subsequently, Arnold et al. [32, 33] studied the dynamic force-speed relation in self-induced vibrations while cutting steel. These

investigations then later helped Tlusty and Polacek [36] and Tobias and Fishwick [10,34] to develop, almost simultaneously, two fundamental chatter models.

First, Tlusty and Polacek [36] proposed a simplified static cutting force model in which the forces are proportional to chip thickness. This model was mainly based on Merchant's investigation [30, 31], and the linear proportional constant was named as total thrust variation factor. The total thrust variation factor was basically the product of the cutting stiffness and the width of cut. The authors found that the smallest thrust factor for chatter occurrence happens on the minimum real part of the structural frequency response function. Tlusty and Polacek highlighted that this approach even allowed the inclusion of multiple degrees of freedom in the solution.

In contrast, Tobias and Fishwick [10, 34] proposed a more general dynamic cutting force model that included a term known as the penetration rate. This term coupled the cutting forces with the vibratory and spindle rotational speeds. The development of this method was based on previous works performed by Arnold [32]. In addition, the model also considered the time delay between consecutive surface waves and multiple-teeth engagement. Tobias showed that, while Tlusty's stability predictions were on the safe side (grey shaded area in Figure 2.1 (a)), they were more conservative in several regions of the stability diagram [9]. In addition, the author explained that these differences are more noticeable at lower spindle speeds because of the penetration rate term. Finally, Tobias emphasised the potential of merging both approaches to build a more robust model [9].

Tlusty replied later [14,37,38] stating that the main aim of previous works was to find the lowest stability limit for an optimal process design. He then enhanced the model based on Tobias's comments, considering aspects such as the phase shifting between the chip thickness and force excitation.

Based on the Tlusty approach, Merritt in [13] showed later that the single point cutting processes can be represented as a feedback loop as shown in Figure 2.2. Thus, control

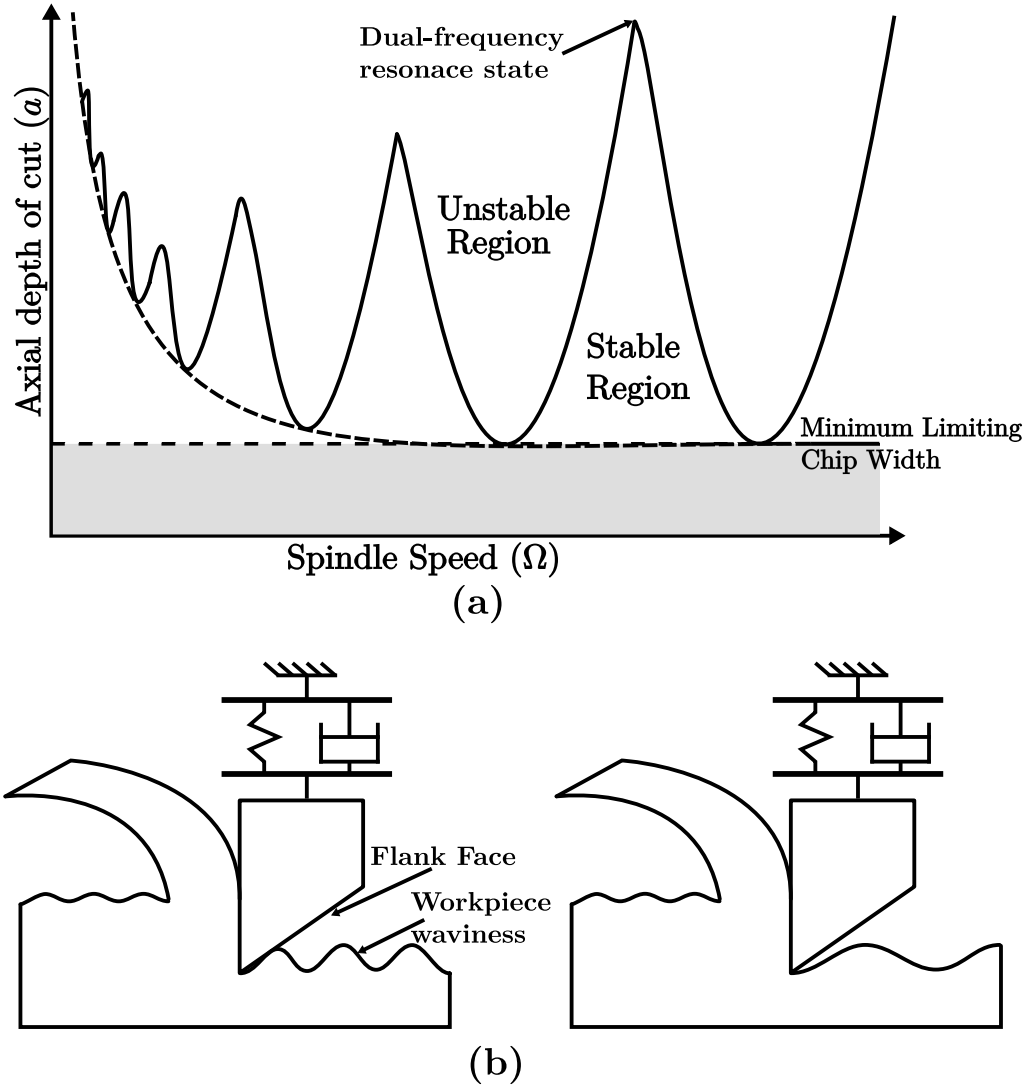

Figure 2.1.: (a) Stability Lobe Diagram (b) Process damping mechanism

theory tools like gain-phase plots of the transfer function can be implemented to analyse the chatter stability of cutting systems. In this research, Merritt neglected the low spindle-speed behaviour presented by Tobias, implying that this condition could be better explained by Kegg in [42]. Kegg in this article explicated that at lower spindle speeds, the wavelength of the waves imprinted on the workpiece surface by the cutter decrease. This then leads to a rubbing between the cutter flank face and these waves as depicted in Figure 2.1 (b). This condition is known today as process damping.

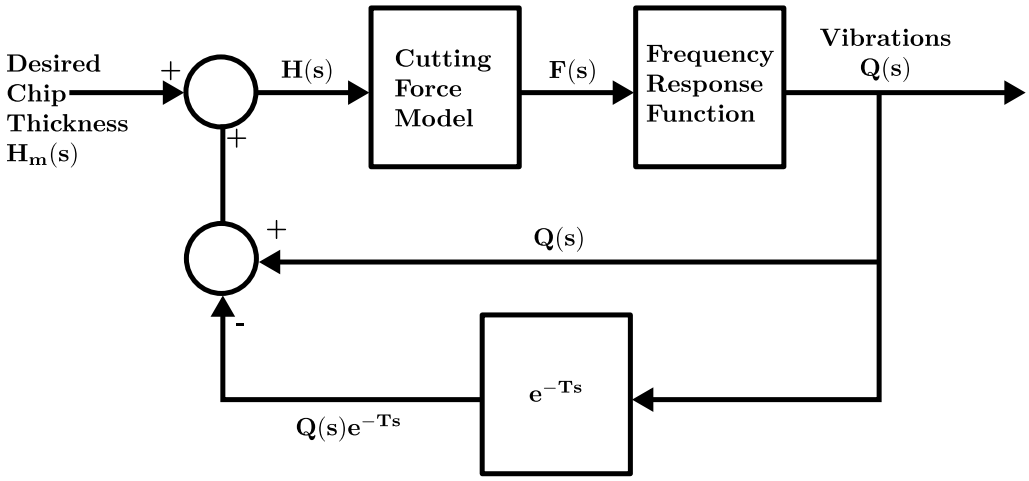

Figure 2.2.: Regenerative feedback loop

Further studies using control theory techniques were carried out. For instance, Sridhar et al. performed a similar investigation than Merritt using milling models with two degrees of freedom [43]. The author presented the process as a connected block diagram that showed the relationship between the different variables. Later, Olgac et al. [44] studied the chatter stability of a single point processes using root-locus plot analysis of time-delayed systems. In this work, Olgac also discussed a phenomenon called dual-frequency resonance that occurs in the intersection of two lobes as shown in Figure 2.1 (a).

Thanks to all these investigations, a more comprehensive machining chatter knowledge was developed. In particular, it was shown that regenerative chatter can be modelled as delayed-differential equations (DDE) with periodic coefficients such as,

$$\dot{\mathbf{q}}(t) = \mathbf{L}(t)\mathbf{q}(t) + \mathbf{R}(t)\mathbf{q}(t-T), \tag{2.1}$$

in which q is a generalised state vector, $\mathbf{L}(t)$ and $\mathbf{R}(\mathbf{t})$ matrix encompassing process related parameters, and T is the fundamental process period. T can be the spindle rotating period for milling process with non-conventional milling tools, or the tooth-passing period for conventional milling cutters. These equations were often solved using time domain simulations (e.g. Smith and Tlusty in [15, 45]), but they were

computationally demanding and impractical. Thus, several analytical approaches have emerged through the years to efficient and reliable predict machining process stability. For instance, the multi-frequency approach (MFA) [46], the time finite element (TFEA) [47], the Chebyshev polynomial approach [48], the semi-discretization method (SDM) [40], and the fully discretized method (FDM) [41] are between the most implemented techniques.

For example, Altintas and Budak in [39] presented the first analytical stability prediction method in the frequency domain for vertical-tooth milling. The methodology applies the Fourier transform to the time domain equation 2.1 leading to,

$$\mathbf{F}(\omega) = \frac{1}{2} a K_t [\mathbf{A}(\omega) * \left\{ \left(1 - e^{-i\omega T}\right) \mathbf{G}(\omega)\mathbf{F}(\omega) \right\}], \tag{2.2}$$

where K_t is a cutting force constant, $\mathbf{A}(\omega)$ is a matrix that considers the periodic angular rotation of the tool, a is the axial depth of cut, $\mathbf{G}(\omega)$ the system's frequency response function, and $*$ denotes the convolution operation. The method then expanded the matrix $\mathbf{A}(\omega)$ into its Fourier series, including only the zeroth-order term into the solution. Later, equation 2.2 was expressed as an eigenvalue problem leading to the critical axial depths of cut and spindle speeds to build the stability lobe diagram of the process. The frequency approach has the benefit of operating directly on raw frequency response functions, without having to estimate modal parameters. The zeroth-order approach has additional advantage of allowing to directly predict the stability lobe diagram in a few seconds without requiring any iterative search algorithm. In general, the method can be reliably used in machining processes with immersions larger than a quarter of the tool diameter, and tooth passing frequencies not exceeding the structural natural modes of vibration. However, although the method worked in most situations, the authors suggested that it required further investigation for helical tools and low cutting immersions. Subsequently, Merdol et al. [46] later tackled these issues, including more harmonics of $\mathbf{A}(\omega)$ in the solution in what is known as the multi-frequency approach MFA. With this enhancement, the method could then predict the stability lobe diagram of highly intermittent milling process at lower immersion and/or

higher spindle speeds. Nevertheless, the method is more time consuming requiring an iterative search of the stability boundaries. Bachrathy and Stepan in [49,50] extended the MFA to more complex milling tool designs. The authors implemented the multi-dimensional bisection method to reduce the computational burden. They showed that the method provided robust stability predictions even with raw, not fitted, noisy frequency response functions. Further MFA enhancements have been performed by Sims in [51] and Otto et al. in [52], in which it was modified for variable helix and pitch milling tools.

As an alternative, Bayly et al. [47, 53] proposed the Time Finite Element Analysis (TFEA) to predict chatter in milling at low immersions. This method assumed $\dot{\mathbf{q}}(t)$, $\mathbf{q}(t-T)$ and $\dot{\mathbf{q}}(t)$ in equation 2.1 as Hermite polynomials. Then, the resulting error in equation 2.1 was weighted by a set of test functions, and its integration was set to zero. Consequently, the process was approximated as a periodic discrete system or map that related the process state vector at one instant $\mathbf{Q_0}$, with the same state vector but at subsequent fundamental periods $\mathbf{Q_T}$ using the transition matrix $\mathbf{\Phi}$ as,

$$\mathbf{Q_T} = \mathbf{\Phi} \mathbf{Q_0}. \tag{2.3}$$

Therefore, the stability of the system could be assessed using the Floquet theory of periodic systems by analysing the eigenvalues of this matrix. Using this method, the authors could predict with significantly higher efficiency the stability of a highly intermittent milling process (e.g. low-radial immersion), capturing extra lobes in the stability diagram. These conditions were non-detected by the zeroth-order frequency approach, requiring the inclusion of higher $\mathbf{A}(\omega)$ harmonics that increased the computational time. The authors indicated that TFEA provided an efficient and accurate approach for low cutting immersions, while for full and near-full immersions, the frequency domain analysis represented the ideal option in these terms. Butcher et al. proposed a similar approach in [48], but approximating delay state vectors as Chebyshev polynomials. Again, the original DDE system was reduced to a group of periodic linear equations for the Chebyshev coefficients. In this case, in addition to providing a

faster chatter prediction for lower immersions, the methodology allowed the implementation of non-linear cutting force models in the chatter stability predictions. Likewise, the stability of the system was then tested using the Floquet theory.

At a similar time, Insperger et al. [40, 54] introduced the semi-discretization method (SDM) for time-delay systems. In this method, fundamental period T is divided into m discrete time intervals such as $T = m\Delta t$ as shown in Figure 2.3. In that case, the state vector $q(t)$ in equation 2.1 at a specific discrete time t_i can be just stated as q_i. Then, for a small Δt value, equation 2.1 can be approximated as,

$$\dot{\mathbf{q}}_i = \mathbf{L}_i \mathbf{q}_i + \frac{1}{2}\mathbf{R}_i \left[\mathbf{q}_{i-m+1} + \mathbf{q}_{i-m}\right], \tag{2.4}$$

in which $\mathbf{q}_{i-m} = \mathbf{q}(t_i - T)$ and $\mathbf{q}_{i-m+1} = \mathbf{q}(t_i - T + \Delta t)$. By doing this, the system is reduced to a series of equations at discrete times, in which the process stability condition can be analysed using the Floquet theory of the transition matrix $\mathbf{\Phi}$ [55]. The SDM proved to be more accurate than the zeroth order frequency approach because instead of averaging the time-variant directional matrix, the method considered it at each discrete sampling interval. Therefore, the accuracy of the SDM is only limited by its sampling interval. Unlike the MFA, the method has the disadvantage of requiring the identification of the structural modal parameters. Consequently, any error incurred in the identification process may also condition the SDM accuracy. Like the MFA, the SDM also requires an iterative search to capture the stability boundaries. Hence, the computation time depends on the number of modes in the system and the sampling interval. Higher orders of the SDM have been proposed by Insperger et al. [56] and Jiang et al. [57], in which the authors implemented linear and quadratic interpolation to approximate $\mathbf{q}(t-T)$ and the periodic matrix $\mathbf{L}(t)$ and $\mathbf{R}$ (equation 2.1), improving the overall convergence rate of the SDM. Further SDM modification for variable helix and pitch milling tools was done by Sims et al. in [58]. Here, the single time delay T in equation 2.1 becomes multiple discrete delays or even distributed delays that vary along the axial axis of the tool.

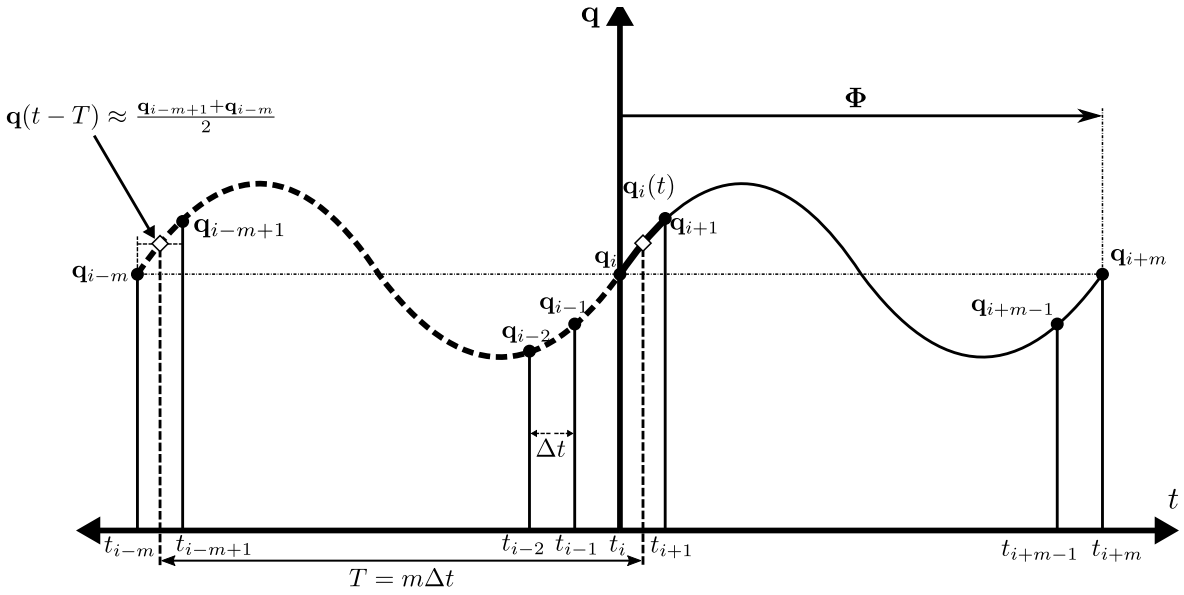

Figure 2.3.: Semi-Discretization Method

Subsequently, Ding et al. [41] proposed the fully discretized method (FDM). This method differs from the SDM in that instead of separately approximating the delayed term $\mathbf{q}(t-T)$ and the time-variant matrix $\mathbf{R}(t)$, the FDM approximates their product by linear interpolation. The authors showed that the FDM had a faster convergence rate than the SDM. Higher orders of the FDM have been proposed by Ding et al. [59], Quo et al. [60], Ozoegwu et al. [61], Tang et al. [62], and Liu et al. [63] showing even better results. However, Insperger in [64] compared the convergence performance between the SDM and FDM. The author concluded that FDM is not a pure full-discretization method. Insperger stated that FDM can be considered as an alternative form of SDM. The author even proved that the first-order SDM has a faster convergence rate than the FDM.

In summary, current developments in regenerative chatter predictions would not be possible without previous investigation that exposed the true physics of chatter. Research about chip formations led to force models, implemented to further modelling of chatter vibrations. Afterwards, the relationship between the cutter geometry and process parameters was visually embodied using block diagrams. Consequently, the

process stability was then studied using control theory means. This synergy then led to developments in analytical approaches for chatter stability such as the MFA, TFEM, SDM, and FDM. With these techniques, the machinist can estimate the cutting conditions for an optimal and chatter-free process. For the current thesis, islands of instability that emerge on the stability diagram of milling with variable-helix tools will be studied using two chatter prediction techniques. These techniques are the SDM and MFA, and in particular, the approaches proposed by Sims in [58] and [51]. While these methods were designed for variable helix and pitch milling tools, they are flexible enough to be implemented with just variable-helix milling tools by setting equal pitches at the tooltip. Consequently, it will be possible to compare the performance of these methods in reliably capturing these unusual conditions. Methods such as the FDM and TFEM will be left out of scope for this thesis, leaving it for future works.

Most analytical chatter predictions techniques allow to determine the chatter stability boundaries of the cutting process based on linear cutting force models. This considerably reduces the complexity of the problem and provides reliable solutions under a specific range of cutting conditions.

Chatter prediction methods divide the spectrum of cutting conditions into stable and unstable regions. Therefore, it enables to study the different vibratory patterns that emerge when transitioning from a stable to an unstable cutting process. Similar analysis has also been done using enhanced non-linear models, exposing further behaviours none captured by the standard linear approaches. Therefore, the following section introduces some of the most relevant works related to bifurcation analysis of milling process.

2.3. Bifurcation analysis of milling process

Being able to predict unstable and stable regions in the stability diagram, several authors have researched the bifurcations that occur in milling. A bifurcation occurs

when a qualitatively different solution of a dynamic system appears when a control parameter (e.g., axial depth of cut, spindle speed) is changed [65]. Authors such as Tlusty et al. [15], Balachandran et al. [66], and Zhao et al. [67], early studied milling bifurcations using numerical simulations. Davies et al. [68] first introduced the use of once-per-revolution sampling and Poincaré map to study the bifurcations that occur in milling. A Poincaré map is the intersection between a dynamic system's periodic orbit (limit cycle) and a Poincaré section (a subspace of lower dimension) that is transversal to the system's flow (Figure 2.4). Honeycutt et al. [69] stated that the bifurcation found in milling are secondary Hopf instability (traditional chatter), and period-n motions (e.g., period one, and period-doubling bifurcations).

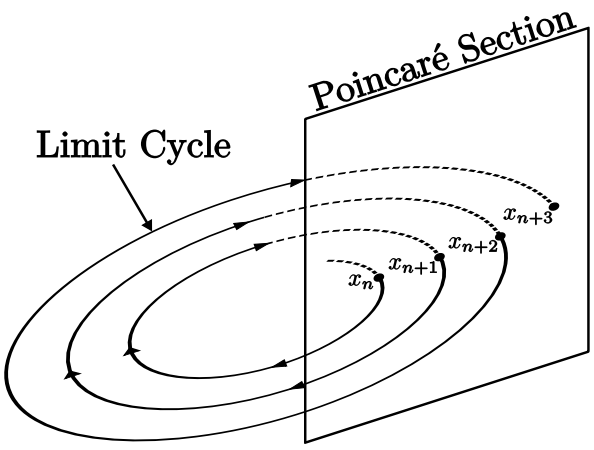

Figure 2.4.: Poincaré map

For periodic stable milling trials, the once-per-revolution values of a state vector should be the same when the process achieves its stationary state [68, 69]. Therefore, the dominant frequency in the process is the fundamental frequency related to periodic forcing. The system response to periodic forces results in a limit cycle that intersects the Poincaré section on the same location every fundamental period T, as illustrated in Figure 2.5 and 2.6 (a).

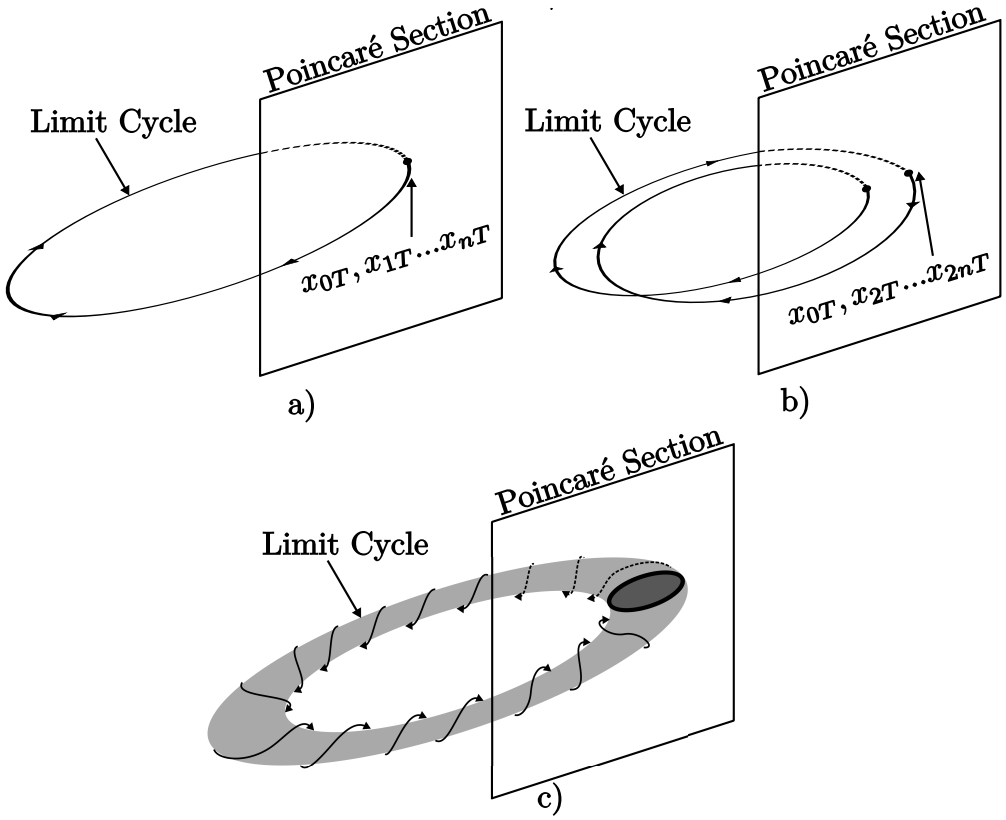

Figure 2.5.: Schematic showing the Poincaré map of a milling process experiencing a: (a) stable condition, (b) unstable period doubling bifurcation, and (c) unstable secondary Hopf bifurcation. T represents the process fundamental period.

As an example of an unstable Period-n bifurcation, Period-2 (or period-doubling) bifurcations are characterised by jumping of the cutter in one fundamental forcing period. Therefore, the limit cycle generated by the periodic force intersects the same location of the Poincaré section every two fundamental forcing periods T, as indicated in Figure 2.5 (b). For two teeth milling cutters, just one tooth of the tool is cutting in the process every two T cycles (Figure 2.6 (b)).

For unstable secondary Hopf bifurcations [68, 69], a quasi-periodic motion emerges because of the appearance of a chatter frequency that co-exists with the fundamental cutting frequency. The periodic orbit then becomes a toroid that intersects the Poincaré

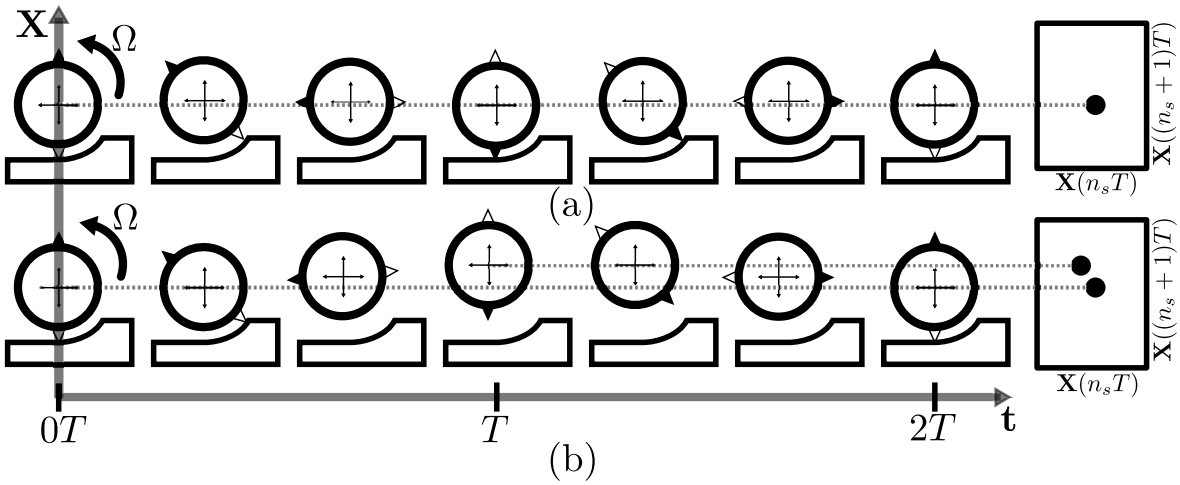

Figure 2.6.: Schematic of milling process and Poincaré plot for a stable (a) and unstable period-doubling case (b)

section at different locations at every fundamental forcing period as shown in Figure 2.5 (c).

Bifurcation analysis has also been implemented to study nonlinearities in the milling process. Nonlinearities in milling can come from sources such as the cutting nonlinear force models [70–72], higher-order structural dynamic stiffness models [70, 73], or/and large displacement [74] that can lead to a loss of tool engagement [75, 76].

The linear cutting force model assumes a linear relationship between the cutting forces F and the uncut chip thickness h being the cutting force stiffness the proportionality constant. However, as it is shown in Figure 2.7 (a), this model does not encompass the complete force dynamics at low and high feed values, showing for example, that there is a force component F_e even at feed equal to zero [77]. Therefore, enhanced models have been proposed such as the power cutting force model [73, 78] or the third order polynomial model [70, 74] that better represent the force feed dynamic behaviour as shown in Figure 2.7 (b) and (c). Bifurcation analysis in milling using these models led to bifurcations behaviours overlooked by the linear models. For example, Zoltan et al. [73] reported uncertain or unsafe zones close to the stability boundaries. In these

regions, better known as bistable zones, stable trials can become subcritical secondary Hopf bifurcation under small perturbations.

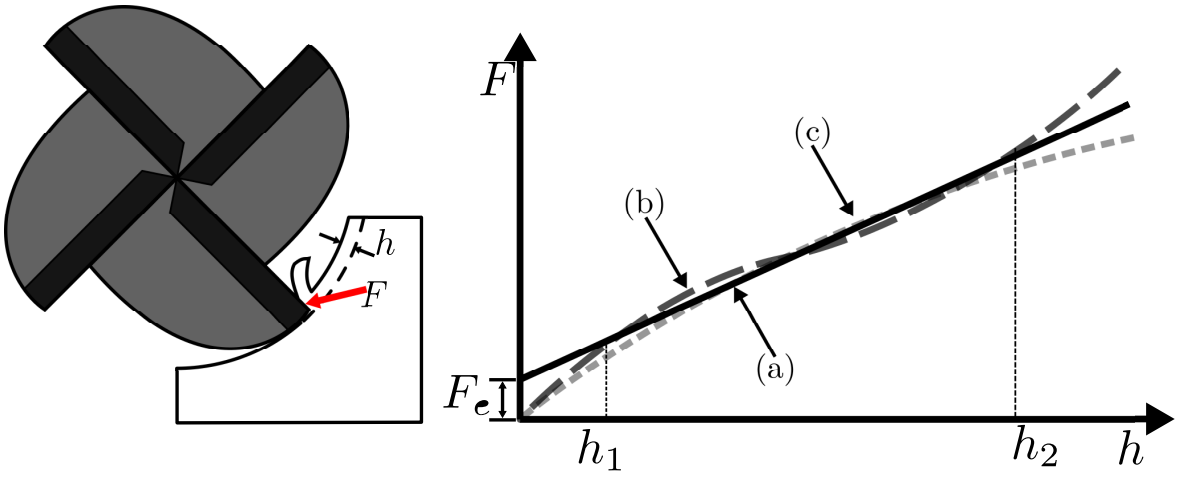

Figure 2.7.: Force vs chip thickness approximation using: (a) linear model, (b) polynomial, and (c) power functions.

Nonlinearities in the structural dynamic models have also been studied by authors such as Hanna et al. [70]. The authors studied the effect of cubic-polynomial stiffness dynamic and cutting force model on the stability of milling process. Hanna found that by including these nonlinearities, several unstable regions were transformed into stable and conditionally stable zones. Weremczuk et al. [79] performed a similar study, additionally exploring the nonlinearities on the bifurcation scenarios. Weremczuk showed that the nonlinearities induced by the force model have a more critical impact on the stability lobe diagram. In simulations, the author could find entire new unstable lobes by including the nonlinear terms, while also showing how stable trials change into subcritical Hopf Bifurcations.

The losing of tool engagement can also induce nonlinearities in the milling process. For example, Zhao et al. [67] studied the milling process implementing a time-domain simulation which incorporated the regenerative effect and loss of tool-workpiece contact.

The authors identified period-doubling bifurcation at low radial immersion and presented bifurcation diagrams to show the stable to unstable transition. Gabor et al. [80] further studied nonlinearities in a high spindle speed milling process. The author reported stable period-2 vibrations outside the unstable period-2 motions predicted by linear models. This phenomenon, named as a fly-over effect, occurs when the tool engages cutting the workpiece in one main cycle, and subsequently flies over the contact region in between. For example, for a two teeth cutter, this means that only one tooth is removing material from the workpiece while the other flies over the cutting region because of the tool vibrations. In addition, for larger amplitude vibration, the time delay (single, multiple or distribute time delays) may depend on previous values of the state variables [81]. This then leads to time and state dependant delayed differential equations which are nonlinear even in the delay term [82]. Bachrathy et al. studied the state-dependent regenerative effect in milling. Bachrathy et al. [75, 76] reported that traditional small oscillation models can overestimate the stable region near-resonant spindle speed velocities. The author could find fold bifurcations regions that create not globally stable, unsafe cutting zones.

In summary, bifurcation analysis has been implemented in milling to study the types of instabilities that emerge while transitioning from a stable to unstable cutting condition. Stable periodic cutting processes are characterised by limit cycle solutions that intersect a Poincaré section in the same locations every fundamental forcing period. This fundamental period varies from the tooth pass period for conventional milling tools to the spindle pass period for non-conventional ones. For linear chatter prediction models, unstable bifurcation cases can be divided into period-n bifurcations and secondary Hopf bifurcation or chatter. In the foremost, the limit cycle solution intersects the Poincaré section every n times. In the latter, a not harmonic frequency of the forcing excitation emerges, leading to multiple intersections of the limit cycle with the Poincaré section resembling an elliptical shape. Chatter prediction methods that employ nonlinear models have also been studied using bifurcation analysis. Sources of

nonlinearities in milling processes can come from cutting force models and/or structural dynamics. Regarding the cutting force model, sources of nonlinearities can come from a nonlinear relationship between the cutting forces and the chip thickness, or enhanced models that allow the inclusions of phenomenons such as the loosing of tool engagement and/or large-amplitude vibrations. Nonlinear structural dynamic sources can come from the use of cubic spring models and/or mass changing models that adjust the FRF according to the material removed from the workpiece. By using these enhanced models, several authors have reported more complex unstable bifurcation conditions and even chaotic behaviours in bifurcation diagrams.

However, while these enhanced non-linear models provide more accurate chatter prediction results, they generally increase the complexity of the modelling equations and the computational time to solve them. On the other hand, linear milling systems provide reliable results within a range of system parameters. For example, Figure 2.7 shows that the linear cutting force model provides a fair approximation for uncut chip thickness from h_1 to h_2. Lower and higher values may diverge from the linear cutting condition. The same analysis can be done for other sources of nonlinearities in which an adequate cutting condition selection reliably allows the linear model assumption.

For the current thesis, the aim is to validate instability islands that emerge when using variable helix milling tools. These islands appear in the stability lobe diagram because of the non-equal helix angles of the tool flutes that alter the chatter condition of the process at higher axial depths of cut. To validate this condition, an instrumented experimental setup is developed. This device has a hall effect sensor that sends a pulse every time it detects a rotating reference in the spindle. These pulses are used as a reference to get once-per-revolution values of the obtained sensorial data. Therefore, it enables to construct recursive or Poincaré plot to analyse types of bifurcation providing an insight into the process dynamics inside and around these islands. To reduce the complexity of the problem, the experimental setup is developed as a linear one-degree-of-freedom flexible workpiece. Also, the machine tool is assumed as infinitely rigid. To

assess this condition, several impact tests are performed on the flexible workpiece and machine tool.

To attain larger depths of cut while assuming linear structural dynamics, a low cutting-force stiffness material is implemented to scale the cutting forces. For this purpose, a thermoplastic named as copolymer acetal is employed as workpiece material. To use the linear cutting force models, it is first investigated in the literature the recommended cutting parameters (such as tool geometry, cutting speeds, chip thickness) that guarantee linearity. Later, a set of milling trials following the mechanistic identification approach are performed to assess this assumption and to determine the cutting force coefficients.

To fulfil this goal, the next section first presents some relevant works related to sensors and signal processing techniques to detect chatter milling processes. Aspects such as the type and the number of sensors and the chatter signal features are vital parameters for a reliable chatter detection system.

2.4. Chatter Detection

Reliable chatter detection is an important aspect to safeguard the workpiece and machine tool integrity. In a production environment, chatter detection can be required online chatter avoidance. By determining the chatter onset, or even forecasting its occurrence, the spindle speed and depths of cut can be automatically adjusted to values with better chatter stability performance. Development environment can also require chatter detection to fine-tune the machining parameters and process design for specific workpiece components, particularly in high-value manufacturing such as aerospace. In research, chatter detection plays a vital role in the model validation process, allowing accurate classification of the stability of machining trials.

Either in offline or online applications, an inadequate sensor choice and detection technique may lead to wrong conclusions and catastrophic results. To detect chatter, process variables can be monitored using sensors such as accelerometers, displacement sensors, microphones, and dynamometers. The state of the process variables can also be indirectly estimated using related variables such as motor current consumption. In addition, the use of sensors requires signal processing techniques to extract features related to chatter. Hence, this section presents some of the most utilised sensors and techniques for this purpose.

2.4.1. Sensors for Chatter Detection

Chatter detection techniques rely heavily on the information provided by sensors. In machining, sensors such as accelerometers, microphones, dynamometers, and displacement sensors are broadly used for this purpose. Therefore, knowing the capabilities and limitations of these devices is essential for a suitable selection. In fact, in most cases multiple sensors are recommended so they can compensate for their limitations in specific applications.

For instance, accelerometers are one of the most implemented sensors for chatter detection because they can robustly reflect the chatter onset at large and low cutting immersions. This reliability is reinforced by their rapid response, suitable for online chatter detection, as mentioned by Cao et al. in [83]. For example, Faseen in [84] compared several sensors for chatter detection in milling. The author highlighted that the fastest response was found using a piezoelectric accelerometer and an eddy current sensor. Nevertheless, Faseen highlighted that accelerometers proved less intrusive with a straightforward implementation. However, applications that require coolant may complicate the sensor's use if a waterproof installation can not be guaranteed.

Regarding microphones, Delio [85] showed the capability of sound signals to better reflect the chatter onset. Delio reached this conclusion when comparing microphones

and force sensors on milling processes at low and high cutting immersions [86, 87]. However, the author stated that background noise may affect signal quality, so noise filtering could be required [84, 88–90]. This adds an extra step in the implementation when compared with accelerometers. In addition, applications requiring spindle and workpiece rotations may complicate the sensor installation. This is because the sensor requires to be orientated and close to the cutting process [91, 92]. The use of coolant may also add another constraint if the microphone is not impermeable.

Chatter detection can be performed using cutting force signals from a table or rotating dynamometer [93–98]. However, several research articles have reported poor force signal performance on reflecting chatter onset [86,99,100]. For example, for low milling cutting immersions, the sensor struggles to reflect chatter due to the short time spent in cutting [85]. If the force magnitudes are also low, it requires a dynamometer with higher sensitivity transducers to capture the dynamics. In addition, to avoid sensor dynamic interference on the measurements, the frequency bandwidth must be as high as possible. For higher cutting force magnitudes, the implementation of larger and more intrusive dynamometers may be required. Therefore, this may lead to a narrower frequency bandwidth due to the additional mass. Another option could be the use of rotating dynamometers, but these sensors increase the tool overhang, thus the flexibility of the spindle-tool holder-tool chain.

Cutting forces can further be indirectly measured from the drives and spindle motor current consumptions [101]. This technique has been implemented by several researchers for chatter detection and tool-condition monitoring [21,102]. This can be done by equating electrical and mechanical power consumption, leading to a cutting forces and motor current linkage. Contrary to dynamometers, this sensor-less approach does not interfere with the machining process in any sense, while providing a good chatter sensitivity at higher and lower immersions [101–104]. However, the thermal dependency of the motor energy utilisation may obscure the chatter feature extraction [105]. Moreover, the tool-toolholder-spindle dynamics are required for the modelling, adding

extra steps for its implementation. Furthermore, the lag time between the chatter onset and the signal arrival may complicate its real time application.

In summary, an adequate sensor selection is critical because it can facilitate the signal processing and feature extraction tasks. This then lead to accurate assertions about the stability condition of the process [106]. In the literature, chatter detection has been performed using sensors such as accelerometers, microphones, and dynamometers. These sensors possess weaknesses and strengths, so more than one of them is often recommended to guarantee effective chatter detection. Thus, the weaknesses of one sensor can be compensated, leading to a more robust detection system. For example, Kuljanic et al. [107, 108] studied a multi-sensor approach for chatter detection. The author found that best results were obtained using microphones, an axial force sensor, and accelerometers in the milling process.

2.4.2. Signal processing and feature extraction for chatter detection

To avoid or suppress chatter, signal processing techniques are required for conditioning and extraction of chatter related features. For instance, techniques such as time-domain analysis, fast Fourier transform, wavelet transform, and Hilbert-Huang transform, have been extensively used for signal processing. Depending on the approach, various metrics and criteria can be defined to characterise the process stability condition. Finally, the chatter characterisation is then performed defining a threshold limit to the features extracted from the signals.

As an example of time-domain analysis, Schmitz [91] implemented the variance of once-per-revolution samples of sound signals as a feature. A periodically sampled signal from a stable milling process is identified by having a low statistical variance because it produces information synchronised with spindle rotation. On the other hand, unstable trials manifest a larger once-per-revolution variance because of the asynchronous motion associated with the process. Later, Shepard [109] followed the same methodology

as Schmitz but using cutting-force signals. Shepard explained that using microphones in a noisy industrial environment may decrease the signal-to-noise ratio. However, the experimental validation revealed several inconsistencies while categorising the stability of some trials, a condition that may be linked to the poor force sensor performance on reflecting chatter.

Furthermore, time-domain analysis has also been implemented for in-process chatter detection. Here, the non-stationary nature of the physical variables requires faster computational times to calculate the features or even to forecast the chatter-stability variations. For example, Li et al. [110] proposed a non-dimensional chatter indicator composed by the root mean square (RMS) calculations of the acceleration signal. First, the individual RMS of five revolutions of the signal was determined. Then, the peak-to-peak distance from these five RMS values was divided by their arithmetic mean value. Finally, the index was calibrated using experimental trials in which a set of thresholds were defined to categorise stable, marginally stable, and unstable chattering processes. In this work, the authors first attempted to implement a dynamometer along with the accelerometers, but the method did not perform adequately using force data. Tangjitsitcharoen et al. [111,112], on the other hand, proposed an approach that implemented the variance ratio of orthogonal cutting forces for chatter identification in ball-end milling. This method comprised a pattern recognition algorithm that classifies stable and unstable milling trials depending on the variance-ratio values. The author suggested that while force magnitudes vary with the machining parameters (e.g. depths of cut and cutting speeds), their variance ratio remain almost unchanged. As a result, the computational requirements of the approach were minimal because it mainly comprised comparing the incoming collected data to pre-calculated thresholds. However, while these thresholds can be used in a wide range of cutting tests, the method requires a large number of cutting tests to determine them.

Yamato et al. [101] proposed an on-line sensor-less chatter detection approach for turning, that implements mechanical energy and electric power factors. Yamato highlighted

that in most research, the threshold definition is unclear and dependent on the cutting conditions and machine tool. In practical industrial scenarios, it is also required a chatter detection method independent of the machining conditions and with a simple preparation. Therefore, the approach proposed by the authors uses the motor current and voltage phase difference to monitor the phase variation between the cutting forces and the tool displacements. This parameter is strongly related to chatter vibrations, and in this approach, it only depends on the frequency disturbances on the system.

While these time-domain approaches proved to be computationally efficient, they do not provide any information about the chatter frequency. This is an essential parameter to either avoid or suppress chatter. Therefore, the fast Fourier transform (FFT) has also been broadly used in the literature to analyse the stability condition of machining processes. This approach calculates the signal's frequency spectrum by expanding the signal into a series of infinite-duration sine and cosine waves. In milling, for example, chatter occurs when non-harmonic frequency components of the excitation forces become dominant. Therefore, the chatter frequencies can be straightforwardly determined, providing a significant advantage over time-domain analysis [1]. For example, Zaghbani et al. [113] implemented a frequency-domain descriptor to analyse the stability of high-speed robotic milling. Essentially, this index is the ratio between the signal's total energy within the steady-state region, to the energy of the signal in a fundamental period. Because a stable milling process is periodic, this descriptor quantifies non-periodic variation in the cutting system. Furthermore, it has the advantage of being bounded between 0 (unstable) to 1 (stable), in which the milling trials with the higher index values provided the best surface finish. The reliability of the method was proven by implementing different sensors such as accelerometers and dynamometers.

Furthermore, the FFT can provide a deeper insight into the cutting process mechanics. For example, Patwari et al. [114] implemented the FFT to investigate the process instabilities induced by the serration formation on the chip thickness of titanium Ti6Al4V in end milling. Using a scanning electron microscope, the authors found that the chip ex-

hibited equally spaced serrated teeth along its main section. It was also found that the teeth frequency depended on the machining system dynamics and the cutting process parameters. Preliminary tests revealed that chatter vibrations were induced whenever the serration frequency was close to the dominant natural frequency of the system.

One of the major disadvantages of the FFT is that because of the unchanging nature of the sinusoidal basis, it cannot be implemented with non-stationary signals. However, this shortcoming can be overcome by implementing the short-time fast Fourier transform (STFT), that windows the signal at equally spaced periods. Consequently, it enables to better capture signal transitory states, allowing to even track the chatter frequencies on the cutting process.

Filippov et al. [115] studied turning chatter behaviour using the STFT of acoustic emission and acceleration data. The authors analysed the time-variant vibration patterns along a slender long shaft, to detect the chatter features that emerge because of the changing dynamics. It was proposed a chatter detection index based on the variance of the signal within the chatter-expected frequency band. The experimental results showed that the acoustic emission signal was more sensitive to the all the stability variations induced by the changing dynamics of the slender shaft, while the acceleration signal mostly detected stable-to-unstable transitions of the process.

An analogous approach was followed by Uekita et al. [116] for deep-hole drilling, applying instead spectral kurtosis operation to the chatter-expected frequency band of the acceleration spectrum. With this approach, the authors could also monitor the cutter condition by tracking chatter features related to tool wear. However, the method reliability strongly depends on the accuracy of the modelling equations, that require a substantial number of pre-trials to determine the different model coefficients.

The STFT, however, has an unavoidable trade-off between frequency and time resolution results of using equal-size windowing [117]. Having good localisation (high resolution) in the time domain produces a poor localisation in the frequency domain

and vice versa. However, this issue can be overcome by implementing the wavelet transform (WT). Contrary to the STFT, this method tackles the resolution problem by using basis functions with variable window sizes. In addition, instead of implementing basis of infinite time duration, this technique expands the signal into a series of finite-duration waves. This allows good frequency resolution at low frequencies, keeping a decent time resolution at higher ones [118]. Thus, this method has become a reliable alternative to the short-time FFT for online chatter detection.

For example, Tangjitsitcharoen [119] proposed and experimentally validated an online chatter detection approach for ball-end milling based on the WT. The author implemented as an index the average-to-absolute ratio of the cutting-force variances in the chatter expected frequency band. The chatter onset was characterised using a threshold or critical value. While the index calculation comprises a larger set of pre-tests, the advantage of this method is that the thresholds are not cutting-condition dependent. Therefore, the same critical values can be reliably used with other spindle speeds or depths of cut.

Zhang et al. [120] proposed an early-stage chatter detection approach for milling, that employed the variational mode decomposition (VMD), the wavelet packet decompositions (WPD), and the entropy of force signals. The VMD can decompose a multi-component signal into a series of sub-signals with specific bandwidth properties in the spectral domain. Additionally, the WPD can split the signal into both low and high passbands. Therefore, both methods were implemented to divide the force signal into two distinct bandwidth groups. Then, the entropy of these groups was determined to estimate their energy distribution levels. Finally, a chatter index was build using these energy values, in which a lower or higher entropy represented a more stable or unstable process state. Although the method showed to be effective in detecting early-stage chatter, the analysis results strongly depend on the researcher experience selecting the suitable wavelet functions and the decomposition levels.

The early-stage chatter detection in boring processes was also studied by Yao et al. in [121]. The authors proposed a method based on the WPD and the support vector machine (SVM). In this method, it was first decomposed the acceleration signal into three frequency-band levels. Then, two chatter features were defined based on the standard deviation of wavelet transform and the wavelet packet energy in the chatter-expected frequency band. Afterwards, an SVM was trained to classify the stability of the cutting process as stable, early-stage chatter, and fully developed chatter. Further model validations showed an accuracy rate of 95% detecting these conditions, in which it could detect chatter even one second before it fully developed. However, as the author suggested, although these chatter features have good performance, they might not be the optimal choices in terms of computing efficiency.

Later, Chen et al. [122] followed a similar approach for online chatter detection of the end milling process. However, in this case, the authors implemented a support vector machine recursive feature elimination (SVM-RFE). This variation of the SVM applies sequential backward elimination to select the optimal feature combination from a pool of options. The author found that using the impulse factor and the auto-correlation function of the signal, the method achieved an accuracy rate of 100% with the lowest computational time from all the combinations.

However, Yuan et al. [123] pointed out the complexity in calculating the chatter features implemented in the literature. The authors highlighted that most of these indexes required extensive pre-experimentation and that they were difficult to interpret. Therefore, it was proposed a chatter detection technique for micro-end milling that uses the wavelet correlation function of two orthogonal acceleration signals as a chatter feature. The authors explained that when chatter occurs, these signals are strongly correlated at the chatter frequency. Therefore, the stability of the process can be assessed by comparing the correlation of these orthogonal signals to a pre-calculated threshold. While it showed to be a simple but effective approach, one of its major drawbacks is requiring multiple sensors.

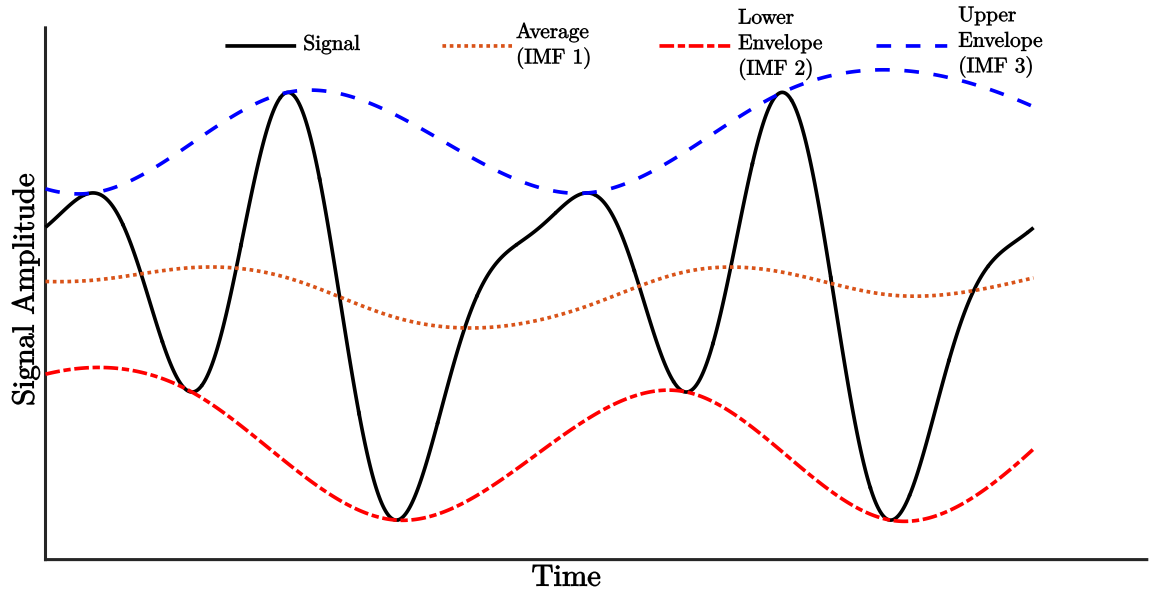

Figure 2.8.: Intrinsic mode functions [127].

One disadvantage of the WT is the arbitrary selection of the mother wavelet, which requires knowledge of the treated function [124]. Furthermore, it does not provide information about the instantaneous chatter frequency that is a critical parameter for chatter avoidance or suppression techniques. However, these drawbacks can be avoided by implementing the Hilbert-Huang transform (HHT) [125, 126]. The HHT is a methodology that decomposes a signal into near or completely orthogonal components known as intrinsic mode functions (IMF) (Figure 2.8). To achieve this, it implements a technique known as empirical mode decomposition EDM to breakdown the signal into IMF without leaving the time domain. This provides an important advantage while analysing non-stationary and non-linear signals. Subsequently, it applies the Hilbert Spectral Analysis (HSA) to the IMF to get their instantaneous frequency values.

Cao et al. [128] proposed a hybrid chatter detection approach that implements the WPT and HHT of acceleration data. In this method, the signal was first decomposed using WPT in several subs-signals containing specific frequency bands from the original. As a result, the noise that is spread across broadband frequencies is then narrowed in these frequency bands. Afterwards, the sub-signal composed by the chatter expected

frequency band was reconstructed, and its frequency spectrum was determined using the HHT. Finally, the author implemented the mean and standard deviation of this spectrum as a chatter index. One of the major disadvantages of this method is that the mean index implemented for chatter detection was not independent of the cutting conditions. Therefore, changes in the machining parameters required further calibration.

Liu et al. [129] proposed a chatter detection method based on the HHT and FFT of cutting force signals. In this approach, after determining the IMF, the authors applied the FFT to every IMF to analyse their frequency content. Contrary to Cao's method, the standard deviation and an energy ratio index of the IMF spectrum were proposed as chatter features to avoid the cutting condition dependency.

Wan et al. [124] investigated the characteristics of chatter at different development stages. For this purpose, the authors proposed a robust chatter detection method that first applied an adaptive filter to remove spindle-related frequency components while amplifying chatter expected frequency bands. Next, Wan used the variance ratio between the filtered and original acceleration signals as chatter index, defining thresholds to characterise marginally stable and fully developed chatter conditions. Finally, the chatter frequencies of the unstable trials were tracked using the HHT. Consequently, this method does not require monitoring a chatter expected frequency bands, that most of the time are arbitrarily defined around the natural frequency of the cutting system. Additionally, the authors experimentally showed the robustness of the method for classifying chatter conditions against transitory events related to unexpected variations in the cutting parameters or discontinuities in the workpiece geometry.

Susanto et al. in [130] evaluated the stability of end-milling process on thin-walled workpieces using the HHT of acceleration and strain gauge data. The authors also explored the robustness of the HHT to detect process disturbances produced by changes

in lubrication, work hardening, and metal inclusions in the workpiece. The author experimentally showed the superiority of the HHT over the STFT, while detecting chatter and these irregularities. In addition, the HHT showed to have better performance when used with the strain gauge sensor.

In summary, several techniques have been implemented for chatter detection, such as time-domain analysis, FFT, STFT, WT, and HHT. Depending on the method, features can be extracted to reflect the chatter onset. For example, time-domain analysis implements many data statistics for chatter characterisation of stationary and nonstationary signals. In contrast, frequency approaches implement the FFT to analyse the signal spectrum. From this spectrum, it constructs indicators with the data gathered on the expected-chatter frequency band. The STFT follows a similar approach, but windowing the nonstationary signals. Nevertheless, its unavoidable time-frequency resolution compromise has led to methods such as the WT and HHT. The WT possesses the disadvantages of the arbitrariness in the mother wavelet choice and its inability to determine the chatter frequency. These disadvantages can be overcome by implementing the HHT. However, one shortcoming of the HHT is that it does not have an inverse function compared with the WT. Furthermore, the HHT is a rather new method when contrasted with the WT. This means faster algorithms and more developments have been performed for WT than the HHT [125].

Based on the revised literature in this section, the sensors and signal processing techniques to be implemented during the experimental observations are defined. The current approach comprises using a microphone, accelerometer, and a Hall effect sensor for chatter detection. As mentioned before, microphones provide reliable chatter information at higher and lower depths of cut. However, chatter related features can be obscured by environmental noise. In case this issue happens, it was decided to use an accelerometer to complement the microphone data, aiming a more robust chatter detection system. Also, the Hall effect sensor allows gathering once per revolution data samples of the acceleration data. With this information, it is possible to build

a Poincaré map to further study the instabilities that occur in unstable trials. This approach then allows a more rigorous analysis from the gathered experimental data.

To define the signal processing technique, it is first considered that the cutting tests in the experimental observations are performed with constant cutting parameters. Thus, aside from the initial and final transitory regions of the trials, the signals from the sensors can be considered stationary. Therefore, the FFT can be reliably implemented as a signal processing technique because none ever-changing dynamic is taking place in the cutting process.

This method and all the approaches found in the literature involve a subjective assessment of the chatter stability boundary. Based on this subjective assessment, a threshold is defined to show the chatter onset. In the current study, a stable milling trial is characterised by having a frequency spectrum in which the fundamental forcing frequency component, or any of its harmonics, dominates or have a larger magnitude. Whenever a chatter frequency (an incommensurate frequency with the spindle pass frequency) has a larger magnitude, the milling trial is categorised as unstable.

Whichever technique is implemented, its results are mainly implemented to actively or passively mitigate chatter conditions, or simply as a chatter analysis tool. Therefore, the next section introduce some of the active and passive chatter mitigation techniques found in the literature.

2.5. Chatter Mitigation

The maximum material removal rate for a milling process is limited by chatter vibrations. The manufacturing industry has sought ways to passively or actively mitigate these vibrations by improving machine tool designs or using additional supporting systems. By doing this, cutting processes can be performed beyond the stability boundaries obtained without these improvements. Active suppression approaches rely heavily

on sensorial information to vary process state variables using actuators [131]. The relationship between the sensor signals and the actuator outputs is defined by a control law that ranges in approach such as classical [132], robust [133], optimal [134], and adaptative control [135]. Online active suppression techniques may also be required for cutting processes based on predictions with high uncertainties. These methods can be implemented with passive approaches such as tuned dampers, mass or friction dampers, viscoelastic inserts on hollow tools, or the use of milling tools with irregular shapes. Therefore, the current section presents a literature review about active and passive approaches to mitigate unwanted chatter vibrations.

2.5.1. Active Chatter Mitigation

Once the chatter indicators extracted from the sensor's signals show the onset of chatter, active chatter mitigation techniques suppress the unwanted vibrations that emerge from this condition [131]. These techniques monitor different process variables such as force, acceleration, sound, and displacement using sensors. Afterwards, the sensor signals are processed and fed to a controller that generates outputs to the actuators depending on the system state. These actuators can be piezoelectric stacks, magnetic and electrostrictive actuators, etc.

Xinhua et al. [134] proposed a delayed state feedback controller based on the discrete optimal control method to suppress milling chatter. Through numerical simulations, the authors tested the approach efficiency in different bifurcation situations. Results suggested that the method achieved the goal of enhancing either the regenerative or forced milling stability.

Dijk et al. [133] proposed a robust control methodology for high-speed milling using μ-synthesis. In this approach, the depth of cut and spindle speed were treated as uncertainties in a prior-stated range, guaranteeing robust milling stability. The author

analysed the controller system behaviour through simulations, but experimental trials were not performed.

Monnin et al. in [136, 137] presented a two-stage optimal control strategy to mitigate milling chatter vibrations. The first stage damps the critical resonance peak, increasing the lower limit of stability of the stability diagram. The second one generates further resonance peaks at particular frequencies, creating higher stability zones around the selected control-design spindle speed. Simulations and experimental results showed the feasibility and effectiveness of the proposed strategy.

Fei et al. [138] proposed an active chatter control strategy for high-speed milling based on H_∞ almost disturbance decoupling method [139]. This method finds the feedback controller that guarantees a stable closed-loop system while attenuating the disturbances to a certain degree. The attenuation accuracy was measured using the H_∞ norm, expressed in terms of a parameter ϵ_1. The author explores the effectiveness of the method under different ϵ_1 values, reaching acceptable results in a broad range. However, the author stated that at low ϵ_1 values, the controller is more sensitive to external perturbations that may lead to undesirable results.

Wan et al. [132] proposed a spindle system for chatter vibration suppression in milling via active damping. This system implements non-contacting two degree of freedom electromagnetic actuators integrated into the spindle design. Additionally, displacement sensors were placed near the actuator to measure the spindle shaft vibrations. These measurements were fed to a proportional-derivative controller. Experimental results with and without the active damping controller showed that the spindle system could effectively suppress chatter vibrations.

Li et al. developed in [135] a model predictive control methodology to suppress chatter in milling process using piezoelectric stack actuators and displacement sensors. The time-varying delayed system was approximated to a linear-time invariant system using

Padé approximation. System simulations with and without the controller showed the chatter suppression effectiveness of the approach.

2.5.2. Passive chatter Mitigation

Passive chatter mitigation increases stability by improving the structural machine-tool design, or by using additional devices to absorb or dissipate the excessive energy. Devices such as tuned dampers, mass or friction dampers, have been used for this purpose. Structural modification includes implementing irregular tools such as variable pitch and helix tools, to disrupt the regeneration effect.

Kim et al. [140] introduced a mechanical damper into a hollow milling tool to reduce chatter vibrations. The relative movement between the tool and the damper caused by the cutting forces generates friction that dissipates the extra energy. Semercigil et al. followed a similar concept [141] but using an impact damper. Ziegert et al. [142] further increased the dissipative effect by inserting a multi-fingered cylindrical insert in the hollow milling tool. Here, besides the friction between the insert outer face and the inner face of the cutter, friction is also generated between the finger's side faces.

Miguelez et al. [143] studied the effect of dynamic absorbers on the chatter stability of boring bars. The author compared two analytical tuning absorber methods, the first one proposed by Den Hartog [144] and the second by Sims [145]. Numerical results suggested that the Sims approach provides wider stability regions than the Den Hartog method. Moradi et al. [146] designed an orthogonal two-degree-of-freedom tunable vibration absorbers to improve chatter milling stability. Moradi developed an algorithm for optimal and robust absorber tuning that includes dynamic model uncertainties. Saadabad et al. [147] optimised the dynamic parameters of a bi-dimensional vibration absorber for peripheral milling. The milling model included tool wear and process damping for more realistic results.

Tuned-mass dampers also provide a reliable passive chatter suppression option. For example, Yang et al. [148] designed and optimally tuned a multiple mass damper for turning chatter mitigation. The author compared the stability effect of having on the system a single and a multiple tuned-mass damper. Results showed that multiple tuned-mass damper provides a more robust system when compared with single ones. Burtscher et al. [149] presented a tuned-mass damper with variable mass. The system comprised a case attached to the main structure by spring and dampers. This case was then filled with oil, adapting its eigenfrequency to the machine-tool dominant ones. A genetic algorithm was implemented for tuning the system to provide the best performance within the workspace.

More radical approaches have recently been taken to suppress chatter. For instance, Zhang et al. in [150, 151] explored the feasibility of submerging the workpiece in a viscous fluid to mitigate milling unwanted vibrations. Zhang could substantially increase the system damping while decreasing the cutting force coefficients. Experimental results suggested that it considerably improved the milling chatter stability while reducing process noise.

Butt et al. [152] suppressed milling chatter in thin-walled workpieces by using contactless eddy-current damping. Butt designed a device mounted on the stationary spindle chassis that holds several neodymium magnets. These magnets induce eddy-current damping forces on the metallic thin-wall being milled. This device was attached to the spindle using motors that rotate it, making it able to machine rounded and more complex thin-wall workpieces.

Wang et al. [153] investigated the possibility of improving milling chatter stability by attaching masses to the workpiece. The author proposed a method that builds an finite-element model using a modal analysis of the original workpiece. This model is later implemented to predict the workpiece dynamic variations due to the added masses and process material removal. These predictions were then implemented to construct

stability diagrams of the pose-dependant process. After, the mass weights, locations, and cutting process parameters are optimised to maximise the material removal rate.

In summary, for applications that require milling cutting conditions beyond stability limits, unwanted chatter vibrations can be suppressed using active and/or passive mitigation approaches. Active approaches monitor the cutting process using sensors such as accelerometers, dynamometers, microphones and feed their signals to a controller. This controller changes the cutting process by sending output signals to actuators based on a control law. The control law can follow approaches such as classical, robust, optimal, and adaptative. In contrast, passive approaches increase chatter stability by improving machine tool design and/or implementing further devices to dissipate or absorb excessive vibrational energy. Additional devices to mitigate chatter can be tuned dampers, mass or friction dampers. Machine tool improvements seek to increase the structural stiffness and/or damping or to use irregular milling tools to suppress regenerative chatter. As will be later shown in this thesis, the use of irregular milling tools provides outstanding chatter stability improvements. However, these tools lead to unusual isolated unstable regions in the stability lobe diagram that need to be avoided to guarantee a chatter-free process. One conclusion drawn from this section is that the effect of the dynamic paraments such as damping or stiffness on these unstable conditions requires further study. For example, as explained in subsequent chapters, these islands are particularly sensitive to structural damping levels and modelling convergence. Therefore, the use of a chatter prediction method with unconverged solutions to tune dampers in a passive approach may lead to overlooked unstable islands, and consequently undesired results. For active approaches, the effect of the actuators on the process can be seen as a virtual damper or/and spring that locally modify the process dynamics. In the same way, the use of models with unconverged solutions may lead to inadequate control actions, resulting in undesired outcomes.

The next section presents the literature review on two types of irregular milling tools, named as variable-pitch milling tools and variable-helix milling tools. That section

presents the most relevant research about these tools and highlights the works in which isolated unstable islands have been found because of the geometrical tool configuration.

2.6. Irregular Milling Tools

Regenerative chatter occurs when consecutive waves imparted by the cutter on the workpiece surface are out of phase. Particularity in milling with conventional cutters, this phenomenon occurs between waves left by consecutive teeth. Therefore, irregular milling tools have been implemented to disrupt this phenomenon, allowing to change the system stability behaviour. Nevertheless, these modifications could be beneficial or detrimental depending of the tool configuration. Therefore, a geometrical optimisation of the tool is required for most cases. Different cutter configurations have been implemented such as variable pitch, variable helix, and even variable helix and pitch milling tools. This section provides a literature review of some relevant works in this area.

2.6.1. Variable Pitch Milling Tools

Hahn was one of the first researchers who proposed a variable-pitch milling tools for chatter suppression [154]. The author highlighted that disrupting the single time delay into multiple discrete ones could lead to more stable milling processes. Later, Slavicek [155] modelled a variable-pitch milling process applying orthogonal chatter theory, and using a two-teeth linear cutter. Stability predictions suggested that it is possible to double the minimum axial depth of cut using these tools. Afterwards, Opitz in [156] considered a rotating tool using an averaged directional factor. As Slavicek, the author also studied a simple variable-pitch tool configuration with two teeth. Thereafter, Vanherck [157] extended Slavicek's work on linear cutters by showing in simulations

the effect of multiple pitches on milling chatter stability. Varterasian in [158] experimentally studied random distribution of pitch angles around the milling tool. Tlusty in [38] optimized variable-pitch milling tool using time domain simulations.

Afterwards, Altintas in [159] presented and experimentally validated an analytical zeroth-order frequency solution for variable-pitch milling tools. The author showed how varying the tool pitches lead to improvements or detriments of the stability boundaries. Budak in [160, 161] proposed a method for optimal pitch selection of linearly arranged variable-pitch tools at a defined spindle speed. Budak showed that the ratio between the variable-pitch stability boundary to the minimum conventional tool stability limit can be substantially maximised. Later, Olgac et al. [162] studied the variable-pitch milling dynamics and stability implementing cluster treatment of characteristics roots technique.

Sellmeier et al. [163] investigated the effect of the system time-dependent terms on the variable-pitch stability diagram at higher immersions. Sellmeier could find several unusual conditions (e.g. stable islands at high depths of cut) in the diagram when compared with conventional tools.

Comak in [164] proposed an iterative optimization method for variable pitch milling tools. In this method, the stability problem was solved for a range of pitches using the zero-order SDM. The method resulted on a three-dimensional stability lobe diagram, in which the third dimension is the pitch parameter. Experimental results validated the optimization outcomes.

Stepan et al. [165] also proposed an iterative method for variable-pitch face-milling tool design. Contrary to Comak in [164], the author considered time-dependant dynamics and more accurate frequency prediction approaches. Iglesias in [166] compared Stepan's iterative approach with the methods proposed by Slavicek [155] and Budak [160, 161]. Numerical and experimental results suggested by Stepan outperformed both methods in

terms of optimal pitch optimisation. The author could experimentally present evidence that the period doubling instabilities related to the pitch pattern arrangement.

In summary, variable-pitch milling cutters differ from conventional milling tools in that they possess non-equal pitches but equal helix angles on the flutes. Therefore, the single time delay that characterises conventional milling tools is then disrupted into multiple discrete delays, allowing them to suppress regenerative chatter. Nevertheless, the chatter stability of these cutters strongly depends on the pitch arrangement around the tool. As a result, their implementation may lead to undesired results if the tools are not adequately optimised for a particular cutting condition.

Variable-pitch milling tools are one of the first irregular milling tool configurations implemented to suppress regenerative chatter. Therefore, compared with other configurations, there are a vast amount of research papers regarding the chatter dynamics and stability of these tools. While the focus of the current thesis is milling with variable-helix cutters, variable-pitch cutters represented the ideal starting point to study the dynamics of irregular milling tools. In fact, early variable-helix research simplified the problem complexity by using pitch averages and solving the problem as a variable pitch one [167, 168]. This then allowed to implement well established variable-pitch design methodologies (e.g. Budak et al. [160, 161]). However, there has been nowadays a growing number of research papers regarding variable-helix milling tools, proposing chatter prediction methodologies as well as reporting unusual conditions such as unstable islands while using these cutters. Therefore, the next section focuses on presenting the literature review about variable-helix milling tools, providing an insight in the methodologies implemented to analyse these cutters.

2.6.2. Variable Helix Milling Tools

Variable helix tools were first described by Stone [167], but they received scant attention for the proceeding four decades. Turner and co-workers [168] reinvigorated the

research when they reported some experimental trials with variable helix tools, along with comparisons to time-domain simulations and an approximate stability model. Variations between the experimental and predicted results were quite significant, and it was suggested that this could be attributed to process damping effects.

Following this, Sims et al. [58] modified the semi-discretisation method to consider variable helix tools. They validated their results against time-domain simulations rather than experimental data, but they did predict islands of instability, unlike the previous studies. In a later study, Yusoff in [24, 169–171] used genetic algorithms to optimise the tool geometry and additionally studied the role of the tool geometry in process damping. They performed some experimental validation of these results, but there was limited evidence for islands of instability in the tests or predictions that they described.

Later, Otto et al. [172, 173] enhanced the regular-tool multi-frequency approach to variable helix and pitch tools. This model considered non-linear cutting force behaviour and cutter run-out in a three-dimensional machine tool and workpiece dynamics. They assessed the validity of the model using data found in the literature.

After, Jin [174] adapted the variable-pitch zeroth-order frequency approach [159] for variable helix tools. As Turner [168], Jin considered the variable helix tool as a variable pitch by averaging the pitches along the flutes. The validity of the model was justified by implementing data encountered in the literature. Jin in [175] applied the same strategy to the semi-discretization method. Wang then implemented this strategy in [176] with the variation of using the largest pitch. Later, based on Wang's approach, Xie [26] studied in simulations the effect of the radial depth of cut on the stability-lobe diagram. In this work, Xie predicted instability islands at a low radial depths of cut in the flip and Hopf regions of the stability diagram. However, the author did not provide further information regarding if the islands in the Hopf region were caused by the highly intermittent nature of the process (parametric islands) or the non-equal

helix angles of the tool.

Afterwards, Sims in [27] proposed an alternative formulation that allowed to visualise the stability of the process using filters. Contrary to Xie in [26], Sims predicted instability islands at full-slotting, suggesting that they result from the non-equal helix angles. Even though this work did not provide experimental data, it explored the potential modelling and validation challenges for these tools.

Later, Sims implemented this work as a backbone to formulate [51] the stability model of these tools employing a harmonic transfer function approach. The first key difference between this work and alternative multi-frequency approaches is the explicit appearance of a phase-changing term in the modelling equations. The second relies on taking advantage of the problem symmetry and the high-frequency behaviour of the dynamic response function to further simplify the problem. The author verified this formulation against simulation data found in the literature.

Otto et al. [177] enhanced and validated the analytical formulation introduced in [172, 173]. In this work, the authors took a similar approach adopted by Sims in [51] to formulate the stability models. Nevertheless, differences between both approaches appear while solving the problem. While Otto identifies the stability boundaries using a winding number of the determinant, Sims implements the generalised Nyquist stability criterion. The latter on enjoying the advantage of not involving calculation of determinants and/or eigenvalues. They verified the formulation against experimental results and presented theoretical comments on the effect of run-out on stability of the process.

Afterwards, based on the comments made by Otto, Jinbo and co-workers [178, 179] retook the study of the run-out effect on the variable-helix and pitch stability. Initially, they characterised the mechanistic force models, including the joint impact of eccentricity and run-out, by using non-linear optimisation. Then, the authors predicted the stability of the process by utilising the generalised Runge-Kutta method. Next,

they performed experimental validation to confirm the simulations. In the preliminary results at a low radial depth of cut, the authors could find changes on the stability frontiers of the system when including these parameters.

To summarise, Stone first described the potential of variable-helix milling tools to suppress regenerative chatter. After forty years of scarce attention, Turner stimulated the research presenting numerical and experimental data. Later, the semi-discretization method was changed by Sims to consider milling tools with non-equal helix angles, while Yusoff implemented this approach to optimise their geometry. Subsequently, Otto extended the multi-frequency approach of conventional milling tools to consider variable helix milling tools, nonlinear cutting force models, and runout. Further studies presented by Jin, Wang, and Xie implemented the zeroth-order frequency approach and the semi-discretization method to study these tools. In these cases, the variable-helix milling tool was approximated as a conventional or variable-pitch one by taking the average or largest pitch along and around the tool. Sims later provided insight into the variable-helix milling dynamics, using filters to allow visualisation of the stability of the process. Based on this work, Sims proposed the multi-frequency method for these tools using a harmonic transfer function approach. The author emphasised a phase-changing term in the equations, not seen in previous multi-frequency methods. Otto proposed a similar approach, and presented a theoretical analysis of the effect of runout on the stability of these tools. Based on Otto's comments, Jinbo et al. performed a numerical and experimental study on the runout effect on the stability of these tools, revealing runout induced variations on the stability at low radial immersion.

From the revised literature, it was noticed that several authors predicted in simulations unusual isolated unstable regions in the stability lobe diagram. However, the authors did not provide experimental evidence to validate, or reasons explaining these conditions. Therefore, the next section presents the literature review about unstable islands beginning with the ones found with conventional milling cutters, and later presenting the studies regarding variable helix instability islands.

2.6.3. Instability Islands

Instability islands with conventional milling tools have been broadly studied and validated by the research community. For example, Szalai [180] and Govekar [181] first reported instability islands in the flip-lobe region. However, the authors did not relate these islands to the helix angle of the flutes. Later, Zatarain [25] enhanced the multi-frequency approach for vertical-flute-milling tools to include the helix angle. In that work, the author noted that at axial depths of cuts that are multiples of the axial pitch, all the harmonics of the directional-factor Fourier expansion become null. Therefore, the zero-order term of the expansion dominates during the process. Because the zero-order solution does not present the added flip lobe, it takes the shape of equally spaced lenticular unstable regions divided by stable areas. A validation performed using a scaled experiment confirmed these findings.

Later, Insperger et al. [182] performed a similar analysis than Zatarain but implementing the semi-discretization method. The authors explained the phenomenon using the Floquet theory of periodic delayed systems. The study showed again that at these multiples, the time-periodic system becomes autonomous. Therefore, the system cannot experience flip instability. Further, they also classified the unstable islands in two categories, named as helix-induced and parametric instability islands. The former regards the condition exposed by Zatarain [25], while the latter, first identified by Szalai and Stepan [180], is independent of the helix angles. Contrary to the helix-induced kind, parametric islands emerge in highly interrupted processes, even in the Hopf region of the stability diagram.

Next, Patel [183] studied both types of instability islands at various cutting conditions. Patel showed that the entry and exit angle of the flutes on the workpiece strongly affects the island locations in the stability diagram. Contrasting with Zatarain in [25], the author used a 3-teeth tool for the validation process. This is because the frequency

spectra from a two-flutes process with run-out has a similar spectrum than a period-doubling motion making it difficult to distinguish between the two phenomena.

Afterwards, Khasawneh et al. [184] investigated the period-doubling islands in milling with simultaneously engaged helical flutes. Contrasting with earlier works, they studied in simulations these islands at higher axial and radial depth of cuts. The authors showed that the period-doubling region could appear at high radial immersion when multiple teeth are simultaneously cutting. They found this with either zero or non-zero helix angles. Additionally, the author showed the active relationship between parity in the number of flutes and the process stability in this region.

As part of the research presented in this thesis, Ureña et al. [185] first attempted to validate a variable-helix instability island using a one-degree-of-freedom scaled experiment. This experimental configuration scaled not only the dynamic of the system but also the cutting-force stiffnesses. The authors performed stability predictions utilising the semi-discretization method, reporting low spindle-speed instability islands away from the flip region. To accomplish this, they implemented a 16 mm variable-helix three-flute tool with equal pitches at the tip. They defined the milling process as up-milling and half-immersion. Therefore, they concluded that these islands emerged because of the distributed delays along the tool caused by the non-equal helix angles. Experimental results corroborated this revealing secondary-Hopf bifurcations inside the island. However, although the results were close to the predictions, it showed the island connected to another lobe. The authors attributed this to convergence issues, dynamic-model inaccuracies, or unmodeled phenomenons.

2.7. Summary

This section presented the literature review regarding several aspects of the milling process relevant to this thesis. It included approaches for prediction, detection, and

mitigation of chatter currently researched or being implemented in industry. The literature review showed how the early cutting models proposed led to chatter stability predictions such as the MFA, SDM, and FDM. It also showed how these cutting force models have been enhanced to include nonlinearities that better reflect the real process's physics. Afterwards, this chapter presented different sensors and signal processing techniques implemented for chatter detection. Later, it was addressed chatter mitigation problem, showing different approaches such as the active and passive ones. Regarding passive chatter mitigation approaches, it was also discussed how the implementation of irregular milling tools can be use cancel regenerative chatter.

Later, some of the most relevant works regarding variable-pitch and variable-helix milling tools were presented. The literature review from these tools, and in particular for variable-helix milling tools, revealed an unusual condition in the stability lobe diagram manifested as isolated unstable regions. As the literature hinted, these unstable islands differ greatly from those found with conventional milling tools. Contrary to regular milling islands, variable-helix instability islands have not been thoroughly researched in the literature. To the best knowledge of the author, no research study has explored the convergence performance of the current chatter stability prediction methods around these conditions. In addition, apart from the validation attempt performed by Ureña et al. [185], no investigation has provided solid experimental data or explanation on why these conditions happen.

Therefore, the current thesis aims to address this knowledge void by implementing a scaled experiment to numerically and experimentally study in depth these conditions. To achieve this, Chapter 3 first presents the theoretical background of two chatter stability prediction approaches, these being the SDM and the MFA. These methods will be then implemented throughout the thesis to capture the instability islands and to compare their convergence performance doing so. Next, Chapter 4 presents in detail the scaled experiment used in this thesis to numerically and experimentally study the stability of variable-helix milling tools. Afterwards, Chapter 5 first explores the effect

of structural damping on the variable-helix stability diagram, and how this parameter is linked to the variable-helix instability islands. Subsequently, a convergence analysis around an instability is performed using the MFA and SDM. Finally, a set of milling trials using the experimental setup are executed to validate the unstable condition.

3. Theoretical Background

3.1. Introduction

The current chapter presents the theoretical background of chatter stability analysis of milling tools. Section 3.2 studies a simple case of regenerative chatter on a single-point cutting process [36]. This section aims to expose the main aspects of this phenomenon [13]. Furthermore, regenerative chatter is shown as a feedback mechanism using a block diagram. Later, key aspects of the process stability are discussed using the stability lobe diagram. Afterwards, two analytical stability prediction techniques for irregular milling tools are presented in the subsequent sections, the first being the Multi-Frequency Approach (MFA), while the second the Semi-Discretization Method (SDM). As mentioned in Chapter 2, the MFA was first introduced by Merdol et al. in [46], while the SDM by Insperger et al. in [40, 54].

In particular, this chapter presents the MFA and SDM modified by Sims in [58] and [51] for variable pitch and variable helix milling tools. In terms of novelty, the current chapter further enhances the MFA to consider helix-induced non-equal cutting force stiffnesses in the models, enabling to study its impact on the stability of the variable-helix milling process. Finally, a case study found in the literature is analysed using both methods to validate the developed simulation programs.

3.2. Regenerative Chatter on Single-Point Cutting Process

Chatter is commonly categorised into primary and secondary. The first chatter category encompasses instabilities induced by the cutting process itself. For example, primary chatter conditions can be induced by friction between the cutter and the workpiece, mode coupling, or thermo-mechanical effects on chip formation. On the other hand, secondary chatter condition, or regeneration chatter, occurs when the wavinesses imprinted on the workpiece surface by subsequent cutter passes are out of phase. Because the focus of this thesis is on regenerative chatter, the current section aims to provide an insight into the characteristics of this phenomenon.

For this purpose, the schematic of a single-point cutter shaping a cylindrical workpiece is shown in Figure 3.1. In this schematic, the workpiece rotates around a rigid pin at a velocity Ω, while the cutter is allowed to vibrate in the y-direction. This model neglects any type of vibrations on the workpiece. Therefore, while the cutter removes a certain amount of materials from the workpiece, it left printed waves on the surface because of these vibrations. Consequently, regenerative chatter then occurs whenever subsequent surface waves are out of phase. This phenomenon can lead to exponentially growing cutting forces that may affect the tool and workpiece integrity.

Figure 3.2 shows a schematic with a closer look of this mechanism after several workpiece rotations. With reference to this schematic, the term h_m is the desired nominal chip thickness, while $h(t)$ is the instantaneous one. This instantaneous chip thickness encompasses can then be express as,

$$h(t) = h_m + (y(t-\tau) - y(t)), \tag{3.1}$$

in which $y(t)$ the current tooth vibration, and $y(t-\tau)$ is the vibration left on the workpiece surface in the previous revolution, characterized by the time delay τ. It is worth mentioning that for cutting processes with multiple teeth as milling, the h_m becomes $h_m \sin\Theta_j$ to consider the angular immersion Θ of the flute j. Now, according to the

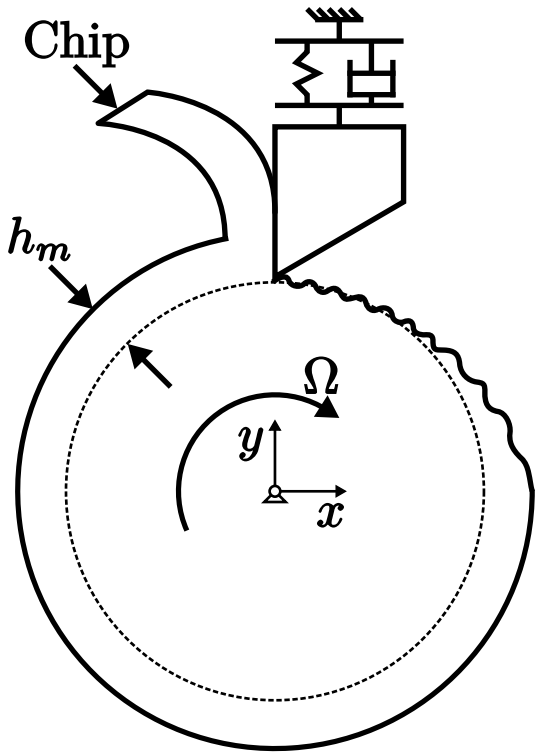

Figure 3.1.: Schematic illustrating a single point cutting process.

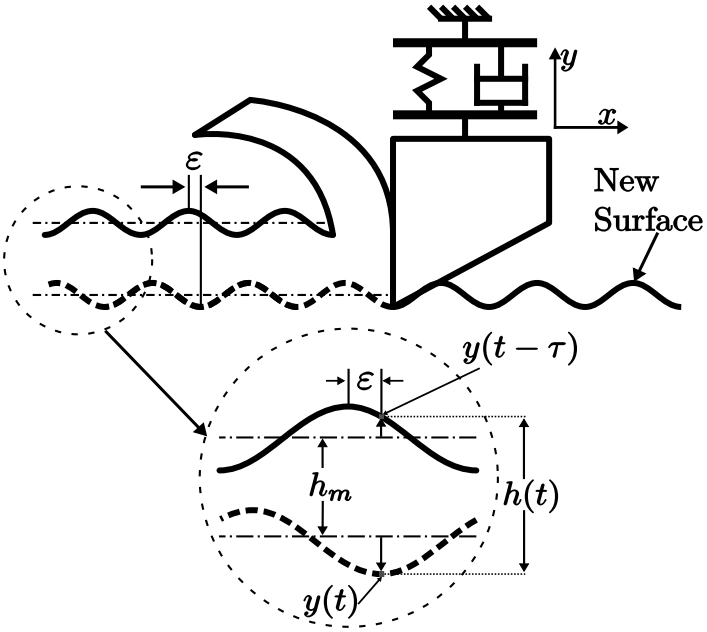

Figure 3.2.: Magnified single point cutting process on an unfolded workpiece describing the regenerative mechanism.

orthogonal cutting theory [77], the process cutting forces are assumed proportional to the cross-sectional area of the chip thickness as follows,

$$F(t) = bK_s h(t) \tag{3.2}$$

in which K_s is a proportionality constant and b is the depth of cut. Moreover, by taking the Laplace transform of the current vibration $\mathcal{L}(y(t)) = Y(s)$ and the cutting forces $\mathcal{L}(F(t)) = F(s)$, these variables are linked by the system's complex transfer function $G(s)$ as follows,

$$Y(s) = G(s)F(s), \tag{3.3}$$

where s is a complex variable, and $Y(s)$ and $F(s)$ are the subsequent complex functions representing the vibration and forces. The relationship between the complex vibration, force, and the instantaneous chip thickness can be obtained by applying the Laplace transform to equations 3.1 and 3.2 obtaining,

$$H(s) = H_m(s) + (e^{-\tau s} - 1)Y(s) \tag{3.4}$$

$$F(s) = bK_s H(s). \tag{3.5}$$

As Merritt presented in [13], the regenerative chatter can be represented as a feedback loop mechanism as it is shown in the block diagram of Figure 3.3. In this diagram, the direct path relates the instantaneous chip thickness with the current vibration. In the feedback path, this vibration is then subtracted by itself modulated by the complex exponential $e^{-\tau s}$ characterised by the time delay τ. This difference is then added to the nominal chip thickness to close the positive feedback block diagram. Now, combining the equations 3.3 and 3.5 gives the following transfer function,

$$\frac{H(s)}{H_m(s)} = \frac{1}{1 + bK_s G(s)(1 - e^{-\tau s})}, \tag{3.6}$$

Therefore, the system stability can be studied analysing the poles of equation 3.6 as,

$$1 + bK_s G(s)(1 - e^{-\tau s}) = 0, \tag{3.7}$$

From control theory [186], the stability boundaries of the system are found whenever the real part of s vanishes. Therefore, by substituting $s = i\omega_c$ ($i = \sqrt{-1}$) into equation 3.7, the closed-loop characteristic equation can be rewritten as,

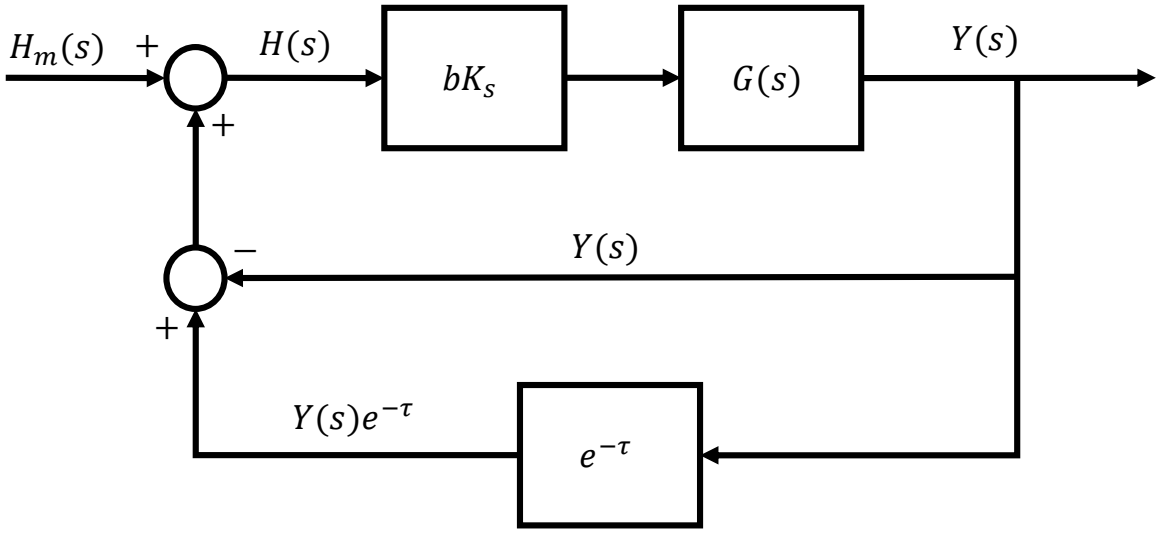

Figure 3.3.: Block diagram showing the interrelationship between the different cutting parameters. The terms $Y(s)$ and $Y(s)e^{-\tau}$ represent the current and delayed vibrations altering the chip thickness $H(s)$.

$$b_{cr}K_sG(i\omega)(1-e^{-\tau i\omega_c})=-1, \tag{3.8}$$

where b_{cr} is the critical depth of cut in which the system becomes marginally stable, vibrating at a frequency ω_c known as the chatter frequency. Now, by defining $\varepsilon=\tau\omega_c$ as the angular phase shift between two consecutive waves, the critical axial depth of cut can be expressed as,

$$b_{cr}=\frac{-1}{K_sG(i\omega)(1-e^{-\varepsilon i})}. \tag{3.9}$$

Consequently, because of the axial depth of cut and K_s are a real positive values, the term $G(i\omega)(1-e^{-\varepsilon i})$ has also to be real but negative to cancel the negative sign in 3.9. This can only be achieved if the vector $G(i\omega)(1-e^{-\varepsilon i})$ is horizontally orientated in the Nyquist plot shown in Figure 3.4. This then means that $G(i\omega)e^{-\varepsilon i}$ is the complex conjugate of $G(i\omega)$, so their imaginary terms cancel each other. Therefore, this term can be reduced to the following expression,

$$G(i\omega)(1-e^{-\varepsilon i})=2Re\left(G(i\omega)\right). \tag{3.10}$$

Additionally, the minimum limiting chip width can be obtained using the minimum real component of the frequency response function as,

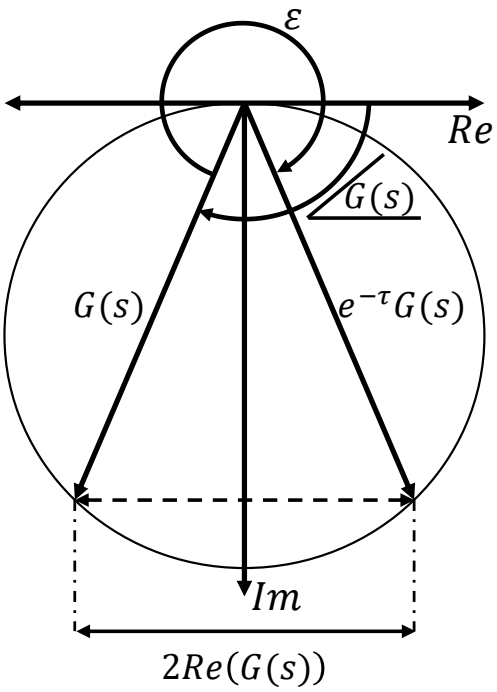

Figure 3.4.: Nyquist diagram

$$b_{min} = \frac{-1}{2K_s Re\left(G(i\omega)\right)|_{min}}. \tag{3.11}$$

By cutting below b_{min}, the process is guaranteed to be stable as shown in Figure 3.5. Subsequently, the ratio between the chatter frequency $\omega_c = 2\pi f_c$ and the rotational frequency f_Ω can be expressed as,

$$\frac{f_c}{f_\Omega} = k + \frac{\varepsilon}{2\pi} \tag{3.12}$$

where k and $\varepsilon/2\pi$ are the subsequent integer and fractional number of waves per revolution. Moreover, the angle ε can be straightforwardly deduced from the diagram 3.4, and written as,

$$\varepsilon = 2\pi - 2\tan^{-1}\left[\frac{Re(G(i\omega))}{Im(G(i\omega))}\right]. \tag{3.13}$$

Therefore, by knowing the system frequency-response function and the cutting parameters, it is possible to build a stability lobe diagram of the process. It is evident that multiple solutions are obtained for a set of parameters due to the term k in the equation 3.12. Note that, the phase difference between the inner and outer waves on the

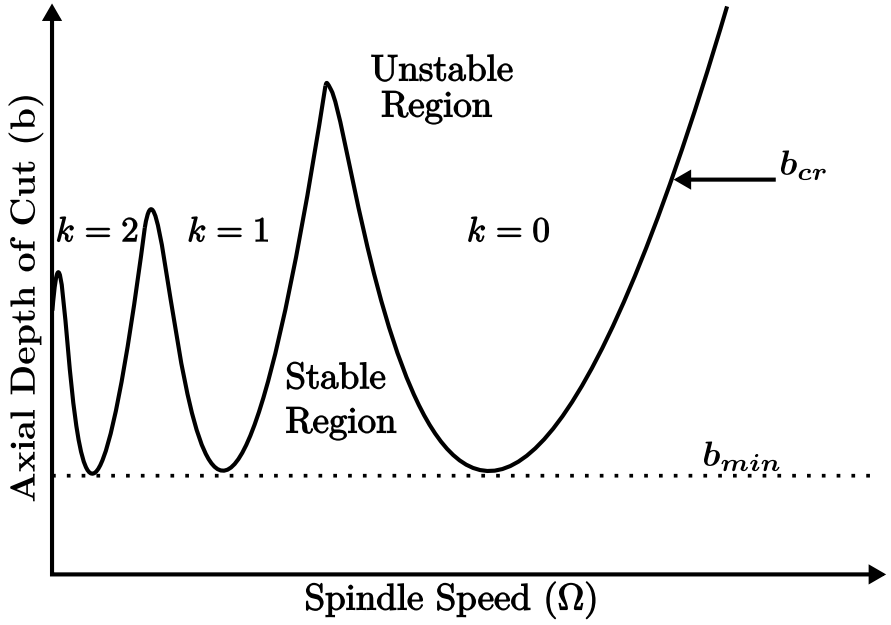

Figure 3.5.: Stability lobe diagram

chip surface ε will be 0 or 2π when the f_c to f_Ω ratio is an integer number. Under this condition, both waves are parallel to each other resulting in a constant chip thickness. However, if the phase difference does not meet these conditions, the chip thickness changes continuously. The essence of this analysis can be extended to cutters with multiple teeth as in milling. However in this case, the non-continuous cutting process performed by the teeth, increases the complexity of the analysis. This complexity is even higher for milling tools with irregular shapes, that requires further modelling to capture the distributed time delays along the tool. Therefore, the next section presents two modelling techniques for irregular milling tools. The first one being the MFA and the second one the SDM. In particular, these modelling techniques can be applied to milling tools with variable pitch and variable helix angles. This thesis places more emphasis on milling tools with variable helix angles as this is the main subject of the investigation.

3.3. Multi-Frequency Approach

The mechanistic force model and the multi-frequency stability approach presented in this section follows the methodology proposed by Sims in [51] for a one-degree-of-freedom system. This method was also based on the multi-frequency approach for conventional milling tools proposed by Merdol in [46]. The current section improves Sims's modelling equations by allowing vibrations in normal and feed direction of the workpiece relative to the tool. Also, it enhances the modelling equations by enabling the inclusion of different cutting force coefficients on the tool flutes. This then allows one to explore the effect of the helix angle on the cutting force coefficients, and therefore on the stability of the variable-helix milling process in subsequent chapters.

3.3.1. Dynamic Cutting Force Model

Based on the geometry of the tool shown in Figure 3.6 (c), we first define the angular location $\phi_j(a)$ of any tooth j as,

$$\phi_j(a) = \phi_{j0} + \beta_j a,$$

where ϕ_{j0} is the angular location of the flute j at the tip of the tool, β_j is the pitch gradient of the same flute, and a is the axial depth of cut. Also, the pitch gradient can be related to the helix angle γ_j and the radius of the tool r by:

$$\beta_j = \frac{\tan \gamma_j}{r}.$$

It is worth mentioning that γ_j is different for every tooth j. Therefore, the angular pitch differences between the flutes of the tool at any axial depth of cut can be expressed as,

$$\Delta\phi_j(a) = \Delta\phi_{j0} + (\beta_l - \beta_j)\, a \ (\text{mod } 2\pi), \tag{3.14}$$

$$l = 1 + j \ (\text{mod } N), \tag{3.15}$$

where N is the number of teeth, and $\Delta\phi_{j0}$ is the pitch at the tip of the tool expressed as $(\phi_{l0} - \phi_{j0})$. In addition, mod denotes modular arithmetic to wrap $\Delta\phi_j(a)$ around

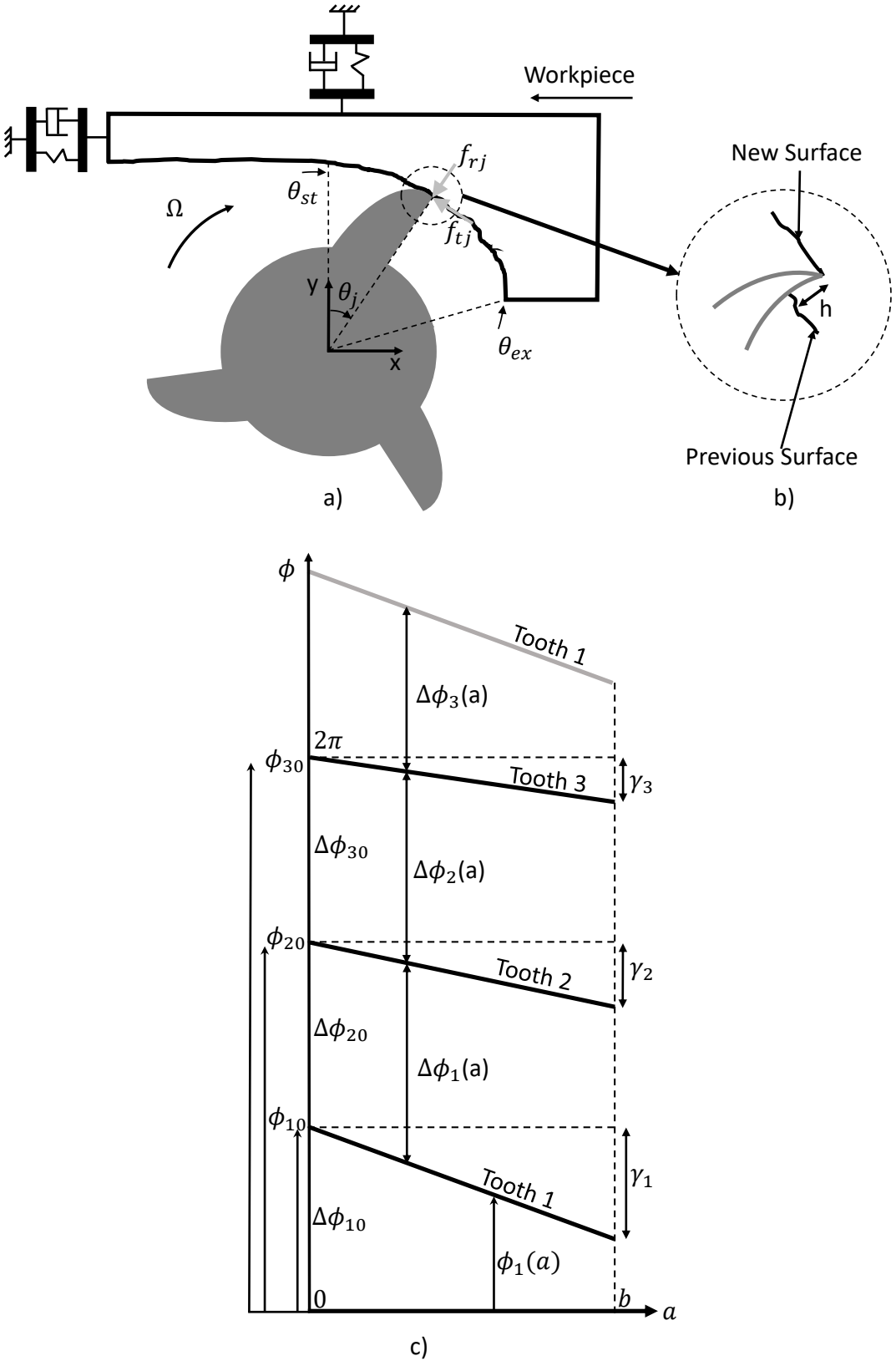

Figure 3.6.: (a) Schematic of the process; (b) Chip thickness removed by the tooth j; (c) Geometrical parameters of the variable helix tool.

the modulus 2π, and l around the modulus N. For variable-helix tools $\Delta\phi_{j0}$ is the same for every two consecutive teeth, so it is taken as a constant. Subsequently, once the tool starts to rotate at a constant spindle velocity Ω, the angle θ_j of the tooth j with respect to the axis $+y$ (Figure 3.6(a)), can be determined as,

$$\theta_j(t,a) = \Omega t + \phi_j(a) \text{ (mod } 2\pi).$$

As shown in Figure 3.6 (a) and (b), the flute j removes a chip thickness $h_j(t,a)$ at the angle $\theta_j(t,a)$. This generates forces acting on the tool in the normal (f_{tj}) and radial (f_{rj}) direction. According to the mechanistic modelling of cutting forces [77], these forces are linearly proportional to the cutting area of the flute giving:

$$f_{tj}(t,a) = K_t^j h_j(t,a) da, \tag{3.16}$$

$$f_{rj}(t,a) = K_r^j f_{tj}, \tag{3.17}$$

in which K_t^j and K_r^j are the constant cutting-force coefficients of the flute j. Now, the chip thickness can be calculated as,

$$h_j(t,a) = g(\theta_j(t,a)) \left(\Delta x(t,a) \sin\theta_j(t,a) + \Delta y(t,a) \cos\theta_j(t,a)\right),$$

where,

$$\Delta x(t,a) = x(t) - x(t - \tau_j(a)),$$
$$\Delta y(t,a) = y(t) - y(t - \tau_j(a))$$

and,

$$\tau_j(a) = \frac{\Delta\phi_j(a)}{\Omega}. \tag{3.18}$$

Meanwhile, $g(\theta_j(t,a))$ represents a binary function that is 1 whenever the flute j is inside the angular cutting region, and 0 otherwise. This angular region is defined by the start angle θ_{st} and the exit angle θ_{ex}. Expressing the normal and tangential forces around the reference frame of Figure 3.6 (a) we obtain,

$$f_{xj}(t,a) = -f_{tj}(t,a)\cos\theta_j(t,a) - f_{rj}(t,a)\sin\theta_j(t,a),$$
$$f_{yj}(t,a) = f_{tj}(t,a)\sin\theta_j(t,a) - f_{rj}(t,a)\cos\theta_j(t,a).$$

Summing the cutting forces contributed by all teeth and integrating the infinitesimal element da from 0 to the axial depth of cut b gives:

$$\mathbf{F} = \sum_{j=1}^{N} \int_{0}^{b} \alpha(\theta_j(t,a)) \Delta q_j(t,a) da, \tag{3.19}$$

where $\alpha(\theta_j(t,a))$ and $\Delta q_j(t,a)$ are the directional matrix and generalised vibration vector given by,

$$\alpha(\theta_j(t,a)) = \tfrac{1}{2} K_t^j g(\theta_j(t,a)) \begin{bmatrix} -\left\{\sin(2\theta_j(t,a)) + K_r^j[1-\cos(2\theta_j(t,a))]\right\} & -\left\{[1+\cos(2\theta_j(t,a))] + K_r^j \sin(2\theta_j(t,a))\right\} \\ [1-\cos(2\theta_j(t,a))] - K_r^j \sin(2\theta_j(t,a)) & \sin(2\theta_j(t,a)) - K_r^j[1+\cos(2\theta_j(t,a))] \end{bmatrix}, \tag{3.20}$$

and,

$$\Delta q_j(t,a) = \begin{bmatrix} x(t) - x(t-\tau_j(a)) \\ y(t) - y(t-\tau_j(a)) \end{bmatrix}. \tag{3.21}$$

3.3.2. Process Stability

To determine the process stability, the directional matrix on equation 3.20 is first expanded into its Fourier series as,

$$\alpha(\theta_j(t,a)) = \sum_{n=-\infty}^{\infty} e^{in(\phi_{j0}+\beta_j a)} \mathbf{A}_j(n) e^{in\Omega t}, \tag{3.22}$$

in which,

$$\mathbf{A}_j(n) = \frac{1}{2\pi} \int_{\theta_{st}}^{\theta_{ex}} \alpha(\theta) e^{-in\theta} d\theta. \tag{3.23}$$

Equation (3.22) reveals an exponential term $e^{in(\phi_{j0}+\beta_j a)}$ named as *phase changing* [51], that was not mentioned in previous multi-frequency derivations [77]. It is worth mentioning that due to the non-equal cutting force coefficients on the teeth, the matrix $\mathbf{A}_j(n)$ is now flute dependent. Subsequently, by replacing equations 3.22 and 3.21 into 3.19 it is obtained,

$$\begin{bmatrix} F_x \\ F_y \end{bmatrix} = \sum_{j=1}^{N} \int_{a=0}^{b} \sum_{n=-\infty}^{\infty} e^{in\phi_j(a)} \begin{bmatrix} A_j^{xx}(n) & A_j^{xy}(n) \\ A_j^{yx}(n) & A_j^{yy}(n) \end{bmatrix} e^{in\Omega t} \begin{bmatrix} x(t) - x(t-\tau_j(a)) \\ y(t) - y(t-\tau_j(a)) \end{bmatrix} da. \tag{3.24}$$

where the expressions for the terms $A^{xx}(n)$, $A^{xy}(n)$, $A^{yx}(n)$, and $A^{yy}(n)$ of the matrix $\mathbf{A}_j(n)$ are given in the appendix A.1. Equation 3.24 can also be expressed in matrix form as,

$$\mathbf{F} = \sum_{j=1}^{N} \int_{a=0}^{b} \sum_{n=-\infty}^{\infty} e^{in\phi_j(a)} \mathbf{A}_j(n) e^{in\Omega t} \left[\mathbf{q}(t) - \mathbf{q}(t - \tau_j(a))\right] da. \tag{3.25}$$

Next, by applying the Fourier transform to equation 3.25, the following frequency domain expression of the force is acquired,

$$\mathbf{F}(i\omega) = \int_{t=0}^{\infty} e^{-\omega t} \sum_{j=1}^{N} \int_{a=0}^{b} \sum_{n=-\infty}^{\infty} e^{in\phi_j(a)} \mathbf{A}_j(n) e^{in\Omega t} \left[\mathbf{q}(t) - \mathbf{q}(t - \tau_j(a))\right] da\ dt. \tag{3.26}$$

Afterwards, taking advantage of the no inter-dependency between any of the summations or limits of integration, this equation can be rewritten as,

$$\mathbf{F}(i\omega) = \sum_{j=1}^{N} \int_{a=0}^{b} \sum_{n=-\infty}^{\infty} e^{in\phi_j(a)} \mathbf{A}_j(n) \int_{t=0}^{\infty} e^{-(i\omega - in\Omega)t} \left[\mathbf{q}(t) - \mathbf{q}(t - \tau_j(a))\right] da\ dt, \tag{3.27}$$

that after expanding the expression inside the time domain integral leads to,

$$\mathbf{F}(i\omega) = \sum_{j=1}^{N} \int_{a=0}^{b} \sum_{n=-\infty}^{\infty} e^{in\phi_j(a)} \mathbf{A}_j(n) \left[\int_{t=0}^{\infty} e^{-(i\omega - in\Omega)t} \mathbf{q}(t) dt - \int_{t=0}^{\infty} e^{-(i\omega - in\Omega)t} \mathbf{q}(t - \tau_j(a)) dt\right] da. \tag{3.28}$$

Now, applying the first and second shift theorems to the terms within the brackets [51], this equation can be simplified as follows,

$$\mathbf{F}(i\omega) = \sum_{j=1}^{N} \int_{a=0}^{b} \sum_{n=-\infty}^{\infty} e^{in\phi_j(a)} \mathbf{A}_j(n) \left[\mathbf{Q}(i\omega - in\Omega) - e^{-\tau_j(a)(i\omega - in\Omega)} \mathbf{Q}(i\omega - in\Omega)\right] da, \tag{3.29}$$

that factorising by the generalised frequency-domain vibration vector $\mathbf{Q}(i\omega - in\Omega)$ results in,

$$\mathbf{F}(i\omega) = \sum_{j=1}^{N} \int_{a=0}^{b} \sum_{n=-\infty}^{\infty} e^{in\phi_j(a)} \mathbf{A}_j(n) \left[1 - e^{-\tau_j(a)(i\omega - in\Omega)}\right] \mathbf{Q}(i\omega - in\Omega) da. \tag{3.30}$$

Therefore, by multiplying both sides of equation 3.30 by the structural frequency response function $G(i\omega)$, the closed loop relationship between the vibration $\mathbf{Q}(i\omega)$ and itself modulated can be obtained as,

$$\mathbf{Q}(i\omega) = \mathbf{G}(i\omega) \sum_{j=1}^{N} \int_{a=0}^{b} \sum_{n=-\infty}^{\infty} e^{in\phi_j(a)} \mathbf{A}_j(n) \left[1 - e^{-\tau_j(a)(i\omega - in\Omega)}\right] \mathbf{Q}(i\omega - in\Omega) da. \tag{3.31}$$

A more general expression of $\mathbf{G}(i\omega)$ at any harmonic p is obtained by rewriting ω as $\omega + p\Omega$ leading to,

$$\mathbf{Q}(i\omega + ip\Omega) = \mathbf{G}(i\omega + ip\Omega) \sum_{j=1}^{N} \int_{a=0}^{b} \sum_{n=-\infty}^{\infty} e^{in\phi_j(a)} \mathbf{A}_j(n) \left[1 - e^{-\tau_j(a)(i\omega - in\Omega + ip\Omega)}\right] \mathbf{Q}(i\omega - in\Omega + ip\Omega) da. \tag{3.32}$$

In addition, defining a new variable σ related to p and n as $\sigma = p - n$, this equation can be restated as,

$$\mathbf{Q}(i\omega + ip\Omega) = \mathbf{G}(i\omega + ip\Omega) \sum_{j=1}^{N} \int_{a=0}^{b} \sum_{p-\sigma=-\infty}^{\infty} e^{i(p-\sigma)\phi_j(a)} \mathbf{A}_j(p-\sigma) \left[1 - e^{-\tau_j(a)(i\omega + i\sigma\Omega)}\right] \mathbf{Q}(i\omega + i\sigma\Omega) da, \tag{3.33}$$

that enables a matrix form notation with p representing the rows and σ the columns as:

$$\hat{q}_p(i\omega) = \mathbf{Q}(i\omega + ip\Omega),$$

$$\hat{g}_{p,p}(i\omega) = \mathbf{G}(i\omega + ip\Omega), \tag{3.34}$$

$$\hat{h}_{p,\sigma}(i\omega) = \sum_{j=1}^{N} \int_{a=0}^{b} e^{in\phi_j(a)} \mathbf{A}_j(n) \left[1 - e^{-\tau_j(a)(i\omega + i\sigma\Omega)}\right], \tag{3.35}$$

$$\hat{q}_p(i\omega) = \hat{g}_{p,p}(i\omega) \sum_{\sigma=-\infty}^{\infty} \hat{h}_{p,\sigma}(i\omega) \hat{q}_\sigma(i\omega). \tag{3.36}$$

Comparing equation 3.35 with the original formulation [51], it is evident that in this case $\mathbf{A}_j(n)$ must remain inside the summation on j. Subsequently, for compactness purpose, equation (3.36) can be written in the following way:

$$\hat{\mathbf{Q}}(i\omega) = \mathbf{G}\hat{\mathbf{H}}(i\omega)\hat{\mathbf{Q}}(i\omega). \tag{3.37}$$

Equation 3.37 represents a multi-input-multi-output system with positive feedback loop defined by the doubly infinite transfer function matrix $\mathbf{\hat{GH}}(i\omega)$. Then, according to the Generalised Nyquist Stability Criterion [187], the system is stable if $\det\left(I - \mathbf{\hat{GH}}(i\omega)\right)$ (where I is the identity matrix) is non-zero and does not encircle the origin in a clockwise sense. While this seems intractable due to the nature of $\mathbf{\hat{GH}}(i\omega)$, further simplifications can be done by exploiting the periodicity of $\mathbf{\hat{GH}}(i\omega)$ and the high frequency behaviour of $G(i\omega)$.

In order to explore the periodicity of equation 3.37, consider the situation when $\omega_1 = \omega + r_h\Omega$. It can be shown that,

$$\hat{g}_{p,p}(i\omega_1) = \mathbf{G}(i\omega + ip\Omega + ir_h\Omega), \tag{3.38}$$

and,

$$\hat{h}_{p,\sigma}(i\omega) = \sum_{j=1}^{N} \int_{a=0}^{b} e^{i(p-\sigma)\phi_j(a)} \mathbf{A}_j(p-\sigma) \left[1 - e^{-\tau_j(a)(i\omega + ir_h\Omega + iq\Omega)}\right]. \tag{3.39}$$

Now, comparing these results with equations 3.34 and 3.35, it can be concluded that,

$$\hat{g}_{p,p}(i\omega + ir_h\Omega) = \hat{g}_{p+r_h,p+r_h}(i\omega), \tag{3.40}$$

and,

$$\hat{h}_{p,\sigma}(i\omega + ir_h\Omega) = \hat{h}_{p+r_h,\sigma+r_h}(i\omega). \tag{3.41}$$

Therefore, the terms of the harmonic transfer function $\mathbf{\hat{GH}}$ are offset diagonally by one row and one column every time the frequency ω increases by Ω. In addition, assuming that the structural dynamic $G(i\omega)$ ends towards zero at a maximum considered frequency ω_{max}, then $\hat{g}_{p,p}(i\omega) = \mathbf{G}(i\omega + ip\Omega)$ will be zero unless,

$$-\omega_{max} < \omega + p\Omega < \omega_{max} \tag{3.42}$$

Afterwards, given the conditions stated in equations 3.40 and 3.41, it can be concluded that the range of ω_{max} requires only be [-Ω/2, Ω/2] before the harmonic transfer

function is duplicated and offset diagonally. Therefore, the maximum frequency to be computed gives rise to a maximum required value for p,

$$-\frac{\omega_{max}}{\Omega} - \frac{1}{2} < p < \frac{\omega_{max}}{\Omega} + \frac{1}{2}, \tag{3.43}$$

that allows to truncate the number of columns in $\hat{g}$ and $\hat{h}$ because other rows will have zero harmonic transfer function.

3.4. Semi-Discretization Method

As previous mention in Chapter 2, the stability of the milling process can also be predicted using the semi-discretization method (SDM). This method was first introduced by Insperger [40, 54], and later modified by Sims in [58] for variable helix and variable pitch tools. The current section summarises the method presented by Sims in [58], first presenting the discretized cutting force model. Later, it shows the state space representation of the dynamic system. Furthermore, it introduces the state-space representation between the displacements and delays terms, which couples the cutting forces with the dynamic system. Next, the stability problem is solved using the Floquet theory of the transition matrix. Finally, the instability bifurcations that occur in the milling process are discussed, analysing the eigenvalues of the transition matrix.

3.4.1. Cutting Force Model

In order to obtain the cutting force model lets first define the sampling time period as T. By doing this, discrete time values can then be expressed as $\bar{k}T$, in which $\bar{k} = 1, 2, \ldots, \infty$. Additionally, discrete local times within each tool revolution can be defined as mT, where $m = 1, 2, \ldots, M$, and M is the number of T samples per revolution. Consequently, the constant spindle speed Ω (rad/s) and sampling period T relationship can be stated as,

$$T = \frac{2\pi}{M\Omega} \tag{3.44}$$

Furthermore, the axial depth of cut b is discretized into l layers of size Δa obtained as $\Delta a = b/l$. Afterwards, for each layer l and tooth j, the dynamic chip thickness can be approximated as,

$$\begin{aligned} h_{l,j} &= g\left(\theta_{l,j}(mT)\right)\left[h_o \sin\left(\theta_{l,j}(mT)\right)\right] \quad \bar{k} = 1, 2, \ldots \\ &+ \left(x(\bar{k}T) - x\left(\bar{k}T - \tau_{l,j}\right)\right)\sin\left(\theta_{l,j}(mT)\right) \\ &+ \left(y(\bar{k}T) - y\left(\bar{k}T - \tau_{l,j}\right)\right)\cos\left(\theta_{l,j}(mT)\right) \quad m = 1, 2, \ldots, M \end{aligned} \tag{3.45}$$

where x and y are the workpiece displacements in x-direction and y-directions. The periodic angular location θ of the flute j on the later l can be obtained as,

$$\theta_{l,j}(mT) = \theta_{l,j}(0T) + \frac{2\pi m}{M} \quad m = 1, 2, \ldots, M, \tag{3.46}$$

and the binary function g from the equation 3.45 that defined when a flute is engaged cutting with workpiece is expressed as,

$$\begin{aligned} g\left(\theta_{l,j}(mT)\right) &= 1 \rightarrow \theta_{st} < \theta_{l,j}(mT) < \theta_{ex} \\ g\left(\theta_{l,j}(mT)\right) &= 0 \rightarrow \theta_{st} < \theta_{l,j}(mT) \cdot or \cdot \theta_{l,j}(mT) > \theta_{ex} \end{aligned} . \tag{3.47}$$

Because only the dynamic component of the chip thickness is linked to the regenerative process stability, its static part $h_o \sin\left(\theta_{l,j}(mT)\right)$ can be neglected from the equation 3.45. Furthermore, time delay for the flute j at the layer l can be expressed as follows,

$$\tau_{l,j} = T \cdot \text{round}\left(M\frac{\Delta\theta_{l,j}}{2\pi}\right), \tag{3.48}$$

where the round function gives as an output its input argument rounded to the nearest integer. It is worth mentioning that for conventional milling tools, this time delay is a constant value independent of the axial depth of cut and flute. Therefore, a intermediate state variable Δ is introduced to described the differences between the current and m previous discrete time displacements as,

$$\begin{aligned} \Delta x_m(\bar{k}T) &= x(\bar{k}T) - x(\bar{k}T - mT) \\ \Delta y_m(\bar{k}T) &= y(\bar{k}T) - y(\bar{k}T - mT). \end{aligned} \tag{3.49}$$

Furthermore, the normal and radial forces acting on every tooth are proportional to the chip thickness as,

$$\begin{aligned} Ft_{(l,j)} &= K_t \Delta a h_{l,j} \\ Fr_{(l,j)} &= K_r Ft_{(l,j)} \end{aligned} . \tag{3.50}$$

These forces can then be expressed in the x and y directions of the global reference frame ((Figure 3.6) a)) obtaining,

$$\left\{ \begin{array}{c} F_x(\bar{k}T) \\ F_y(\bar{k}T) \end{array} \right\} = \mathbf{R}(mT) \left\{ \begin{array}{c} \Delta x(\bar{k}T) \\ \Delta y(\bar{k}T) \end{array} \right\} \text{ with } m = 1, 2, \ldots, M, \tag{3.51}$$

in which the time-varying periodic matrix $\mathbf{R}$ is formed by the following terms:

$$\begin{aligned} r_{1,\bar{k}}(mT) &= \frac{1}{2}\Delta a K_t \sum_{j=1}^{N}\sum_{l=1}^{L} h\left(\bar{k}, \tau_{l,j}\right) \overline{a}_{xx}\left(\theta_{l,j}(mT)\right) \\ r_{2,\bar{k}}(mT) &= \frac{1}{2}\Delta a K_t \sum_{j=1}^{N}\sum_{l=1}^{L} h\left(\bar{k}, \tau_{l,j}\right) \overline{a}_{xy}\left(\theta_{l,j}(mT)\right) \\ r_{1,M+\bar{k}}(mT) &= \frac{1}{2}\Delta a K_t \sum_{j=1}^{N}\sum_{l=1}^{L} h\left(\bar{k}, \tau_{l,j}\right) \overline{a}_{yx}\left(\theta_{l,j}(mT)\right) \\ r_{2,M+\bar{k}}(mT) &= \frac{1}{2}\Delta a K_t \sum_{j=1}^{N}\sum_{l=1}^{L} h\left(\bar{k}, \tau_{l,j}\right) \overline{a}_{yy}\left(\theta_{l,j}(mT)\right) \end{aligned} . \tag{3.52}$$

In this equation, the delay term is defined by the unit step function h as,

$$\begin{aligned} h\left(\bar{k}, \tau_{l,j}\right) &= 1 \rightarrow \bar{k} = \tfrac{\tau_{l,j}}{T} \\ h\left(\bar{k}, \tau_{l,j}\right) &= 0 \rightarrow \bar{k} \neq \tfrac{\tau_{l,j}}{T} \end{aligned} \tag{3.53}$$

and the averaged directional factors are obtained using the following expression,

$$\begin{aligned} \overline{a}_{xx} &= g\left(\theta_{l,j}\right) \frac{M}{4\pi} \left[\cos 2\theta - 2K_r\theta + K_r \sin 2\theta\right]_{\theta_{l,j}(mT)-\pi/M}^{\theta_{l,(mT)}+\pi/M} \\ \overline{a}_{xy} &= g\left(\theta_{l,j}\right) \frac{M}{4\pi} \left[-\sin 2\theta - 2\theta + K_r \cos 2\theta\right]_{\theta_{l,j}(mT)-\pi/M}^{\theta_{l,j}(mT)+\pi/M} \\ \overline{a}_{yx} &= g\left(\theta_{l,j}\right) \frac{M}{4\pi} \left[-\sin 2\theta + 2\theta + K_r \cos 2\theta\right]_{\theta_{l,j}(mT)-\pi/M}^{\theta_{l,j}(mT)+\pi/M} \\ \overline{a}_{yy} &= g\left(\theta_{l,j}\right) \frac{M}{4\pi} \left[-\cos 2\theta - 2K_r\theta - K_r \sin 2\theta\right]_{\theta_{i,j}(mT)-\pi/M}^{\theta_{l,(mT)}(mT)+\pi/M} \end{aligned} . \tag{3.54}$$

3.4.2. State Space Formulation

Assuming that the tool does not rotate along the x-axis and y-axis of Figure 3.6, all the layers along the tool experience the same displacements x and y. Therefore, assuming D number of total states to represent x and y vibrations, the continuous state space form of the dynamic system can be stated as,

$$\begin{aligned} \{\dot{\mathbf{q}}_s\}_{[D\times 1]} &= \mathbf{A}_s\mathbf{q}_s + \mathbf{B}_s \begin{Bmatrix} F_x \\ F_y \end{Bmatrix}, \\ \begin{Bmatrix} x \\ y \end{Bmatrix} &= \mathbf{C}_s\mathbf{q}_s(\bar{k}T) \end{aligned} \tag{3.55}$$

Additionally, this continuous system can be discretised obtaining,

$$\begin{aligned} \mathbf{q}_m(\bar{k}T+T) &= \mathbf{A}_m\mathbf{q}_m(\bar{k}T) + \mathbf{B}_m \begin{Bmatrix} F_x(\bar{k}T) \\ F_y(\bar{k}T) \end{Bmatrix} \\ \begin{Bmatrix} x(\bar{k}T) \\ y(\bar{k}T) \end{Bmatrix} &= \mathbf{C}_s\mathbf{q}_m(\bar{k}T) \end{aligned} \tag{3.56}$$

where the exponential function can be used to obtain the matrix $\mathbf{A}_m$, and $\mathbf{B}_m$ as,

$$\begin{bmatrix} [\mathbf{A}_m]_{[D\times D]} & [\mathbf{B}_m]_{[D\times 2]} \\ \mathbf{X}_{[2\times D]} & \mathbf{W}_{[2\times D]} \end{bmatrix}_{[(D+2)\times(D+2)]} = \exp\left(T \begin{bmatrix} [\mathbf{A}_s]_{[D\times D]} & [\mathbf{B}_s]_{[2\times D]} \\ [\mathbf{0}]_{[2\times D]} & [\mathbf{0}]_{[2\times 2]} \end{bmatrix} \right)$$

A discrete time state space representation of the tool vibration and delay state relationship can be stated as,

$$\begin{aligned} \mathbf{q}_z(\bar{k}T+T) &= \mathbf{A}_z\mathbf{q}_z(\bar{k}T) + \mathbf{B}_z \begin{Bmatrix} x(\bar{k}T) \\ y(\bar{k}T) \end{Bmatrix} \\ \begin{Bmatrix} \Delta x(\bar{k}T) \\ \Delta y(\bar{k}T) \end{Bmatrix} &= \mathbf{C}_z\mathbf{q}_z(\bar{k}T) + \mathbf{D}_z \begin{Bmatrix} x(\bar{k}T) \\ y(\bar{k}T) \end{Bmatrix}, \end{aligned} \tag{3.57}$$

where,

$$
\begin{aligned}
A_z &= \begin{bmatrix} \begin{bmatrix} \{0\dots0\}_{[M-1]} & 0 \\ [I]_{[(M-1)\times(M-1)]} & \{0\dots0\}^T_{[M-1]} \end{bmatrix} & [0] \\ [0] & \begin{bmatrix} \{0\dots0\}_{[M-1]} & 0 \\ [I]_{[(M-1)\times(M-1)]} & \{0\dots0\}^T_{[M-1]} \end{bmatrix} \end{bmatrix} \\
B_z &= \begin{bmatrix} \left\{1\,\{0\dots0\}^T_{[M-1]}\right\} & \{0\dots0\}^T_{[M-1]} \\ \{0\dots0\}^T_{[M]} & \left\{1\,\{0\dots0\}^T_{[M-1]}\right\} \end{bmatrix} \\
C_z &= \begin{bmatrix} -[I]_{[M\times M]} & [0] \\ [0] & -[I]_{[M\times M]} \end{bmatrix} \\
D_z &= \begin{bmatrix} \{1\dots1\}^T_{[M]} & \{0\dots0\}^T_{[M]} \\ \{0\dots0\}^T_{[M]} & \{1\dots1\}^T_{[M]} \end{bmatrix}.
\end{aligned}
\tag{3.58}
$$

3.4.3. System Coupling and Solution

The final system model can be found combining the forces in the equation 3.51, and the state space representation of the dynamic system and delay to displacement relationship in equations 3.56, and 3.57 to obtain,

$$
\begin{Bmatrix} \mathbf{q}_m(\bar{k}T+T) \\ \mathbf{q}_z(\bar{k}T+T) \end{Bmatrix} = \mathbf{A} \begin{Bmatrix} \mathbf{q}_m(\bar{k}T) \\ \mathbf{q}_z(\bar{k}T) \end{Bmatrix} + \mathbf{BC}(mT) \begin{Bmatrix} \mathbf{q}_m(\bar{k}T) \\ \mathbf{q}_z(\bar{k}T) \end{Bmatrix}, \tag{3.59}
$$

in which the matrices A, B, and C are determined with the following expressions [186],

$$
\begin{aligned}
\mathbf{A} &= \begin{bmatrix} \mathbf{A}_m & [\mathbf{0}] \\ \mathbf{B}_z\mathbf{C}_s & \mathbf{A}_z \end{bmatrix} \\
\mathbf{B} &= \begin{bmatrix} \mathbf{B}_m \\ [\mathbf{0}]_{[2M\times 2]} \end{bmatrix} \\
\mathbf{C}(mT) &= \begin{bmatrix} \mathbf{R}(mT)\mathbf{D}_z\mathbf{C}_s & \mathbf{R}(mT)\mathbf{C}_s \end{bmatrix}
\end{aligned}
\tag{3.60}
$$

Therefore, the variation of the system states along consecutive tool revolutions is finally stated as,

$$\left\{ \begin{array}{c} \mathbf{q}_m(\bar{k}T + MT) \\ \mathbf{q}_z(\bar{k}T + MT) \end{array} \right\} = (\mathbf{A} + \mathbf{BC}(MT))(\mathbf{A} + \mathbf{BC}((M-1)T))(\ldots)(\mathbf{A} + \mathbf{BC}(T)) \left\{ \begin{array}{c} \mathbf{q}_m(\bar{k}T) \\ \mathbf{q}_z(\bar{k}T) \end{array} \right\}, \tag{3.61}$$

or expressed in a more compact form as,

$$\mathbf{Q}_{i+1} = \mathbf{\Phi}\mathbf{Q}_i, \tag{3.62}$$

in which $\mathbf{\Phi}$ represents the transition matrix [188]. Consequently, the system stability is governed by the characteristic multipliers or eigenvalues μ of $\mathbf{\Phi}$. As shown in Figure 3.7, asymptotically stable cutting systems are obtained whenever these eigenvalues are within a unit circle. On the other hand, marginally stable systems are characterised by having at least one eigenvalue μ on the unit circle, while the rest are within the circle. In this condition, the eigenvalue on the unit circle defines the system stability boundary. Furthermore, the system becomes unstable if at least one eigenvalue is outside the unit circle, leading to chatter vibrations.

At this point, all stability analysis was performed for the approximated discrete-time system on equation 3.59. Nevertheless, the eigenvalues of the discrete-time system μ can be transformed to continue ones [186] using the following relationship,

$$\lambda = \frac{\ln \mu}{T} = \sigma_c \pm j\omega_c, \tag{3.63}$$

in which σ_c and ω_c are the subsequent real and imaginary component of the continues-time eigenvalue λ. The system vibration can also be determined from the imaginary part of λ as,

$$f_{sv} = \left\{ \pm f_c + k_c \frac{2\pi}{T} \right\} \text{rad/s} = \left\{ \pm \frac{\omega_c}{2\pi} + k_c \frac{\Omega}{60} \right\} \text{Hz}, \quad k_c = \ldots, -1, 0, 1, \ldots, \tag{3.64}$$

adjusted to 2π multiples of the spindle pass frequency Ω due to the non-unique transformation from discrete to continuous system. Now, for unstable milling systems, the

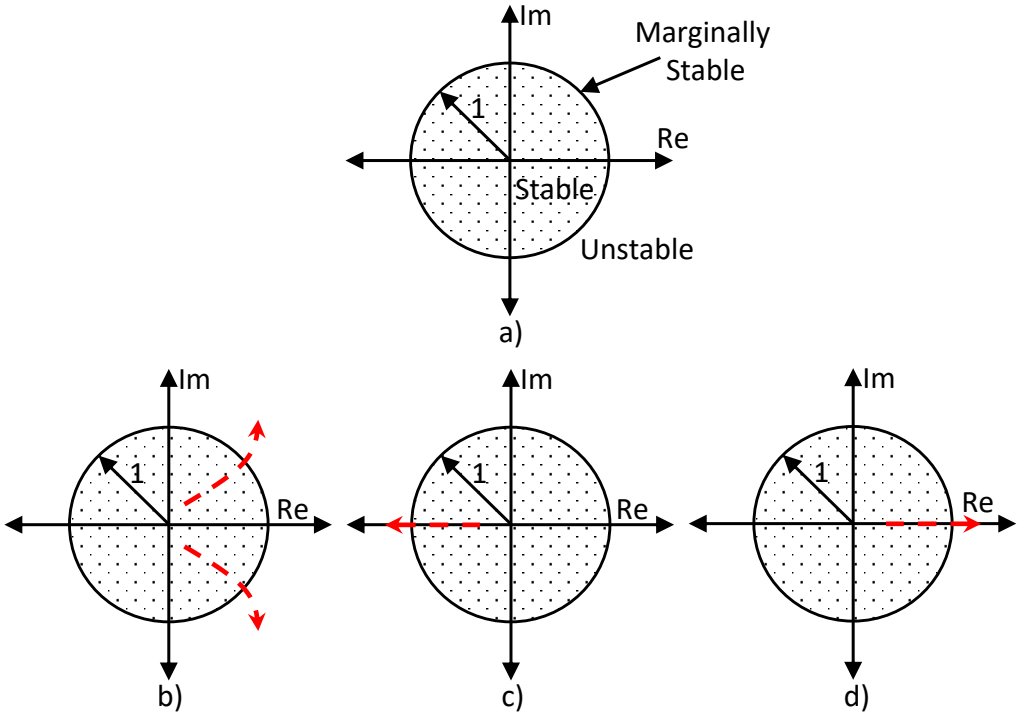

Figure 3.7.: Diagram (a) shows a unitary circle defining the stability of the discrete map. Depending on how the eigenvalues leave the circle, the types of bifurcations that can be experienced in milling are secondary Hopf (a), period-doubling (c), and period one (d) bifurcations.

eigenvalues μ can bifurcate outside the unitary circle in three different ways as shown in Figure 3.7. The first one corresponds to a secondary Hopf bifurcation that occurs whenever the solution involves a complex conjugate eigenvalue μ leaving the unit circle as in Figure 3.7 b). This type of instability is characterized by the following chatter frequency,

$$f_{Hopf} = \left\{ \pm f_c + k_c \frac{2\pi}{T} \right\} \text{rad}/s = \left\{ \pm \frac{\omega_c}{2\pi} + k_c \frac{\Omega}{60} \right\} Hz, \quad \text{k}_\text{c} = \ldots, -1, 0, 1, \ldots. \tag{3.65}$$

The second type of instability bifurcation corresponds to the period doubling bifurcation. In this case, the eigenvalue μ is lesser than -1, leading to a chatter frequency of,

$$f_{PD} = \left\{ \frac{\pi}{T} + k_c \frac{2\pi}{T} \right\} \text{rad}/s = \left\{ \left(\frac{1}{2} + k_c \right) \frac{\Omega}{60} \right\} Hz, \quad \text{k}_\text{c} = \ldots, -1, 0, 1, \ldots. \tag{3.66}$$

Finally, the last type of bifurcation is the period one bifurcation. This type of bifurcation occurs when μ is larger than one (Figure 3.7 d)), giving a chatter frequency of,

$$f_{PO} = \left\{0 + k_c \frac{2\pi}{T}\right\} rad/s = \left\{0 + k_c \frac{\Omega}{60}\right\} Hz, \quad \mathrm{k_c} = \ldots, -1, 0, 1, \ldots \tag{3.67}$$

3.5. Case study

The current section aims to verify the correct operation of the SDM and MFA programs developed for the chatter prediction of variable helix and pitch milling tools. This is achieved by using the machining scenario presented by Wang in [176], which presents simulation data using structural dynamic models vibrating in the feed and normal directions. Consequently, this then allows for verifying the enhancements performed to the MFA (Sims in [51]) in this chapter.

The machining scenario provided by Wan is outlined in Table 3.1, and the results are shown in Figure 3.9. Dashed black lines represent the outcomes obtained from the SDM, while the blue lines the result from the MFA. The ω_{max} implemented in this simulation (equation 3.43) was 1000 Hz. At this frequency, the FRF of the system in the x and y directions (Figure 3.6) decayed 95% and 98% of the maximum peaks at the resonant frequencies (Figure 3.8). Consequently, this frequency value was chosen as an acceptable value to truncate the harmonic transfer function $\mathbf{G\hat{H}}(i\omega)$ in equation 3.37. For this comparison, the M value (equation 3.44) was chosen as 360 because no significant change in the stability boundaries was noticed beyond this value. Even though there are slight differences at spindle speeds higher than 4500 rpm and lower than 2250 rpm, in general, the overall simulation outcomes suggest that the MFA and SDM follow the same chatter stability boundaries. In addition, these results match the stability charts predicted by Wang in [176] using a simplified version of the SDM.

Further experimental validation of the models will be performed in the forthcoming sections using a scaled experimental setup for variable-helix milling cutters. This setup

was tuned to enable the presence of variable-helix islands of instability, conditions rarely found in simulation throughout the literature. As a matter of fact, to the best knowledge of the author, no formal experimental verification has been done about it. It is worth mentioning that while these chatter prediction methods are developed for variable helix and pitch milling mechanisms (Figure 3.6), they can be straightforwardly used with non-equal helix ones by simply keeping equally spaced the pitches between the flutes at the tooltip.

Parameter	**Value**
ω_{nx}, ω_{ny}	563.55Hz, 516.21Hz
m_x, m_y	1.4986kg, 1.199kg
ζ_x, ζ_y	5.58%, 2.5%
ϕ_{10}, ϕ_{20}, ϕ_{30}, ϕ_{40}	0°, 70°, 180°, 250°
γ_1, γ_2, γ_3, γ_4	30°, 40°, 30°, 40°
Radial Immersion	50%
Tool Diameter	19.5 mm
Kt	697 N/mm^2
Kr	256 N/mm^2
Cutting Condition	Down-milling

Table 3.1.: Machining scenario for the two degree of freedom case.

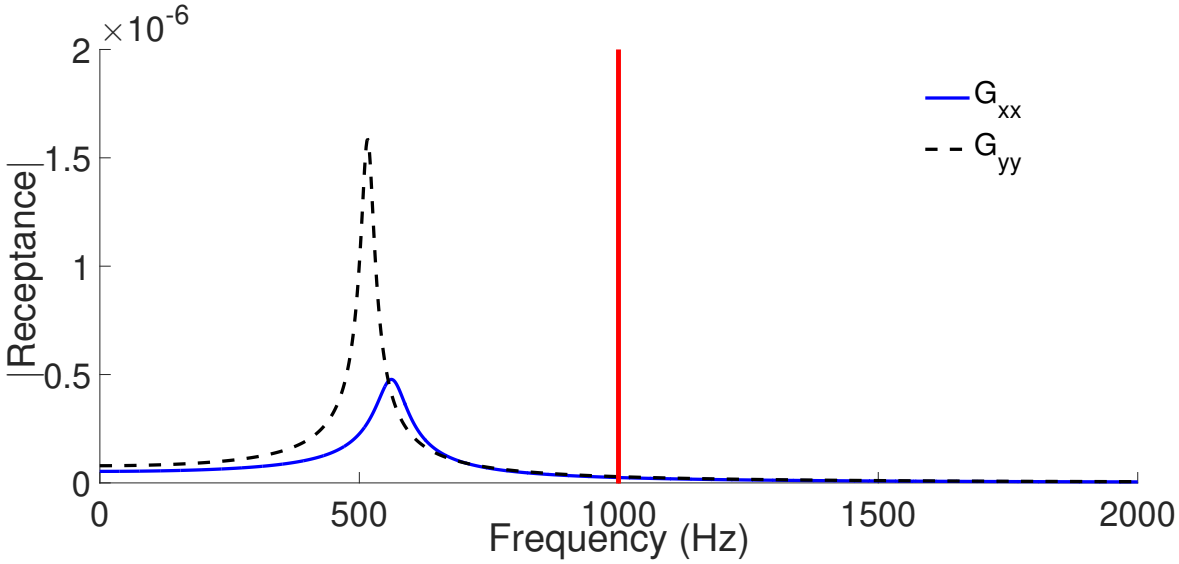

Figure 3.8.: Frequency response function in the X and Y directions from the case study implemented to validate the SDM and MFA programs.

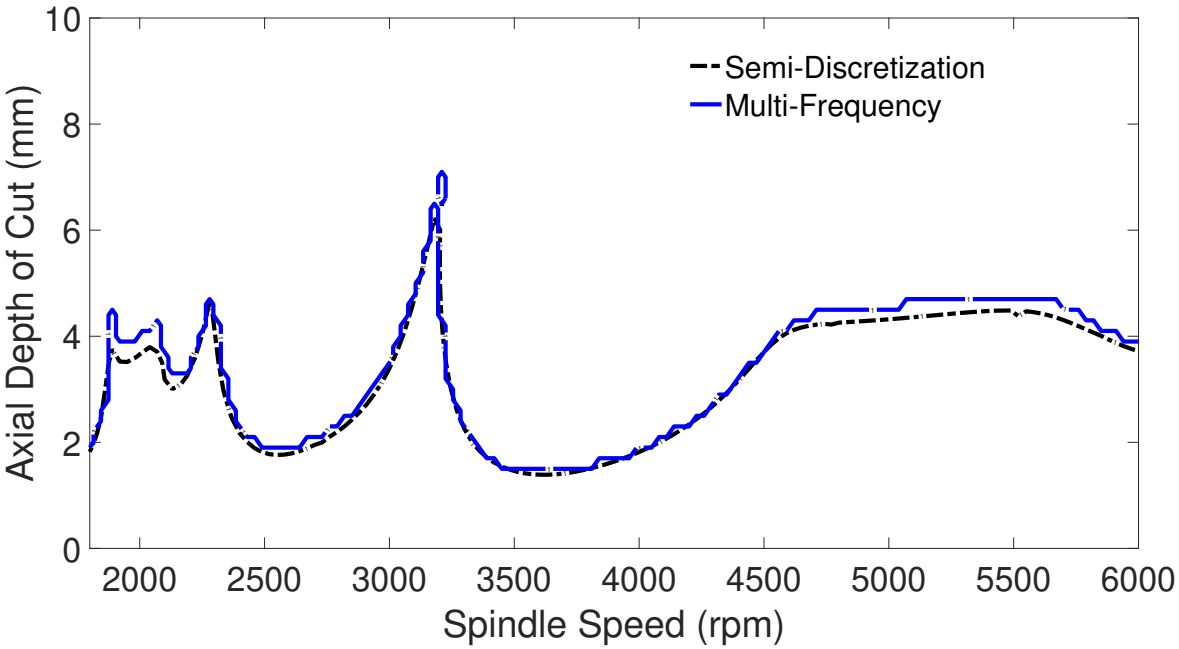

Figure 3.9.: Comparison between the Multi-Frequency and Semi-Discretization approaches ($\omega_{max} = 1000$ Hz, $M = 360$).

3.6. Summary

In summary, Sections 3.3 and 3.4 have presented the MFA and SDM methods to predict chatter stability with variable helix and pitch milling tools. From this, it can be seen that both methods begin with the same assumptions regarding the physical system under consideration (for example, linear cutting force coefficients). The SDM method then requires a modal model of the frequency response function, whereas the MFA method operates directly on the numerical frequency response function. The SDM involves a decision on the number of modes to be included in the model, as well as the number of discretization steps M in the solution. In contrast, the MFA requires an assumption on the truncation frequency ω_{max} to automatically adjust the number of harmonics p in the solution (equation 3.37). This differs from previously reported multi-frequency solutions [46], in which the number of harmonics was constant indistinctly of the spindle speed and manually chosen. Finally, the programs developed following both techniques were verified using the machining scenario and simulations found in the literature.

The next chapter first presents the instrumented experimental setup used in this thesis to validate chatter predictions. This setup comprises a customised variable-helix milling tool and an instrumented flexure device supporting a workpiece with low cutting force coefficients. In particular, the implemented material is a thermoplastic known as a copolymer acetal. This innovative approach allows for attaining larger axial depths of cut while assuming linear structural dynamics. Therefore, the system enables the appearance of islands of instability in the variable-helix stability lobe diagram predicted using SDM and MFA. The islands are then validated conducting cutting trials, and the effectiveness of the methods while capturing these condition is tested.

The forthcoming chapter also studies the effect of the helix-induced cutting-coefficient variations on the stability lobe diagram. In the literature, one of the main assumptions of chatter prediction methods is assuming identical cutting force coefficients on

the teeth of variable-helix milling tools. However, it is known that the magnitude of these coefficients strongly depends on the geometry of the milling cutter, and in particular, of the helix angle. For this purpose, tailored one-flute milling tools are utilised to determine the individual cutting-force coefficients of a custom-made variable helix milling cutter. Chatter stability predictions using the non-equal coefficient MFA (Section 3.3) are then compared to the conventional MFA, to evaluate the impact of these modifications on the variable-helix stability lobe diagram.

4. Validation of Variable-Helix Stability Diagram

4.1. Introduction

In milling, one approach to suppress regenerative chatter is the use of tools with non-uniform helix angles. Here, variations of the helix angles between adjacent teeth can change the chatter stability, albeit with more complex dynamics and stability of the system. This is because it leads to periodic, piecewise, distributed-time delayed differential equations with no closed-form solution. Consequently, there have been several studies that have developed alternative analytical formulations of variable helix chatter stability (e.g. the SDM and MFA presented in Chapter 3). Whilst some of these have included detailed experimental validation, in general, there is limited validation of the different analysis methods [26, 51, 58, 170, 176–179]. In particular, the potential for variable helix tools to stabilise at higher axial depths of cut is of significant practical value but needs detailed experimental validation.

Contrary to the conventional milling process, the stability lobe diagram of variable-helix milling cutters can exhibit a process re-stabilisation at axial depths of cut beyond the chatter boundaries. This occurs because of the continuous pitch variations along the axial length of the tool, induced by the non-equal helix on the flutes. As a result, this property may lead to undesirable islands of instability in the stability charts. These conditions are rarely found in the literature, and to the best knowledge of the author, no experimental data has been provided to validate their existence. Most of the information found in the literature comprises chatter predictions verified using cutting process simulations [26, 27, 189–191].

Hence, the present chapter aims to fulfil this void in the knowledge by experimentally validating an island of instability using a novel scaled experimental configuration. This setup comprises a one-degree-of-freedom flexible device supporting a low cutting-force stiffness material, known as copolymer acetal. By implementing a single-degree-of-freedom device, the before-mentioned high complexity of the problem is considerably reduced, preventing that other phenomenon (e.g. mode coupling) to obscure these islands. In addition, using a low cutting-coefficient material, it enables the assumption of linear structural dynamics even at higher depths of cuts. Using a metal along with the flexible device may generate high amplitude vibrations (even at relatively lower depths of cut), that may lead to non-linear dynamic states. As presented in Chapter 2, non-linear conditions such as large-amplitude vibrations or the loosing of tool engagement may require the use of more advanced techniques to solve the state dependant delay differential equations.

To develop the experimental setup, Section 4.2 discusses the relationship between the chip thickness and cutting forces while cutting this material. It will be shown how the material properties, cutting conditions, and geometrical parameters of the tool influence this relationship. Subsequently, it defines the range of these variables in which a linear assumption is valid. To verify these hypotheses, the experimental linear mechanistic approach for conventional milling cutters will be implemented. The premises of this method is that, for shear-type chip formation, there is a linear relationship between the uncut chip thickness and the cutting forces in an stable process, being the cutting coefficients the proportional constants. Consequently, deviation from this relationship may suggest a non-shear induced complex chip formation.

Later, the one-degree-of-freedom assumption of the flexible rig supporting the workpiece will be verified using impact tests in Section 4.3. The overall sought dynamic behaviour is that the only source of flexibility that leads to regenerative chatter is the vibration of the workpiece in the normal direction. The feed direction, on the other hand, will be assumed as infinitely rigid. Thus, the frequency response functions of the

device obtained from the tap testing experiments in these directions will be compared. In addition, to fulfil the one-degree-of-freedom assumption, it is required the machine tool to be significantly stiffer than the workpiece. Therefore, the only flexibility source leading to chatter comes from the workpiece. Otherwise, the combined workpiece-tool dynamics of the cutting system should be considered solving the problem, promoting further non-modelled behaviours. For the current purpose, the infinitely rigid machine tool condition will be assessed by comparing the frequency response function of the machine tool and flexible workpiece.

Subsequently, Section 4.4 will predict the variable-helix stability diagram using the MFA that was enhanced in Chapter 2 to consider non-equal cutting force coefficients. This stability chart will then be compared to the one obtained from the unmodified MFA, to study the impact of this model enhancement on the stability chart. Regarding the milling cutters, in this study, a customised 16 mm of diameter 3-teeth variable-helix milling tool with helix angles of 25°, 15°, and 10° will be implemented. In addition, three additional tailored 16 mm of diameter one-flute tools with helix angles of 25°, 15°, and 10° will be used to separately determine the cutting force constants of every tooth of the variable-helix milling cutter. Also, the cutting force coefficients of an additional 16 mm of diameter 3-teeth conventional milling tool with a helix angle of 25° will be calculated for comparison reasons. All the milling tools utilised in this thesis are made of solid carbide.

Afterwards, the entire setup will be validated in Sections 4.5 and 4.6 performing milling trials around a potential island of instability, in which the performance of the SDM and MFA capturing this condition will be tested against the preliminary results. Finally, there will be presented the conclusions and discussions in Section 4.7 about the assumptions, experimental procedures, and results obtained throughout this chapter.

4.2. Workpiece Material

The current thesis aims to predict and validate islands of instability on the stability lobe diagram of variable-helix milling tools. For this purpose, it implements a workpiece material with lower cutting force coefficients. Thus, it enables achieving larger axial depths of cuts, wherein overall the process is more prone to develop these unstable isolated conditions. To predict the variable-helix stability lobe diagram, the SDM and MFA (Chapter 3) will be implemented. These techniques have in common assuming a linear relationship between the cutting forces and the chip thickness (equations 3.17 and 3.50), in which the cutting force coefficients are the proportional constants [30,31]. This section aims to investigate the machining conditions and tool geometrical parameters that ensure reliable implementation of the linear cutting force models with the chosen material. This step is crucial because, even for metal alloys, machining processes performed beyond the linearity limits require advanced yet complex models to capture the full process dynamics [192], as explained in Section 2.3.

To explain the key requirements to use the mechanistic linear cutting-force model, lets first refer to the schematic (a) in Figure 4.1. This schematic shows a single-edge orthogonal cutting process in which a cutter removes an amount of material of thickness d_c from a workpiece, generating the forces F_c and F_t. One of the fundamental assumptions of this model is that the material mostly yields because of a shear force along an infinitely thin plane defined by the line through the points A and B in Figure 4.1 (b) [77]. This plane is orientated at an angle ϕ_s known as the shear angle. The linear orthogonal cutting force model assumes that the shear angle ϕ_s, and consequently the normal (σ_s) and shear (τ_s) stresses, remain as constant. As a result, the cutting forces can be assumed as proportional to the uncut chip thickness d_{uc}. While this analysis was first performed on metal alloys, there are research in the literature from over six decades ago highlighting that some plastics satisfy these constraints under certain conditions [193–195]. In these studies, it was shown that parameters such as

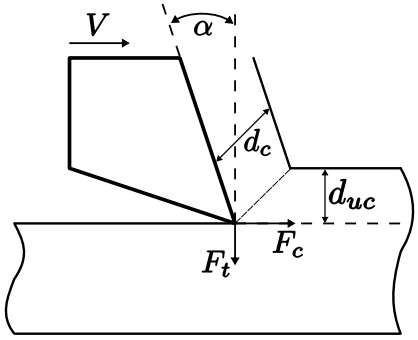

(a)

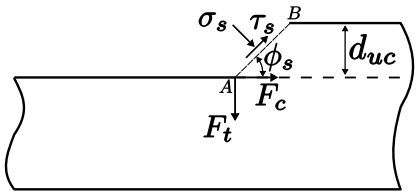

(b)

Figure 4.1.: Schematic diagram showing: (a) Orthogonal cutting (two-dimensional) (b) Shear stress τ_s and angle ϕ_s in orthogonal cutting [30, 31, 193].

the tool rake angle and the cutting speed strongly influence the relationship between the cutting forces and the chip thickness. Hence, these investigations are used in this thesis as a reference to define the tool the geometry and cutting conditions that could ensure linearity throughout the prediction and validation of the variable-helix instability islands.

4.2.1. Chip Formation in Thermoplastics and Thermosets

Contrary to metals, thermoplastics and thermosets experience five types of chip formation [196]. Two of these types are continuous mechanisms while the remaining ones discontinuous. The continuous types are known as flow and shear types, while the discontinuous classes as simple shear, complex, and crack types. The continuous flow kind, a condition not found in metals, is characterised by removing the chip under high elastic deformations. It mainly occurs at lower cutting speeds when the material

shows a higher elasticity. Similar to metals, the continuous shear-type chip formation is produced by shearing the material at small intervals along the shearing plane. This plane is orientated at the minimum-work direction to tear up the chip, and the shear strain along this plane is considerably lower than the limiting rupture strain. In contrast, the simple discontinuous-shear type is distinguished by experience larger shear intervals and shear strains at the shear plane higher than the limiting rupture strain. Therefore, the chip formation is frequently interrupted resulting in a poor final surface quality on the workpiece. The discontinuous-complex type mainly occurs using cutters with a negative rake angle. This type is characterised by producing the chip from a combined effect of large compressive and shear stresses. Furthermore, the discontinuous crack type occurs in brittle materials at larger depths of cut, using cutters with an excessively large rake angle. Here, cracks develop on the tooltip while the chip is forming. This then results in a chip collapse causing hackle marks on the workpiece surface.

Regarding the two continuous chip formation types, there have been reports that the assumption of constant shear angle is valid in many thermoplastics and thermosets under certain cutting conditions [193, 197, 198]. In particular, the thermoplastic known as copolymer acetal showed to have unique properties that bridge the gap between metals and plastics [193]. Based on the recommendations provided by these studies, this thermoplastic was then chosen as workpiece material for the current thesis.

4.2.2. Machinability of Copolymer Acetal

Copolymer acetal is a semi-crystalline thermoplastic that provides a high machinability, with a low environmental sensitivity to factors such as humidity. Harper and Chanda [199, 200] considered this material as an engineering plastic with working temperatures of up to 120 °C. More advanced engineering plastics like PEEK and PPS have higher working temperatures of about 230 °C, but lower machinability. Also, they can cost 15

times the price of acetal [201–203]. Table 4.1 outlines some relevant thermomechanical properties of copolymer acetal. Furthermore, as a comparison, it also presents the same properties for aluminium 6061-O, and titanium Ti 6Al-4V. The Young's modulus of the copolymer acetal is approximately forty-two times smaller than titanium and twenty-five times smaller than aluminium. Similar relationships can also be found between the shear modulus values. However, the mechanical properties of acetal strongly depend on the temperature and strain rate, affecting also the chip formation while cutting this material [204–207].

As an instance, Figure 4.2 (a) shows the stress-strain curves of acetal at 20 °C, 40 °C, and 60 °C. This figure reveals a decreasing trending on the ultimate and yield strength while the temperature is increased. The temperature also affects the Young's modulus of the thermoplastic, as shown in Figure 4.3. For example, a change in temperature from 25 °C to 40 °C represents a decrease of 15% on the Young modulus. As a comparison, Figure 4.2 (b) depicts the stress-strain curves of titanium at 880 °C, 1100 °C, in which a similar decreasing strength tendency can be observed.

In addition, copolymer acetal exhibits a considerably higher specific heat with a lower density when contrasted to titanium and aluminium. Therefore, temperature increments in acetal will be higher when equal volumes of each material are exposed to the same amount of heat. Also, the thermal conductivity of copolymer acetal is lower than its metallic counterparts, even though the ones for acetal and titanium are not quite distant when compared to aluminium. Consequently, over 99% of the heat generated while cutting this thermoplastic with a metallic tool is transferred to the cutter, while the difference to the workpiece. Furthermore, because this heat cannot be diffused toward the interior workpiece mass, only the surface layer of the thermoplastic experiences a major increase in temperature [193]. Lakshmi in [213] observed this phenomenon measuring the maximum workpiece temperature in the cutting interface of single-edge cutting of acetal at various depths of cut and cutting speeds. At the cutting speed of 36 m/min, the author performed cutting trials at different chip thickness from

	Material		
Property	**Copolymer Acetal**	**Aluminium (6061-O)**	**Titanium (Ti 6Al-4V)**
Densitiy (g/cm^3)	1.41	2.7	4.43
Tensile yield strength (MPa)	68.33	55.2	880
Tensile ultimate strength (MPa)	66.74	124	950
Young's Modulus (GPa)	2.7	68.9	113.8
Elongation at break (%)	30	25	14
Poisson's ratio (-)	0.37	0.33	0.342
Shear strength (MPa)	55.2	82.7	550
Shear modulus (GPa)	1.01	26	44
Specific heat (J/kg/°C)	1460	896	526.3
Thermal conductivity (W/m/°C)	0.31	180	6.7
Coefficient of linear thermal expansion ($\mu°C^{-1}$)	92	23.6	8.6
Melting temperature (°C)	170	616.85	1660

Table 4.1.: Mechanical properties of copolymer acetal, aluminium 6061-O, and titanium Ti 6Al-4V [199, 200, 208, 209].

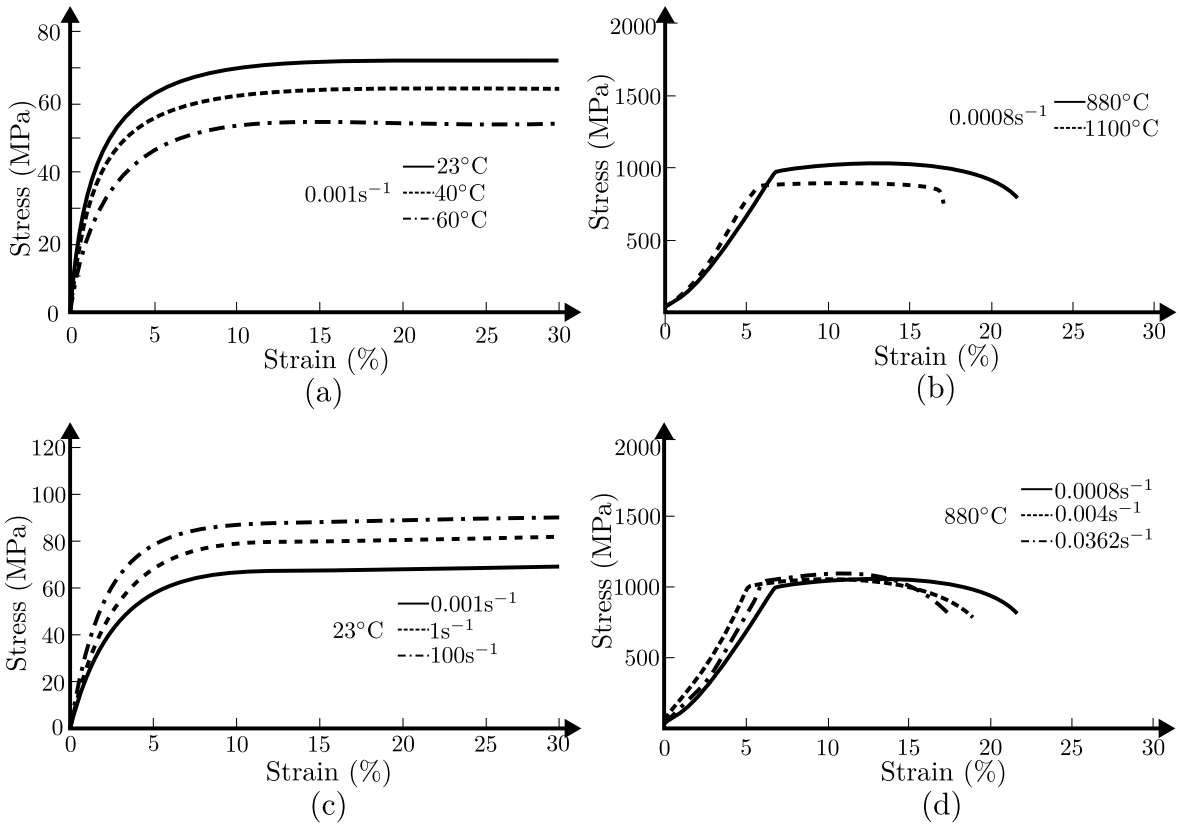

Figure 4.2.: Temperature and strain rate effect on the stress-strain plots of Acetal and Titanium Ti 6Al-4V [204, 210–212].

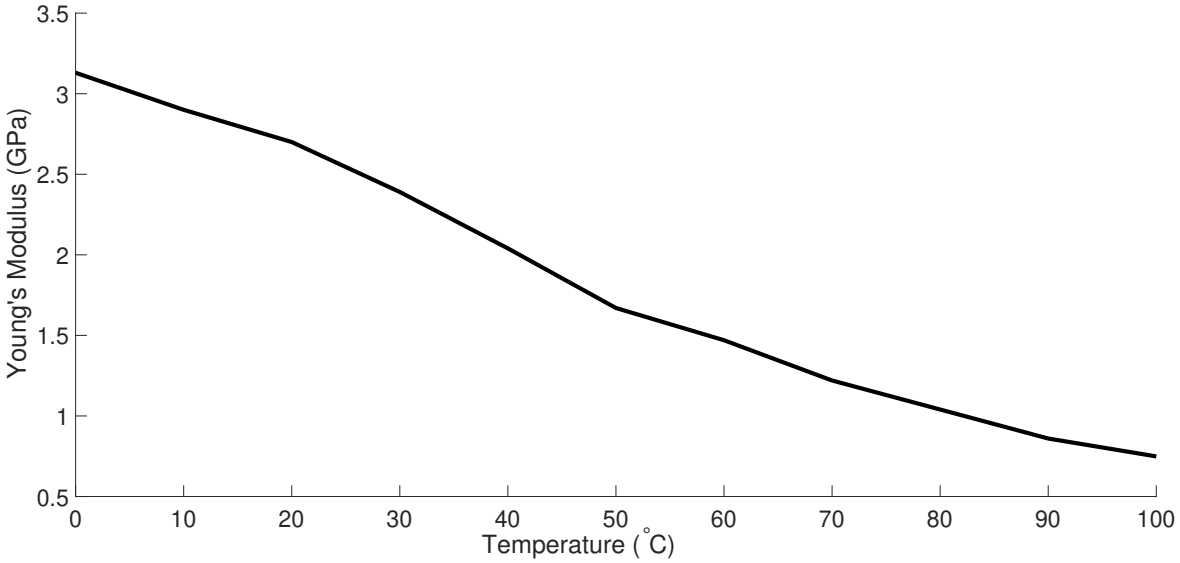

Figure 4.3.: Variation of the Young's modulus with temperature for acetal [204, 212].

0.2 to 0.8 mm. Later, at the chip thickness of 0.2 mm, the author carried out cuts at cutting speeds ranging from 36 m/min to 141 m/min. Both sets of trials shown an almost constant temperature that did not exceed 45 °C for the constant spindle speed test, while 35 °C for the constant chip thickness one. In these cases, the majority of the heat generated was conducted and dissipated by the metallic tool. In titanium for example, a similar condition can be observed resulting in rapid tool wear and poor surface integrity, because of the higher cutting force magnitudes when compared to acetal.

The mechanical properties of acetal are also strain-rate dependant. For example, Figure 4.2 (c) shows the stress-strain curve for acetal at different strain rates. At higher strain rates, a more brittle fracture occurs resulting in a higher ultimate and yield strength with a shorter ultimate elongation. This occurs because the material does not have enough time to flow and accommodate the applied load [204, 212]. Conversely, the strength lowers as the strain rate decreases showing a more ductile material behaviour with a longer ultimate elongation at break. A similar response is observed for titanium in Figure 4.2 (d), but not as pronounced as in acetal.

In essence, the mechanical properties of the workpiece material experience two different local stimuli while being cut. The first one relates to the shear and tensile strength reduction caused by the temperature increment linked to the heat generated in the cutting zone. On the other hand, the material also undergoes a higher strain (cutting speed) resulting in higher tensile and shear strengths. Hence, as suggested in [196, 198, 213], the resultant overall effect of the temperature and strain rate while cutting this material is better assessed using the shear stress τ_s at the shear plane. These research showed that at a specific cutting speed (strain rate), for example, a constant shear stress condition within a range of uncut chip thickness means that the superposition of the strain-rate and temperature effects compensate each other. Therefore, this then allowed the authors to implement the linear cutting force model to predict the cutting forces within this uncut chip thickness range. However, it was suggested that to ensure

linearity, the tool's rake angle and the range of cutting speeds and chip thicknesses should be carefully selected for a particular material [193].

Rao et al. in [197] proved that the constant shear angle assumption is valid for the continuous type chip formations while performing single-edge orthogonal cutting of acetal and nylon. Under this assumption, the authors could predict the cutting forces using the linear orthogonal model. However, the results for acetal showed that at rake angles larger than 15°, the chip formation changed from continuous to discontinuous. Kobayashi in [193] attributed this to the higher strain rate induced by sharp-edge tools with larger rake angles, that lead to a more brittle chip fracture. Kobayashi further explored the machinability of acetal on single-edge cutting at different rake angles and cutting speeds. Figure 4.4 presents some results provided by the author, showing the relationship between F_c and d_c at various rake angles and cutting speeds of 97 m/min and 70 m/min. The author normalised F_c by the width of the cut to compare the results with similar tests results presented by Rao in [197]. At 97 m/min, rake angles larger than 15° lead to non-linear behaviours between d_c and F_c. Rake angle values below 15° provided more linear results for a broad range of d_c. As Rao, the author reported a continuous chip formation in the linear region, while the opposite in the non-proportionality areas. In addition, for a chip thickness d_c of 0.123 mm, the relationship between the F_c, F_t and V at different rake angles is shown in Figure 4.5. In general, for rake angles between 0° to 20°, the relation between F_c, F_t and V in the range from 50 m/min to 400 m/min can be assumed as linear. Below 50 m/min, the plot moves upward with a slight curvature.

While the current thesis regards a multiple-edge cutting process like milling, the previous analysis and results on the single-edge cutting of acetal can be implemented as a reference to define several experimental parameters. For example, the primary rake angles of the teeth, cutting speeds, and the feeds per tooth. By doing this, the primary aim is to keep the tool geometry and cutting conditions within a range that allows implementing the linear cutting force model to predict the chatter stability charts of

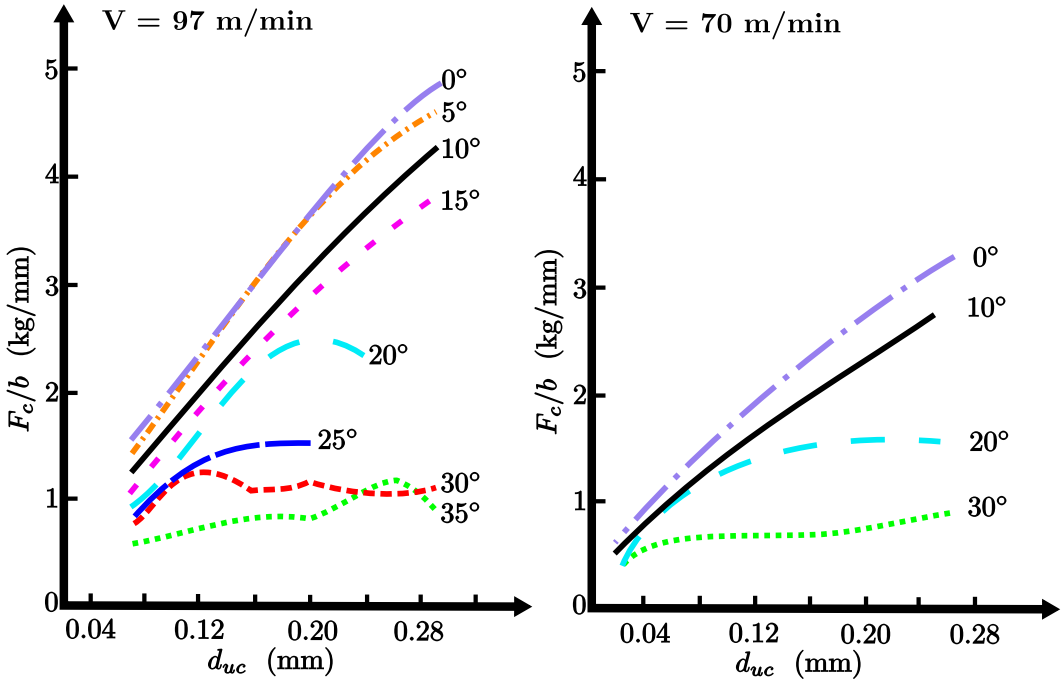

Figure 4.4.: Relationship between cutting force parallel to direction of cut and depth of cut for acetal at V = 97 m/min and V = 70 m/min [193, 197].

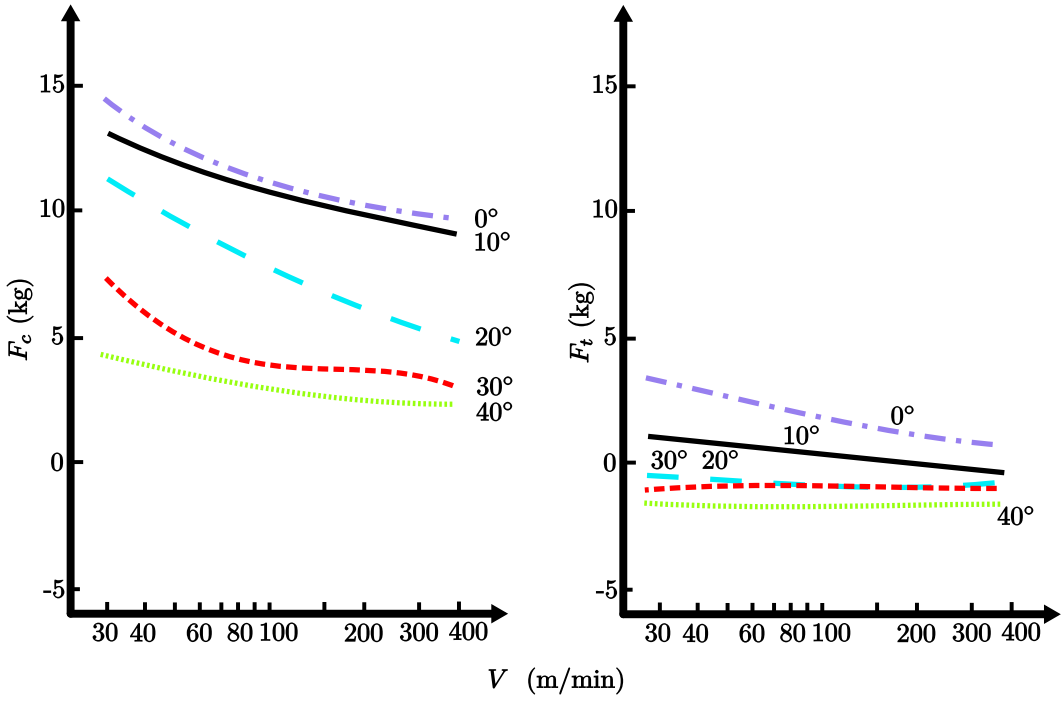

Figure 4.5.: Variation of cutting forces with cutting speed and tool rake angle for acetal. Depth of cut was 0.123 mm [193, 197].

variable-helix milling tools. Following Kobayashi and Rao's data, for the current thesis, the teeth primary rake angles were chosen as 10°. Furthermore, the cutting speeds for all the tests were kept between 50 m/min to 400 m/min, while the feed per tooth between 0.05 mm/tooth to 0.2 mm/tooth. Subsequently, the next section tests the linearity assumptions using the mechanistic approach presented by Altintas in [77]. Also, this test provides the cutting force coefficients required to predict chatter stability using linear cutting force models.

4.2.3. Cutting force coefficients

The mechanistic force model implemented in this investigation (equation 3.17) assumes that the cutting forces are proportional to the uncut chip thickness. This may not be true for all the milling cases, leading to the use of non-linear models to describe the process [71,79,214,215]. Hence, in [77] Altintas presented a method to test the linearity assumption. In this method, the average forces linearly relate to the feed per tooth, being the cutting force coefficients proportional to the line slopes. Because this method can only be applied to conventional milling tools, this section utilised single-flute milling cutters to estimate separately the coefficients of a variable-helix milling tool.

Following this approach, three one-flute tools of 16 mm of diameter and helix angles of 25°, 15°, and 10° were employed to determine the cutting force coefficients independently. The same methodology was applied to the conventional tool of 25° of helix angle. This approach also allowed detecting any significant variation in the coefficients because of the helix angle. All the solid carbide tools implemented in the experiment were part of the same material batch, guaranteeing homogeneity in the results.

Therefore, per every tool, a group of full-slotting trials at 5 mm of axial depth of cut was performed at feed-per-tooth values of 0.05, 0.1, 0.15 and 0.2 mm/tooth. The entire procedure was executed at spindle speeds of 1300, 2800, and 4300rpm to further study any variation due to cutting speed. By doing so, the minimum cutting speed attained

Spindle Speed (rpm)	Cutting Speed (m/min)	Number of cutting flutes	Helix Angles (deg.)	K_t (N/mm^2)	K_n (N/mm^2)	K_a (N/mm^2)
1300	65.34	3	25	142.19	18.89	58.93
		1	25	136.55	11.44	55.98
		1	15	131.86	15.16	28.61
		1	10	130.70	17.10	14.51
2800	140.74	3	25	104.00	13.27	45.59
		1	25	102.96	15.97	50.72
		1	15	106.42	16.15	2.72
		1	10	97.12	14.70	1.74
4300	216.14	3	25	102.36	17.46	46.49
		1	25	100.02	13.96	46.78
		1	15	101.17	17.76	26.52
		1	10	99.12	17.56	21.58

Table 4.2.: Cutting Force Coefficients for a conventional milling tool of 25° of helix angle, and one-flute tools with helix angles of 25°, 15°, and 10°.

in this experiment was of 65 m/min, while the maximum speed was of 216 m/min. Table 4.2 summarises the results obtained from these experimental tests.

Regarding Table 4.2, for the spindle speed of 1300 rpm, the cutting force coefficients decrease in magnitude while decreasing the helix angle. For K_t and K_r these changes appeared to be small, while the K_a experienced a more dramatic change. The same pattern occurs for the spindle speeds of 2800 and 4300 rpm. In addition, the magnitude of the coefficients decreases when the spindle speed increases. This variation may be because of the workpiece softening resulting from the temperature increments at higher speeds, a behaviour common in metal alloys.

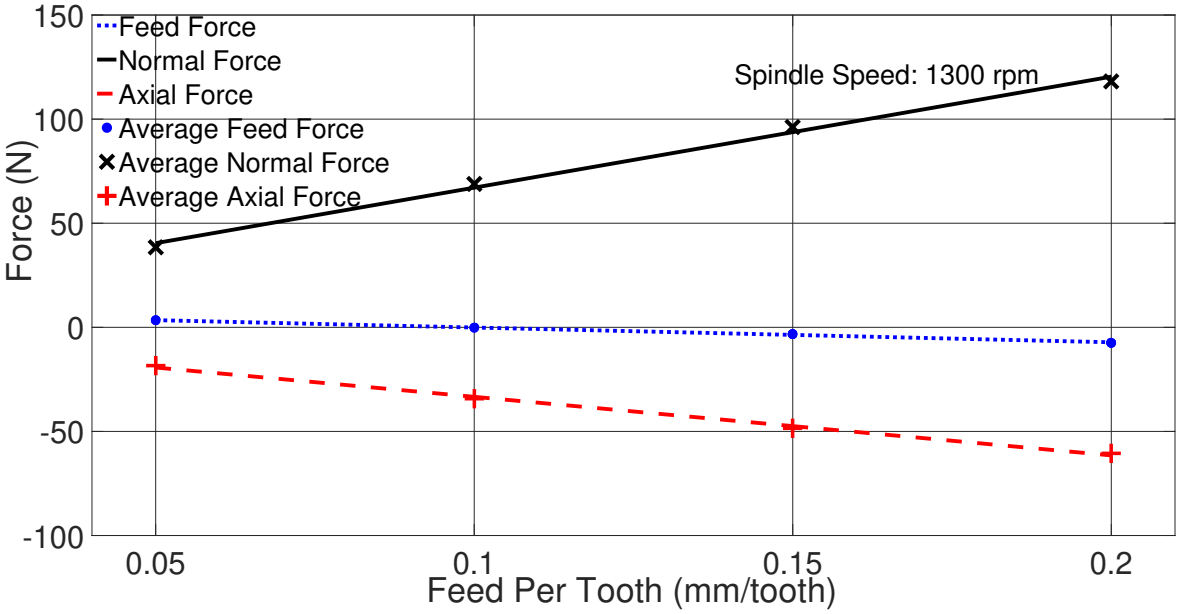

Figure 4.6.: Experimental results showing the relationship between the feed-per-tooth, and the average forces for a conventional milling tool with 25° of helix angle.

Subsequently, Figure 4.6 shows the relation between the feed per tooth and the average forces for the conventional tool at 1300 rpm. It is clear from this plot that the feed per tooth is proportional to the average forces in the feed, normal, and axial directions. Therefore, the assumption of a linear-force model with this plastic is reasonable [193, 196,216]. The same behaviour was found in the results obtained from the one-flute-tool tests, as it is shown in Appendix B.1.

4.3. Experimental Flexure Device

One of the main aims of the current project is to validate a variable-helix island of instability. To do so, it is assumed that the structural dynamics of the cutting system behaves as a one-degree-of-freedom flexible workpiece. This then reduces the complexity of the analysis removing further aspects that may obscure the study of variable-helix

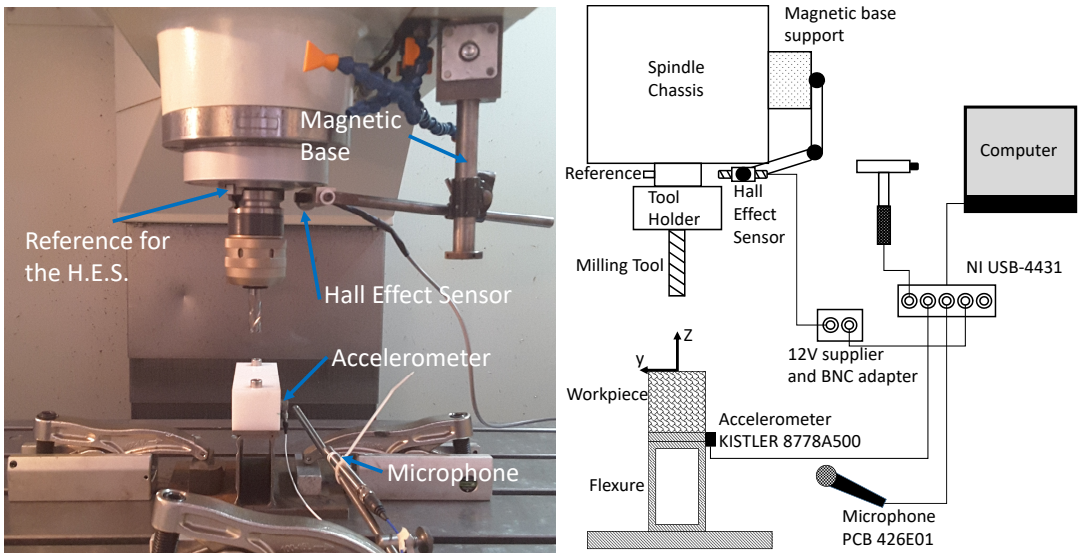

(a) (b)

Figure 4.7.: (a) Experimental Configuration,(b) Schematic of the Instrumentation.

instability islands (e.g. mode-coupling vibrations). Authors like Zatarain, Smith, and Yusoff [25, 171, 217] have successfully implemented similar one-degree-of-freedom systems, but the higher force magnitudes while cutting the metal-alloy workpieces limited their studies to lower depths of cut.

The setup proposed in this project for the variable-helix chatter stability validations is shown in Figure 4.7 (a) and (b). It comprises a copolymer acetal block of 150mm of length, 50mm of depth, and 40mm of height attached to the flexure device using screws. This flexure is then mounted on a CNC machine (XYZ 1060 HS VMC) and fixed using clamps.

To detect chatter in milling trials, the flexure was instrumented with a uni-axial accelerometer (KISTLER model 8776A50) attached with wax, and a microphone (PCB-377B20 with a pre-amplifier PCB-426E01) as shown in the schematic of Figure 4.7 (b). To study the types of bifurcation occurring in the unstable tests, once-per-revolution values were obtained from the acceleration time series by using the data collected from a Hall-effect sensor. This sensor was configured to provide a voltage pulse every time it

detected a rotating reference on the spindle, as shown in Figure 4.7 (a). Finally, all the sensors were connected to a data acquisition device (NI DAQ USB-4431) and sampled at a rate of 6 kHz. The data acquisition device was then linked to a laptop by USB.

4.3.1. Tap test analysis of flexure device

The FRF of the flexure device with the attached workpiece was determined using a hammer impact test. From this experiment, it was also possible to assess the validity of assuming a one-degree-of-freedom flexible workpiece. To explain the procedure followed, Figure 4.8 (a), (b), and (c) show the workpiece's reference frame, the accelerometer placements, and the locations where the structure was impacted.

With reference to Figure 4.8 (b), the chatter stability simulations in this project assumed that the system is flexible in the y-direction while infinitely rigid in the x-direction. While this condition is not fully possible in reality, this test aims to compare the device's FRFs in the x and y directions at different z-locations (Figure 4.8 (a)), to evaluate if this premise is valid at some degree.

Therefore, four locations were defined on the workpiece face perpendicular to the y-axis. These locations in the z-axis are 0 mm, 14 mm, 28 mm, and 46 mm (Figure 4.8 (a)). Subsequently, the accelerometer was placed on the opposite workpiece face on the z-location of 0 mm, as shown in Figure 4.8 (b). Next, the workpiece was impacted on the previously defined locations, while always keeping the accelerometer in the same position. Afterwards, a similar procedure was followed for the workpiece faces perpendicular to the x-direction, as depicted in Figure 4.8 (c).

The FRFs obtained for the y-direction are shown in Figure 4.9 (a). The continuous black line represents the dynamic response at 0 mm, the dashed blue line at 14 mm, the dotted line at 28 mm, and the dashed and dotted line at 46 mm. These results suggest

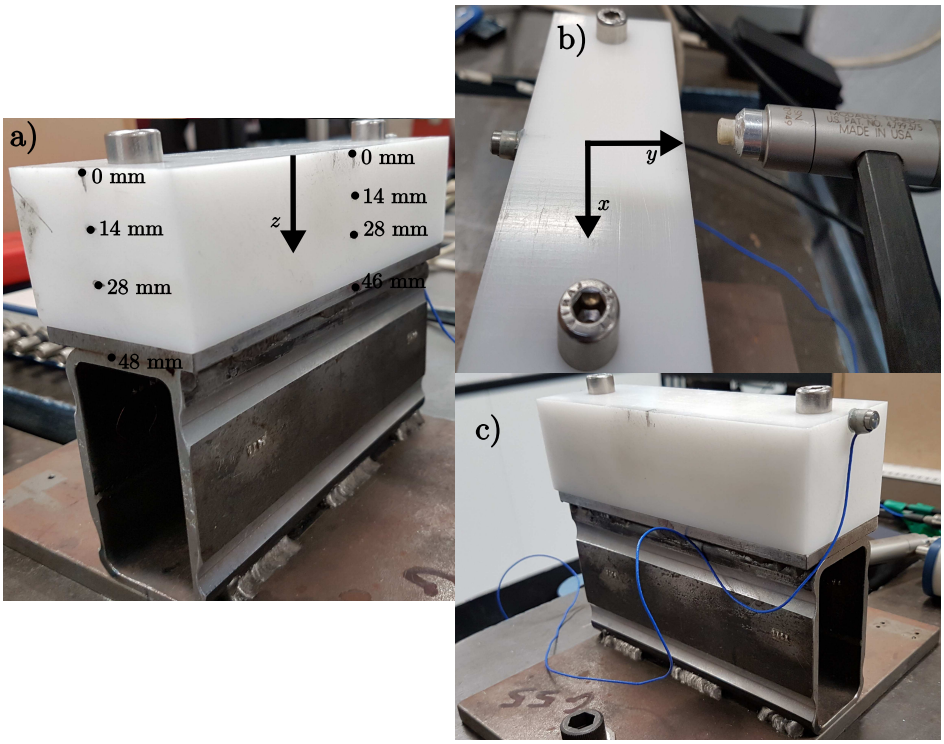

Figure 4.8.: Figure describing the impact test procedure on flexure device. This figure shows: (a) The locations where the structure was impacted, (b) The workpiece reference frame and the accelerometer placement for the y-direction test, and (c) the accelerometer location for the x-direction tests.

that the dynamic response along the height of the workpiece does not experience significant variations. This behaviour is better reflected by normalised modal displacements shown in Figure 4.10, that shows that the displacement difference between the top and bottom of the workpiece is within less than 10%.Thus, it is reasonable to assume that the workpiece is stiff enough to assume that it will vibrate as a whole with the upper metallic platform of the flexure device.

Furthermore, Figure 4.9 (b) shows the flexure's FRFs in the x and y directions. The continuous black line and the dashed blue line represent the y-direction FRFs at the z-locations of 0 mm and 46 mm. Additionally, the dotted red line and the green dashed and dotted line represent the x-direction FRFs at the heights of 0 mm and 48 mm. These results suggest that flexure is considerably stiffer in the x-direction when compared to the y-direction, allowing to assume x-direction as rigid.

The estimated flexure device's modal natural frequency, damping ratio, and stiffness were of 290 Hz, 0.67%, and 3.55 kN/mm. This device is 86 times more flexible than the system comprising the cutting tool, tool holder, and the spindle at the tooltip. The FRF of this system is presented in Figure 4.11, showing a dominant resonant frequency of 4331 Hz in x and y directions. Therefore, the assumption of a rigid machine tool is also valid, meaning that the only source of instability in the processes comes from the workpiece vibrations in the y-direction.

4.4. Variable-helix chatter stability predictions with unequal cutting force coefficients

Having determined the cutting force coefficients in Section 4.2.3 and flexure device's FRF in Section 4.3, the current section aims to determine the effect of using different cutting force coefficients on the stability lobe diagram of variable helix milling tools. While several research projects have previously studied the effect of the helix angles on

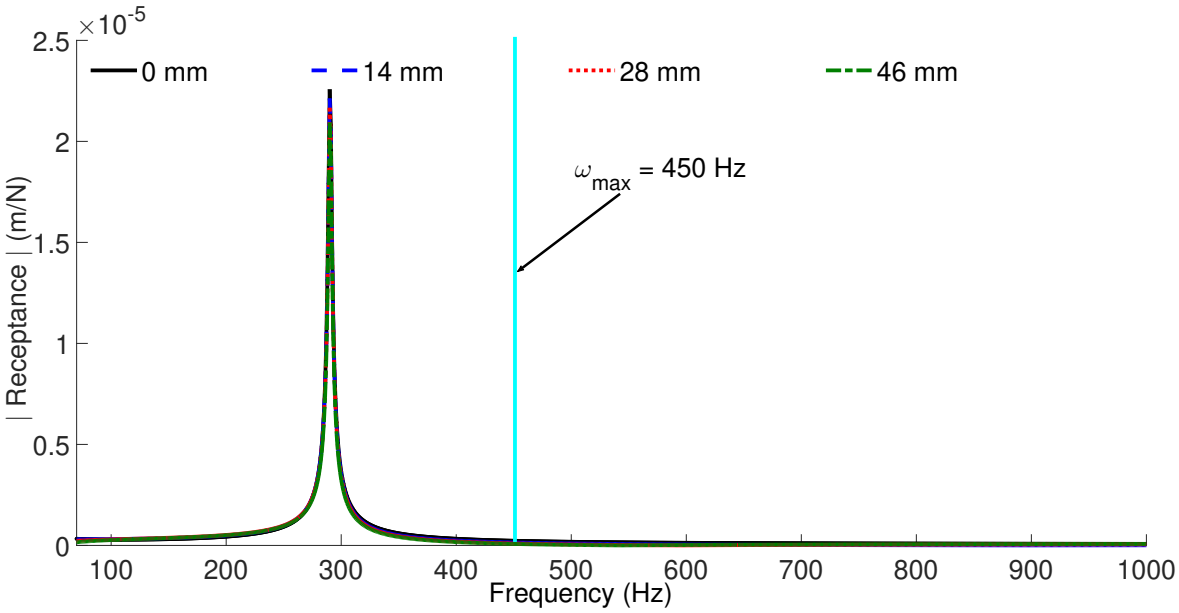

(a)

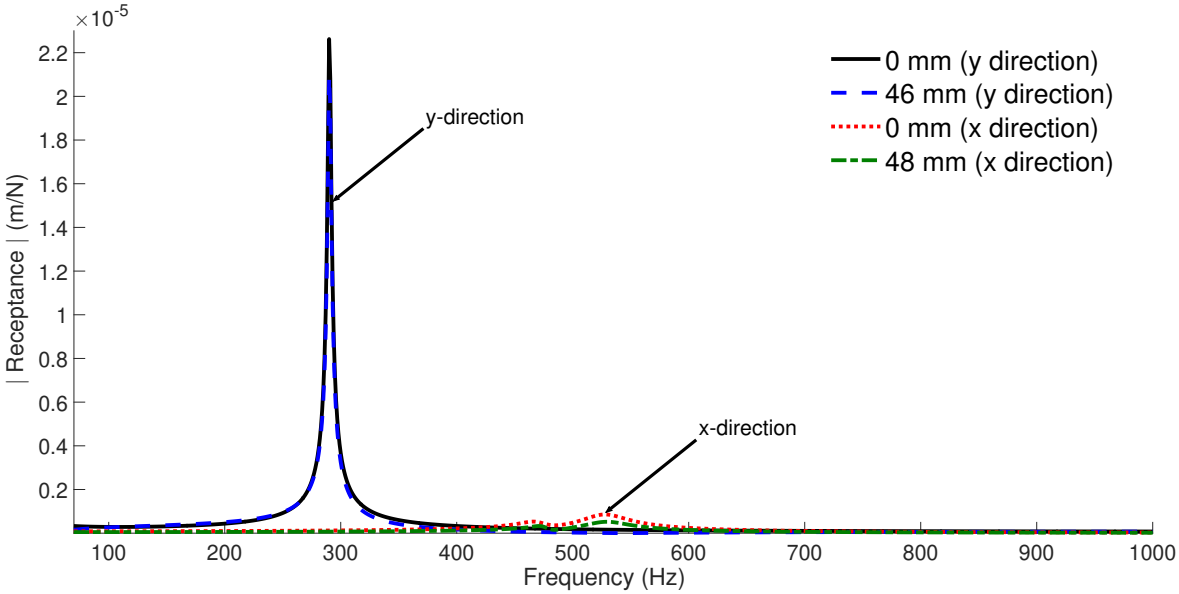

(b)

Figure 4.9.: (a) FRF of the flexure device in the y-direction at different location along the workpiece, (b) Comparison between the flexure's FRFs along the y- and x- directions ($\omega_{max} = 450$ Hz).

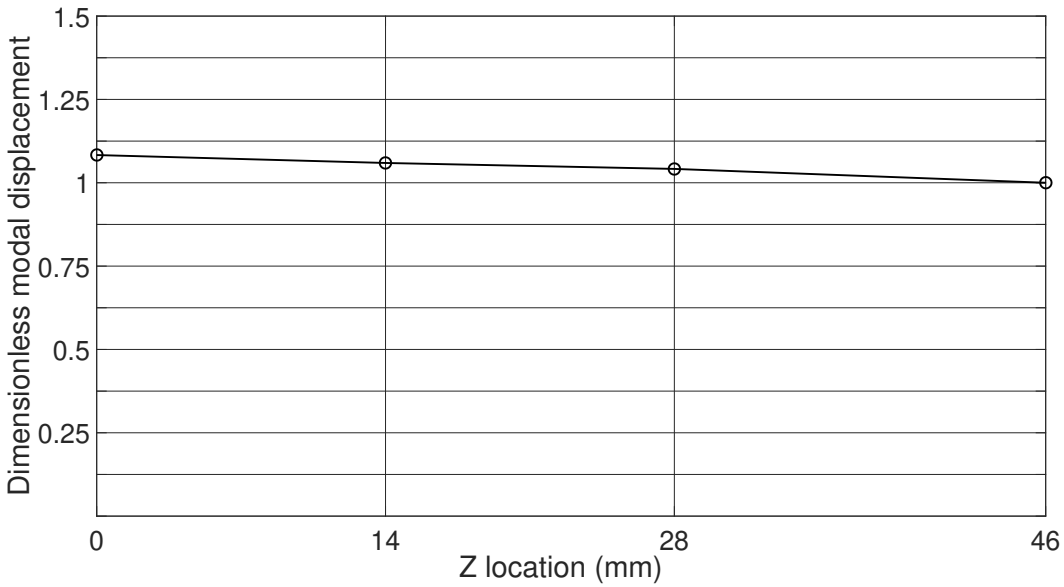

Figure 4.10.: Dimensionless modal displacement.

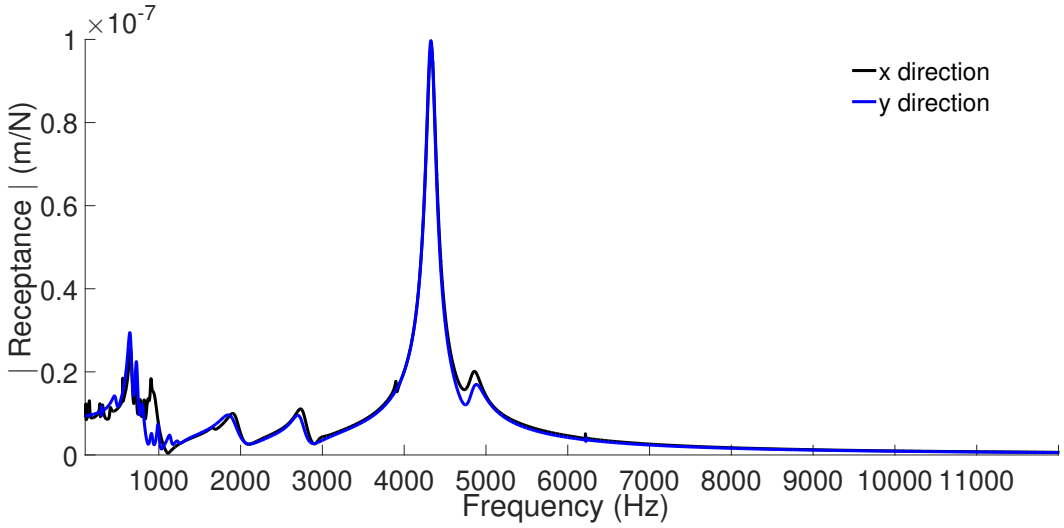

Figure 4.11.: Frequency Response Function of the CNC machine.

the cutting forces either on conventional and variable-helix milling cutters [218–220], none of them has shown how the coefficient variations affect the process stability.

Consequently, to explore this issue, the current section implements the modified MFA (Chapter 3) that allows cutting force modelling with non-equal coefficients on the teeth. Then, chatter stability predictions are calculated assuming a non-equal coefficient variable-helix cutter with 25°, 15°, and 10° of helix angles. Subsequently, as a comparison, they are also estimated using the standard unmodified MFA. The machining scenario in this study is shown in Table 4.3, in which the single-flute cutting force coefficients implemented for the simulations are the ones estimated at 1300rpm (Table 4.2). The MFA was configure with a ω_{max} (equation 3.43) of 450 Hz, and subsequent axial depth of cut and spindle speed increments of $\Delta a = 0.1$ mm, and $\Delta\Omega = 15$ rpm.

The chatter stability predictions are shown in Figure 4.12. These results suggest that the stability boundary variations because of the helix-induced non-equal coefficients are negligible. One of the main reasons of this minor effect could be the relatively small helix angle differences. For example, Ozturk in [218] explored the effect of the helix angle on the cutting force coefficients in a broader angular range, finding more significant variations on the coefficients. However, the author did not study how this is reflected on the process stability using a variable-helix milling tool.

For the current thesis, based on the results found in this section, the stability predictions perform in subsequent chapters will implement the cutting force coefficients obtained from the conventional milling tool. At this stage, several assumptions have been made regarding the material machinability, one-degree-of-freedom behaviour of the flexure device, and the effect of helix angles on the cutting force coefficients. Therefore, the next three sections aim to validate experimentally these premises by first analysing the chatter stability of the variable-helix cutter tool with 25°, 15°, and 10° of helix angles using the SDM and MFA. Afterwards, a set of cutting trials are performed around a potential island of instability in the stability chart to determine if the

Parameter	**Value**
ω_{ny}	290 Hz
k_y	3.55 kN/mm
ζ_y	0.67%
ϕ_{10}, ϕ_{20}, ϕ_{30}	0°, 120°, 240°
γ_1, γ_2, γ_3	25°, 15°, 10°
Radial Immersion	50%
Tool Diameter	16 mm
Material	Copolymer Acetal
Conventional Milling Tool Coefficients:	
K_t	142.2 N/mm^2
K_r	18.9 N/mm^2
Single Flute Milling Tool Coefficients:	
K_t^{25}, K_t^{15}, K_t^{10}	136.55 N/mm^2, 131.55 N/mm^2, 130.70 N/mm^2
K_r^{25}, K_r^{15}, K_r^{10}	11.44 N/mm^2, 15.16 N/mm^2, 17.10 N/mm^2
Cutting Condition	Up-milling
Normal Direction (flexible)	y (Figure 4.7)
Feed Direction (rigid)	$+x$ (Figure 4.7 pointing outside the page)

Table 4.3.: Machining Scenario

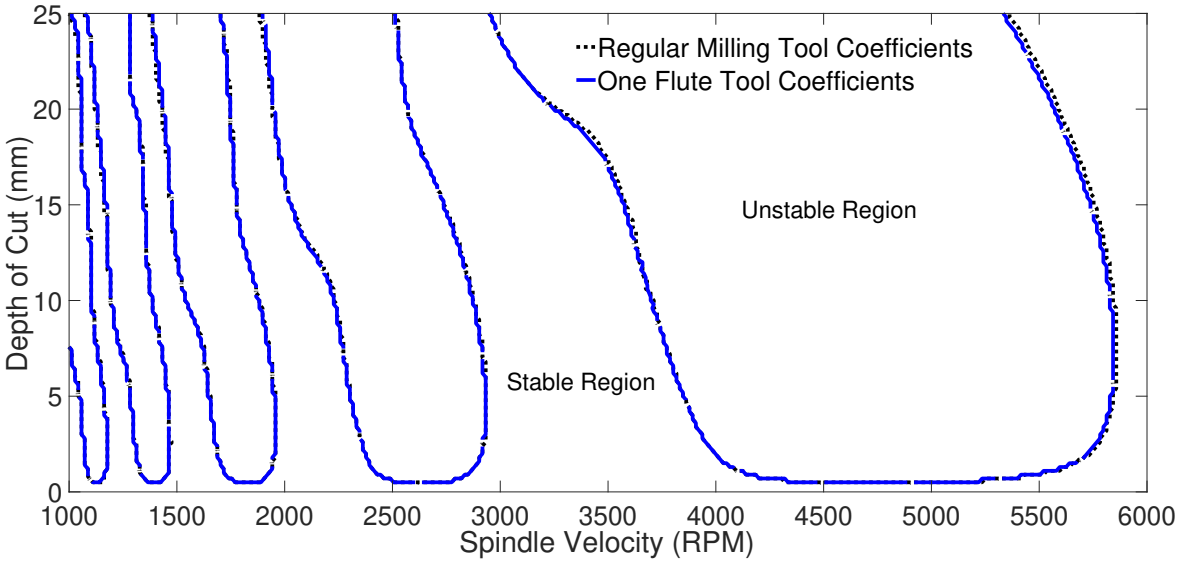

Figure 4.12.: Chatter stability predictions using the modified MFA to consider non-equal cutting force coefficients on the teeth. The results are compared with the MFA predictions obtained using equal cutting force coefficients on the flutes.

system behaves as expected. Finally, conclusions are drawn regarding the simulations and experimental outcomes, and it is discussed the accuracy of the chatter prediction methods and potential dynamic modifications on the setup that may lead to islands of instability.

4.5. Stability Predictions with SDM and MFA

The machining scenario implemented for the simulations is summarised in Table 4.3. As previously mentioned in Section 4.4, the cutting force coefficients used for the chatter predictions are the ones obtained with the conventional milling tool with 25° of helix angle. Furthermore, the SDM and MFA were configured to predict stability at axial depth of cut steps Δa of 0.1 mm, and spindle speed increments $\Delta\Omega$ of 15 rpm. Additionally, the SDM was configured with an m parameter (equation 3.44) of 500,

while the MFA with an ω_{max} (equation 3.43) of 450 Hz. This frequency is shown in Figure 4.9, along with the system's frequency response function. Due to the nature of the MFA, the number of harmonics p used in the solution at every spindle speed Ω is automatically adjusted following the relationship in equation 3.43.

The simulation's outcomes using both methods are shown in Figure 4.13 (a) and (b). The continuous blue lines and discontinuous black lines in these plots represent the subsequent predictions for the SDM and MFA. Also, the parameter k in these plots indicates the number of waves per revolution printed on the workpiece surface by the tool flutes. As a comparison, Figure 4.13 (a) and (b) also show in discontinuous red lines the stability predictions for a conventional milling tool with 25 degrees of helix angle. From these plots, it is evident that the conventional and variable-helix milling tools behave similarly at lower axial depths of cut because the variable-helix cutter has equal pitches at the tooltip. However, at higher axial depths, the pitches between the flutes tend to continuously change altering the regenerative stability condition of the process. Consequently, this may lead to further stabilisation of the variable-helix milling process at higher depths of cuts when compared to conventional ones.

For example, at the spindle speed of 2500 rpm ($k = 2$ lobe in Figure 4.13 (a)), the lower chatter stability boundary predicted for both tools and methods is of approximately 2 mm. After this axial depth of cut value, the process becomes unstable for both tool configurations and chatter prediction approaches. Subsequently, while the process at larger depths of cut continues being unstable for the conventional milling tool, the variable-helix cutter experiences a further process stabilisation at 17 mm for the SDM, and 18 mm for the MFA. Consequently, these results suggest that by adequately fine-tuning a variable-helix milling tool for a particular application, it is possible to achieve axial depths of cut that could be unattainable with conventional ones without chatter.

Furthermore, Figure 4.13 reveals several discrepancies between the stability predictions with the SDM and MFA. The most remarked differences are the isolated instability

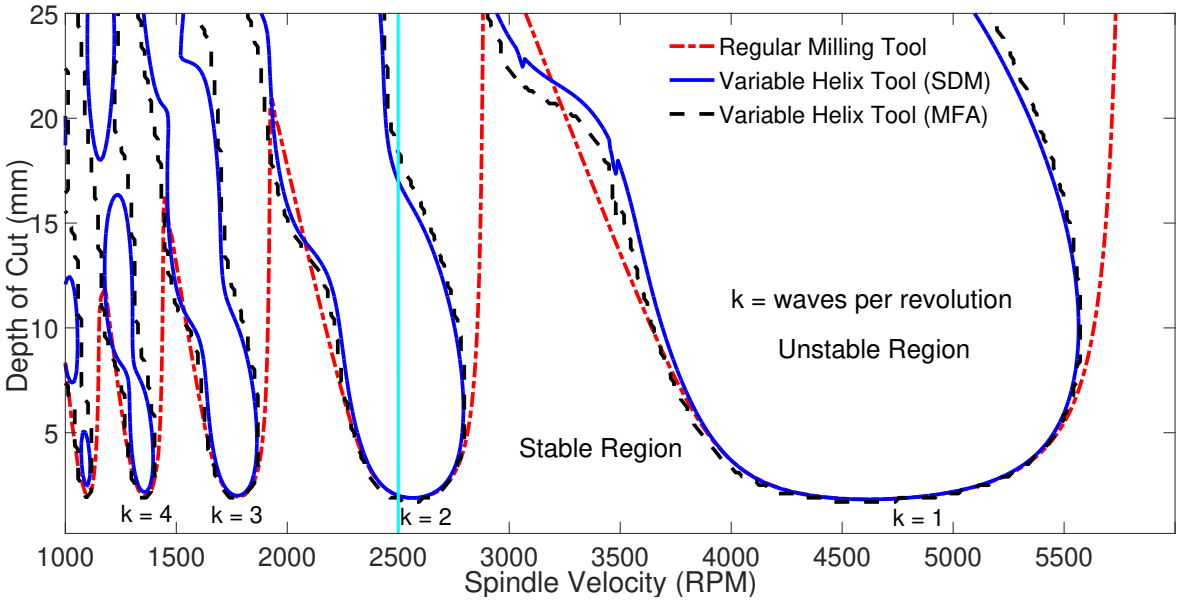

(a)

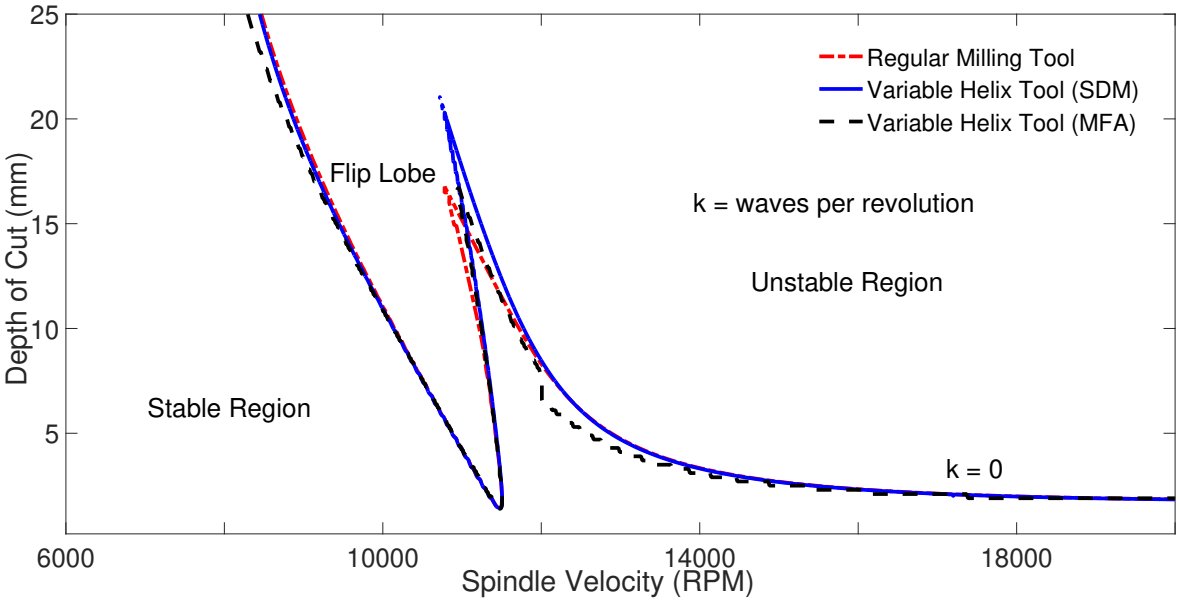

(b)

Figure 4.13.: Stability lobe diagrams obtained using the MFA and SDM for a conventional milling tool with 25° of helix angle, and a variable-helix cutter with helix angles of 25°, 15°, and 10° . The stability lobe diagram was divided into a low-spindle speed region from 1000 to 6000 rpm (a), and a high spindle speed area from 6000 to 20000 rpm (b) to show the flip or added lobe.

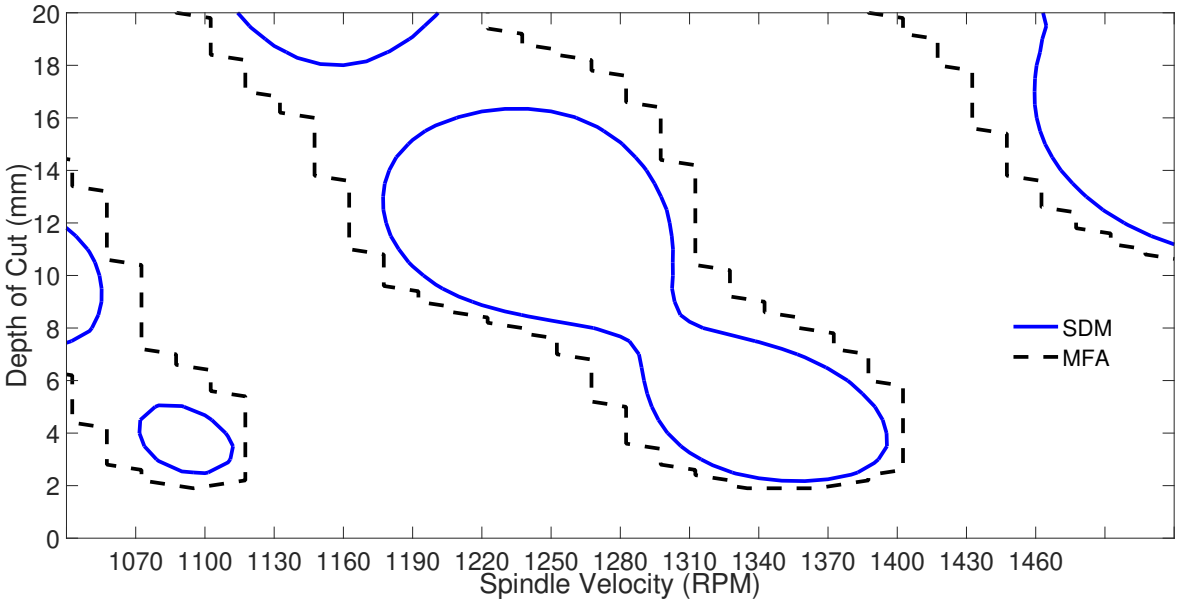

Figure 4.14.: The stability predictions obtained using SDM suggest the appearance of an instability island, while the MFA suggests otherwise.

islands predicted by the SDM for the $k = 4$ and $k = 5$ lobes, conditions not found by the MFA. These islands are shown in Figure 4.14. It is worth mentioning that these instability islands occurred far away from the flip lobe of the stability diagram that is shown in Figure 4.13 (b). Additionally, the radial immersion of tool engagement is 50%. Thus, as explained in Chapter 2 for conventional milling tools, these conditions suggest that these isolated unstable regions are not either parametric or helix-induced islands of instability. Consequently, it was concluded that its appearance could be mainly because of the non-equal helix angles on the milling tool. Therefore, the $k = 4$ island was chosen as the ideal condition for the experimental validation stage in the forthcoming section.

4.6. Experimental procedure and results

The instability island revealed by the SDM in the previous section is shown in Figure 4.14. Around this condition, a series of 126 cutting trails were defined comprising 14

spindle velocities starting from 1070 rpm to 1460 rpm at increments of 30 rpm. The milling tests were executed at a feed per tooth of 0.1 mm/tooth, such as the minimum cutting speed attained in these trials was of 53.7 m/min, and the highest of 73.3 m/min.

Per every spindle speed, two acetal workpieces were required to complete the nine tests at different axial depths of cut. On the first workpiece, six milling trials were performed from 18 mm to 8 mm at steps of 2 mm of the axial depth of cut. On the other hand, three milling tests were executed on the second workpiece from 6 mm to 2 mm at steps of 2 mm of the axial depth of cut.

At every spindle speed condition, the cutting bed of the machine tool was first placed in its initial position as shown in Figure 4.15 (a). In this location, the tool axis was aligned with the z axis of Figure 4.15 (a). Furthermore, the tooltip was 18 mm in the z-axis (axial depth of cut) and 13 mm in the x-axis. Afterwards, the data acquisition system and the spindle were initiated and the workpiece was fed into the milling tool 38 mm in the x-direction producing a half immersion cut of 25 mm of cutting length. Next, the cutting bed stopped feeding the workpiece, and the axial depth of cut was decreased by 2 mm. Subsequently, another half immersion cut of 25 mm of length was completed, as illustrated in Figure 4.15 (c). This operation was executed six times on the first workpiece resulting in a final workpiece geometry as depicted in Figure 4.15 (d) and (e).

After switching off the data acquisition system and the spindle, the workpiece was removed from the flexure device. Next, the second workpiece was fixed on the flexure and the cutting bed was placed again in its initial location. The axial depth of cut (z-axis) on this occasion was 6 mm. Subsequently, the acquisition system and spindle were started and the remaining three milling trials at the particular spindle speed were completed.

This entire procedure was repeated at the subsequent spindle speeds and the final results are shown in the stability lobe of Figure 4.16. In this diagram, green dots

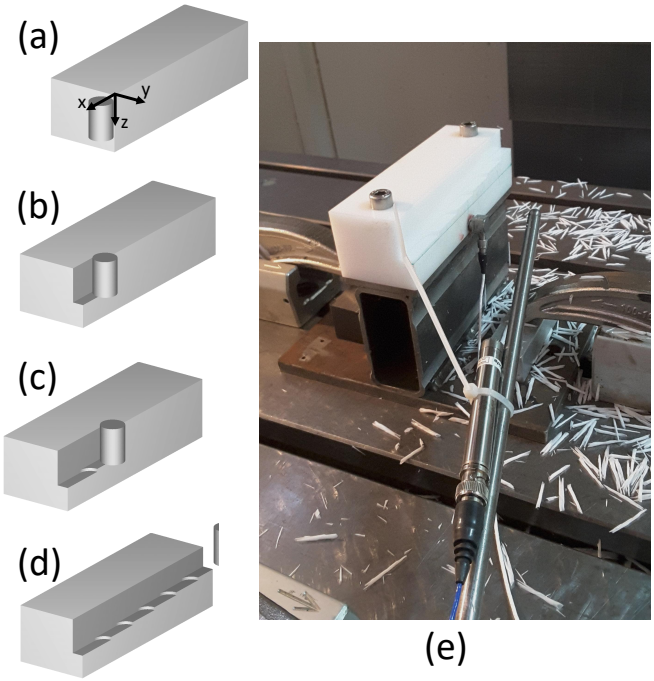

Figure 4.15.: Experimental Procedure.

represent stable cuts, orange diamonds marginally stable cuts, and red squares unstable ones. Additionally, the discontinuous black lines represent the stability predictions obtained with the MFA, while the continuous blue lines the SDM ones. The overall experimental outcome in Figure 4.16 suggest a reasonable good agreement between the results and both predictions. However, the MFA predictions seem to better resemble the preliminary results when compared with the SDM.

For each test described in Figure 4.16, the acceleration once-per-revolution samples were used to construct a delayed Poincaré section as shown in section 2.2. It was later used to qualitatively classify the process stability. In addition, the Fast Fourier Transform of the audio and acceleration signals were computed. The criteria to categorise the stability condition of the trials are as follows. If the delayed Poincaré section appears as a dot, it suggests a stable process because it gives the same solution every revolution. Note that for a variable-helix tool, the fundamental period is the tool rotational period rather than the tooth-passing one. Therefore, a stable Fast-Fourier-Transform

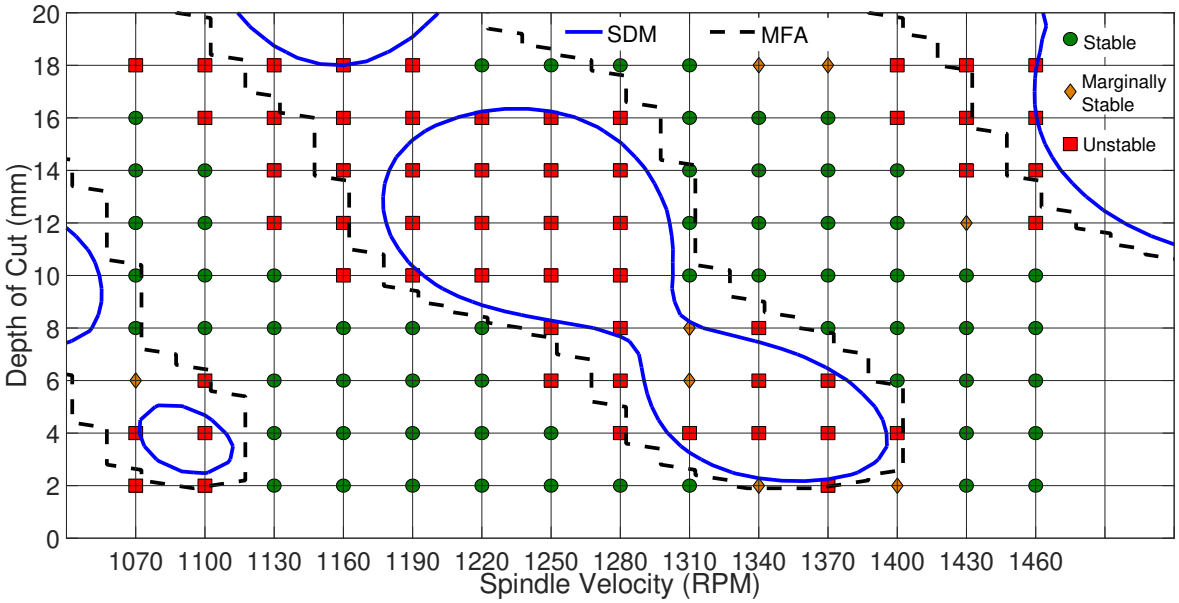

Figure 4.16.: Instability island and results obtained from the milling trials.

(FFT) spectrum shows the spindle-pass frequency or any of its harmonics as dominant in the process. For the acceleration signal, it was observed that whenever the Poincaré section suggested a stable trial, the acceleration FFT indicated the same.

However, whenever the stability condition suggested by the sound and acceleration FFT does not agree, the trial were concluded as marginally stable. Thus, in a fully stable test, the Poincaré section along with the acceleration and sound FFT indicate a stable process.

As an example, Figure 4.17 shows the detailed behaviour at 1100 rpm for depths of cut from 2 to 8 mm. The plots located on the left of Figures 4.17 (a), (b), (c), and (d) show the acceleration time series in blue lines with the once per revolution samples superimposed as red dots. In addition, it shows the steady state region in a green rectangle used to build the Poincaré plot shown on the right side of Figures 4.17 (a), (b), (c), and (d). It can be seen that the cut at 2 mm (Figure 4.17 (a)) is unstable as the simulation predicted, with the once-per-revolution sampled acceleration indicating quasi-periodic motion that is indicative of a Hopf bifurcation [80] and the acceleration

and microphone spectra indicating a chatter frequency of 289.7 Hz as indicated in the Fourier transform of the Figure 4.18 (a). At 4 mm and 6 mm (Figure 4.17 (b) and (c)), the cutting process is still unstable, until 8 mm (Figure 4.17 (d)) when the system becomes stable. The system continues being stable until 16 mm when it became unstable again exhibiting a chatter frequency of 263.9 Hz as it is shown in the Figure 4.18 (b).

As another example, for the spindle speed of 1400 rpm, the cutting trial at 2 mm is a period double unstable cut with a chatter frequency of 280 Hz, as it is shown in the Figure 4.19 (a). This represents the 6th harmonic of the double of the spindle pass frequency 23.33 Hz. When the axial depth of cut is increased to 4 mm (Figure 4.19 (b)), again a quasi-periodic response is found in the Poincaré plot suggesting the appearance of a Hopf bifurcation. Next, the subsequent milling cuts at 6 and 8 mm (Figures 4.19 (c) and (d)), become stable as indicated in the Poincaré plot. As is shown in the Figure 4.16, the cutting trials at 1400 rpm remain stable until 16 mm when the cutting process becomes unstable.

Contrary to the SDM predictions, the experimental results shown in Figure 4.16 suggest that no instability island is located in this cutting region. The instability sector showed by the SDM as an island appears connected to another lobe as suggested by the MFA. It is clear from the predictions in Figures 4.13 and 4.14 that at lower axial depths of cut and higher spindle speeds, both methods provide similar solutions. For example, stability predictions at spindle speeds higher than around 1500 rpm (Figure 4.13) are similar for both methods at low and high axial depths of cut. However, at spindle speeds below this value, both methods considerably differ when the axial depth of cut is increased beyond approximately 5 mm.

From both simulations, the MFA shows to better follow the shape described by the experimental results, although its predictions appear to be slightly skewed to the right. This condition at higher axial depths of cut appears to be caused by a changing in

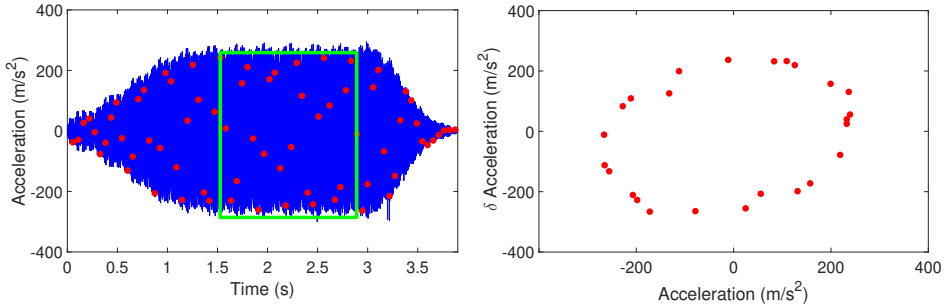

(a)

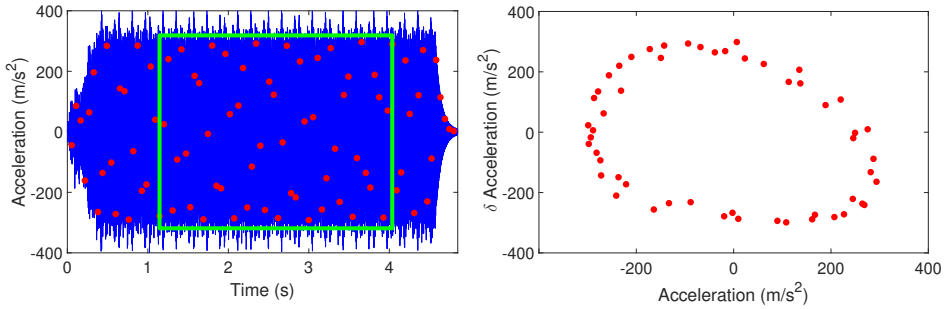

(b)

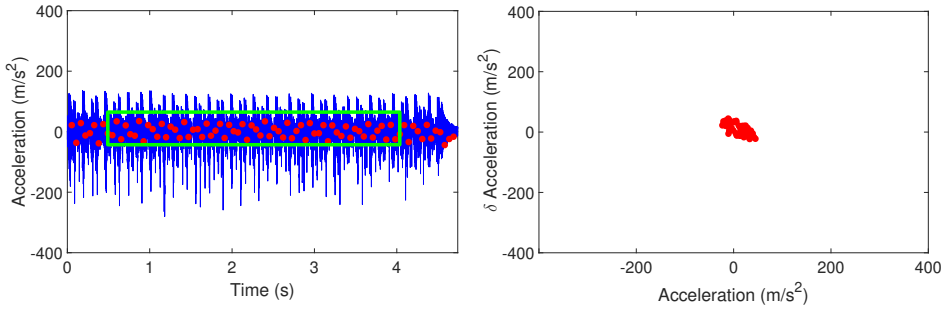

(c)

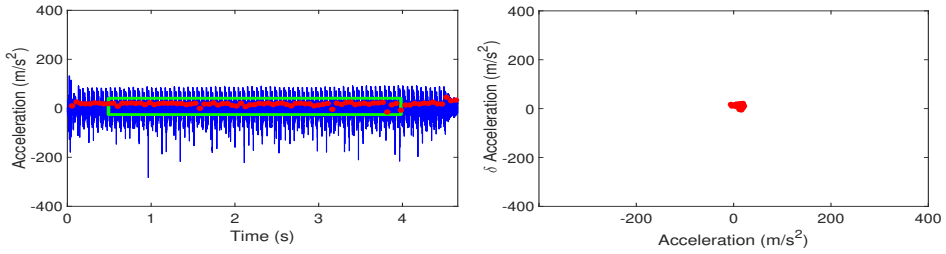

(d)

Figure 4.17.: Time series (blue line) and once per revolution samples (red dots) of the acceleration data at a spindle speed of 1100 rpm and axial depth of cut of 2mm (a), 4mm (b), 6mm (c), and 8mm (d). The steady state region of the process is defined by the green rectangle.

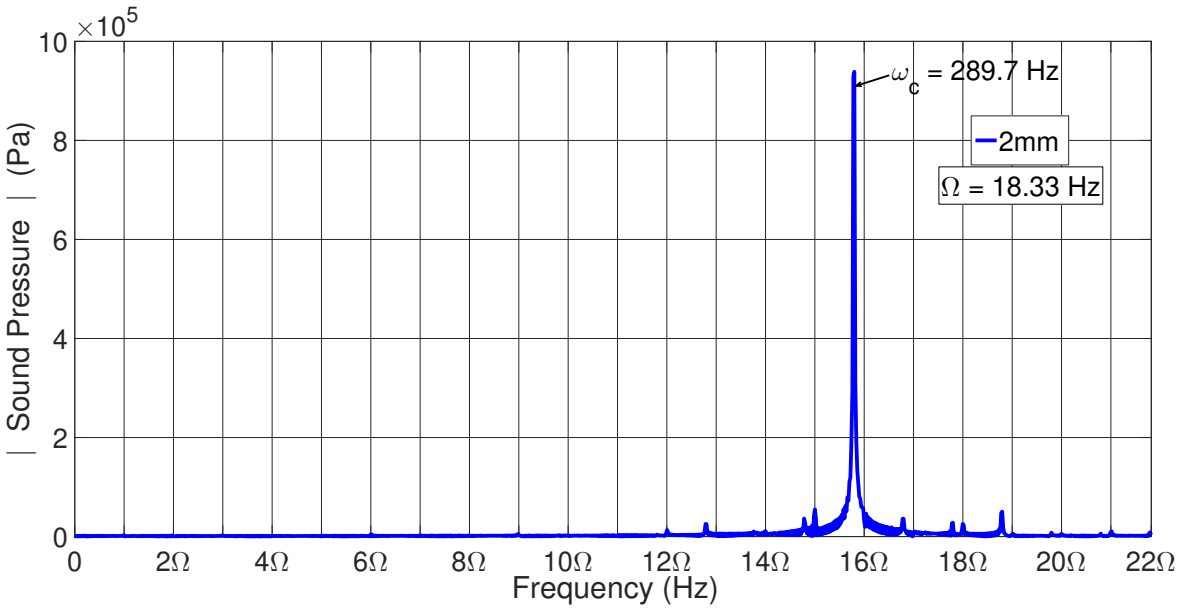

(a)

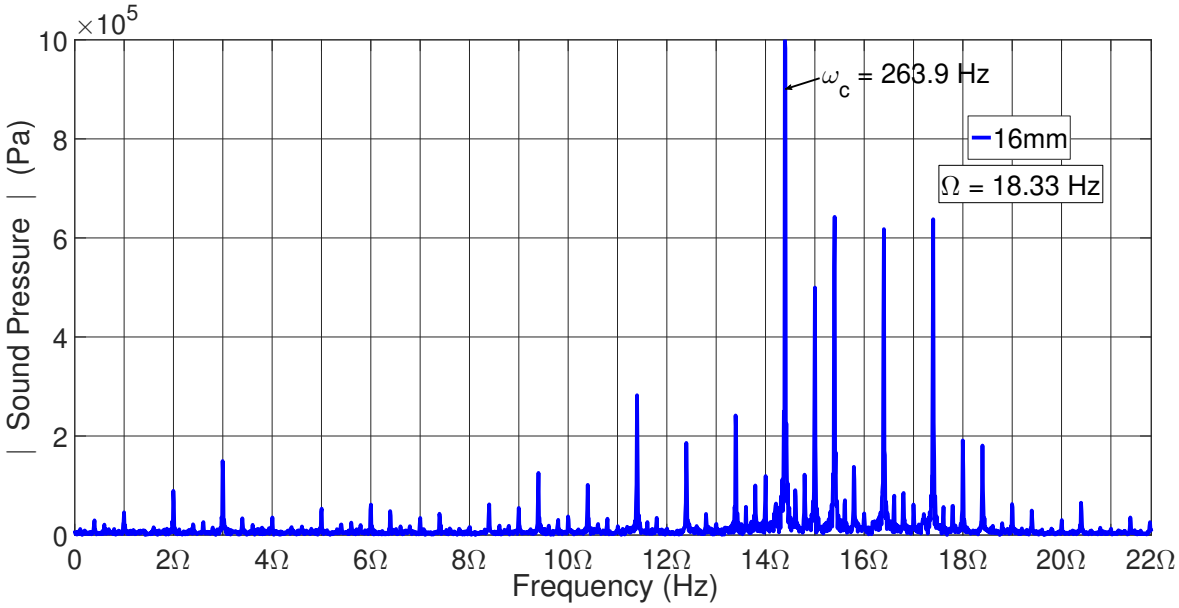

(b)

Figure 4.18.: Frequency spectrum of the audio signal for the milling trial at 1100rpm and 2mm (a) and 16mm (b) depth of cut.

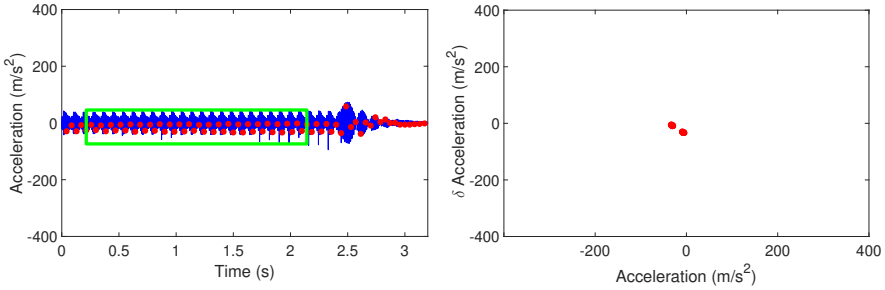

(a)

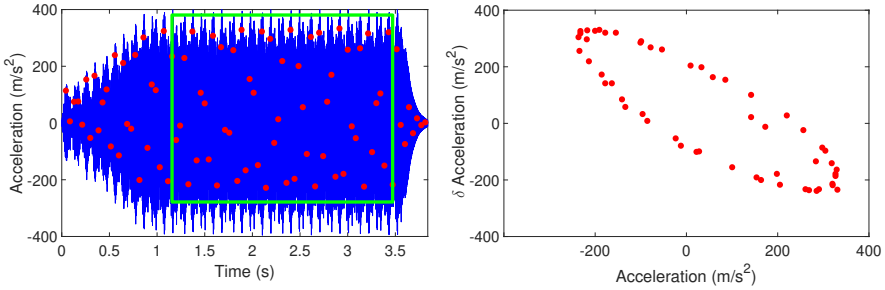

(b)

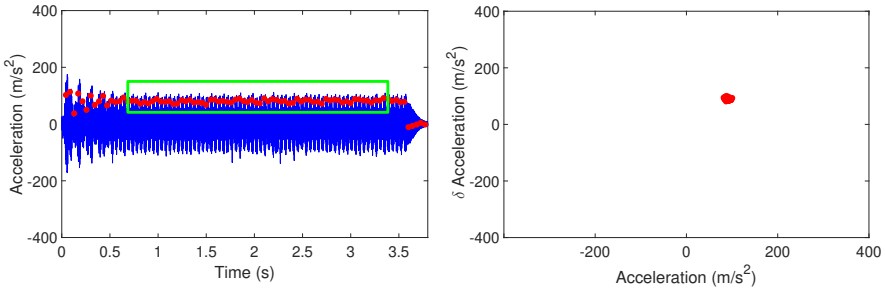

(c)

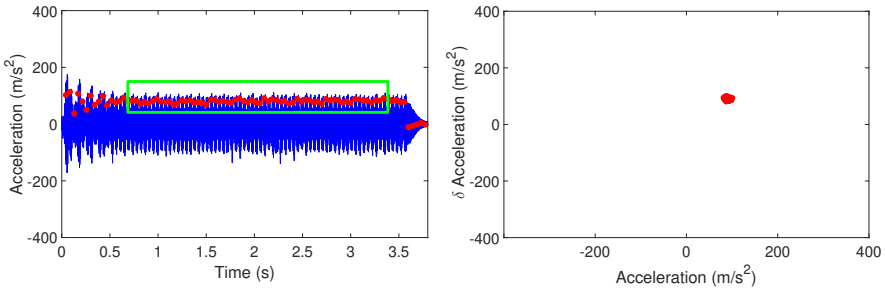

(d)

Figure 4.19.: Time series (blue line) and once per revolution samples (red dots) of the acceleration data at a spindle speed of 1400 rpm and axial depth of cut of 2mm (a), 4mm (b), 6mm (c), and 8mm (d). The steady state region of the process is defined by the green rectangle.

the natural frequency of the system, that is induced by the material removed from the workpiece. However, while the SDM resembles the same shifting phenomenon, it seems to be unable to predict the lobe connection detected by the MFA. This behaviour suggests that the SDM struggles to converge to a solution due to the additional high-frequency vibrations induced by the distributed time delays at higher depths of cut. This condition seems to be aggravated at lower spindle speeds since larger spindle-pass periods allow these vibrations to remain longer. To explore this issue in more detail, the next chapter includes a convergence study for both methods.

4.7. Conclusions and Discussion

From the previous analytical and experimental study, the following conclusions can be achieved. First, it can be concluded that the linear mechanistic cutting force model can be implemented to predict the cutting forces of copolymer acetal. In the current thesis, it was proposed a custom-made 3-teeth variable-helix milling cutter with helix angles of 25°, 15° and 10°. The cutting force coefficients of this tool were independently determined using customised one-flute tools and the standard mechanistic identification method. Additionally, a conventional 3-teeth milling tool with a helix angle of 25° was employed to further comparison. The trials performed on copolymer acetal following the mechanistic approach revealed that the average cutting forces linearly relates to the feed per tooth, being the cutting force coefficients proportional to the line slopes. This relationship was found using the single-flute and three-flute tools at several cutting speeds, agreeing with the data found in the literature. Additional chatter stability validations using a variable-helix milling tool further confirmed the reliability of implementing the linear models. Furthermore, simulations were performed using the MFA that was modified to consider non-equal cutting force coefficients. The simulation's outcomes led to the conclusion that the impact of the helix-induced coefficient variations on the chatter stability boundaries can be neglected for the specific tool under

study. While there were fluctuations between the coefficients because of the helix angle, these variations were translated into minor changes on the stability boundaries.

Regarding the dynamic behaviour of the experimental setup, the workpiece and machine tool impact test results confirmed that the one-degree-of-freedom flexible workpiece assumption is valid. The workpiece's FRF in the flexible direction exhibited an isolated resonant frequency of 290 Hz. Impact tests performed along the height of the workpiece and flexure device revealed negligible changes, showing that the workpiece and flexure were linearly vibrating as a complete entity with no rotation. This then guaranteed a one-degree-of-freedom behaviour, while cutting the workpiece at larger axial depths of cut. Moreover, the workpiece FRF in the direction orthogonal to the flexible one revealed that the workpiece is considerable more rigid, further validating the one-degree-of-freedom hypothesis. In addition, the machine tool's FRF showed that workpiece system is 86 times more flexible than the machine. Consequently, it can be assumed a rigid machine tool whose structural dynamics can be neglected from the chatter stability analysis.

From the chatter stability simulations performed using the SDM and MFA, it was found several discrepancies between the methods at lower spindle speeds. The most remarkable difference was an unstable island predicted by the SDM, a phenomenon not captured by the MFA. In general, the results from the experimental tests conducted around this condition mostly agreed with both predictions at lower axial depths of cut. However, the MFA better fits the overall shape of the preliminary outcomes at higher axial depths of cut, although the results appeared to be slightly skewed. This shifting on the chatter boundaries at a higher axial depth of cut seems to be caused by the changes on the system's natural frequency because of the material removed from the workpiece. For example, per every spindle speed in the stability lobe diagram of Figure 4.16, two copolymer acetal workpiece were implemented. In the first one, there were executed the trials from 18 mm to 8 mm at steps of 2 mm. The remaining three trials from 6 mm to 2 mm were conducted on the second workpiece. It is clear

from Figure 4.16 that the shifting is more pronounced on the trials performed on the first workpiece where more material was subtracted. In addition to reducing the workpiece mass, this condition could also alter the dynamic structural stiffness of the system because of the workpiece geometry modifications. These continuous changes on the workpiece natural frequencies seem to alter locally the chatter boundaries [221]. Future works can implement enhanced models such as the ones proposed by Shi and Budak in [222, 223], in which the FRF of the flexible workpiece is updated based on the material removed in the cutting process.

The SDM inability to predict the lobe connection could be related to convergence issues, emerging from the formulation nature of the stability problem. As shown in Chapter 3, the accuracy of the SDM relies on the value M (equation 3.44), that represents the number of equally spaced elements in which the spindle rotation is divided. This parameter remained constant indistinctly of the spindle speed. On the other hand, the MFA accuracy depends on the number of harmonics p, that are considered when solving the stability problem. However, contrary to the SDM, this parameter is not fixed. The MFA takes advantage of the FRF property of tending to zero at higher frequencies, to self-adjust p to the spindle speed based on a truncation frequency ω_{max}. For the chatter stability simulations presented in Figure 4.16, both SDM and MFA predictions showed to be similar at higher spindle speeds, where a fewer number harmonics p or lower M values are necessary to predict the boundaries. However, at lower spindle speeds, a higher number of harmonics p or M values are required to capture the full process dynamics. This occurs due to the higher frequency content on the workpiece vibrational spectrum resulting from the longer spindle-pass periods. In addition, this condition seems to be aggravated at higher axial depths of cut because of the helix-induced time delay variations along the axial length of the tool that further modulate the frequency spectrum. It seems that the MFA self-adjusted nature makes the approach more robust to these changes when compared with the SDM.

However, although the MFA better adjusted the preliminary results, the discrepancies found with the SDM made it unclear whether the studied region contained an island, or further unmodeled experimental uncertainties altered the preliminary results. Therefore, the next section first seeks to perform a convergence analysis of both methods to provide an insight into the performance of these techniques, predicting the chatter stability of variable-helix milling tools. In addition, the next chapter pursues to shed some light on the dynamic conditions that lead to islands of instability in the stability lobe diagram, and in particular, structural damping. Several research articles have suggested that this parameter plays an essential role in the chatter stability behaviour of variable-helix milling tools at lower spindle speeds [27].

4.8. Summary

In summary, this section experimentally and investigated the potential of variable-helix milling tools to stabilise at higher axial depths of cut. In particular, it studied the islands of instability that emerge in the stability lobe diagram because of the non-equal tool helix angles. To do this, a scaled experiment was implemented comprising a one-degree-of-freedom flexure device holding a low-cutting force coefficient workpiece. By using this setup, it was possible to assume linear structural dynamics at higher depths of cut. Furthermore, this section also studied the impact of the flute helix angle on the cutting coefficients and therefore on the stability lobe diagram. For the case studied, it was shown that the helix-related variations on the coefficients can be translated into negligible changes in the stability diagram.

During the investigation, considerable discrepancies between the SDM and MFA predictions were found. While the SDM showed an instability island in the stability lobe diagram, the MFA did not present this condition. However, though the final results showed a good agreement with both predictions, the MFA better matched the experimental results.

Consequently, the next chapter presents an converge study for the SDM and MFA. In addition, it investigate the role of structural damping on the appearance of instability islands. These two aspects are of vital importance because as it was shown in Chapter 2, chatter vibrations can be passively or actively suppressed by increasing the level of structural damping. Therefore, implementing non-converged stability approaches may lead to undetected instability islands causing undesired outcomes.

5. Damping Analysis and Validation of Variable-Helix Instability Island

5.1. Introduction

Preliminary experimental results presented in Chapter 4 first attempted to validate a potential instability island revealed by the SDM. This presumed island was not captured by the MFA, that showed that it was connected to another lobe. The experimental validation around this condition in Chapter 4 agreed with the MFA, arousing the question of whether the SDM may be experiencing convergence difficulties. Therefore, the current chapter seeks to address the issues exposed in Chapter 4 regarding variable-helix islands of instability and the SDM convergence. To do this, it first demonstrates that islands of instability only emerge at relatively high levels of structural damping. Subsequently, by performing a convergence analysis using the SDM and MFA, it also proves that instability islands are particularly susceptible to model convergence effects. At this stage, the damping and convergence analysis revealed a damping-induced variable-helix instability island using the cutter with 25°, 15°, and 10° of helix angles. Moreover, an additional customised solid-carbide variable-helix tool with helix angles of 25°, 15°, and 15° is introduced in this chapter, whose stability analysis also revealed a similar instability island. Therefore, the model predictions with both tools are validated using the experimental configuration presented in Chapter 4, with the modification of using constrained layer damping (CLD) to adjust the damping to desired levels. To the author's knowledge, this provides the first experimental and analytic study of unstable islands in variable-helix milling, while also showing the

importance of accurate damping estimates and convergence studies within the stability predictions.

The organisation of this chapter is as follows. Section 5.2 performs a structural damping analysis in which the structural damping is systematically increased in simulations to show the effect of this parameter on the chatter stability of variable-helix tools. This section also presents the structural modifications performed to the experimental setup to increase the damping using the CLD. Next, Section 5.3 performs a convergence analysis for the SDM and MFA around an instability island found using the CLD treated setup. Finally, Section 5.4 presents the procedure and experimental results obtained from the instability island's validation.

5.2. Damping analysis

One of the first authors to highlight the importance of damping on milling process with variable helix cutters was Sims in [27]. In this work, the author suggested that the system's structural dynamic is crucial in the variable-helix stability condition at a high axial depth of cut. This conclusion was achieved by analysing in simulations a regenerative-delayed-transfer function of a two teeth variable-helix tool. The author found that the real and imaginary components of this function are inversely proportional to the axial depth of cut and frequency. Thus, this means that the regenerative effect has less influence on the process stability because of the continuous variation of the time delays along the tool. Therefore, the dynamic response of the system has a higher impact on the process stability. This then led to the question that if the variable-helix milling process could be more sensitive to structural damping than conventional ones.

Based on these suggestions, the present section explores the role of damping on the existence of islands of instability while milling with variable-helix cutters. For this

purpose, the chatter stability behaviour of the milling tool with helix angles of 25°, 15°, and 10° is investigated under different levels of structural damping. It is worth mentioning at this stage that the system's frequency response function implemented for the chatter stability predictions slightly changed from the ones used in Chapter 4. This was caused by changes to the workpiece geometry to allow more cutting trials per copolymer acetal block. The new dimensions of the workpiece are a length of 170 mm, a depth of 44 mm, and a height of 38 mm. While doing these modifications, we attempted to keep the workpiece's mass as similar as possible to the original one, aiming to not significantly change the natural frequency of the system. Furthermore, a grinding procedure was applied to the internal faces of the side walls that connect the workpiece supporting platform and the fixed base of the flexure device (Figure 5.1). This was performed as a pre-treatment for a damping modification that required these surfaces as smooth as possible. These modifications are explained in subsequent sections. The FRF of the flexure device supporting the new workpiece is shown as a discontinuous black line in Figure 5.2. It is worth mentioning that this FRF only reflects the flexure dynamics after the grinding procedure, with no additional damping modifications. Furthermore, as a comparison, the same figure shows the FRF of the original system as a continuous blue line. The modal dynamic parameters estimated from the new FRF are a natural frequency of 296.82 Hz, a damping ratio of 0.153%, and stiffness of 3.85 kN/mm.

Consequently, the chatter stability predictions obtained using the MFA are shown in Figure 5.3 (a) and (b). The machining scenario implemented to perform these simulations is summarised in Table 5.1. Similarly as in Chapter 4, the MFA was configured with an ω_{max} of 450 Hz, Δa of 0.1 mm, and $\Delta\Omega$ of 15 rpm. From this plot, the discontinuous black line represents the stability predictions using the conventional tool, while the continuous blue line the ones with the variable helix cutter. Additionally, the value of k represents the number of waves per revolution imprinted by the tool on the workpiece surface. Subsequently, to explore the effect of damping on the chatter

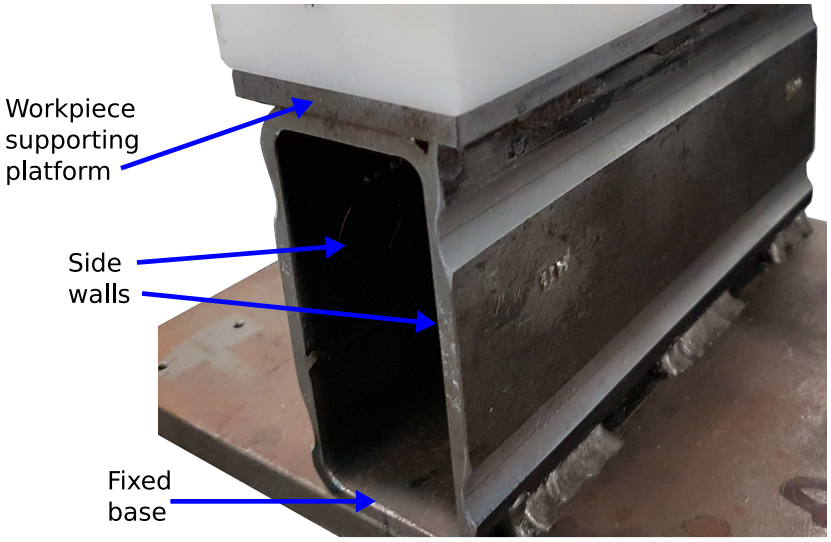

Figure 5.1.: Flexure device before CLD treatment

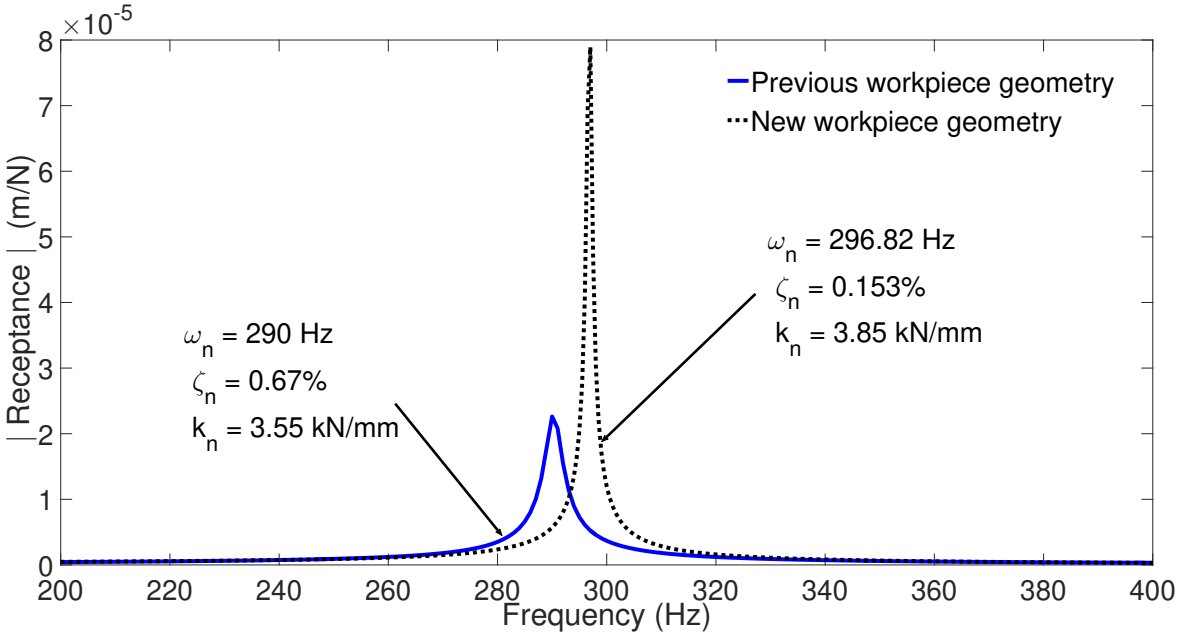

Figure 5.2.: Frequency response function of the flexure device with new workpiece geometry.

Parameter	**Value**
ω_{ny}	296.82 Hz
k_y	3.85 kN/mm
ζ_y	0.153%
ϕ_{10}, ϕ_{20}, ϕ_{30}	0°, 120°, 240°
γ_1, γ_2, γ_3	25°, 15°, 10°
Radial Immersion	50%
Tool Diameter	16 mm
Material	Copolymer Acetal
Kt	142.2 N/mm^2
Kr	18.9 N/mm^2
Cutting Condition	Up-milling
Normal Direction (flexible)	y (Figure 4.7)
Feed Direction (rigid)	$+x$ (Figure 4.7 pointing outside the page)

Table 5.1.: Machining Scenario

stability of this tool, the damping ratio was multiplied by a factor d_f while unchanging the remaining modal parameters, tool geometry, force coefficients, and simulation variables. Afterwards, the chatter stability of the updated system was determined and the outcomes at different d_f values are shown in Figure 5.4 (a) and (b).

In general, the plot shown in Figures 5.4 (b) suggests that the damping effect at higher spindle speeds ($k = 0$ and $k = 1$ lobes) only increases the minimum limiting axial depths of cut. On the other hand, low spindle speed lobes ($k \geq 2$ in Figure 5.4 (a)) reveal the appearance of several islands of instability at higher damping levels. For the $k = 2$ lobe, the predictions indicate that both ends of the lobe become closer while increasing the damping. However, the ends of the lobe around the spindle speed of 2500 rpm and 15 mm of the depth of cut become closer at a faster rate than the other

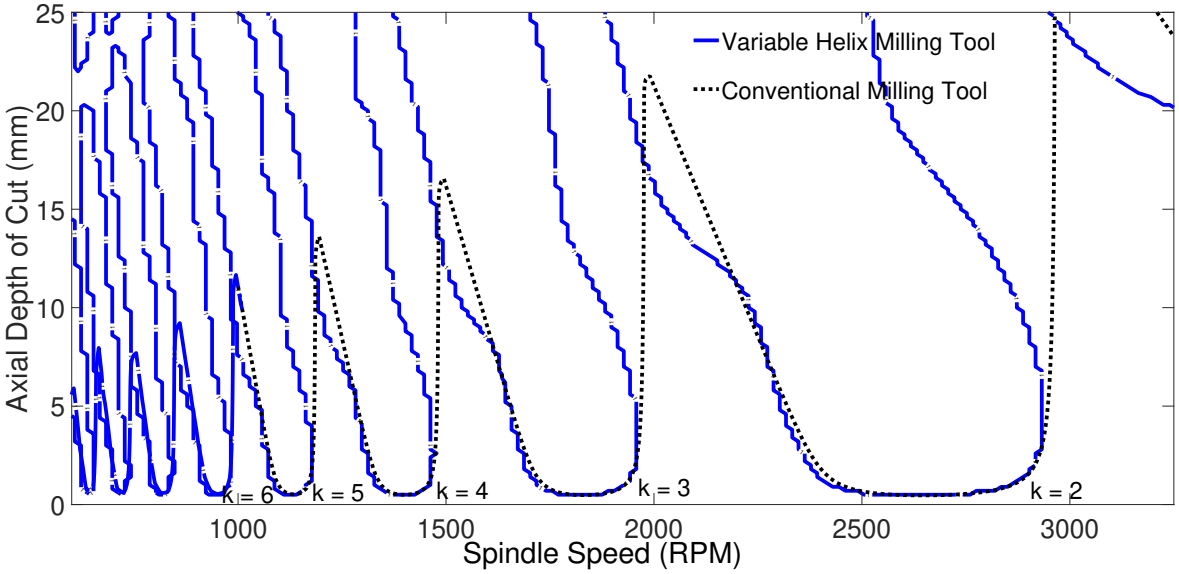

(a)

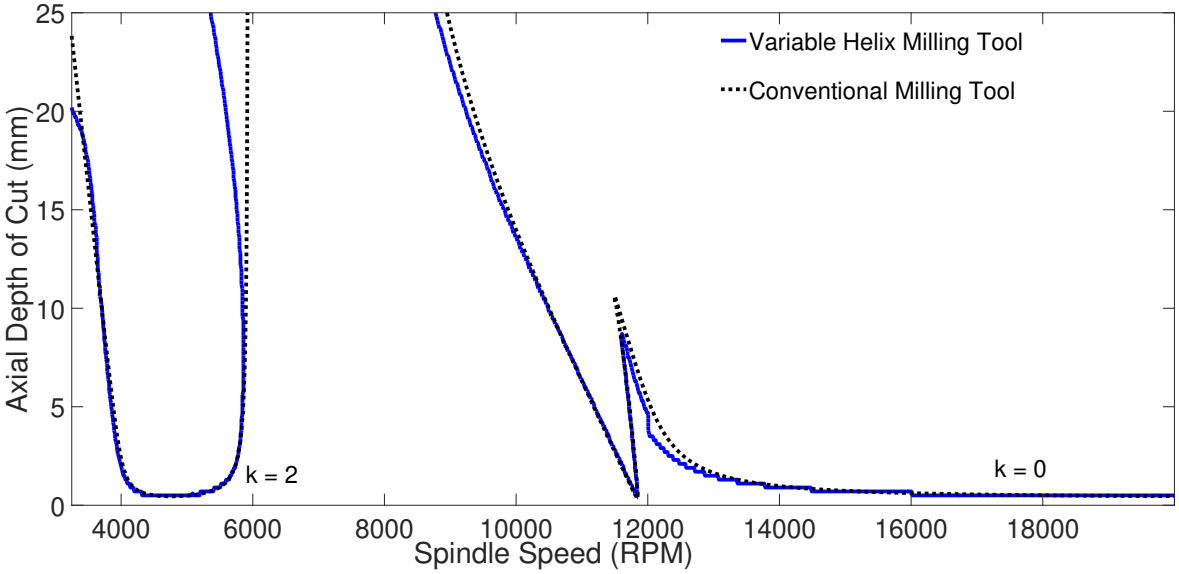

(b)

Figure 5.3.: MFA chatter stability predictions of the CLD treated system for the variable-helix milling tool with helix angles of 25°, 15°, and 10° for the spindle speed ranges from (a) 500 rpm to 3250 rpm and (b) 3250 rpm to 20000 rpm.

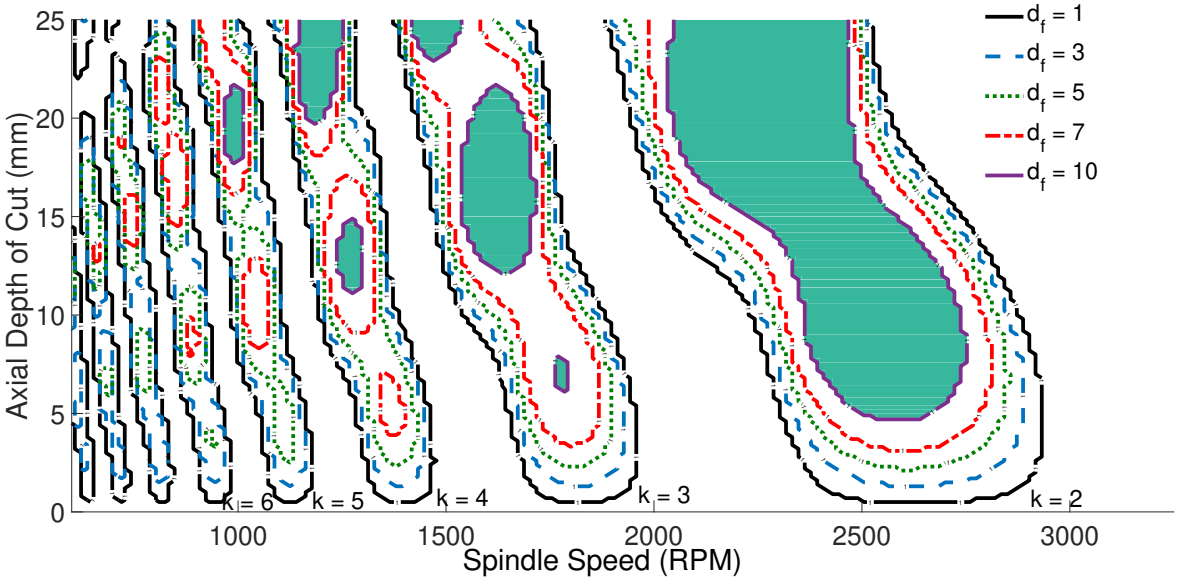

(a)

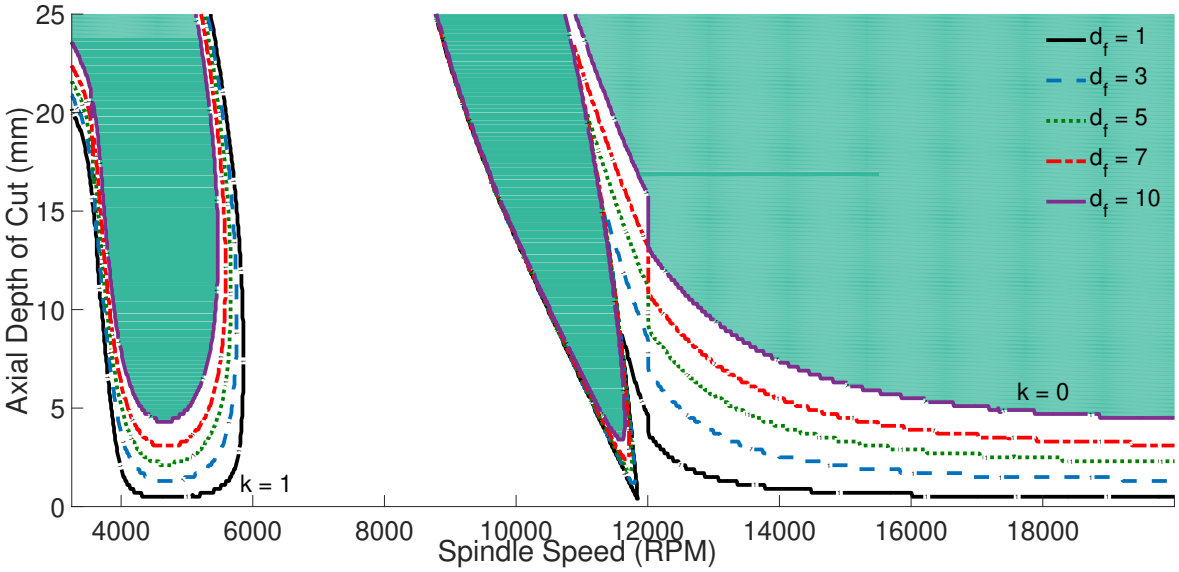

(b)

Figure 5.4.: Damping effect on the MFA chatter stability predictions of a variable-helix milling tool with helix angles of 25°, 15°, and 10° for the spindle speed ranges from (a) 500 rpm to 3250 rpm and (b) 3250 rpm to 20000 rpm. The damping ratio was increased by a factor d_f as $\zeta_n = d_f(0.153\%)$.

lobe regions. While the same behaviour occurs for the higher order lobes at $k = 3$ and $k = 4$, there are particular damping levels in which the lobes split into several unstable islands. For example, for the $k = 3$ lobe, when damping is ten times its original values, this lobe is divided into three regions. The first one is a small instability island starting at around 5 mm, another larger instability island at 12 mm, and an unstable region from 23 mm to 25 mm. The same behaviour occurs for the $k = 4$ lobe, but in this occasion at a damping ratio of seven times the original value. For this lobe in particular, when d_f is increased to 10, the small instability island located around 1500 rpm and 5 mm disappears. It is also noticed how the size of the instability island between 15 mm and 10 mm reduces in size when d_f increases from 7 to 10.

5.2.1. Structural dynamics

Based on the finding presented in Section 5.2, the current section seeks to increase the structural damping of the flexure device to recreate the conditions necessary for the appearance of an island of instability. For this purpose, constrained layered damping (CLD) are applied to the flexure device as shown in Figure 5.5 (b). CLD comprises a layer of viscoelastic material attached by an adhesive to the most significant curvature regions of a host structure [224–227]. Then, when the structure deforms, it induces a shear deformation in the viscoelastic material that dissipates energy. To further increase the shear effect, a metallic laminate is attached to the other side of this layer to constrain its deformation.

In this device, Figure 5.1 suggests that the primary sources of flexibility in this structure are the metallic side walls. For instance, when a force is applied to the workpiece, these plates bend pivoting around the grooves on the walls. Therefore, it was decided to place the CLD on the inside faces of the side walls. To install the CLD on the targeted locations, the aimed surfaces were first subjected to a grinding procedure. This was done seeking to remove unevennesses from the designated regions. As the supplier

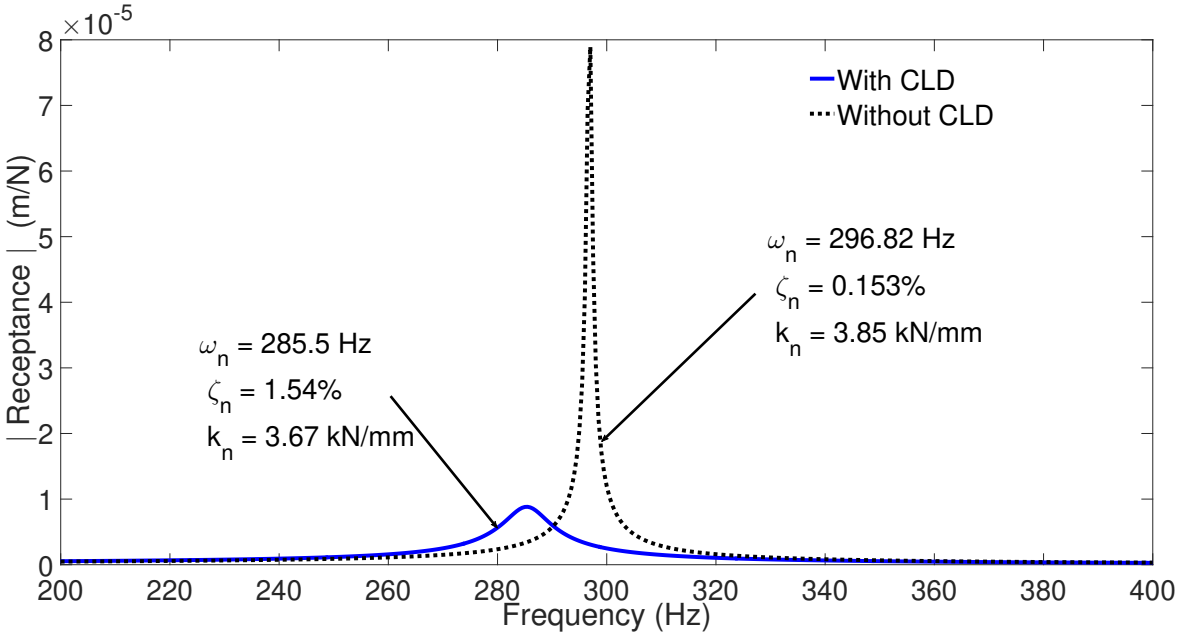

(a)

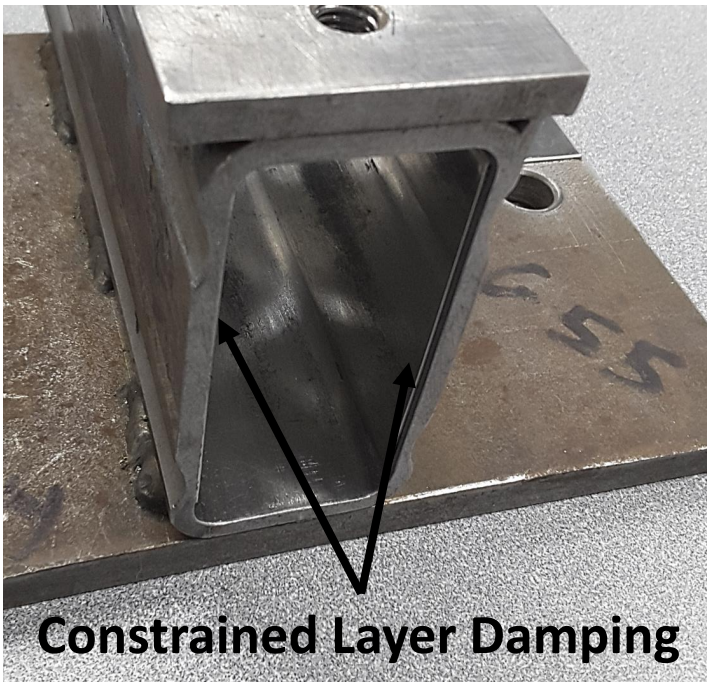

(b)

Figure 5.5.: (a) Frequency response function of the flexure without the constrained layer damping (black line) and with it (blue line). The natural frequency and stiffness of the system were slightly reduced while the damping was drastically increased by a factor of 10. (b) Placement of the CLD on the experimental flexure device.

suggested, the surface roughness of these regions was left within 0.1 mm to guarantee an effective performance. Subsequently, the areas were cleaned using a solvent to remove any residue or contaminant that may affect the CLD adherence. Next, the CLDs were attached to the host structure and kept under pressure using vices for about twenty-four hours. Afterwards, the pressure vices were removed from the flexure device, as it is shown in Figure 5.5 (b). Finally, an impact hammer test was performed to the CLD-treated system with the workpiece attached, to determine the FRF of the enhanced configuration. The obtained results are shown in Figure 5.5 (a), in which the estimated modal parameters are a natural frequency of 285.5 Hz, a modal stiffness of 3.65 kN/mm, and a damping ratio of 1.54%. This damping level is approximately ten times the value in the initial structure with the new workpiece. Finally, Figure 5.6 (a) and (b) show the stability lobe diagrams obtained with the CLD treated setup and the milling tools with helix angles of $25°/15°/15°$ and $25°/15°/10°$.

5.3. Convergence analysis

The present section aims to compare the convergence performance of the SDM and MFA around one of the instability islands found with the CLD treated system in Section 5.2.1. In particular, the island under study in this section is the one presented in Figure 5.6 (b), located in the $k = 3$ lobe between 12 and 22 mm of axial depth of cut. This instability island is shown in Figure 5.7.

From this island, the spindle speed of 1560 rpm was chosen to compare the SDM and MFA. At this spindle speed, the stability problem for the MFA was first solved assuming $p = 1$ (equation 3.43) harmonics in the solution. Afterwards, this value was increased by one harmonic until $p = 30$, and at every iteration, the upper and lower chatter stability boundaries of the island were predicted. Next, a similar procedure was followed for the SDM, in which number of samples per revolution M (equation

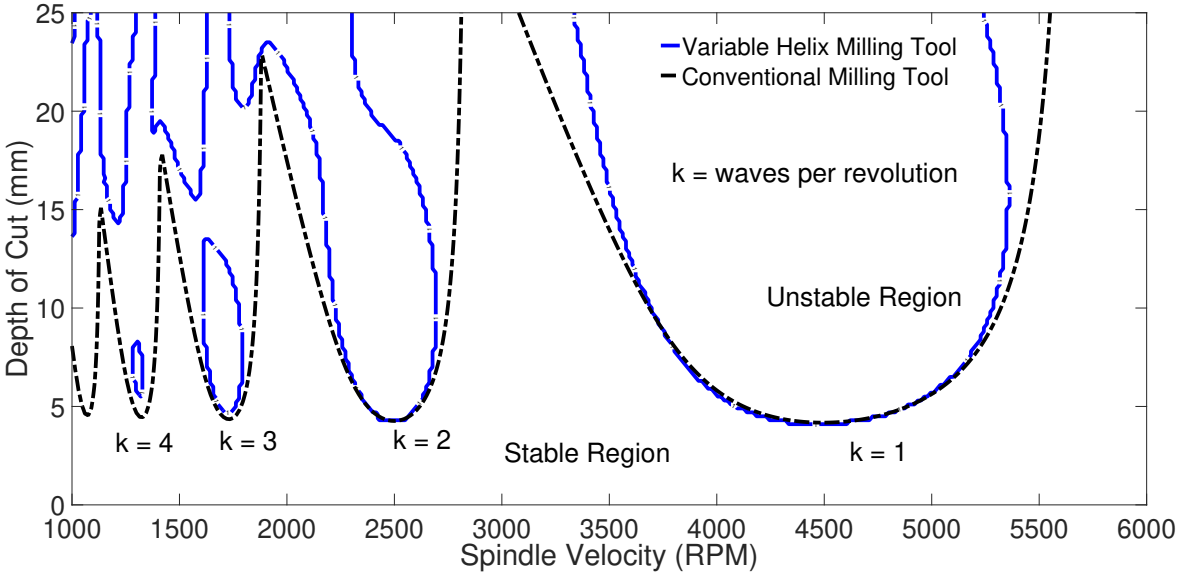

(a)

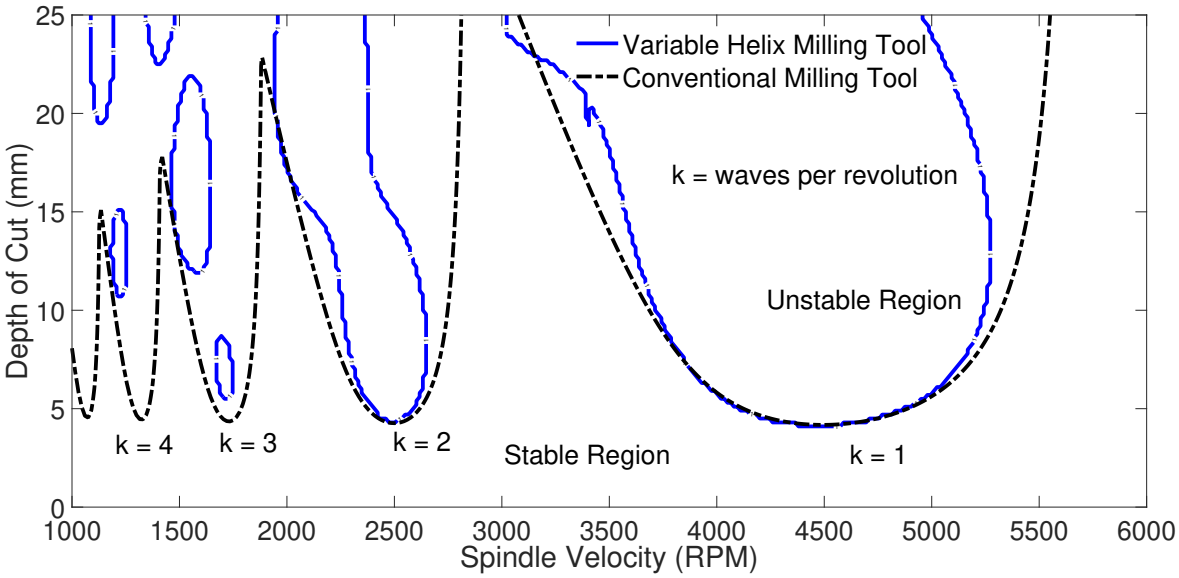

(b)

Figure 5.6.: MFA chatter stability predictions of the CLD treated system and the variable-helix milling tools with: (a) 25°, 15° and 15° and (b) 25°, 15°, and 10° of helix angle.

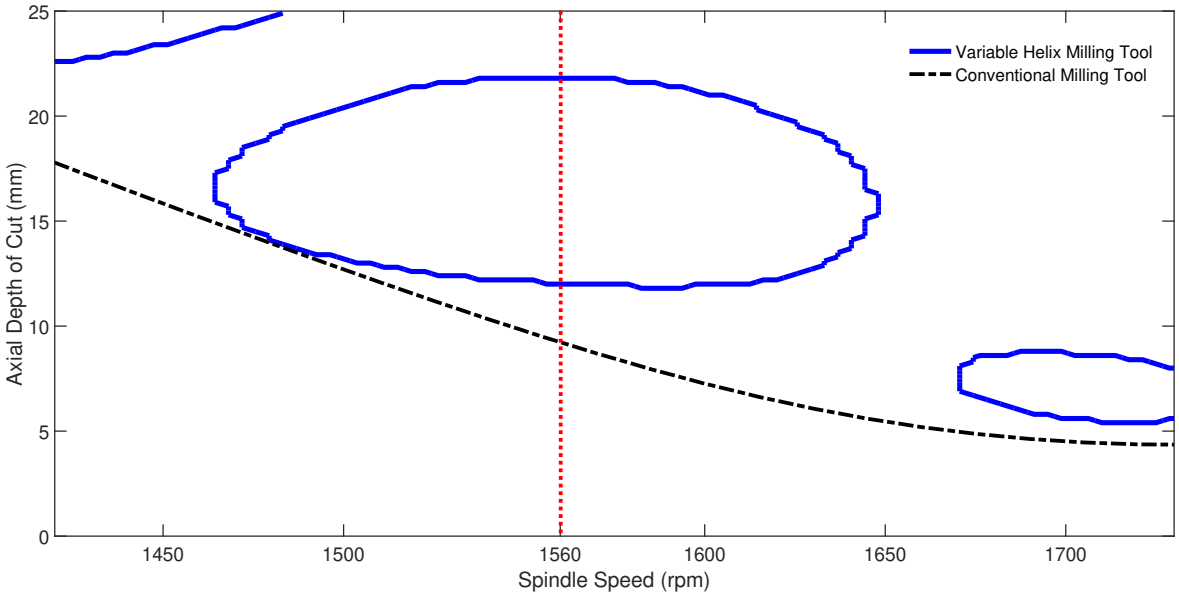

Figure 5.7.: Instability island predicted by the MFA using the CLD treated system along with the variable-helix milling tools with 25°, 15° and 10° of helix angle.

3.44 in Chapter 3) was normalised at multiples of the natural frequency η as,

$$M = \frac{60\eta f_n}{\Omega}, \tag{5.1}$$

in which f_n is the system's natural frequency in Hz and Ω is the spindle speed in rpm. The obtained results are shown in Figure 5.8, where the y-axis denotes the axial depth of the cut, the upper x-axis represents the number of harmonics p, and the lower x-axis the multiples of the natural frequency η.

From Figure 5.8, the blue dots and upper x-axis show that the minimum p value to at least detect one of the island boundaries is $p = 11$. Below this harmonic value, the MFA does not detect the instability condition in the milling process. At $p = 11$, the MFA only detects the lower boundary of the island, but fails to capture the further stabilization at higher depths of cut. Nevertheless, the MFA starts to detect the upper stability boundary of the island at $p = 12$. Later, while increasing p, these boundaries decreased or increased until they settle at 22 and 12 mm. The first boundary to

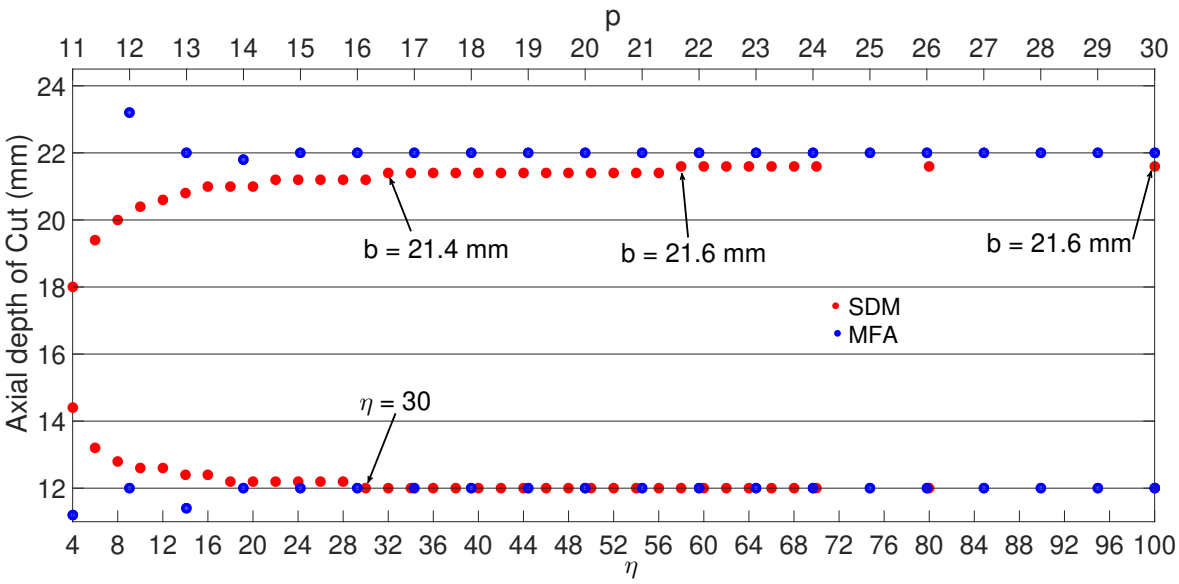

Figure 5.8.: Convergence Analysis for the MFA and SDM.

converge was the lower one at a $p = 14$, while the upper boundary at $p = 15$. For higher values of p, the stability boundaries remain unchanged at 22 and 12 mm, indicating that the minimum convergence p value is 15. At the spindle speed of 1560 rpm, this represents an ω_{max} of 403 Hz in the equation 3.43 presented in Chapter 3.

On the other hand, the results for the SDM (red dots and lower x-axis in Figure 5.8) suggest that the method struggles to converge to final solutions. For instance, the lower stability boundary converges to the same solutions as the MFA at $\eta = 30$. At this value, the upper boundary is 0.8 mm away from the solution estimated by the MFA. At higher sampling frequencies, the upper boundary slowly moved toward the value predicted by MFA, but it never achieves this at the largest simulated η value of 100.

As a computing performance comparison between MFA and SDM, chatter stability simulations were performed at 1560 rpm using the minimum convergence parameters for the MFA, and a $\eta = 30$ for the SDM. This was implemented on a computer with 16 GB of RAM, and an Intel(R) Core(TM) i7-6700k running at 4 GHz. From these simulations, the MFA could predict the boundaries in 0.55 minutes while the SDM in

32.1 minutes. This then means the MFA was 58 times faster than the SDM. However, although the computing-time difference may be caused by code optimisation, the convergence analysis revealed that the MFA provides a converged and more accurate solution than the SDM. This crucial property is of more vital importance while predicting the chatter stability boundaries of high-precision milling processes.

A convergence analysis was also performed for the SDM and MFA using the conventional milling tool with 25° of helix angle. In this case, the chatter stability boundaries were predicted while varying p from 1 to 30 for the MFA, and η from 4 to 30 for the SDM.

The convergence results are shown in Figure 5.9. For the MFA, the method predicts an stability boundary at 7.8 mm when $p = 11$, and remains at this axial depth of cut value until $p = 13$. At $p = 14$, the stability boundary converges to 8.6 mm where it stays until the end of the simulation. Comparing this behaviour with the variable-helix milling tool, $p = 14$ also represents the minimum number of harmonics required by the lower stability boundary of the island to converge to a final solution in Figure 5.8. Regarding the SDM, it initially predicts a stability boundary of 9.6 mm at $\eta = 4$, but gradually converges toward the boundary calculated by MFA at higher values of η. SDM finally settles at 8.6 mm when $\eta = 23$. In contrast to the variable-helix milling tool, this η value is less than the minimum required by the lower island boundary to settle in a final solution ($\eta = 30$ in Figure 5.8).

Another comparison can be done by manually selecting and keeping as constant the value of p indistinctly of the spindle speed as Altintas in [77]. In contrast, the approach presented in Chapter 3 automatically adjust the p value at a spindle speed Ω by the maximum FRF frequency ω_{max} (equation 3.43).

Simulations performed using different p values are shown in Figure 5.10, in which the continuous blue line represents the chatter stability predictions implementing the MFA of Chapter 3, and the discontinuous red, green, and black subsequent stability

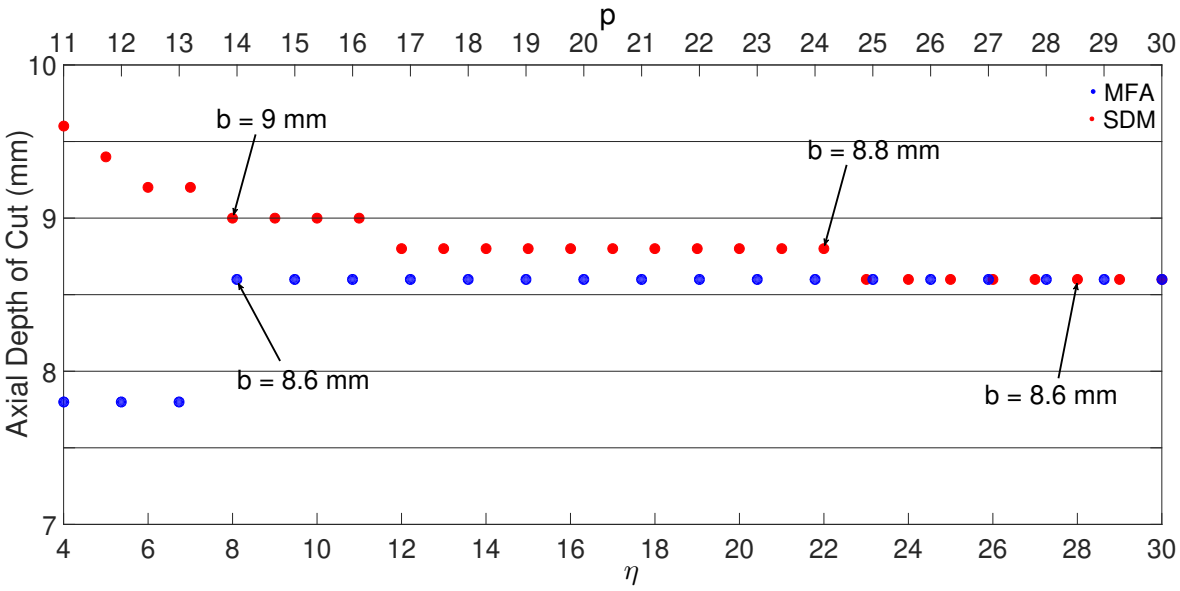

Figure 5.9.: Convergence Analysis for the MFA and SDM using the conventional milling tool.

predictions using a fixed number of harmonics of $p = 10$, $p = 11$, and $p = 12$. For $p = 12$, the results suggest that while the method captures the island of instability, lower spindle-speed regions of the unstable island appear to be skewed to the left. Afterwards, at $p = 11$, the method detects the island as connected to a small unstable region on the upper left corner of the diagram. Finally, the method fails to capture the island of instability at $p = 10$ and presents it as an unstable lobe. Consequently, while implementing the fixed harmonic p approach, it is recommended to perform a convergence analysis at the lowest analysed spindle speed, to determine the maximum number of harmonics to predict the stability lobe diagram. Otherwise, the method could fail in capturing the stability boundaries, resulting in unwanted chatter vibrations in practice. The reason for performing this analysis at the lowest spindle speed is that it represents the largest fundamental excitation period of the periodic dynamic cutting system. Therefore, the tool and workpiece are allowed to vibrate for a longer period before completing the main cutting cycle. This condition is translated into a higher frequency content in the vibrational spectrum. Consequently, this requires more p

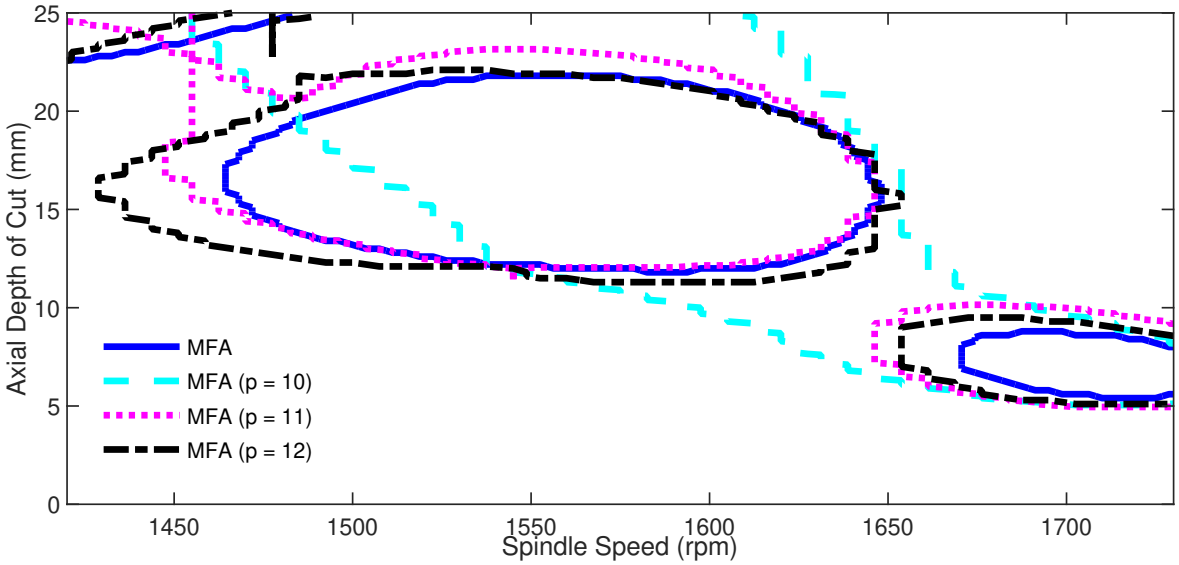

Figure 5.10.: Chatter stability prediction around an instability island at different p values. The method implemented in these simulations assumes a fixed number of harmonics p at every spindle speed. As a comparison, the predictions obtained using the method proposed in Chapter 3 are overlaid as continuous blue lines.

harmonics in the solution to capture the full process dynamics.

5.4. Experimental validation of a variable-helix island of instability

A similar experimental procedure as in Chapter 4 is followed in this section to experimentally validate the instability island predicted using the CLD-treated workpiece dynamic. Due to the increment on the length of the workpiece, a group of seven trials can be performed on the workpiece instead of six. Furthermore, in contrast with the experiment in Chapter 4, the milling trails on this occasion are executed at non-equally spaced axial depths of cut to allow performing more tests in regions of particular interest. Additionally, extra tests were done around specific areas to better estimate

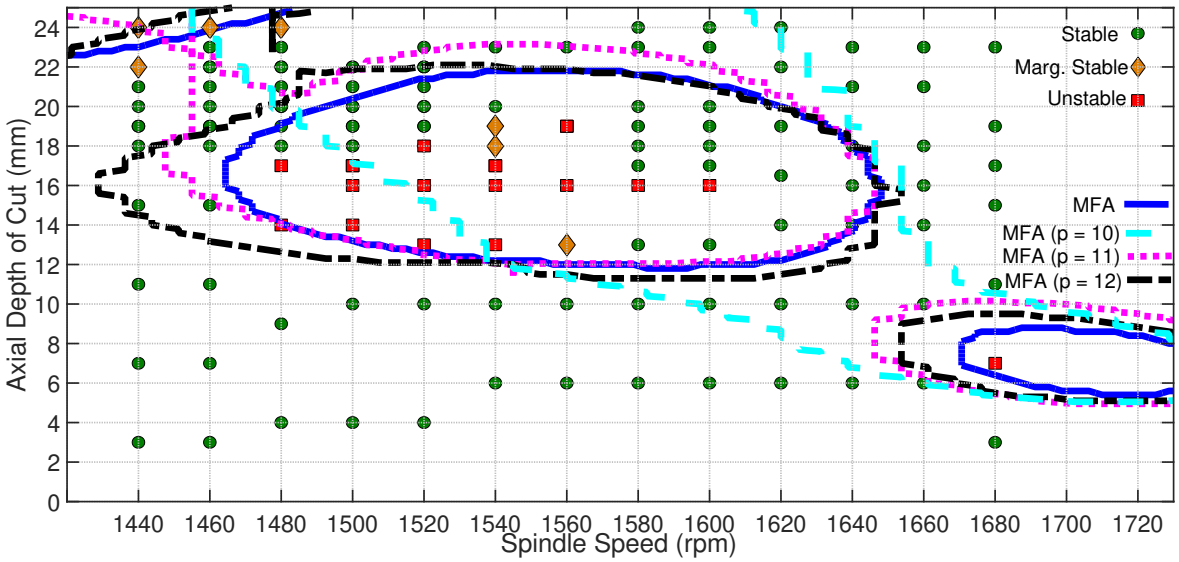

Figure 5.11.: Experimental results from the validation of the chatter stability prediction of a island of instability obtained with a milling tool with 25°, 15° and 10° of helix angles.

the boundaries near the island. The trials were executed using a feed per tooth of 0.05 mm/tooth, half immersion, and up-milling condition. The results are summarised in the stability lobe of Figure 5.11. Here, green dots represent stable tests while red squares are unstable ones. Marginally stable cases are shown as orange diamond markers. Overall, good agreement was found between the experiments and the estimated stability boundaries. Most importantly, the experiments show an instability island close to the predicted behaviour.

For example, a detailed analysis of the results obtained at 1540 rpm is described in Figure 5.12. Here, the left column shows the acceleration time series in blue lines, with once-per-revolution samples superimposed as red dots. The green square indicates the steady-state region, manually chosen to build the Poincaré section shown on the right side.

It is clear from Figure 5.12 (a) that the process at 6 mm is stable. This was also reflected in the acceleration and sound FFT spectrums. At 13 mm, the Poincaré section

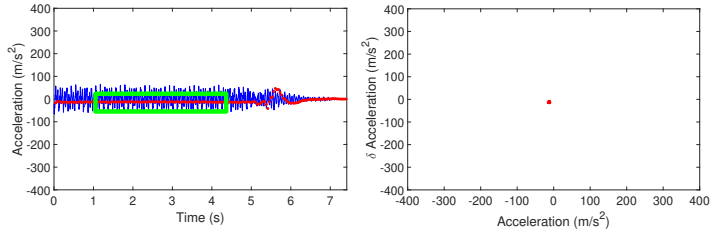

(a)

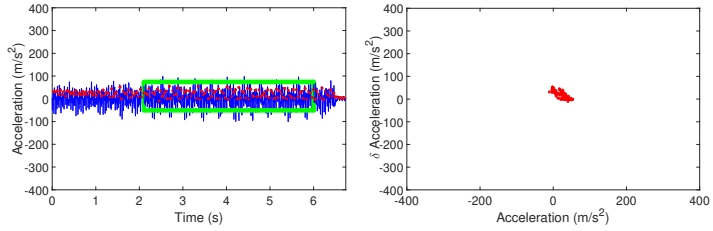

(b)

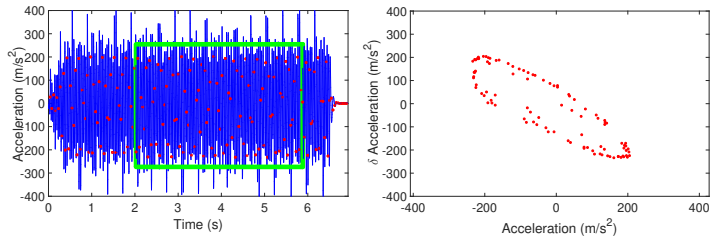

(c)

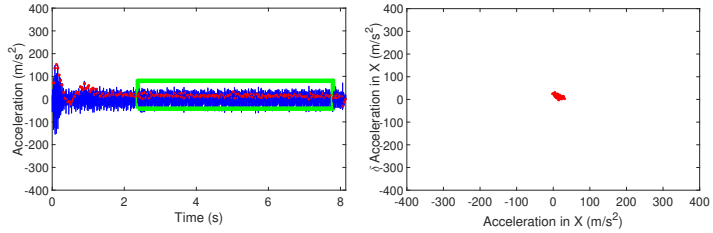

(d)

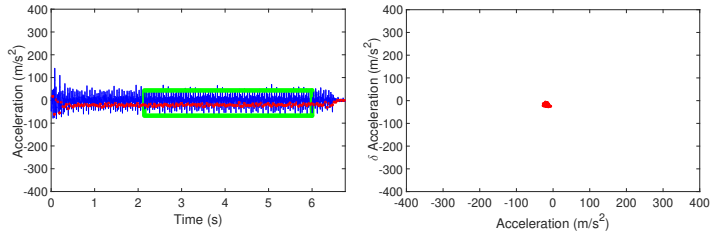

(e)

Figure 5.12.: Time series (blue line) and once per revolution samples (red dots) of the acceleration data at a spindle speed of 1540 rpm and axial depth of cut of 6mm (a), 13mm (b), 16mm (c), 19mm (d), and 20mm (e). The steady state region of the process is defined by the green rectangle.

reveals a small transition to a quasi-periodic motion, associated with a secondary Hopf bifurcation [228]. As the axial depth of cut is increased to 16 mm, the magnitude of this quasi-periodic motion also increases. At 19 mm, even though the acceleration FFT and Poincaré section suggested that the process was stable, the sound signal FFT revealed the opposite. Figure 5.13 (a) and (b) show that the dominant frequency at 19 mm does not coincide with multiples of the tool-rotation frequency (25.67 Hz). Therefore, the trial was declared as marginally stable. Later at 20 mm, the process becomes fully stable, showing that the dominant frequency corresponds to a tool-passing-frequency harmonic.

Additionally, Figure 5.14 shows the surface profile for the milling trials at 10 mm (a), 13 mm (b), 16 mm (c), 19 mm (d), and 20 mm (d). The y axis from these plots represents the surface profile in μm, while the x axis is the tested length. Because of several accessibility issues performing the tests, the measurements were performed diagonally to the feed direction. In general, these results agree with previous conclusions about the stability condition of the trials.

While the preliminary outcomes manifested the presence of an island of instability, it is noticeable that this island appears to be smaller than the predicted one. These discrepancies may result from the frequency and temperature dependency of the CLD viscoelastic material [229–231]. First, the loading frequency plays a key role because it relates to the strain-rate dependency of the material. This is caused by the molecule rearrangements inside the material while being deformed. Secondly, an increment or decrement in temperature can subsequently result in a strengthening or weakening of the molecular bonds, impeding or promoting their relative motion. Consequently, these combined effects can change the material loss factor and shear modulus, altering the overall damping effect [229, 232]. To explore the impact of this issue on the current island, a stability simulation was performed by artificially increasing the damping of the original system by 30%. The remaining simulation parameters were left unchanged. Figure 5.15 shows the original and modified islands of instability, as well as the ex-

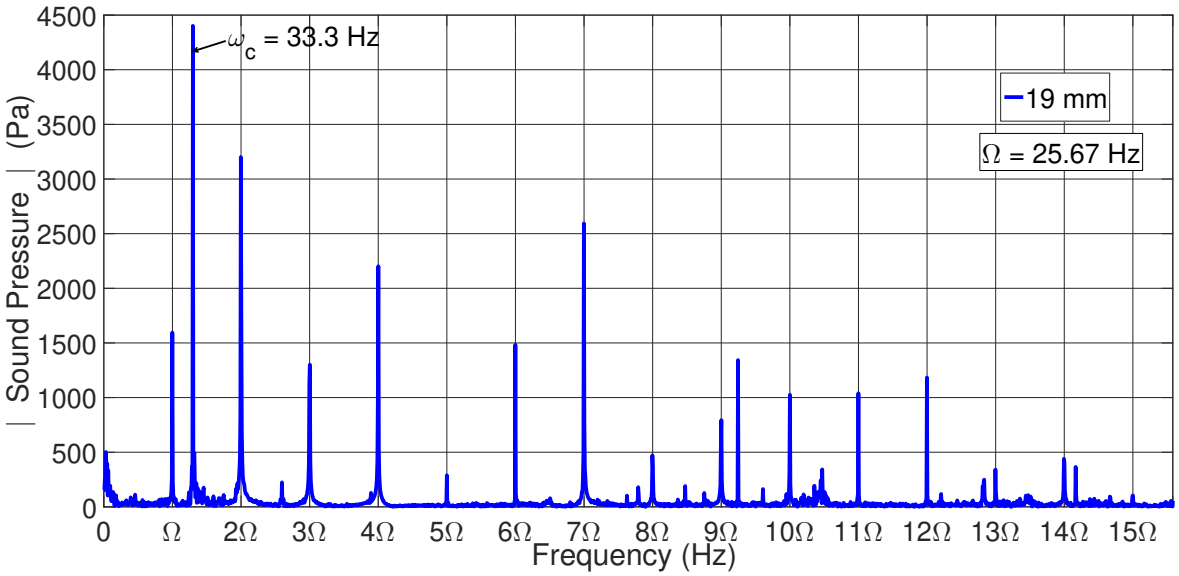

(a)

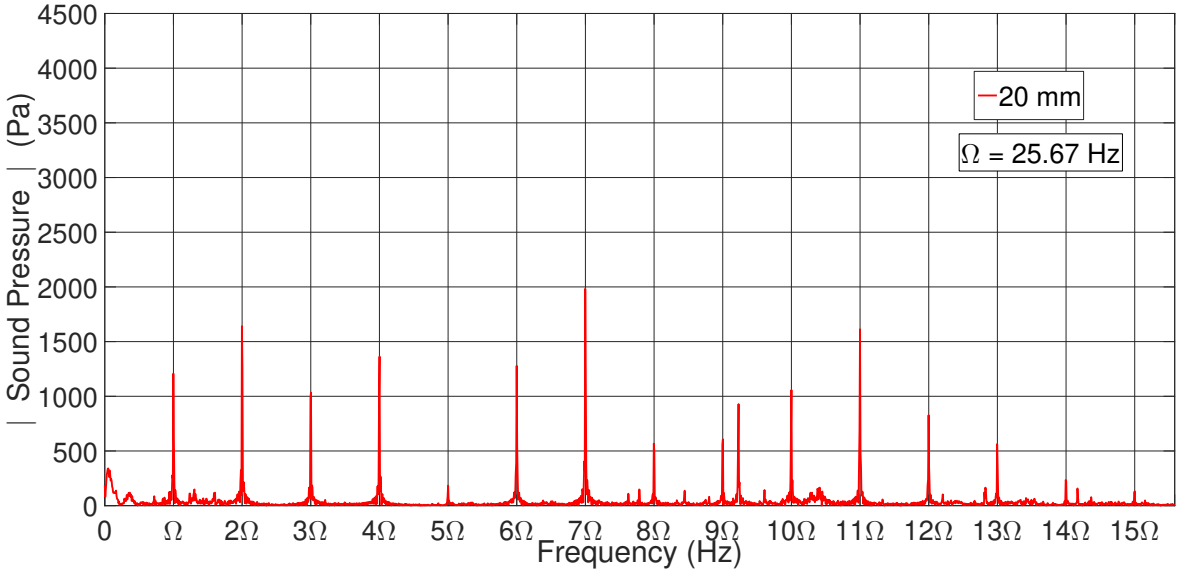

(b)

Figure 5.13.: Frequency spectrum of the audio signal for the milling trial at 1540rpm and 19mm (a) and 20mm (b) depth of cut.

perimental results. The simulation outcomes suggest a better approximation to the experimental results. As in Section 4.7, the preliminary outcomes appear to be shifted to the left. Again, this may be caused by the mass removed from the workpiece, that locally alters the chatter stability boundaries.

To further validate the modelling approach, a similar procedure was performed for the island of instability found in the $k = 3$ lobe with the milling tool of 25°, 15°, and 15° (Figure 5.6 (a)). The experimental results are summarised in Figure 5.16. Even though the results appeared to be slightly shifted up and to the right from the predictions, the overall shape suggests an isolated island. The discrepancies could be attributed to small variations in the boundary conditions (e.g. clamping forces) that may change the workpiece natural frequency.

For this tool, a ramped-axial-depth-of-cut test was also performed using a ramped workpiece with a similar mass as the original one. The experiment was configured such as the axial depth of cut varied from 3 mm to 17 mm across the 170 mm length of the cut. The results are shown in Figure 5.17. Here, the acceleration data (blue lines) and the once-per-revolution samples (red dots) are plotted against the axial depth of cut (lower x axis) and time (upper x axis). The test starts as a stable process after a small transitory region. Later, at about 4.5 mm of axial depth of cut, a period-doubling bifurcation hints that the process is moving towards a more unstable state inside the island. Afterwards, a continuous secondary Hopf bifurcations from 4.5 to 14 mm of the axial depth of cut shows that the process is unstable inside the island. After this, the process becomes stable until the end of the trial. These results agree with the stability predictions presented in Figure 5.16.

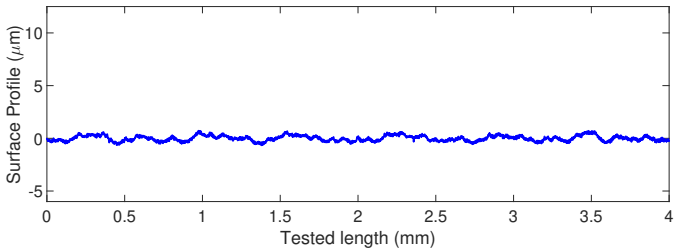

(a)

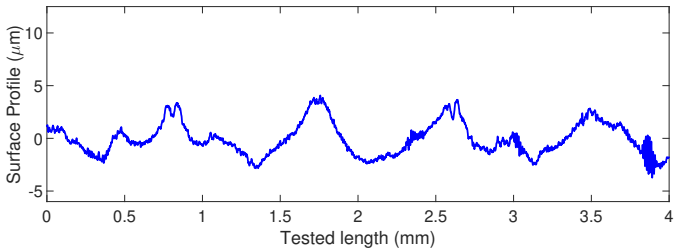

(b)

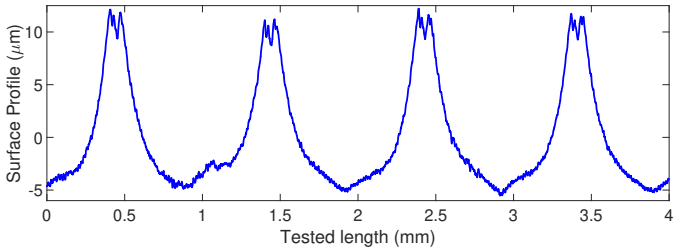

(c)

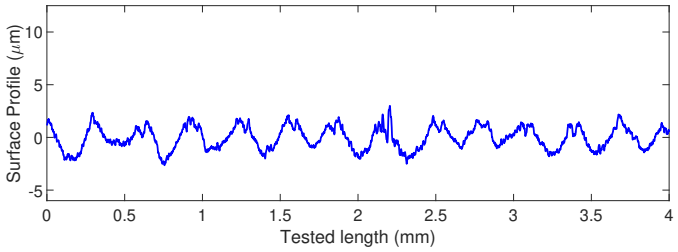

(d)

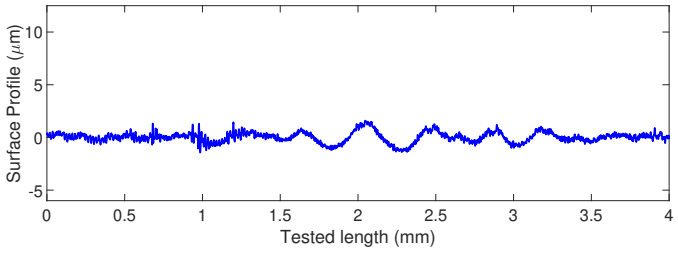

(e)

Figure 5.14.: Workpiece surface profile data at a spindle speed of 1540 rpm and axial depth of cut of 6mm (a), 13mm (b), 16mm (c), 19mm (d), and 20mm (e).

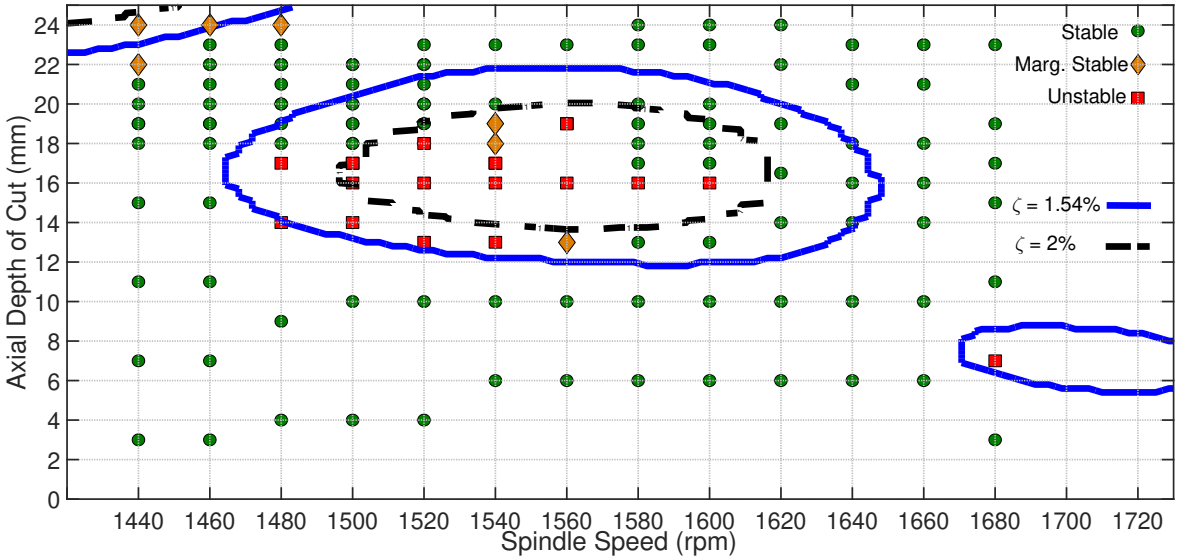

Figure 5.15.: Comparison between the islands of instability obtained with the original system, and a hypothetical system with 30% higher modal damping.

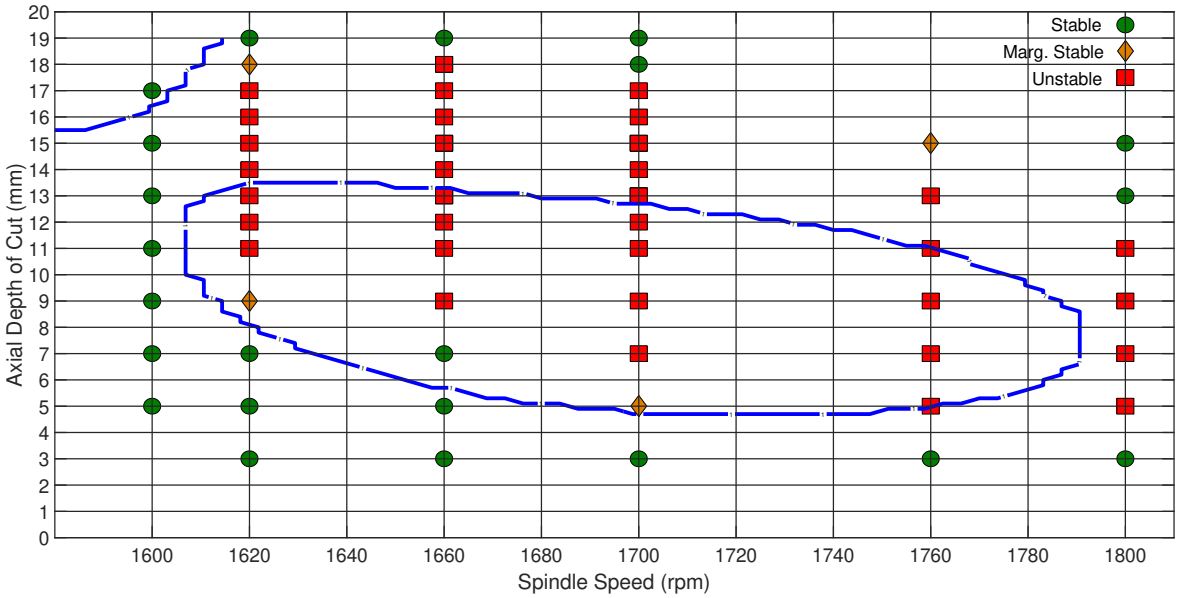

Figure 5.16.: Instability island found with a milling tool with 25°, 15° and 15° of helix angles.

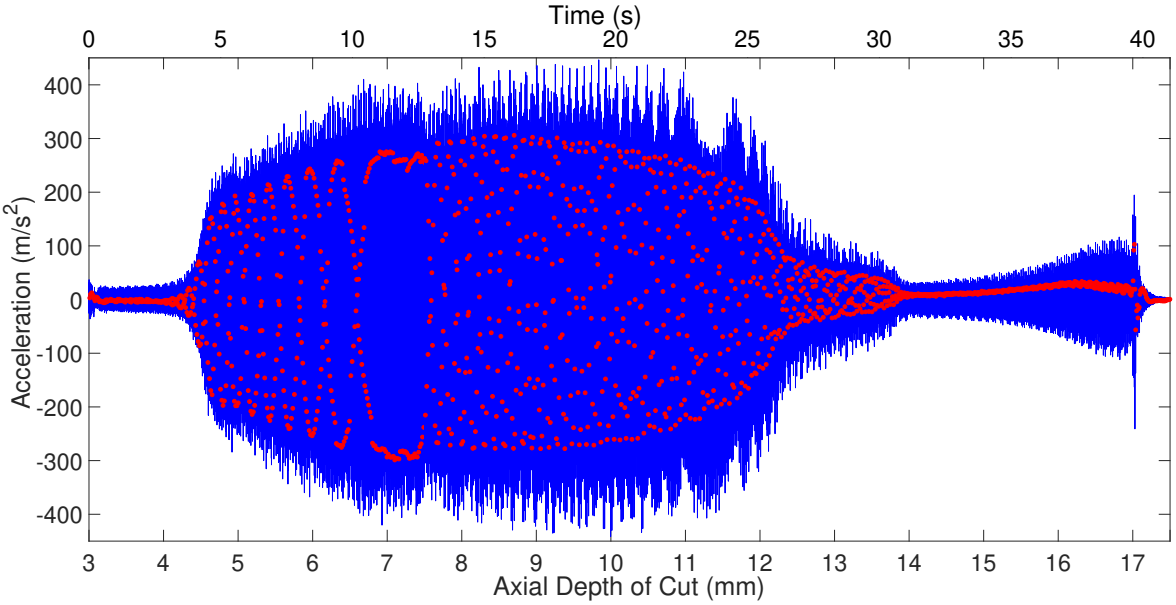

Figure 5.17.: Acceleration and once-per-revolution values of the ramped workpiece test with the tool of 25°,15°, and 15° of helix angles, at 1760rpm.

5.5. Summary

The current chapter presented the damping and convergence analysis and the experimental validation of instability islands using a one-degree-of-freedom scaled experiment. The analysis was performed using a milling tool of 16 mm of diameter and helix angles of 25, 15, and 10 degrees. For the damping analysis, the dynamic parameters of the original experimental setup were initially implemented to determine a stability diagram. Afterwards, the structural damping was systematically increased in the simulations while keeping the remaining dynamic parameters constant. The simulation outcomes revealed that at particular levels of damping, the lobes in the diagram split into several isolated unstable regions. If the damping is then further increased, these regions can be eliminated from the diagram. To validate this phenomenon, constrained layer damping was used to increase the damping of the experimental setup. By doing so, this parameter was increased 10 times, while keeping small changes in the other dynamic parameters. As a result, it was possible to recreate one of the stability diagrams

constructed in the damping analysis, in which several unstable islands were found.

Subsequently, a convergence analysis around one unstable island was performed using the SDM and MFA. In this study, at a particular spindle speed, the lower and upper stability boundaries of the island were calculated using both methods. The results revealed that the SDM struggled to converge to final solutions when compared to the MFA. While both methods converged to the same solution for the lower boundary, the SDM slowly approached but did not converge to a definite upper boundary value as did the MFA. These results then suggest that the isolated unstable region shown by the SDM in Chapter 4 was indeed connected to the main lobe, as the MFA predicted.

Before the validation process, stability predictions were also obtained for a milling tool of 16 mm of diameter and helix angles of 25, 15, and 15 degrees. Again, several instability islands were found in the spindle speed vs axial depth of the cut diagram.

Next, a set of experimental trials were carried out around particular instability islands for both tools, aiming to capture these conditions. The final results suggested that the islands were in the tested regions. A ramped workpiece test was further performed for the island obtained with the 25, 15, and 15 degrees of the helix angle tool. At a particular spindle speed, this workpiece configuration allowed to increase gradually the axial depth of cut across the entire island height. Time-series and once-per-revolution acceleration plots showed the stable-to-unstable stability transitions while getting inside the island, and from unstable to stable while leaving it.

6. Conclusions and Future Works

6.1. Thesis Summary

The current thesis began with Chapter 1, presenting a brief introduction to different aspects regarding milling. It first defined milling process and discussed the different milling configurations. Afterwards, the vibrations that occur in milling were discussed, giving special emphasis to the type studied in this work named regenerative chatter vibrations. Later, Chapter 1 discuss the different approaches for chatter suppression, showing that the focus of the project is the one using variable-helix milling cutters. Afterwards, the instability islands that emerge using these tools are presented, and they are compared with the islands found with conventional milling tools. The last section showed the thesis aim and objectives, along with a thesis outline.

Chapter 2 presented the thesis literature review, beginning from some early chatter studies. The chapter then showed how these early works served as a backbone for most advanced chatter prediction methods such as the MFA, SDM and the FDM. Later, the chapter presented several chatter detection techniques, discussing the different sensors and signal processing methods implemented for this purpose. Afterwards, active and passive chatter suppression approaches were discussed, a section in which the literature reviewed was focused on the passive approach of using variable-helix milling tools. Finally, the literature review about islands of instability in the milling process was outlined, presenting the most relevant works about this topic.

Next, the theoretical background of regenerative chatter was introduced in Chapter 3. This chapter started studying the regenerative effect on a single point cutting process. By using this simple example, key features of regenerative chatter stability were described. Subsequently, it presented the two analytical chatter stability prediction approaches for variable-helix milling cutters, these being the SDM and the MFA. The programs used throughout the project were then tested using a case study found in the literature.

Afterwards, Chapter 4 aimed to validate the variable-helix stability lobe diagram at a larger axial depth of cut using a scaled experiment. The experimental setup consisted of an instrumented one-degree-of-freedom flexure device that held a workpiece made of copolymer acetal. With this setup, it was possible not only to scale the system dynamics but also the cutting force coefficients allowing to reach larger depths of cut while assuming linear dynamics. Besides, Chapter 4 explored the effect of the flutes helix angles on the cutting force coefficients, concluding that these effects were translated into minimal variations in the stability lobe diagram. Chapter 4's last section validated the variable-helix stability diagram around a potential instability island.

Finally, Chapter 5 demonstrated the effect of structural damping on the occurrence of variable-helix unstable islands. It was shown in simulations that increasing the level of structural damping to certain levels, the lobes in the stability diagram may split into isolated unstable regions. Then, the convergence of the SDM and MFA were tested around a defined unstable island. It was found that the SDM struggled to converge to island boundaries at a particular spindle speed, while the MFA could settle on solutions at a faster convergence rate.

6.2. Conclusions and Original Contributions

In this thesis, the dynamics of variable helix milling tools have been explored using a novel stability analysis approach with rigorous experimental validation. It can be concluded that:

1. Variable-helix tools can exhibit large islands of instability on the stability lobe diagram.

2. The islands of instability have been shown to be highly dependent on the structural damping values within the system.

3. The stability analysis methods for variable-helix tools are particularly susceptible to convergence issues.

4. Using a multi-frequency solution approach based upon a harmonic transfer function ensures a guaranteed convergence of the stability prediction, overcoming this convergence issue. The approach relies upon the Fourier series and the first and second shift theorems.

Some of the original contributions to knowledge found in this thesis are:

1. Enhancement of the MFA to consider non-equal cutting force coefficients on the flutes, as well as vibrations in the feed and normal direction.

   The MFA for variable helix and pitch milling tools proposed by Sims in [51] was initially developed assuming vibrations only in the feed direction. Additionally, it assumes equal cutting force coefficients on the tool flutes regardless of the helix angle. However, it is known from the literature that the helix angle affects these coefficients, so variable-helix milling tools possess non-equal cutting constants on the flutes. Consequently, the modelling equations implemented in the current thesis were enhanced in Chapter 3 to allow this condition. In Chapter

4, the stability lobe diagram of a variable-helix milling tool with 25°, 15° and 10° of helix angle was predicted using the modified and the original MFA. For modified MFA, the coefficients of every tool flute were separately estimated using single-tooth milling cutters. Furthermore, for the original MFA, the cutting force coefficients were determined using a conventional milling tool with 25° of helix angle. A subsequent comparison between the chatter predictions from both methods revealed minor discrepancies. However, these minor variations could be related to the smaller helix angle differences between tool flutes. It was found in the literature studies about the effect of the helix angle on the magnitude of the coefficients, that exposed considerably larger coefficient variations with more pronounce tool configurations [218–220]. Future works may seek to explore this phenomenon with other more complex irregular milling cutter configurations (e.g. harmonically varied and serrated tools), in which helix angle on the flutes experience further non-constant variations (Figure 1.4).

2. The experimental validation for the first time of variable-helix instability islands using an scaled experiment.

   These unstable islands were validated using an instrumented scaled experiment that comprises a one-degree-of-freedom flexure device, and the novelty of employing a workpiece made of lower-cutting-force coefficients. This novel approach allows us to assume low-order linear structural dynamics through a broader spectrum of axial depths of cut in the stability charts. Additionally, it substantially lessens the tool-wear mechanism throughout the experiments, facilitating the isolation of tool geometry effect on the stability lobe diagram. Consequently, this experimental setup provides a reliable, faster, and cost-effective way to validate chatter-stability models of non-conventional milling tools. Previous studies using one-degree-of-freedom devices and variable-helix milling tools utilised metal alloys as workpiece materials [25, 171, 217]. Therefore, the high-magnitude cutting forces did not allow studying the processes at larger depths of cut without

inducing in the system a highly nonlinear vibratory state. As a result, the re-stabilisation property of variable-helix cutters at larger axial depths of cut had not been experimentally explored across the literature. This characteristic plays a key role in the emergence of instability islands in the stability lobe diagram.

The material implemented in the current thesis was a thermoplastic known as copolymer acetal. It was found throughout the literature that the linear mechanistic cutting force model has been extensively implemented to predict the machining forces with this thermoplastic within specific cutting conditions [25, 171, 217]. However, cutting trials performed outside these regions exhibited complex non-linear force behaviours that require enhanced models to describe the cutting mechanics. To test linearity in the current thesis, a set of experiments using single-flute milling tools were defined using the mechanistic identification method of cutting force coefficients. The cutting conditions selected for these tests were based on experimental data found in the literature that provided an overall perspective about cutting force behaviour of this thermoplastic. The preliminary results from the tests validated the linearity assumption, showing a linear relationship between the average cutting forces and the feed per tooth within the selected cutting conditions. Consequently, the cutting force coefficients were calculated using the proportionality constants from these linear relationships [77].

Subsequently, the one-degree-of-freedom assumption of the experimental setup was tested analysing the FRF of the flexure with the workpiece attached and the machine tool. These FRF measurements were obtained from impact tests. The tap testing revealed that only source of flexibility leading to regenerative chatter was the workpiece compliance in the normal direction. Afterwards, the experimental configuration was instrumented with an accelerometer and microphone for chatter detection. Additionally, a Hall Effect sensor was employed to gather once-per-revolution samples of the acceleration data. Therefore, it was possible to analyse the bifurcations that emerge from unstable trials.

Although a potential island of instability was found in Chapter 4 using a milling tool with 25°, 15°, and 10° of helix angle, it was later found that the island was connected to another lobe. Nevertheless, these experimental results further validated the assumptions made regarding the dynamic behaviour of the system and the machinability of the thermoplastic. Additionally, they validated the property of the variable-helix milling tools to further re-stabilise at larger axial depths of cut when compared with conventional ones. Subsequently, a damping analysis in Chapter 5 helped to recreate the conditions leading to a variable-helix instability island with the before mentioned tool. Further chatter predictions performed using another variable-helix milling cutter with 25°, 15°, and 15° of helix angle also reveal islands of instability. In these cases, experimental results around these conditions agreed with the island predictions, representing the first-ever experimentally captured islands of instability in the literature.

The scaled experimental setup with reduced dynamics considerably simplified the complexity of the problem. This then isolated the effect of the tool geometry and damping that lead to the variable-helix islands of instability. However, to recreate these unstable conditions in industrial setups while machining metal alloys raises several challenges. First, the higher cutting forces generated with metal alloys can excite multiple modes of vibrations of the machine tool and workpiece in different directions. Therefore, the combined dynamics of both the machine tool and workpiece must be included in the stability analysis, leading to further unstable coupling behaviours that could undermine the re-stabilisation property of the variable-helix milling tools. Additionally, it was shown that this condition mainly emerges at larger axial depths of cut, where the regenerative effect is mostly altered by the continuous pitch variation. However, increasing the depths of cut to such levels may induce a symmetry-breaking condition in which the higher force vibrations change the tool-workpiece engagement, as shown by Totis in [233]. This then results in further non-linearities in the cutting process

that are not captured by linear dynamic milling models. To avoid this issue, it can be implemented variable-helix milling tools with higher pitch gradient (equations 3.3.1 and 3.14). Therefore, a greater regenerative-effect alteration can be achieved at lower axial depths of cut. As a result, it may be possible to generate islands of instability at relatively lower axial depths of cut, where the before-mentioned issues are not so prominent. However, the chip evacuation should be taken into consideration when designing the geometrical configuration of the variable helix milling cutter.

3. Proving the effect of the structural damping on the occurrence of variable-helix milling islands of instability.

   Similar as with conventional milling tools, increasing the structural damping of a dynamic cutting system with variable-helix milling tools leads to an increment of the absolute minimum axial depth of cut of the stability lobe diagram. However, with a variable-helix milling process, this may also promote a splitting of the lobes into several unstable isolated regions. Simulations performed in Chapter 5 using different levels of structural damping showed that some regions within the unstable lobes converged faster to stable states than others when the damping was increased. This behaviour was particularly noticeable at lower spindle speeds when the lobes were narrower. This splitting condition may be related to the continuous helix-induced pitch variations between the teeth along the axial length of the variable-helix tool. From previous studies about the optimisation of variable-pitch milling tool, it is known that some pitch configurations may lead to a better chatter performance than others [160, 161]. Some researches have also shown how undesired vibrations can be attenuated, or even completely suppressed, by simply fine-tuning the pitch arrangement of a variable-pitch milling tool [234]. These studies implemented indexes to quantify the regenerative-effect levels of a cutting process in particular locations of the stability lobe diagram [170, 235]. With variable helix milling tools, because of the pitch angles vary along the axial

length of the cutter, there should be unstable regions in the stability lobe diagram with higher and lower regenerative impact [236–238]. Therefore, unstable areas with a lower regenerative effect may converge faster to stable conditions when the damping is increased, leading to the before-mentioned splitting of the lobe. Nevertheless, this phenomenon requires further investigations, so it will be the subject of future works.

Using dampers to dissipate excessive vibratory energy is one of the most implemented ways to suppress chatter in the industry. Extensive research has been done about active and passive damping approaches [239], that has shown significant improvements in the chatter performance of milling processes. However, special caution should be taken while implementing these methods with variable-helix milling tools, or irregular milling cutters in general. For example, thin-walled components have been machined with irregular milling tools [151, 152]. Because of the lower dynamic stiffness of the workpiece, active fixtures have been employed to increase the damping and stiffness of the workpiece. However, while this approach can provide substantial chatter improvement, it may cause islands of instability that can pass undetected if they are not analysed with converged chatter prediction methods.

4. Demonstrating that these islands are particularly sensitive to convergence issues of the implemented chatter prediction method.

   This finding is of significant importance because it shows that using a non-converged chatter prediction method may lead to considerable inaccuracies in stability lobe diagram of variable-helix milling tools. In Chapter 4, for example, the SDM predicted an island of instability in the stability chart while the MFA showed otherwise. Further experimental results later agreed with the MFA predictions, suggesting that SDM may have convergence issues around this condition. Subsequently, a convergence analysis was performed around a variable-helix

instability island, that was found from a damping analysis in Chapter 5. The simulation outcomes confirmed the initial assumptions about SDM convergence, showing that the method struggles to settle into solutions when compared with the MFA.

5. The redaction of the conference papers: *Stability of variable helix milling: model validation using scaled experiments* and *Convergence Analysis of the Multi-Frequency Approach around an Instability Island*, published in the 8th CIRP Conference on High Performance Cutting and the 17th CIRP Conference on Modelling of Machining Operations.

6.3. Future Works

Based on the experience acquired through the thesis development, the following recommendations can be made for eventual future research:

- During the validation process, one of the main challenges experienced by the author was the variations of structural damping. These oscillations maybe because of the CLD temperature sensitivity, manufacturing inaccuracies, and/or unequal clamping between the workpieces. Even though these fluctuations were small, they may affect in some sense the experimental results, due to the sensitivity of the islands to the dynamic parameter. Experiments performed using the same setup without the CLD provided an even closer agreement. Therefore, an improved experimental setup can be developed to allow a more controlled linear damping variation, e.g. eddy current damping, that may overcome this problem. Further modifications can be done to explore also the stiffness variations effects on variable-helix instability islands.

- While the current study focused on the instability islands that emerge while using variable-helix milling tools, future works may explore unstable or even stable

islands with more complex tool setups. Irregular configurations such as the variable helix and pitch tools, serrated milling cutters, and harmonically varied helix milling tools may generate interesting phenomenons in the stability lobe diagram. For example, computer simulations in the literature have shown that harmonically varied helix milling tool (Figure 1.4) can lead to islands of instability [189]. Regarding serrated milling tools, these characteristics can be studied using different serration patterns (e.g. circular, sinusoidal, or trapezoidal). In every case, advanced multi-variable optimisation techniques such as the genetic algorithms can be implemented for searching unstable islands in the stability charts. For this purpose, the structural damping and key geometrical features of the tool can be used as variables in the optimisation problem. The objective functions can be based on regenerative indexes measuring the severity of regenerative effect in particular regions of the stability lobe diagram.

- In Chapter 4, for the cutting system implemented, it was mentioned that the flute helix effects on the cutting force coefficients and the stability lobe diagram were negligible. Nevertheless, this assumption may not be true for milling systems using more complex cutter configurations such as harmonically varied and serrated milling tools. In these cases, the coefficients may become functions dependent on the axial and/or radial depths of cut to take into account the local variations throughout the flutes. These models can be calibrated utilising experimental data and advanced optimisation techniques (e.g. evolutionary algorithms).

- The experimental configuration used in this project assumed a one-degree-of-freedom flexible workpiece, to avoid that further phenomena such as mode coupling may obscure the experimental results. Future works may also explore the variable-helix islands occurrence using a flexible two-degree-of-freedom system. For example, it can be implemented a scaled two-degree-of-freedom setup similar to the one proposed by Rubeo et al. in [240]. This experimental configuration even allows changing the damping, mass, and stiffness of the workpiece to

satisfy experimental requirements. Therefore, it may enable tuning the workpiece structural dynamics for a specific variable-helix milling tool, to generate islands of instability in the stability lobe diagram. Using a flexible configuration like this while machining metal alloys may require reducing the radial depths of cut of the milling processes. This to allow attaining larger axial depths of cut where instability islands are more prone to emerge. Consequently, this may also demand taking into account the tool runout while predicting these unstable islands. For example, Otto et al. in [173] predicted the stability lobe diagram of a variable-helix cutter with and without runout. While the differences between the diagrams at full slotting were negligible, the author found several discrepancies at 25% of radial immersion. Machining metal alloys may further require implementing coolant instead of dry cuts, as in the current study. Therefore, this reduces the cutting temperatures and forces, limiting the tool wear that may negatively affect the preliminary results.

- Future works may also seek to determine variable-helix instability islands using enhanced chatter prediction models. These improved models can include non-linearity sources from either the cutting force process (e.g. power or polynomial force models), or the structural dynamics (e.g. cubic stiffness). Comparing the stability predictions and performing a bifurcation analysis using both the linear and non-linear models can provide insight on the impact of these non-linearities on variable-helix unstable islands.

7. Bibliography

[1] T. Schmitz, *Machining Dynamics, Frequency Response to Improved Productivity.* Springer, 2009.

[2] H. A. Youssef and H. El-Hofy, *Machining Technology: Machine Tools and Operations.* CRC Press, 2008.

[3] C. J. Li, H. C. Tseng, M. S. Tsai, and C. C. Cheng, "Novel servo-feed-drive model considering cutting force and structural effects in milling to predict servo dynamic behaviors," *International Journal of Advanced Manufacturing Technology*, vol. 106, no. 3-4, pp. 1441–1451, 2020.

[4] T. Mohanraj, S. Shankar, R. Rajasekar, N. R. Sakthivel, and A. Pramanik, "Tool condition monitoring techniques in milling process-a review," *Journal of Materials Research and Technology*, vol. 9, no. 1, pp. 1032–1042, 2020.

[5] G. Wu, W. Pan, X. Wang, J. Mo, and S. Ding, "Chatter and deformation in machining thin-walled flexible components," *IOP Conference Series: Materials Science and Engineering*, vol. 423, no. 1, 2018.

[6] I. Del Sol, A. Rivero, L. N. L. de Lacalle, and A. J. Gamez, "Thin-wall machining of light alloys: A review of models and industrial approaches," *Materials*, vol. 12, no. 12, 2019.

[7] S. Seguy, G. Dessein, and L. Arnaud, "Surface roughness variation of thin wall milling, related to modal interactions," *International Journal of Machine Tools and Manufacture*, vol. 48, no. 3-4, pp. 261–274, 2008.

[8] B. Stone, *Chatter and Machine Tools*. Springer, 2014.

[9] S. A. Tobias, *Machine-tool vibration*. J. Wiley, 1965.

[10] S. A. Tobias and W. Fishwich, "Theory of Regenerative Machine Tool Chatter (II)," *The Engineer*, vol. 205, no. I, pp. 238–239, 1958.

[11] E. Budak and Y. Altintas, "Analytical Prediction of Chatter Stability in Milling, Part I: General Formulation," *Journal of Dynamic Systems, Measurement, and Control*, vol. 120, no. 1, pp. 22–30, 1998.

[12] E. Budak and Y. Altintas, "Analytical prediction of chatter stability in milling, Part II: Application of the general formulation to common milling systems," *Journal of Dynamic Systems, Measurement, and Control*, vol. 120, no. 1, pp. 31–36, 1998.

[13] H. E. Merrit, "Theory of Self-Excited Machine-Tool Chatter: Contribution to Machine-Tool Chatter Research," *Journal of Manufacturing Science and Engineering*, vol. 17, pp. 447–454, 1965.

[14] J. Tlusty, "A method of analysis of machine tool stability," in *Proceedings of the 6th International Machine Tool Design and Research Conference*, 1965, pp. 5–14.

[15] J. Tlusty and F. Ismail, "Basic Non-Linearity in Machining Chatter," *CIRP Annals - Manufacturing Technology*, vol. 30, no. 1, pp. 299–304, 1981.

[16] M. A. Laboratories, "CUTPRO Fundamentals of Machining," 2013.

[17] A. Kaufnerová and J. Kutlwašer, "Measuring stability of the cutting process when turning using txf metalmax software," *Annals of DAAAM and Proceedings of the International DAAAM Symposium*, vol. 30, no. 1, pp. 982–988, 2019.

[18] R. F. Harik, H. Gong, and A. Bernard, "5-axis flank milling: A state-of-the-art review," *CAD Computer Aided Design*, vol. 45, no. 3, pp. 796–808, 2013.

[19] R. B. D. Pereira, L. C. Brandão, A. P. de Paiva, J. R. Ferreira, and J. P. Davim, "A review of helical milling process," *International Journal of Machine Tools and Manufacture*, vol. 120, no. May, pp. 27–48, 2017.

[20] Y. Altintas, "Virtual High Performance Machining," *Procedia CIRP*, vol. 46, pp. 372–378, 2016.

[21] Y. Altintas and D. Aslan, "Integration of virtual and on-line machining process control and monitoring," *CIRP Annals - Manufacturing Technology*, vol. 66, no. 1, pp. 349–352, 2017.

[22] G. Quintana and J. Ciurana, "Chatter in machining processes: A review," pp. 363–376, 2011.

[23] H. Gao, X. Liu, S. Y. Liang, and L. Wang, "A review of chatter vibration research in milling," *Chinese Journal of Aeronautics*, no. September 2018, 2019.

[24] A. Yusoff and N. Sims, "Optimisation of variable helix end milling tools by minimising self excited vibration," *Journal of Physics: Conference Series*, vol. 181, 2009.

[25] M. Zatarain, J. Muñoa, G. Peigne, and T. Insperger, "Analysis of the influence of mill helix angle on chatter stability," *CIRP Annals - Manufacturing Technology*, vol. 55, no. 1, pp. 365–368, 2006.

[26] Q. Xie, "Dynamics and stability predictions of variable helix milling," in *Conference on Mechatronics, Electronic, Industrial and Control Engineering*, 2015, pp. 282–286.

[27] N. D. Sims, "Fast chatter stability prediction for variable helix milling tools," *Proceedings of the Institution of Mechanical Engineers, Part C: Journal of Mechanical Engineering Science*, vol. 230, no. 1, pp. 133–144, 2016.

[28] F. W. Taylor, "The Art of Cutting Metals," *American society of mechanical engineers*, vol. 63, no. 1618, pp. 25 929–25 931, 1907.

[29] H. Ernst, *Physics of Metal Cutting in Machining of Metals*. American Society for Metals, 1938.

[30] M. E. Merchant, "Mechanics of the metal cutting process. I. Orthogonal cutting and a type 2 chip," *Journal of Applied Physics*, vol. 16, no. 5, pp. 267–275, 1945.

[31] E. Merchant, "Mechanics of the metal cutting process. II. Plasticity conditions in orthogonal cutting," *Journal of Applied Physics*, vol. 16, no. 6, pp. 318–324, 1945.

[32] R. N. Arnold, *The Mechanism of Tool Vibration in the Cutting of Steel: Cutting Tools Research: Report of Sub-committee on Carbide Tools*. Institution of Mechanical Engineers, 1945.

[33] P. R. N. Arnold and G. A. Hankins, "The Mechanics of the Cutting Operation," *Proceedings of the Institution of Mechanical Engineers*, vol. 155, no. 1, pp. 238–240, 1946.

[34] S. Tobias and W. Fishwich, "Theory of Regenerative Machine Tool Chatter (I)," *The Engineer*, vol. 205, pp. 199–203, 1958.

[35] C. Andrew and S. A. Tobias, "A critical Comparision of two current theories of machine tool chatter," *International Journal of Machine Tool Design and Research*, vol. 1, pp. 325–335, 1961.

[36] J. Tlusty and M. Polacek, "The stability of machine tools against self-excited vibrations in machining," in *Proceedings of the ASME International Research in Production Engineering*, vol. 1, Pittsburgh, USA, 1963, pp. 465–474.

[37] J. Tlusty and P. MacNeil, "Dynamics of Cutting Forces in End Milling," *Annals of the CIRP*, vol. 24, no. 1, pp. 21–25, 1975.

[38] J. Tlusty, F. Ismail, and W. Zaton, "Use of Special Milling Cutters Against Chatter," pp. 408–415, 1983.

[39] Y. Altintas and E. Budak, "Analytical Prediction of Stability Lobes in Milling," *CIRP Annals - Manufacturing Technology*, vol. 44, no. 1, pp. 357–362, 1995.

[40] T. Insperger and G. Stépán, "Semi-discretization method for delayed systems," *International Journal for Numerical Methods in Engineering*, vol. 55, no. 5, pp. 503–518, 2002.

[41] Y. Ding, L. Zhu, X. Zhang, and H. Ding, "A full-discretization method for prediction of milling stability," *International Journal of Machine Tools and Manufacture*, vol. 50, no. 5, pp. 502–509, may 2010.

[42] R. L. Kegg, "Cutting dynamics in machine tool chatter," *J. of Engng. for Indust.*, vol. 87, pp. 464–470, 1965.

[43] R. Sridhar, R. E. Hohn, and G. W. Long, "A General Formulation of the Milling Process Equation," *Journal of Engineering for Indus*, pp. 317–324, 1968.

[44] N. Olgac and M. Hosek, "A new perspective and analysis for regenerative machine tool chatter," vol. 38, pp. 783–798, 1998.

[45] S. Smith and J. Tlusty, "Efficient Simulation Programs for Chatter in Milling," *CIRP Annals - Manufacturing Technology*, vol. 42, no. 1, pp. 463–466, 1993.

[46] S. D. Merdol and Y. Altintas, "Multi Frequency Solution of Chatter Stability for Low Immersion Milling," *Journal of Manufacturing Science and Engineering*, vol. 126, no. 3, p. 459, 2004.

[47] P. V. Bayly, J. E. Halley, B. P. Mann, and M. A. Davies, "Stability of Interrupted Cutting by Temporal Finite Element Analysis," *Journal of Manufacturing Science and Engineering*, vol. 125, no. 2, p. 220, 2003.

[48] E. A. Butcher, H. Ma, E. Bueler, V. Averina, and Z. Szabo, "Stability of linear time-periodic delay-differential equations via Chebyshev polynomials," *International Journal for Numerical Methods in Engineering*, vol. 59, no. 7, pp. 895–922, 2004.

[49] D. Bachrathy and G. Stepan, "Improved prediction of stability lobes with extended multi frequency solution," *CIRP Annals - Manufacturing Technology*, vol. 62, no. 1, pp. 411–414, 2013.

[50] G. Stepan, J. Munoa, T. Insperger, M. Surico, D. Bachrathy, and Z. Dombovari, "Cylindrical milling tools: Comparative real case study for process stability," *CIRP Annals - Manufacturing Technology*, vol. 63, no. 1, pp. 385–388, 2014.

[51] N. D. Sims, "Multi-frequency Chatter Analysis Using the Shift Theorem," *Procedia IUTAM*, vol. 22, pp. 3–9, 2017.

[52] A. Otto, S. Rauh, S. Ihlenfeldt, and G. Radons, "Stability of milling with non-uniform pitch and variable helix Tools," *International Journal of Advanced Manufacturing Technology*, vol. 89, no. 9-12, pp. 2613–2625, 2017.

[53] P. V. Bayly, B. P. Mann, T. L. Schmitz, D. A. Peters, G. Stepan, and T. Insperger, "Effects of Radial Immersion and Cutting Direction on Chatter Instability in End-Milling," no. July 2015, 2008, pp. 351–363.

[54] T. Insperger and G. Stépán, "Updated semi-discretization method for periodic delay-differential equations with discrete delay," *International Journal for Numerical Methods in Engineering*, vol. 61, no. 1, pp. 117–141, 2004.

[55] T. Insperger and G. Stépán, *Semi-Discretization for Time-Delay Systems*, 2011.

[56] T. Insperger, G. Stépán, and J. Turi, "On the higher-order semi-discretizations for periodic delayed systems," *Journal of Sound and Vibration*, vol. 313, no. 1-2, pp. 334–341, 2008.

[57] S. Jiang, Y. Sun, X. Yuan, and W. Liu, "A second-order semi-discretization method for the efficient and accurate stability prediction of milling process," *International Journal of Advanced Manufacturing Technology*, vol. 92, no. 1-4, pp. 583–595, 2017.

[58] N. D. Sims, B. Mann, and S. Huyanan, "Analytical prediction of chatter stability for variable pitch and variable helix milling tools," *Journal of Sound and Vibration*, vol. 317, no. 3-5, pp. 664–686, 2008.

[59] Y. Ding, L. Zhu, X. Zhang, and H. Ding, "Second-order full-discretization method for milling stability prediction," *International Journal of Machine Tools and Manufacture*, vol. 50, no. 10, pp. 926–932, 2010.

[60] Q. Quo, Y. Sun, and Y. Jiang, "On the accurate calculation of milling stability limits using third-order full-discretization method," *International Journal of Machine Tools and Manufacture*, vol. 62, pp. 61–66, 2012.

[61] C. G. Ozoegwu, S. N. Omenyi, and S. M. Ofochebe, "Hyper-third order full-discretization methods in milling stability prediction," *International Journal of Machine Tools and Manufacture*, vol. 92, pp. 1–9, 2015.

[62] X. Tang, F. Peng, R. Yan, Y. Gong, Y. Li, and L. Jiang, "Accurate and efficient prediction of milling stability with updated full-discretization method," *International Journal of Advanced Manufacturing Technology*, vol. 88, no. 9-12, pp. 2357–2368, 2017.

[63] Y. Liu, D. Zhang, and B. Wu, "An efficient full-discretization method for prediction of milling stability," *International Journal of Machine Tools and Manufacture*, vol. 63, no. May 2010, pp. 44–48, 2012.

[64] T. Insperger, "Full-discretization and semi-discretization for milling stability prediction: Some comments," *International Journal of Machine Tools and Manufacture*, vol. 50, no. 7, pp. 658–662, 2010.

[65] T. L. Schmitz and A. Honeycutt, "The Extended Milling Bifurcation Diagram," *Procedia Manufacturing*, vol. 1, pp. 466–476, 2015.

[66] B. Balachandran and M. Zhao, "A Mechanics Based Model for Study of Dynamics of Milling Operations," *Meccanica*, vol. 35, no. 2, pp. 89–109, 2000.

[67] M. X. Zhao and B. Balachandran, "Dynamics and stability of milling process," *International Journal of Solids and Structures*, vol. 38, no. 10-13, pp. 2233–2248, 2001.

[68] M. A. Davies, B. Dutterer, and J. Pratt, "On the Dynamics of High-Speed Milling with Long, Slender Endmills," *CIRP Annals - Manufacturing Technology*, vol. 47, no. 1, pp. 55–60, 1998.

[69] A. Honeycutt and T. L. Schmitz, "Milling bifurcations: A review of literature and experiment," *Journal of Manufacturing Science and Engineering, Transactions of the ASME*, vol. 140, no. 12, pp. 1–19, 2018.

[70] N. H. Hanna and S. A. Tobias, "A theory of nonlinear regenerative chatter," *Journal of Manufacturing Science and Engineering, Transactions of the ASME*, vol. 96, no. 1, pp. 247–255, 1974.

[71] H. Moradi, M. R. Movahhedy, and G. Vossoughi, "Linear and Nonlinear Model of Cutting Forces in Peripheral Milling: A Comparison Between 2D and 3D Models," in *Volume 3: Design and Manufacturing, Parts A and B*. ASME, 2010, pp. 955–962.

[72] B. P. Mann, N. K. Garg, K. A. Young, and A. M. Helvey, "Milling bifurcations from structural asymmetry and nonlinear regeneration," *Nonlinear Dynamics*, vol. 42, no. 4, pp. 319–337, 2005.

[73] Z. Dombovari and G. Stepan, "On the bistable zone of milling processes," *Philosophical Transactions of the Royal Society A: Mathematical, Physical and Engineering Sciences*, vol. 373, no. 2051, 2015.

[74] H. M. Shi and S. A. Tobias, "Theory of finite amplitude machine tool instability," *International Journal of Machine Tool Design and Research*, vol. 24, no. 1, pp. 45–69, 1984.

[75] D. Bachrathy, G. Stépán, and J. Turi, "State Dependent Regenerative Effect in Milling Processes," *Journal of Computational and Nonlinear Dynamics*, vol. 6, no. 4, p. 041002, 2011.

[76] D. Bachrathy and G. Stepan, "Fold bifurcation in the state-dependent delay model of milling - Analytical and numerical solutions," in *Proceedings of the*

ASME Design Engineering Technical Conference, vol. 4, no. PARTS A AND B, 2011, pp. 521–527.

[77] Y. Altintas, *Manufacturing Automation: Metal Cutting Mechanics, Machine Tool Vibrations, and CNC Design.* Cambridge University Press, 2012.

[78] J. Tlusty and G. Tlusty, *Manufacturing Processes and Equipment.* Prentice Hall, 2000.

[79] A. Weremczuk, R. Rusinek, and J. Warminski, "Bifurcation and stability analysis of a nonlinear milling process," *AIP Conference Proceedings*, vol. 1922, 2018.

[80] G. Stepan, R. Szalai, B. P. Mann, P. V. Bayly, T. Insperger, J. Gradisek, and E. Govekar, "Nonlinear Dynamics of High-Speed Milling - Analyses, Numerics, and Experiments," *Journal of Vibration and Acoustics*, vol. 127, no. 2, p. 197, 2005.

[81] P. Kim and J. Seok, "Bifurcation analyses on the chatter vibrations of a turning process with state-dependent delay," *Nonlinear Dynamics*, vol. 69, no. 3, pp. 891–912, 2012.

[82] T. G. Molnár, T. Insperger, and G. Stépán, "State-dependent distributed-delay model of orthogonal cutting," *Nonlinear Dynamics*, vol. 84, no. 3, pp. 1147–1156, 2016.

[83] H. Cao, X. Zhang, and X. Chen, "The concept and progress of intelligent spindles: A review," *International Journal of Machine Tools and Manufacture*, vol. 112, no. October 2016, pp. 21–52, 2017.

[84] R.P.H. Faassen, "Chatter prediction and control for high-speed milling:modelling and experiments," Ph.D. dissertation, Eindhoven University of Technology, 2007.

[85] T. Delio, "Use of Audio Signals for Chatter Detection and Control," *Journal of Manufacturing Science and Engineering*, vol. 114, no. 2, p. 146, 1992.

[86] M. L. Polli, W. L. Weingaertner, R. B. Schroeter, and J. D. De Oliveira Gomes, "Analysis of high-speed milling dynamic stability through sound pressure, machining force and tool displacement measurements," *Proceedings of the Institution of Mechanical Engineers, Part B: Journal of Engineering Manufacture*, vol. 226, no. 11, pp. 1774–1783, 2012.

[87] G. Quintana, J. Ciurana, I. Ferrer, and C. A. Rodríguez, "Sound mapping for identification of stability lobe diagrams in milling processes," *International Journal of Machine Tools and Manufacture*, vol. 49, no. 3-4, pp. 203–211, 2009.

[88] L. Sallese, N. Grossi, A. Scippa, and G. Campatelli, "Investigation and Correction of Actual Microphone Response for Chatter Detection in Milling Operations," *Measurement and Control (United Kingdom)*, vol. 50, no. 2, pp. 45–52, 2017.

[89] H. Cao, Y. Yue, X. Chen, and X. Zhang, "Chatter detection in milling process based on synchrosqueezing transform of sound signals," *International Journal of Advanced Manufacturing Technology*, vol. 89, no. 9-12, pp. 2747–2755, 2017.

[90] V. S. Edouard Riviere O. Van den Abeele, Enrico Filippi , Pierre Dehombreux, "Chatter detection techniques using microphone," *7th National Congress on theoretical and applied Mechanics (NCTAM 2006), Mons*, 2006.

[91] T. L. Schmitz, K. Medicus, and B. Dutterer, "Exploring once-per-revolution audio signal variance as a chatter indicator," *Machining Science and Technology*, vol. 6, no. 2, pp. 215–233, 2002.

[92] J. Rech, F. Dumont, A. Le Bot, and P. J. Arrazola, "Reduction of noise during milling operations," *CIRP Journal of Manufacturing Science and Technology*, vol. 18, pp. 39–44, 2017.

[93] M. Hidayah, J. Ghani, M. Nuawi, and C. Haron, "A Review of Utilisation of Cutting Force Analysis In Cutting Tool Condition Monitoring," *International Journal of Engineering & Technology IJET-IJENS*, vol. 15, no. 28, pp. 150 203–4848, 2015.

[94] M. Luo, Z. Chong, and D. Liu, "Cutting forces measurement for milling process by using working tables with integrated PVDF thin-film sensors," *Sensors (Switzerland)*, vol. 18, no. 11, 2018.

[95] Y. Li, Y. Zhao, J. Fei, Y. Qin, Y. Zhao, A. Cai, and S. Gao, "Design and development of a three-component force sensor for milling process monitoring," *Sensors (Switzerland)*, vol. 17, no. 5, 2017.

[96] M. Sortino and F. Miani, "Application of a Rotating Dynamometer for Cutting Force Measurement in Milling," *AMST'02 Advanced Manufacturing Systems and Technology*, no. April 2015, 2013.

[97] M. Liu, J. Bing, L. Xiao, K. Yun, and L. Wan, "Development and testing of an integrated rotating dynamometer based on fiber bragg grating for four-component cutting force measurement," *Sensors (Switzerland)*, vol. 18, no. 4, 2018.

[98] A. Ghani and M. Nuawi, "Integrated rotating dynamometer for milling or drilling process," 2016.

[99] K. K. Singh, R. Singh, and V. Kartik, "Comparative Study of Chatter Detection Methods for High-Speed Micromilling of Ti6Al4V," *Procedia Manufacturing*, vol. 1, pp. 593–606, 2015.

[100] P. Huang, J. Li, J. Sun, and J. Zhou, "Vibration analysis in milling titanium alloy based on signal processing of cutting force," *International Journal of Advanced Manufacturing Technology*, vol. 64, no. 5-8, pp. 613–621, 2013.

[101] S. Yamato, T. Hirano, Y. Yamada, R. Koike, and Y. Kakinuma, "Sensor-less on-line chatter detection in turning process based on phase monitoring using power factor theory," *Precision Engineering*, vol. 51, pp. 103–116, 2018.

[102] R. Koike, Y. Kakinuma, T. Aoyama, and K. Ohnishi, "Evaluation of Sensor-less Identification Method for Stable Spindle Rotation against Chatter with Milling Simulation Analysis," *Procedia CIRP*, vol. 46, pp. 169–172, 2016.

[103] E. Soliman and F. Ismail, "Chatter detection by monitoring spindle drive current," *International Journal of Advanced Manufacturing Technology*, vol. 13, no. 1, pp. 27–34, 1997.

[104] H. Caliskan, Z. M. Kilic, and Y. Altintas, "On-Line Energy-Based Milling Chatter Detection," *Journal of Manufacturing Science and Engineering*, vol. 140, no. 11, p. 111012, 2018.

[105] D. Aslan and Y. Altintas, "On-line chatter detection in milling using drive motor current commands extracted from CNC," *International Journal of Machine Tools and Manufacture*, vol. 132, no. February, pp. 64–80, 2018.

[106] O. V. Arriaza, Z. Tumurkhuyagc, and D. W. Kim, "Chatter Identification using Multiple Sensors and Multi-Layer Neural Networks," *Procedia Manufacturing*, vol. 17, pp. 150–157, 2018.

[107] E. Kuljanic, M. Sortino, and G. Totis, "Multisensor approaches for chatter detection in milling," *Journal of Sound and Vibration*, vol. 312, no. 4-5, pp. 672–693, 2008.

[108] E. Kuljanic, G. Totis, and M. Sortino, "Development of an intelligent multisensor chatter detection system in milling," *Mechanical Systems and Signal Processing*, vol. 23, no. 5, pp. 1704–1718, 2009.

[109] J. S. Shepard, "Chatter Simulation and Detection in CNC Milling," 2017.

[110] H. Li, X. Jing, and J. Wang, "Detection and analysis of chatter occurrence in micro-milling process," *Proceedings of the Institution of Mechanical Engineers, Part B: Journal of Engineering Manufacture*, vol. 228, no. 11, pp. 1359–1371, 2014.

[111] S. Tangjitsitcharoen and T. Moriwaki, "Intelligent identification of turning process based on pattern recognition of cutting states," *Journal of Materials Processing Technology*, vol. 192-193, pp. 491–496, 2007.

[112] S. Tangjitsitcharoen and N. Pongsathornwiwat, "Development of chatter detection in milling processes," *The International Journal of Advanced Manufacturing Technology*, vol. 65, no. 5-8, pp. 919–927, 2013.

[113] I. Zaghbani, M. Lamraoui, V. Songmene, M. Thomas, and M. El Badaoui, "Robotic High Speed Machining of Aluminum Alloys," *Advanced Materials Research*, vol. 188, no. June 2015, pp. 584–589, 2011.

[114] M. A. U. Patwari, A. K. M. N. Amin, and W. F. Faris, "Influence of Chip Serration Frequency on Chatter Formation During End Milling of Ti6Al4V," *Journal of Manufacturing Science and Engineering*, vol. 133, no. 1, p. 011013, 2011.

[115] A. V. Filippov, V. E. Rubtsov, S. Y. Tarasov, O. A. Podgornykh, and N. N. Shamarin, "Detecting transition to chatter mode in peakless tool turning by monitoring vibration and acoustic emission signals," *International Journal of Advanced Manufacturing Technology*, vol. 95, no. 1-4, pp. 157–169, 2018.

[116] M. Uekita and Y. Takaya, "Tool condition monitoring technique for deep-hole drilling of large components based on chatter identification in time-frequency domain," *Measurement: Journal of the International Measurement Confederation*, vol. 103, pp. 199–207, 2017.

[117] H.-G. Stark, *Wavelets and Signal Processing.* Berlin/Heidelberg: Springer-Verlag, 2005.

[118] O. Rioul and M. Vetterli, "Wavelets and Signal Processing," *IEEE Signal Processing Magazine*, vol. 8, no. 4, pp. 14–38, 1991.

[119] S. Tangjitsitcharoen, "Analysis of Chatter in Ball End Milling by Wavelet Transform," vol. 6, no. 11, pp. 1075–1081, 2012.

[120] Z. Zhang, H. Li, G. Meng, X. Tu, and C. Cheng, "Chatter detection in milling process based on the energy entropy of VMD and WPD," *International Journal of Machine Tools and Manufacture*, vol. 108, pp. 106–112, 2016.

[121] Z. Yao, D. Mei, and Z. Chen, "On-line chatter detection and identification based on wavelet and support vector machine," *Journal of Materials Processing Technology*, vol. 210, no. 5, pp. 713–719, 2010.

[122] G. S. Chen and Q. Z. Zheng, "Online chatter detection of the end milling based on wavelet packet transform and support vector machine recursive feature elimination," *International Journal of Advanced Manufacturing Technology*, vol. 95, no. 1-4, pp. 775–784, 2018.

[123] Y. Yuan, X. Jing, H. Li, K. F. Ehmann, and D. Zhang, "Chatter detection based on wavelet coherence functions in micro-end-milling processes," *Proceedings of the Institution of Mechanical Engineers, Part B: Journal of Engineering Manufacture*, 2018.

[124] S. Wan, X. Li, W. Chen, and J. Hong, "Investigation on milling chatter identification at early stage with variance ratio and Hilbert-Huang transform," *International Journal of Advanced Manufacturing Technology*, vol. 95, no. 9-12, pp. 3563–3573, 2018.

[125] Ž. B. Jakovljević, "Comparative analysis of hilbert huang and discrete wavelet transform in processing of signals obtained from the cutting process: An intermittent turning example," *FME Transactions*, vol. 41, no. 4, pp. 342–348, 2013.

[126] N. E. Huang and S. S. P. Shen, *Hilbert-Huang Transform and Its Applications*. World Scientific, 2005.

[127] K. Wallis, G. Akers, P. Collins, R. Davis, A. Frazier, M. Oxley, and A. Terzuoli, "Complex empirical mode decomposition, Hilbert-Huang transform, and fourier transform applied to moving objects," *International Geoscience and Remote Sensing Symposium (IGARSS)*, no. 1, pp. 4395–4398, 2012.

[128] H. Cao, Y. Lei, and Z. He, "Chatter identification in end milling process using wavelet packets and Hilbert-Huang transform," *International Journal of Machine Tools and Manufacture*, vol. 69, pp. 11–19, 2013.

[129] M.-k. Liu, Q. M. Tran, Y.-w. Qui, and C.-h. Chung, "Chatter Detection in Milling Process Based on Time-Frequency Analysis," 2017, p. V001T02A025.

[130] A. Susanto, C. H. Liu, K. Yamada, Y. R. Hwang, R. Tanaka, and K. Sekiya, "Application of Hilbert-Huang transform for vibration signal analysis in end-milling," *Precision Engineering*, vol. 53, no. March, pp. 263–277, 2018.

[131] N. van Dijk, *Active chatter control in high-speed milling process*. Eindhoven University of Technology, 2011.

[132] S. Wan, X. Li, W. Su, J. Yuan, J. Hong, and X. Jin, "Active damping of milling chatter vibration via a novel spindle system with an integrated electromagnetic actuator," *Precision Engineering*, no. 28, pp. 1–8, 2019.

[133] N. J. M. V. Dijk, N. V. D. Wouw, E. J. J. Doppenberg, H. A. J. Oosterling, and H. Nijmeijer, "Robust Active Chatter Control in the High-Speed Milling

Process," *IEEE Transactions on Control Systems Technology*, vol. 20, no. 4, pp. 901–917, 2012.

[134] X. Long, S. Ren, and P. Zheng, "Delayed State Feedback Control for Milling Process," *Procedia IUTAM*, vol. 22, pp. 115–122, 2017.

[135] D. Li, H. Cao, X. Zhang, X. Chen, and R. Yan, "Model predictive control based active chatter control in milling process," *Mechanical Systems and Signal Processing*, vol. 128, no. 28, pp. 266–281, 2019.

[136] J. Monnin, F. Kuster, and K. Wegener, "Optimal control for chatter mitigation in milling-Part 1: Modeling and control design," *Control Engineering Practice*, vol. 24, no. 1, pp. 156–166, 2014.

[137] J. Monnin, F. Kuster, and K. Wegener, "Optimal control for chatter mitigation in milling-Part 2: Experimental validation," *Control Engineering Practice*, vol. 24, no. 1, pp. 167–175, 2014.

[138] F. Shi, H. Cao, D. Li, X. Chen, and X. Zhang, "Active chatter control in high speed milling processes based on Hinf almost disturbance decoupling problem," *Procedia CIRP*, vol. 78, pp. 37–42, 2018.

[139] S. Weiland and J. C. Willems, "Almost Disturbance Decoupling with Internal Stability," pp. 277–286, 1989.

[140] N. H. Kim, D. Won, and J. C. Ziegert, "Numerical analysis and parameter study of a mechanical damper for use in long slender endmills," *International Journal of Machine Tools and Manufacture*, vol. 46, no. 5, pp. 500–507, 2006.

[141] S. Semercigil and L. Chen, "Preliminary Computations for Chatter Control in End Milling," *Journal of Sound and Vibration*, vol. 249, no. 3, pp. 622–633, 2002.

[142] J. C. Ziegert, C. Stanislaus, T. L. Schmitz, and R. Sterling, "Enhanced damping in long slender end mills," *Journal of Manufacturing Processes*, vol. 8, no. 1, pp. 39–46, 2006.

[143] M. H. Miguélez, L. Rubio, J. A. Loya, and J. Fernández-Sáez, "Improvement of chatter stability in boring operations with passive vibration absorbers," *International Journal of Mechanical Sciences*, vol. 52, no. 10, pp. 1376–1384, 2010.

[144] J. P. D. Hartog, "Mechanical Vibrations," *The Journal of the Royal Aeronautical Society*, vol. 61, no. 554, pp. 139–139, feb 1957.

[145] N. D. Sims, "Vibration absorbers for chatter suppression: A new analytical tuning methodology," *Journal of Sound and Vibration*, vol. 301, no. 3-5, pp. 592–607, 2007.

[146] H. Moradi, M. R. Movahhedy, and G. Vossoughi, "Tunable vibration absorber for improving milling stability with tool wear and process damping effects," *Mechanism and Machine Theory*, vol. 52, pp. 59–77, 2012.

[147] N. A. Saadabad, H. Moradi, and G. Vossoughi, "Global optimization and design of dynamic absorbers for chatter suppression in milling process with tool wear and process damping," *Procedia CIRP*, vol. 21, pp. 360–366, 2014.

[148] Y. Yang, J. Muñoa, and Y. Altintas, "Optimization of multiple tuned mass dampers to suppress machine tool chatter," *International Journal of Machine Tools and Manufacture*, vol. 50, no. 9, pp. 834–842, 2010.

[149] J. Burtscher and J. Fleischer, "Adaptive tuned mass damper with variable mass for chatter avoidance," *CIRP Annals - Manufacturing Technology*, vol. 66, no. 1, pp. 397–400, 2017.

[150] Z. Zhang, H. Li, G. Meng, and S. Ren, "Milling chatter suppression in viscous fluid: A feasibility study," *International Journal of Machine Tools and Manufacture*, vol. 120, no. October 2016, pp. 20–26, 2017.

[151] Z. Zhang, H. Li, X. Liu, W. Zhang, and G. Meng, "Chatter mitigation for the milling of thin-walled workpiece," *International Journal of Mechanical Sciences*, vol. 138-139, no. February, pp. 262–271, 2018.

[152] M. A. Butt, Y. Yang, X. Pei, and Q. Liu, "Five-axis milling vibration attenuation of freeform thin-walled part by eddy current damping," *Precision Engineering*, vol. 51, no. May 2017, pp. 682–690, 2018.

[153] M. Wan, X. B. Dang, W. H. Zhang, and Y. Yang, "Optimization and improvement of stable processing condition by attaching additional masses for milling of thin-walled workpiece," *Mechanical Systems and Signal Processing*, vol. 103, pp. 196–215, 2018.

[154] R. Hahn, "Metal-cutting chatter and its elimination," *Transactions of ASME*, vol. 75, no. 6, p. 1073, 1953.

[155] J. Slavicek, "The Effect of Irregular Tooth Pitch on Stability of Milling," pp. 15–22, 1965.

[156] H. Opitz, E. U. Dregger, and H. Roese, "Improvement of the dynamic stability of the milling process by irregular tooth pitch," p. 213, 1966.

[157] P. Vanherck, "Increasing Milling Machine Productivity By Use of Cutters With Non-Constant Cutting-Edge Pitch," *Advances in Machine Tool Design and Research*, pp. 947–960, 1967.

[158] J. H. Varterasian, "White Noise A Deterrent to Milling Cutter Chatter.pdf," *Manufacturing Engineering and Management*, 1971.

[159] Y. Altintas, S. Engin, and E. Budak, "Analytical Stability Prediction and Design of Variable Pitch Cutters," *Journal of Manufacturing Science and Engineering*, vol. 121, no. July 1998, pp. 173–178, 1999.

[160] E. Budak, "An Analytical Design Method for Milling Cutters With Nonconstant Pitch to Increase Stability, Part 1: Theory," *Journal of Manufacturing Science and Engineering*, vol. 125, no. 1, p. 35, 2003.

[161] E. Budak, "An Analytical Design Method for Milling Cutters With Nonconstant Pitch to Increase Stability, Part 2: Application," *Journal of Manufacturing Science and Engineering*, vol. 125, no. 1, p. 35, 2003.

[162] N. Olgac and R. Sipahi, "Dynamics and stability of variable-pitch milling," *JVC/Journal of Vibration and Control*, vol. 13, no. 7, pp. 1031–1043, 2007.

[163] V. Sellmeier and B. Denkena, "Stable islands in the stability chart of milling processes due to unequal tooth pitch," *International Journal of Machine Tools and Manufacture*, vol. 51, no. 2, pp. 152–164, 2011.

[164] A. Comak and E. Budak, "Modeling dynamics and stability of variable pitch and helix milling tools for development of a design method to maximize chatter stability," *Precision Engineering*, vol. 47, pp. 459–468, 2017.

[165] G. Stepan, D. Hajdu, A. Iglesias, D. Takacs, and Z. Dombovari, "Ultimate capability of variable pitch milling cutters," *CIRP Annals*, vol. 67, no. 1, pp. 373–376, 2018.

[166] A. Iglesias, Z. Dombovari, G. Gonzalez, J. Munoa, and G. Stepan, "Optimum Selection of Variable Pitch for Chatter Suppression in Face Milling Operations," *Materials*, vol. 12, no. 1, p. 112, 2018.

[167] B. J. Stone, "The Effect on the Chatter Behavior of Machine Tools of Cutters with Different Helix Angles on Adjacent Teeth," pp. 169–180, 1970.

[168] S. Turner, D. Merdol, Y. Altintas, and K. Ridgway, "Modelling of the stability of variable helix end mills," *International Journal of Machine Tools and Manufacture*, vol. 47, no. 9, pp. 1410–1416, 2007.

[169] A. R. Yusoff, S. Turner, C. M. Taylor, and N. D. Sims, "The role of tool geometry in process damped milling," *The International Journal of Advanced Manufacturing Technology*, vol. 50, no. 9-12, pp. 883–895, oct 2010.

[170] A. R. Yusoff and N. D. Sims, "Optimisation of variable helix tool geometry for regenerative chatter mitigation," *International Journal of Machine Tools and Manufacture*, vol. 51, no. 2, pp. 133–141, 2011.

[171] A. R. Yusoff, N. D. Sims, and S. Turner, "Experimental Validation of Chatter Stability for Variable Helix Milling Tools," *IOP Conference Series: Materials Science and Engineering*, vol. 26, p. 012010, dec 2011.

[172] A. Otto and G. Radons, "Frequency domain stability analysis of milling processes with variable helix tools," *Nineth International Conference on High Speed Machining*, vol. 1, no. 0, pp. 1–6, 2012.

[173] A. Otto and G. Radons, "The Effect of Runout on the Stability of Milling with Variable Helix Tools," *Proceedings of the 23th International Congress of Theoretical and Applied Mechanics*, 2012.

[174] G. Jin, Q. Zhang, H. Qi, and B. Yan, "A frequency-domain solution for efficient stability prediction of variable helix cutters milling," *Proceedings of the IMechE, Part C: Journal of Mechanical Engineering Science*, vol. 228, no. 15, pp. 2702–2710, 2014.

[175] G. Jin, Q. Zhang, S. Hao, and Q. Xie, "Stability prediction of milling process with variable pitch and variable helix cutters," *Proceedings of the Institution of*

Mechanical Engineers, Part C: Journal of Mechanical Engineering Science, vol. 228, no. 2, pp. 281–293, 2014.

[176] Y. Y. Wang, T. Wang, Z. Yu, Y. Zhang, Y. Y. Wang, and H. Liu, "Chatter prediction for variable pitch and variable helix milling," *Shock and Vibration*, vol. 2015, 2015.

[177] A. Otto, S. Rauh, S. Ihlenfeldt, and G. Radons, "Stability of milling with non-uniform pitch and variable helix Tools," *International Journal of Advanced Manufacturing Technology*, vol. 89, no. 9-12, pp. 2613–2625, 2017.

[178] J. Niu, Y. Ding, L. M. Zhu, and H. Ding, "Mechanics and multi-regenerative stability of variable pitch and variable helix milling tools considering runout," *International Journal of Machine Tools and Manufacture*, vol. 123, no. August, pp. 129–145, 2017.

[179] J. Niu, J. Peng, Y. Ding, and L. M. Zhu, "Evaluation indicators of the runout effects on milling forces and regenerative stability," *8th CIRP Conference on High Performance Cutting (HPC 2018)*, vol. 77, pp. 98–101, 2018.

[180] R. Szalai and G. Stépán, "Stability Boundaries of High-Speed Milling Corresponding to Period Doubling Are Essentially Closed Curves," in *ASME International Mechanical Engineering Congress and Exposition*, 2003, pp. 63–68.

[181] E. Govekar, J. Gradišek, M. Kalveram, T. Insperger, K. Weinert, G. Stépán, and I. Grabec, "On stability and dynamics of milling at small radial immersion," *CIRP Annals - Manufacturing Technology*, vol. 54, no. 1, pp. 357–362, 2005.

[182] T. Insperger, J. Muñoa, and J. Munoa, "Unstable islands in the stability chart of milling processes due to the helix angle," *CIRP - 2nd International Conference on High Performance Cutting (HPC)*, 2006.

[183] B. R. Patel, B. P. Mann, and K. A. Young, "Uncharted islands of chatter instability in milling," *International Journal of Machine Tools and Manufacture*, vol. 48, no. 1, pp. 124–134, 2008.

[184] F. A. Khasawneh, O. A. Bobrenkov, B. P. Mann, and E. A. Butcher, "Investigation of Period-Doubling Islands in Milling With Simultaneously Engaged Helical Flutes," *Journal of Vibration and Acoustics*, vol. 134, no. 2, p. 021008, 2012.

[185] L. Ureña, E. Ozturk, and N. Sims, "Stability of variable helix milling: model validation using scaled experiments," *8th CIRP Conference on High Performance Cutting (HPC 2018)*, vol. 77, pp. 449–452, 2018.

[186] K. Ogata, *Modern Control Engineering*, ser. Instrumentation and controls series. Pearson, 2010.

[187] M. C. Smith, "On the generalized nyquist stability criterion," *International Journal of Control*, vol. 34, no. 5, pp. 885–920, 1981.

[188] D. Debeljković, *Time-Delay Systems*, D. Debeljković, Ed. InTech, 2011.

[189] Z. Dombovari and G. Stepan, "The Effect of Helix Angle Variation on Milling Stability," *Journal of Manufacturing Science and Engineering*, vol. 134, no. 5, p. 051015, 2012.

[190] Z. Dombovari, D. Bachrathy, and G. Stepan, "Optimization of edge geometry of cylindrical milling tools to enhance dynamic stability," *Proceedings of the ASME Design Engineering Technical Conference*, vol. 6, no. 2, pp. 1–5, 2019.

[191] M. Sanz, A. Iglesias, J. Munoa, and Z. Dombovari, "The Effect of Geometry on Harmonically Varied Helix Milling Tools," *Journal of Manufacturing Science and Engineering*, vol. 142, no. 7, pp. 1–6, 2020.

[192] K. A. M. Adem, R. Fales, and A. S. El-gizawy, "Identification of cutting force coefficients for the linear and nonlinear force models in end milling process using average forces and optimization technique methods," pp. 1671–1687, 2015.

[193] A. Kobayashi, *Machining of plastics*. McGraw-Hill, 1967.

[194] A. Kobayashi and K. Saito, "On the Cutting Mechanism of High Polymers," *Journal of Polymer Science*, vol. 58, no. 1962, pp. 1377–1395, 1962.

[195] A. C. Mehta, "Study of effect of speed, feed, and tool rake angle in machining plastics," Master's Thesis, Kansas State University, 1963.

[196] Y. Patel, "The Machining of Polymers," Doctoral Thesis, Imperial College London, 2008.

[197] U. M. Rao, J. D. Cumming, and E. G. Thomsen, "Some Observations on the Mechanics of Orthogonal Cutting of Delrin and Zytel Plastics," *Journal of Engineering for Industry*, vol. 86, no. 2, p. 117, 1964.

[198] K. Q. Xiao and L. C. Zhang, "The role of viscous deformation in the machining of polymers," *International Journal of Mechanical Sciences*, vol. 44, no. 11, pp. 2317–2336, 2002.

[199] C. A. Harper, *Modern Plastics Handbook*, ser. McGraw-Hill handbooks. Mcgraw-hill, 2000.

[200] M. Chanda and K. R. Salil, *Plastic Technology Handbook*, 2006.

[201] T. U. Jagtap and H. A. Mandave, "Machining of Plastics: A Review," *International Journal of Engineering Research and General Science*, vol. 3, no. 2, pp. 577–581, 2015.

[202] R. Keresztes, G. Kalácska, L. Zsidai, and Z. Dobrocsi, "Machinability of engineering polymers," *Sustainable Construction and Design*, no. 1, pp. 106–114, 2011.

[203] Curbell Plastics, "Curbell plastics engineering materials guide," p. 93, 2012.

[204] P. Volgers and A. Winkler, "Analysis of DuPont engineering polymers - challenges and solutions," *2017 Science in the Age of Experience*, no. May, 2017.

[205] S. Jeet, "An Overwiew on Machining of Engineering Polymers," vol. 9, no. 4, pp. 46–50, 2018.

[206] C. Ticona, "Designing with Celcon acetal copolymer," 2002.

[207] C. Ticona, "Designing With Plastic: The Fundamentals," p. 84, 2009.

[208] G. Welsch, R. Boyer, and E. W. Collings, *Materials Properties Handbook: Titanium Alloys*, ser. Materials properties handbook. ASM International, 1993.

[209] A. H. Committee, *Properties and Selection: Nonferrous Alloys and Special-Purpose Materials*, ser. Metals handbook. ASM International, 2018.

[210] O. M. Ivasishin, S. V. Akhonin, D. G. Savvakin, V. A. Berezos, V. I. Bondarchuk, O. O. Stasyuk, and P. E. Markovsky, "Effect of microstructure, deformation mode and rate on mechanical behaviour of electron-beam melted Ti-6Al-4V and Ti-1.5Al-6.8Mo-4.5Fe alloys," *Progress in Physics of Metals*, vol. 19, no. 3, pp. 309–336, 2018.

[211] S. Wei, P. Deng, Q. Jiangtong, and Y. Jin, "Tensile deformation behavior of Ti-6Al-4V sheet at elevated temperature," *Materials Research Express*, vol. 6, no. 11, 2019.

[212] S. R. Raisch and B. Möginger, "High rate tensile tests - Measuring equipment and evaluation," *Polymer Testing*, vol. 29, no. 2, pp. 265–272, 2010.

[213] L. Devamma, "Studies on machinability of engineering materials," PhD, Bangalore University, 2014.

[214] G. Stepan, Z. Dombovari, and J. Muñoa, "Identification of cutting force characteristics based on chatter experiments," *CIRP Annals - Manufacturing Technology*, vol. 60, no. 1, pp. 113–116, 2011.

[215] M. A. Rubeo and T. L. Schmitz, "Milling Force Modeling: A Comparison of Two Approaches," *44th Proceedings of the North American Manufacturing Research Institution of SME*, vol. 5, pp. 90–105, 2016.

[216] G. Williams, Y. Patel, and B. R. K. Blackman, "An Analysis of Cutting and Machining using Fracture Mechanics Concepts," *ECF17, Brno 2008*, vol. 1, pp. 106–136, 2013.

[217] A. Honeycutt and T. L. Schmitz, "Experimental Validation of Period-n Bifurcations in Milling," *Procedia Manufacturing*, vol. 5, pp. 362–374, 2016.

[218] E. Ozturk, O. Ozkirimli, T. Gibbons, M. Saibi, and S. Turner, "Prediction of effect of helix angle on cutting force coefficients for design of new tools," *CIRP Annals - Manufacturing Technology*, vol. 65, no. 1, pp. 125–128, 2016.

[219] G. Jin, H. Li, Z. J. Li, and G. X. Sun, "A method to predict the cutting force for end mills with variable-pitch and variable-helix angle," *IOP Conference Series: Materials Science and Engineering*, vol. 392, no. 6, 2018.

[220] Q. Guo, B. Zhao, M. Y. Zhang, Y. Jiang, and Y. Zhang, "A separate-edge force coefficients' calibration method using specific condition for cutters with variable helix and pitch angles combining the runout effect," *International Journal of Advanced Manufacturing Technology*, vol. 93, no. 5-8, pp. 1737–1749, 2017.

[221] L. Pejryd and M. Eynian, "Minimization of chatter in machining by the use of mobile platform technologies," *The 5th International Swedish Production Symposium, SPS12*, no. January, pp. 179–189, 2012.

[222] E. Budak, L. T. Tunç, S. Alan, and H. N. Özgüven, "Prediction of workpiece dynamics and its effects on chatter stability in milling," *CIRP Annals - Manufacturing Technology*, vol. 61, no. 1, pp. 339–342, 2012.

[223] J. Shi, Q. Song, Z. Liu, and X. AI, "A novel stability prediction approach for thin-walled component milling considering material removing process," *Chinese Journal of Aeronautics*, vol. 30, no. 5, pp. 1789–1798, 2017.

[224] R. Plunkett and C. T. Lee, "Length Optimization for Constrained Viscoelastic Layer Damping," *The Journal of the Acoustical Society of America*, vol. 48, no. 1B, pp. 150–161, 1970.

[225] R. Stanway, J. A. Rongong, and N. D. Sims, "Active constrained-layer damping: A state-of-the-art review," *Proceedings of the Institution of Mechanical Engineers, Part I: Journal of Systems and Control Engineering*, vol. 217, no. 6, pp. 437–456, sep 2003.

[226] B. M. Shafer, "An overview of constrained-layer damping theory and application," vol. 065023, pp. 065 023–065 023, 2013.

[227] S. C. Huang, C. Y. Tsai, and C. L. Liou, "A general vibration theory for constrained layer damping-treated thick sandwich structures," *Journal of Sandwich Structures and Materials*, vol. 18, no. 3, pp. 343–373, 2016.

[228] J. M. T. Thompson and H. B. Stewart, *Nonlinear Dynamics and Chaos*. Wiley, 2002.

[229] G. R. Tomlinson, "The use of constrained layer damping in vibration control," *International Journal of Mechanical Sciences*, vol. 32, no. 3, pp. 233–242, 1990.

[230] P. P. Hujare and A. D. Sahasrabudhe, "Experimental Investigation of Damping Performance of Viscoelastic Material Using Constrained Layer Damping Treatment," *Procedia Materials Science*, vol. 5, pp. 726–733, 2014.

[231] D. H. Lee, "Optimal placement of constrained-layer damping for reduction of interior noise," *AIAA Journal*, vol. 46, no. 1, pp. 75–83, 2008.

[232] J. F. Madeira, A. L. Araújo, and C. M. Mota Soares, "Multiobjective optimization of constrained layer damping treatments in composite plate structures," *Mechanics of Advanced Materials and Structures*, vol. 24, no. 5, pp. 427–436, 2017.

[233] G. Totis, T. Insperger, M. Sortino, and G. Stépán, "Symmetry breaking in milling dynamics," *International Journal of Machine Tools and Manufacture*, vol. 139, no. November 2018, pp. 37–59, 2019.

[234] N. Suzuki, T. Kojima, R. Hino, and E. Shamoto, "A novel design method of irregular pitch cutters to attain simultaneous suppression of multi-mode regenerations," *3rd CIRP Conference on Process Machine Interactions*, vol. 4, pp. 98–102, 2012.

[235] K. Takuya, N. Suzuki, R. Hino, and E. Shamoto, "A novel design method of variable helix cutters to attain robust regeneration suppression," *Procedia CIRP*, vol. 8, pp. 363–367, 2013.

[236] T. Hayasaka, A. Ito, and E. Shamoto, "Generalized design method of highly-varied-helix end mills for suppression of regenerative chatter in peripheral milling," *Precision Engineering*, vol. 48, pp. 45–59, 2017.

[237] A. Ito and E. Shamoto, "An Innovative Machining Strategy for Efficient Peripheral Finishing of Hard Materials," pp. 1–9, 2014.

[238] A. Ito and E. Shamoto, "Proposal of low-radial and high-axial immersion machining of hard materials with highly-varied-helix end mill - Experimental verification of proposed method and its comprehension by regenerative-effect cancelation diagram," *Seimitsu Kogaku Kaishi/Journal of the Japan Society for Precision Engineering*, vol. 81, no. 9, pp. 867–874, 2015.

[239] B. B. Muhammad, M. Wan, J. Feng, and W. H. Zhang, "Dynamic damping of machining vibration: a review," *International Journal of Advanced Manufacturing Technology*, vol. 89, no. 9-12, pp. 2935–2952, 2017.

[240] M. A. Rubeo, K. Kiran, and T. L. Schmitz, "The Design of a Multiple Degree of Freedom Flexure Stage with Tunable Dynamics for Milling Experimentation."

A. APPENDIX A

A.1. Directional-coefficient Fourier-series expansion

```
Axxn = -0.1e1 ./ pi .* Kt .* ((i) .* Kr .* exp((-1.*i) .* n .* c) .* cos(2 .* c) .* n .^ 2 + (-1.*i) .* Kr .* exp((-1.*i) .* n .* d) .* cos(2 .* d) .* n .^ 2 + (-1.*i) .* Kr .* exp((-1.*i) .* n .* c) .* n .^ 2 + (i) .* Kr .* exp((-1.*i) .* n .* d) .* n .^ 2 + (-1.*i) .* exp((-1.*i) .* n .* c) .* sin(2 .* c) .* n .^ 2 + (i) .* exp((-1.*i) .* n .* d) .* sin(2 .* d) .* n .^ 2 - 2 .* Kr .* exp((-1.*i) .* n .* c) .* sin(2 .* c) .* n + 2 .* Kr .* exp((-1.*i) .* n .* d) .* sin(2 .* d) .* n + (4.*i) .* Kr .* exp((-1.*i) .* n .* c) + (-4.*i) .* Kr .* exp((-1.*i) .* n .* d) - 2 .* exp((-1.*i) .* n .* c) .* cos(2 .* c) .* n + 2 .* exp((-1.*i) .* n .* d) .* cos(2 .* d) .* n) ./ n ./ (n .^ 2 - 4) ./ 4;

Axyn = 0.1e1 ./ pi .* Kt .* (i .* Kr .* exp(-i .* n .* c) .* sin(2 .* c) .* n .^ 2 + -i .* Kr .* exp(-i .* n .* d) .* sin(2 .* d) .* n .^ 2 + i .* exp(-i .* n .* c) .* cos(2 .* c) .* n .^ 2 + -i .* exp(-i .* n .* d) .* cos(2 .* d) .* n .^ 2 + 2 .* Kr .* exp(-i .* n .* c) .* cos(2 .* c) .* n - 2 .* Kr .* exp(-i .* n .* d) .* cos(2 .* d) .* n + i .* exp(-i .* n .* c) .* n .^ 2 + -i .* exp(-i .* n .* d) .* n .^ 2 - 2 .* exp(-i .* n .* c) .* sin(2 .* c) .* n + 2 .* exp(-i .* n .* d) .* sin(2 .* d) .* n + -4.*i .* exp(-i .* n .* c) + 4.*i .* exp(-i .* n .* d)) ./ n ./ (n .^ 2 - 4) ./ 4;

Ayyn = 0.1e1 ./ pi .* Kt .* (i .* Kr .* exp(-i .* n .* c) .* cos(2 .* c) .* n .^ 2 + -i .* Kr .* exp(-i .* n .* d) .* cos(2 .* d) .* n .^ 2 + i .* Kr .* exp(-i .* n .* c) .* n .^ 2 + -i .* Kr .* exp(-i .* n .* d) .* n .^ 2 + -i .* exp(-i .* n .* c) .* sin(2 .* c) .* n .^ 2 + i .* exp(-i .* n .* d) .* sin(2 .* d) .* n .^ 2 - 2 .* Kr .* exp(-i .* n .* c) .* sin(2 .* c) .* n + 2 .* Kr .* exp(-i .* n .* d) .* sin(2 .* d) .* n + -4.*i .* Kr .* exp(-i .* n .* c) + 4.*i .* Kr .* exp(-i .* n .* d) - 2 .* exp(-i .* n .* c) .* cos(2 .* c) .* n + 2 .* exp(-i .* n .* d) .* cos(2 .* d) .* n) ./ n ./ (n .^ 2 - 4) ./ 4;

Ayxn = 0.1e1 ./ pi .* Kt .* (i .* Kr .* exp(-i .* n .* c) .* sin(2 .* c) .* n .^ 2 + -i .* Kr .* exp(-i .* n .* d) .* sin(2 .* d) .* n .^ 2 + i .* exp(-i .* n .* c) .* cos(2 .* c) .* n .^ 2 + -i .* exp(-i .* n .* d) .* cos(2 .* d) .* n .^ 2 + 2 .* Kr .* exp(-i .* n .* c) .* cos(2 .* c) .* n - 2 .* Kr .* exp(-i .* n .* d) .* cos(2 .* d) .* n + -i .* exp(-i .* n .* c) .* n .^ 2 + i .* exp(-i .* n .* d) .* n .^ 2 - 2 .* exp(-i .* n .* c) .* sin(2 .* c) .* n + 2 .* exp(-i .* n .* d) .* sin(2 .* d) .* n + 4.*i .* exp(-i .* n .* c) + -4.*i .* exp(-i .* n .* d)) ./ n ./ (n .^ 2 - 4) ./ 4;
```

B. APPENDIX B

B.1. Cutting Force Coefficients

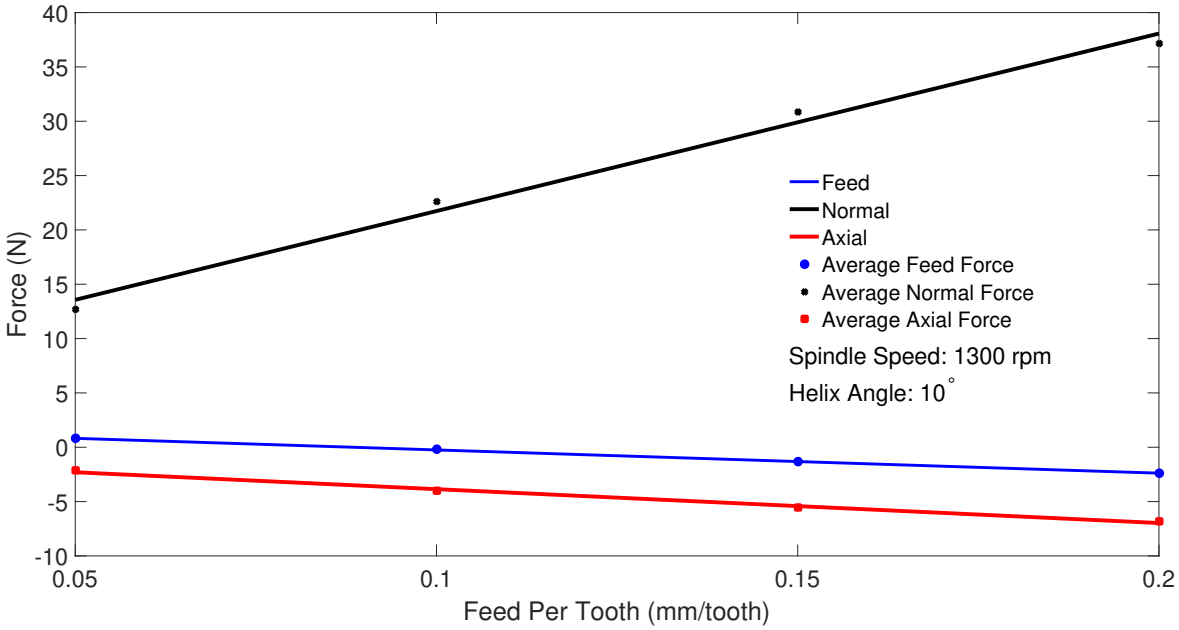

Figure B.1.: Experimental results showing the relationship between the feed-per-tooth, and the average forces for the one-flute tool with 10° of helix angle.

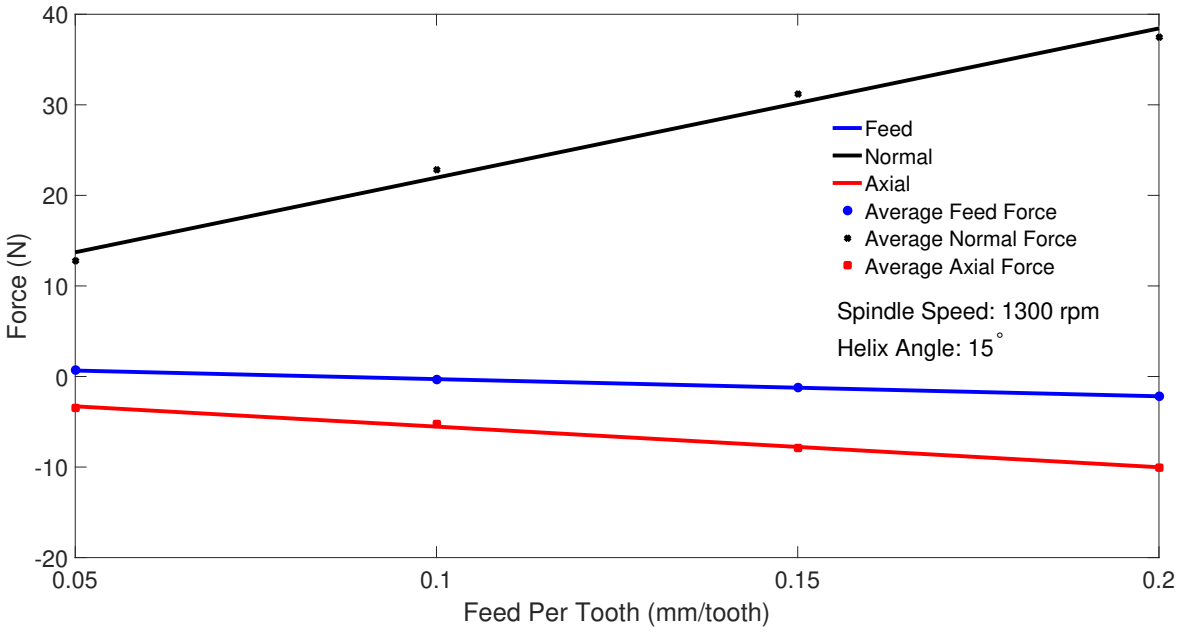

Figure B.2.: Experimental results showing the relationship between the feed-per-tooth, and the average forces for the one-flute tool with 15° of helix angle.

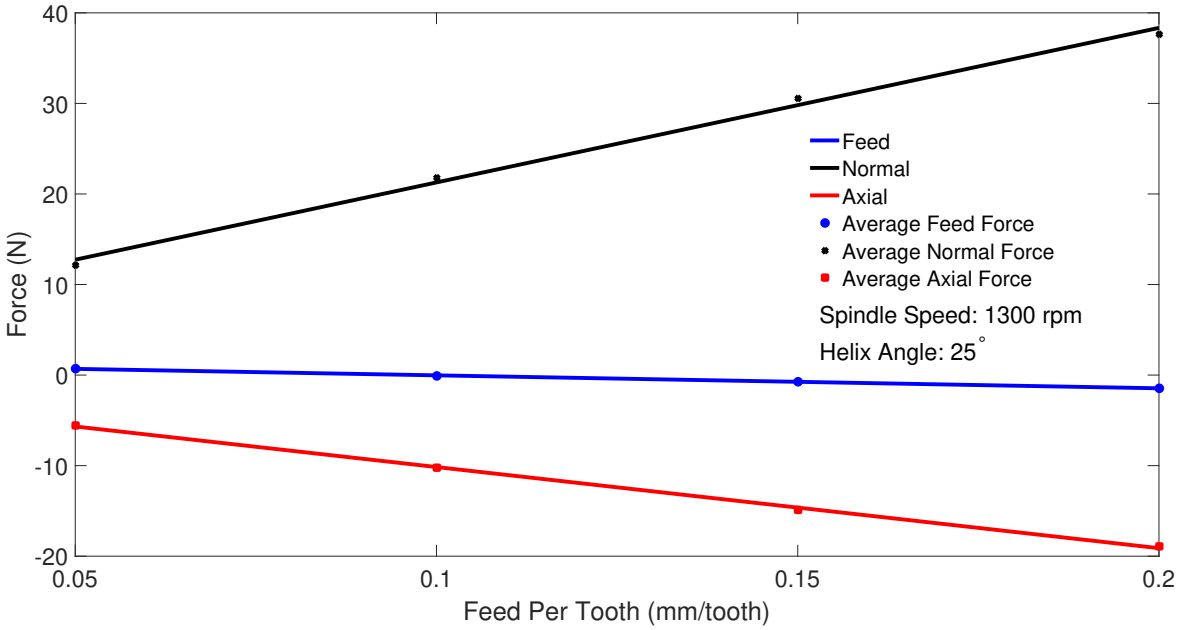

Figure B.3.: Experimental results showing the relationship between the feed-per-tooth, and the average forces for the one-flute tool with 25° of helix angle.

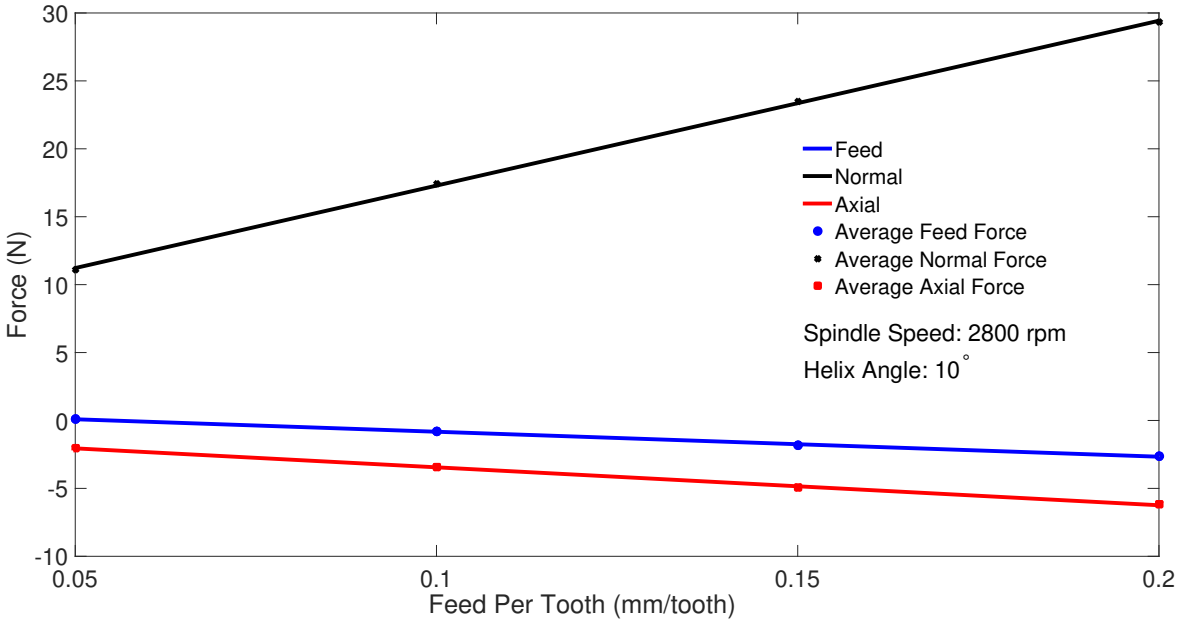

Figure B.4.: Experimental results showing the relationship between the feed-per-tooth, and the average forces for the one-flute tool with 10° of helix angle.

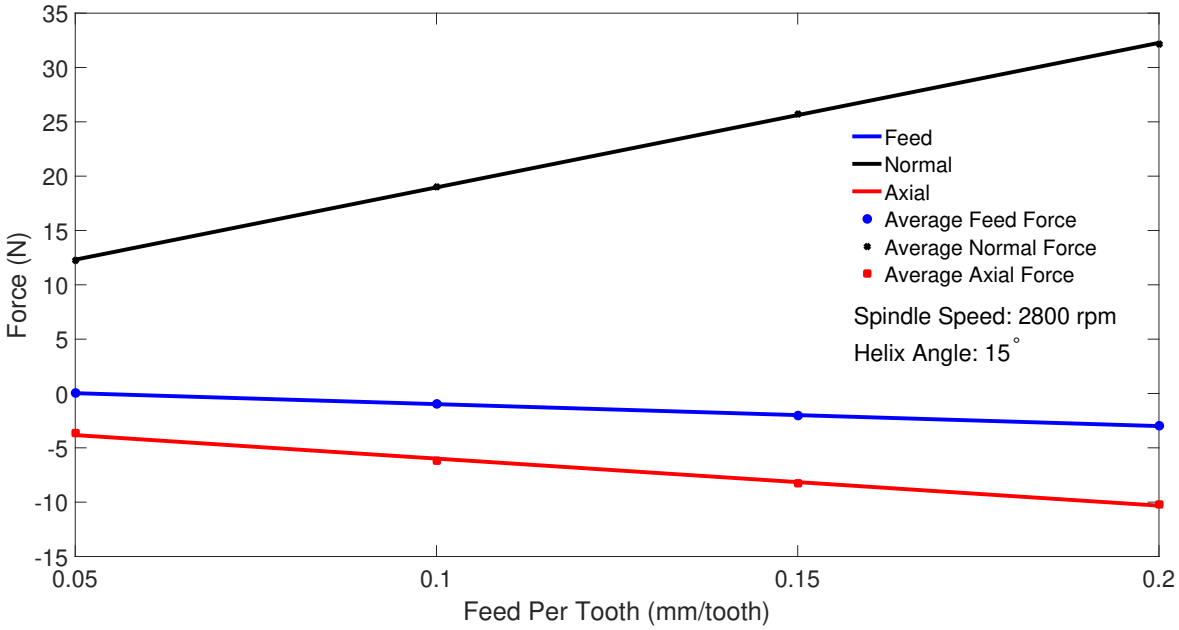

Figure B.5.: Experimental results showing the relationship between the feed-per-tooth, and the average forces for the one-flute tool with 15° of helix angle.

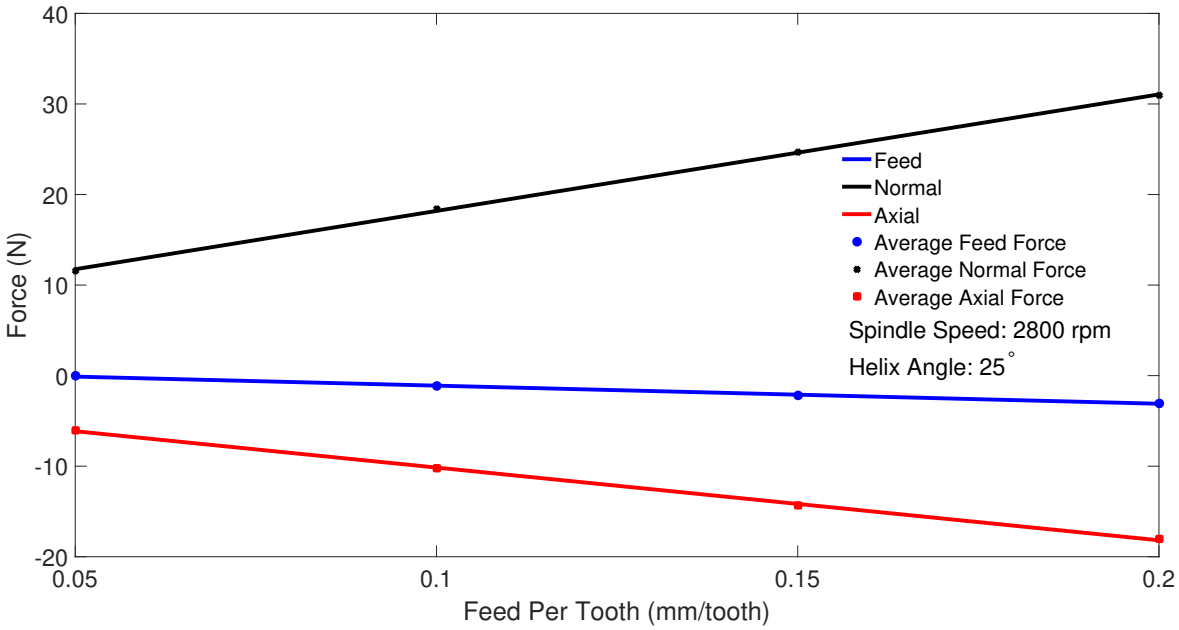

Figure B.6.: Experimental results showing the relationship between the feed-per-tooth, and the average forces for the one-flute tool with 25° of helix angle.

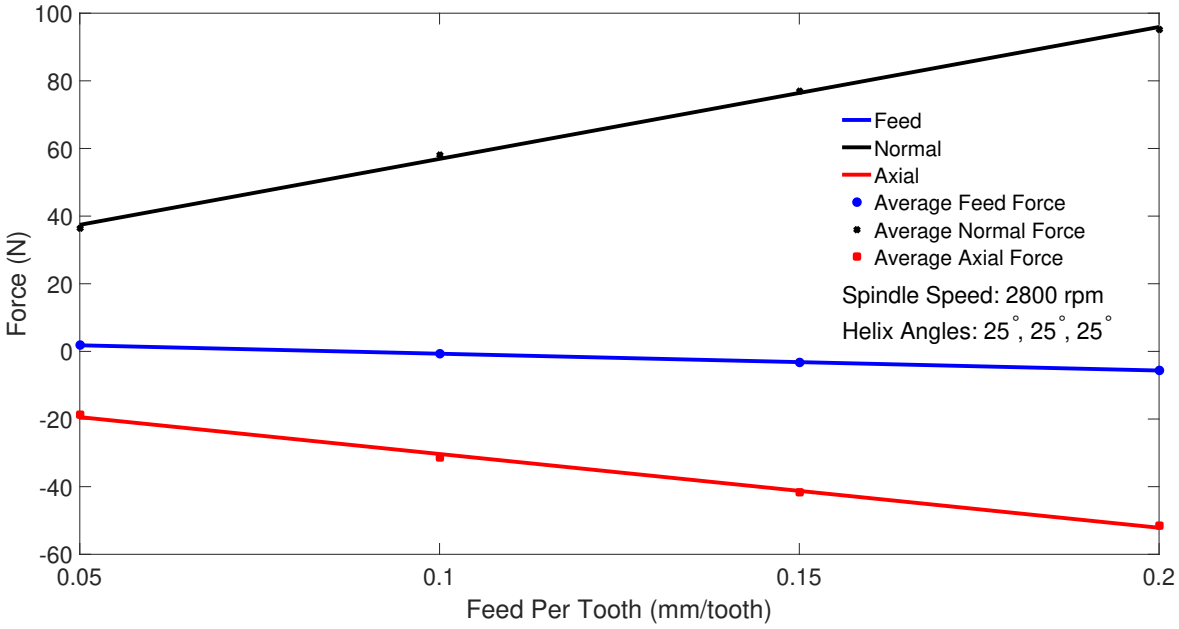

Figure B.7.: Experimental results showing the relationship between the feed-per-tooth, and the average forces for a conventional milling tool with 25° of helix angle.

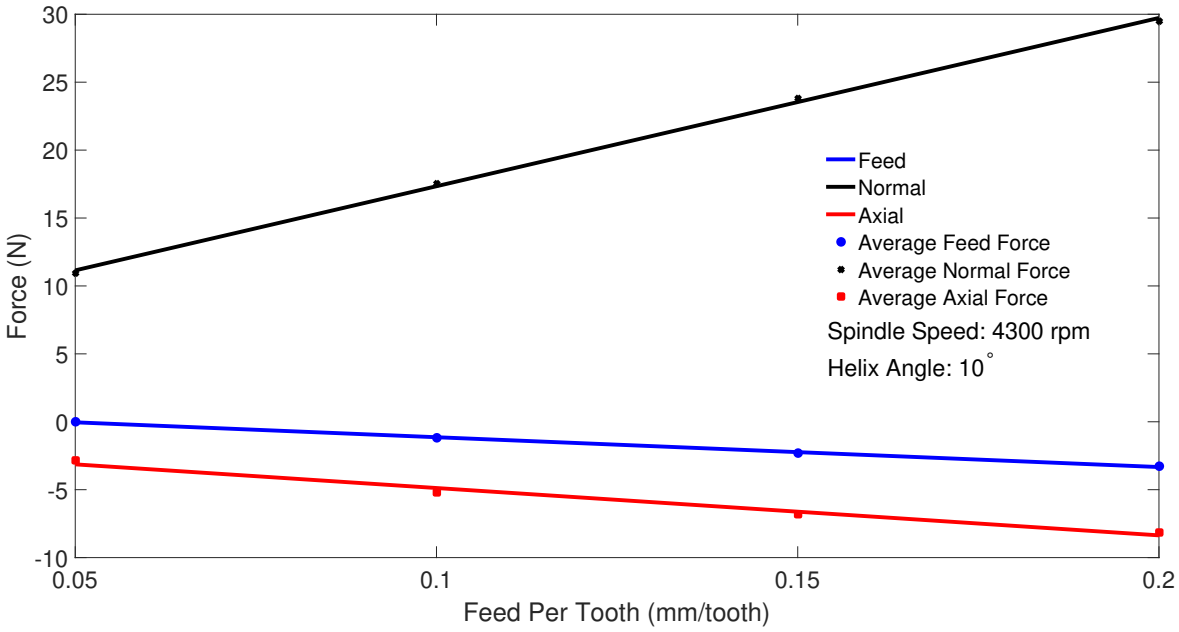

Figure B.8.: Experimental results showing the relationship between the feed-per-tooth, and the average forces for the one-flute tool with 10° of helix angle.

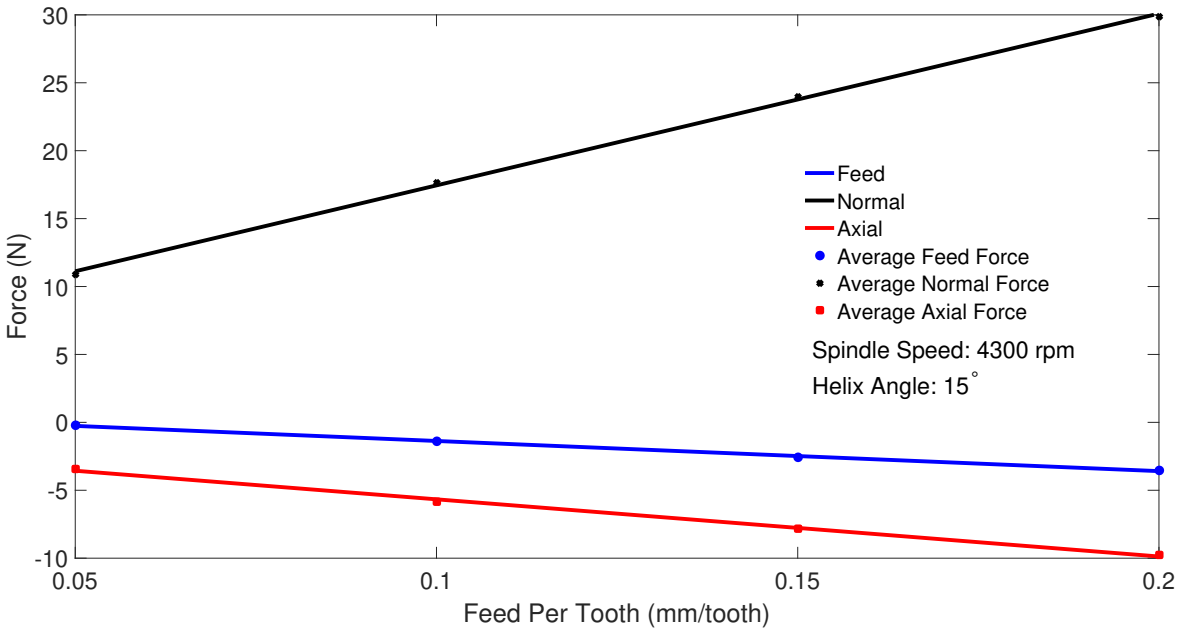

Figure B.9.: Experimental results showing the relationship between the feed-per-tooth, and the average forces for the one-flute tool with 15° of helix angle.

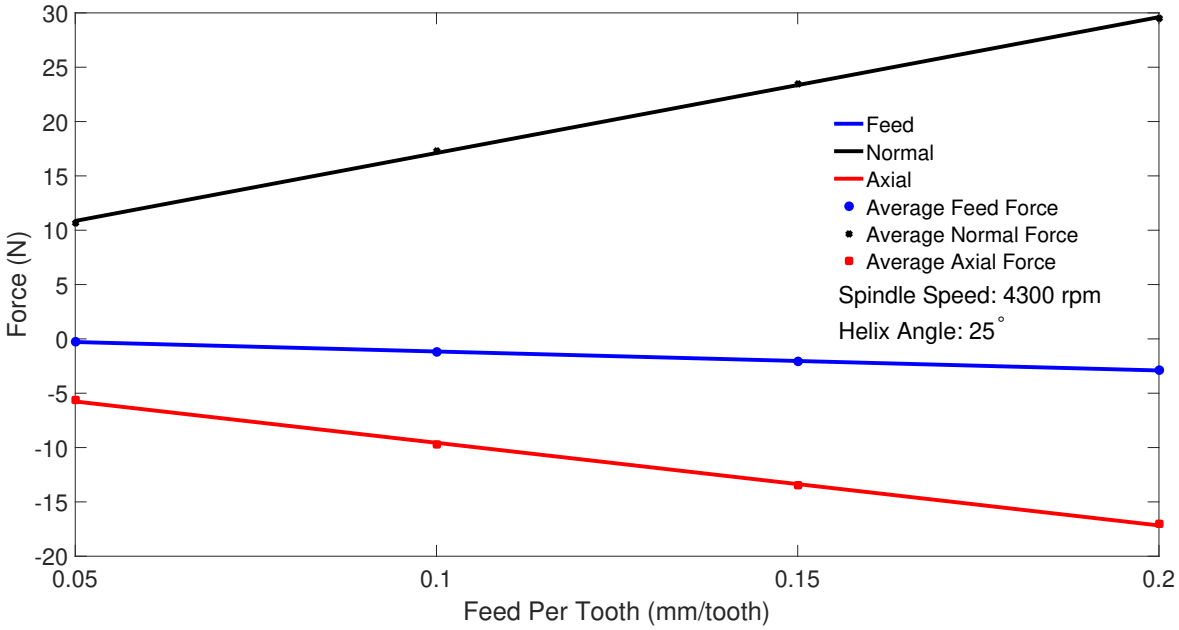

Figure B.10.: Experimental results showing the relationship between the feed-per-tooth, and the average forces for the one-flute tool with 25° of helix angle.

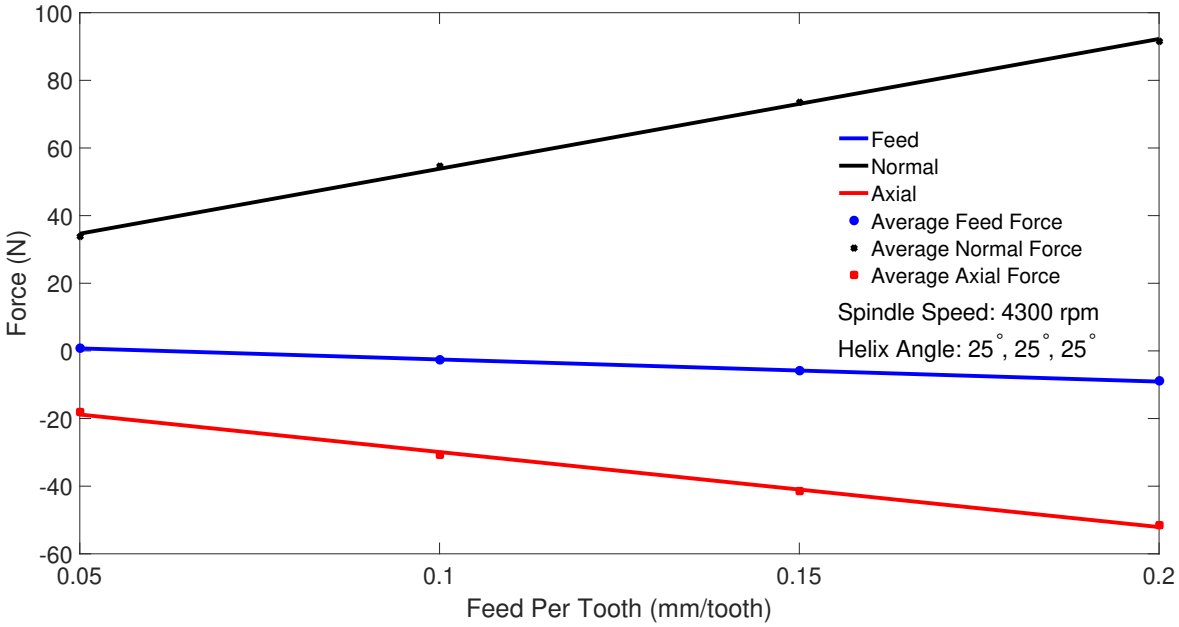

Figure B.11.: Experimental results showing the relationship between the feed-per-tooth, and the average forces for a conventional milling tool with 25° of helix angle.

C. APPENDIX C

C.1. Research Papers

Available online at www.sciencedirect.com

ScienceDirect

Procedia CIRP 77 (2018) 449–452

www.elsevier.com/locate/procedia

8th CIRP Conference on High Performance Cutting (HPC 2018)

Stability of variable helix milling: model validation using scaled experiments

L. Ureña[a,*], E. Ozturk[a], N. Sims[b]

[a]Department of Mechanical Engineering, The University of Sheffield, Mappin Street, Sheffield, S1 3JD, UK
[b]Advanced Manufacturing Research Center with Boeing, Wallis Way, Rotherham, S60 5TZ, UK

* Corresponding author. Tel.: +44-0114-222-7700. *E-mail address:* ueluis1@sheffield.ac.uk

Abstract

Regenerative chatter is widely known to be one of the main obstacles to improving the productivity of machining. In milling, one approach to suppress regenerative chatter is the use of milling tools with non-uniform helix angles. There have been a number of studies that have developed alternative analytical formulations of variable helix chatter stability. Whilst some of these have included detailed experimental validation, in general, there is a limited validation of the different analysis methods. In particular, the potential for variable helix tools to stabilise at higher axial depths of cut is of significant practical value but needs detailed experimental validation. The present study aims to provide variations to commonly used configurations, by implementing copolymer acetal as a workpiece material mounted on an intentionally flexible platform. Using this configuration, the force magnitudes can be reduced to lower levels, whilst also ensuring that low-order linear structural dynamics can be assumed even at high axial depths of cut. This provides a pathway to validate the stability predictions for variable helix tools, even if further work is then needed in order to understand non-linearity and other un-modelled effects. Based on the experimental data, the accuracy of the model predictions, and the validity of the model assumptions are discussed. Finally, conclusions are drawn regarding the potential for well-designed variable helix tools to offer significant performance improvements in practical applications.

Keywords: Milling; Variable Helix Tools; Machining Dynamics; Copolymer Acetal; Chatter

1. Introduction

Regenerative chatter is widely known to be one of the main obstacles to improving the productivity of machining. In milling, it occurs when the waviness printed on the workpiece surface by one tooth, is out of phase with the waviness left by the previous tooth. Hence, the chip thickness, and therefore the forces, may grow exponentially. This can result in a poor surface finish, tool wear, as well as catastrophic damage to the machine. In the long run approach to suppress regenerative chatter is the use of milling tools with non-equal helix angles.

There have been a number of studies that have developed alternative analytical formulations of variable helix chatter stability [1–3]. Whilst some of these have included detailed experimental validation [4,5], in general, there is a limited validation of the different analysis methods. In particular, the potential for variable helix tools to stabilize at higher axial depths of cut is of significant practical value but needs detailed experimental validation.

The present study seeks to address this issue, using a workpiece material with low cutting stiffness in contrast to previous studies. Consequently, low-order linear structural dynamics can be assumed even at high axial depths of cut due to the relatively low cutting forces. Copolymer acetal was used as the workpiece material, mounted on an intentionally flexible platform. This provides a pathway to validate the stability predictions for variable helix tools, even if additional work is then needed in order to comprehend non-linearity and other un-modelled effects.

The first and second section of this paper presents the experimental configuration implemented in the experiment and a case study. Subsequently, section three shows and discusses the results obtained from some of the cutting trials. Finally, conclusions are drawn regarding the potential for well-designed variable helix tools to offer significant performance improvements in practical applications.

10.1016/j.procir.2018.08.277

2. Variable Helix Milling Model and Stability

The state-space form of a single-degree-of-freedom milling system can be expressed as [6],

$$\dot{\mathbf{x}}(t) = \mathbf{A}\mathbf{x}(t) + \mathbf{B}(t,a)\mathbf{x}(t) - \mathbf{B}(t,a)\mathbf{x}(t-T) \quad (1)$$

With the vector $\mathbf{x}$ and matrices $\mathbf{A}$ and $\mathbf{B}$ defined as:

$$\dot{\mathbf{x}}(t) = \begin{pmatrix} x(t) \\ \dot{x}(t) \end{pmatrix}, \mathbf{A} = \begin{pmatrix} 0 & 1 \\ -{\omega_{nx}}^2 & -2\zeta_x\omega_{nx} \end{pmatrix}, \mathbf{B}(t,a) = \begin{pmatrix} 0 & 0 \\ -\frac{aK_t h(t,a)}{m_x} & 0 \end{pmatrix}$$

The term x refers to the displacement of the workpiece in the normal direction (Figure 2). On the other hand, the terms ω_{nx}, ζ_x and m_x refer to the modal natural frequency, damping ratio and mass of the flexure system in the x direction. The y (feed) direction is assumed to be rigid. Subsequently, $h(t,a)$, a, K_t and T represent the chip thickness, axial depth of cut, tangential cutting stiffness, and the spindle-pass period. In addition, the chip thickness can be expresses as,

$$h(t,a) = \sum_{j=1}^{N} g(\phi_j(t,a)) \cos(\phi_j(t,a)) \left[\sin(\phi_j(t,a)) - K_{ra}\cos(\phi_j(t,a))\right],$$

in which $\phi_j(t,a)$ is the angular position of the teeth j, K_{ra} the ratio of radial cutting stiffness to the tangential one, N the number of teeth, and g is a binary function that is 1 when the tooth is engaged in the workpiece and 0 otherwise.

The stability lobe diagram of the milling process can be obtained by using the Semi-Discretization Method (SDM) as described in [7,8]. In this method, the spindle-pass period T is divided into m discrete time intervals Δt such as $T = m\Delta t$. This then leads to a series of equations at discrete time interval as,

$$z_{i+1} = [\Phi] z_i.$$

According to the Floquet theory, the milling process is unstable if any of the eigenvalues of the transition matrix $[\Phi]$ have a modulus greater than one, marginally stable if the modulus is equal to 1, and stable if all the modulus are less than 1.

3. Experimental Configuration

The experimental configuration implemented in the current project is shown in Figure 1. It consists of an instrumented flexure device mounted on a CNC machine (XYZ 1060 HS VMC). Whilst many studies have used an intentionally flexible workpiece (e.g. [9,10]), they have typically used Aluminium alloy or other engineering alloys as the workpiece material. As a consequence, whilst the structural dynamics can be approximated with a low-order linear model, the resulting stability boundaries can be very low due to the flexibility of the structure and relatively high cutting force coefficients. To overcome this, the present study uses copolymer acetal as the workpiece material. Consequently, both the workpiece structural stiffness and its cutting stiffness are intentionally controlled in order to achieve thorough experimental validation.

4. Workpiece Material

Acetal is a semi-crystalline thermoplastic that provides a high machinability and low sensitivity to environmental factors such as temperature or humidity. In the plastic triangle [11,12],

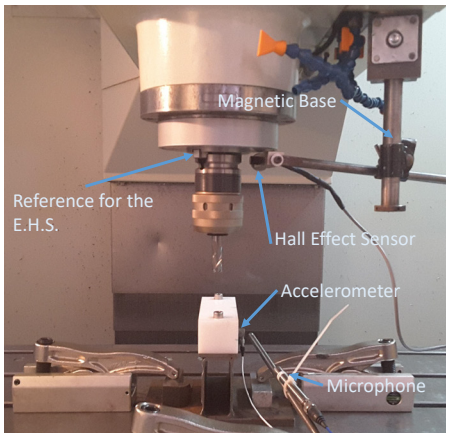

Fig. 1. Experimental Configuration

it falls within the category of engineering plastic with working temperatures of up to 100 $^{\circ}C$. More advanced engineering plastics like PEEK and PPS possess higher working temperatures of about 150 $^{\circ}C$ but lower machinability with a cost of 15 times the price of acetal [13,14].

In addition, acetal can also be divided into two categories named as copolymer and homopolymer. Even though these two materials behave similarly, the main disadvantage of the homopolymer is the high centerline porosity compared with copolymer side. To avoid any difficulty due to this issue, it was decided to select copolymer acetal as the workpiece material.

5. Instrumentation

In order to detect chatter in the cutting trials, the flexure was instrumented with a uniaxial accelerometer (KISTLER model 8776A50) attached with wax, and a microphone (PCB-377B20 with pre-amplifier PCB-426E01) as shown in Figure 2. In addition, to study the types of bifurcation evident in the unstable tests, once-per-revolution values were obtained from the acceleration time series by using the data obtained from a Hall-effect sensor. This sensor was configured such that it provides a voltage pulse periodically with the rotation of the spindle.

The sensors were connected to a data acquisition device (NI DAQ USB-4431) with a sampling frequency of 6kHz. The dynamic response of the flexure (with attached workpiece) was tested using an impact hammer, giving a natural frequency of 290 Hz, damping ratio of 0.67%, and modal stiffness of 3.55 kN/mm.

6. Case study

A custom end mill with 3 teeth, 16 mm diameter and angles of 25, 15 and 10 degrees on the flutes was used. This configuration was chosen in order to ensure unusual stability prediction when machining the workpiece. The cutting force coefficients were measured using standard techniques [15], giving $K_t = 142.2\ kN/mm^2$, $K_r = -18.9\ kN/mm^2$ and $K_a = 58.9\ kN/mm^2$. The SDM was configured to predict stability in up-milling with 8 mm radial immersion, and a feed direction normal to the flexural mode of vibration. Predictions

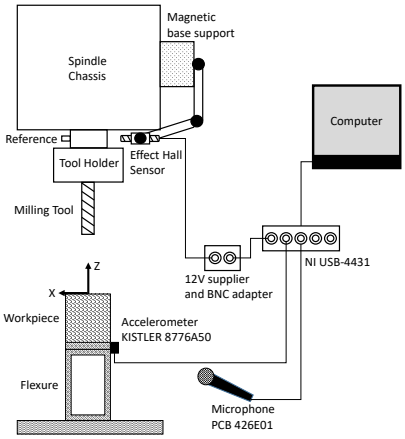

Fig. 2. Schematic of the Instrumentation

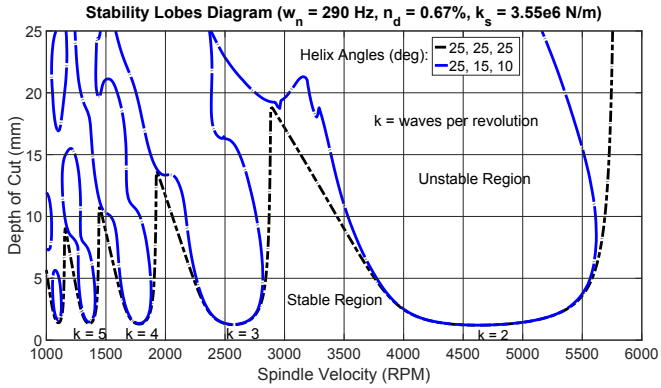

Fig. 3. Stability lobe diagram for a standard and a variable helix tool

were made with steps of 0.1 mm in the axial length of the tool, increments of 5 rpm in the spindle velocity and an angular discretization of the tool of 1 degree. The predicted chatter stability is shown in the Figure 3.

With reference to Figure 3, as the spindle speed reduces, the 'lobe number' (denoted k in Figure 3) increases. This integer denotes the number of oscillations per tool rotation. Above k=4 the lobes are predicted to become isolated islands of instability, which is a form of stability that is rarely seen with traditional uniform-helix tools. Consequently, a small region around k=5 was selected for experimental validation. In this region, a set of 135 cutting trails were configured, consisting of 15 spindle velocities starting from 1070 rpm to 1490 rpm at increments of 30 rpm. For every spindle velocity, 9 cuts were performed from 2 mm to 18 mm at step increments of 2 mm. This section of the stability lobe diagram is shown in Figure 4.

7. Results

The results obtained from the cutting trials are shown in the stability lobe of the Figure 4. In this diagram, green dots represent stable cuts and crosses represent unstable trials. It can be seen that a reasonably good agreement between the results and the simulations was found. As an example, Figure 5 shows the detailed behaviour at 1100 rpm for depths of cut from 2 to 8 mm. The plots a), c), e), g), on the left side of this figure show the acceleration data in blue lines with the

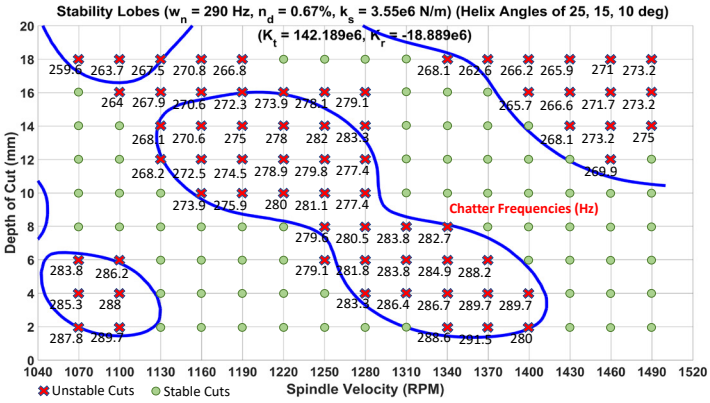

Fig. 4. Instability island and results obtained from the milling trials.

once per revolution samples superimposed with red dots. In addition, it shows the steady state region in a green rectangle used to build the Poincare plot shown in the plots b), d), f), h). It can be seen that the cut at 2 mm (Figure 5 a)) is unstable as the simulation predicted, with the once-per-revolution sampled acceleration indicating quasi-periodic motion that is indicative of a Hopf bifurcation [16] and the acceleration and microphone spectra indicating a chatter frequency of 289.7 Hz as indicated in the Fourier transform of the Figure 7 a). At 4 mm and 6 mm (Figure 5 d) and f)), the cutting process is still unstable with a chatter frequencies of 288 Hz and 286 Hz. Subsequently, the system becomes stable at 8 mm (Figure 5 h)). The system continues being stable until 16 mm which exhibits a chatter frequency of 263.9 Hz as it is shown in the Figure 7 b).

As another example, for the spindle speed of 1400 rpm, the cutting trail at 2 mm is a period double unstable cut with a chatter frequency of 280 Hz, as it is shown in the Figure 6 b). This represents the 6th harmonic of the double of the spindle pass frequency 23.33 Hz. When the axial depth of cut is increased to 4 mm (Figure 6 d)), again a quasi-periodic response is found in the Poincare plot suggesting the appearance of a Hopf bifurcation. Next, the subsequent milling cuts at 6 and 8 mm (Figures 6 f) and h)), become stable as indicated in the Poincare plot. As is shown in the Figure 4, the cutting trials at 1400 rpm remain stable until 16 mm when the cutting process becomes unstable with a chatter frequency of 265.7 Hz.

8. Conclusion

One of the strategies for disrupting regenerative chatter vibrations is the implementation of irregular tools in milling and in particular the use of variable helix tools. In this project, the implementation of copolymer acetal as workpiece material is proposed for the validation of stability processes with variable helix milling tools. This provides two important advantages in the validation process; First, the relatively low cutting stiffness allows one to assume low-order linear structural dynamics even at a high axial depth of cut. Second, this implementation increases drastically the usability of the tools, minimising the risk that potential geometrical discrepancies of the tools or even wear may affect the final results. This can considerably accelerate the validation stage of the geometrical design of variable helix tools for practical purposes.

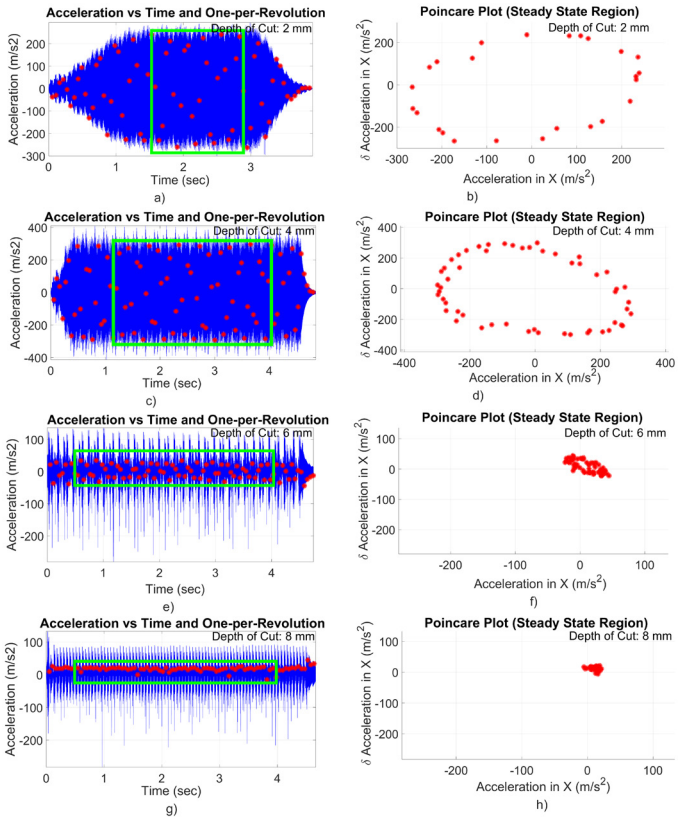

Fig. 5. Acceleration Data, One-Per-Rev values and Poincare Plot for: a) b) 2mm, c) d) 4mm, e) f) 6mm, g) h) 8mm (Spindle Speed: 1100rpm, Feed per Tooth: 0.1 mm/tooth).

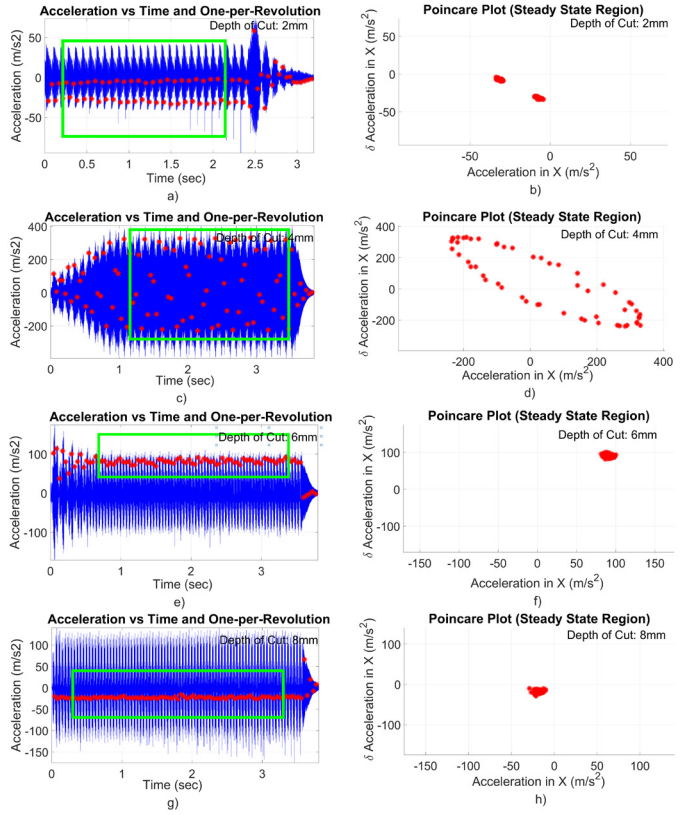

Fig. 6. Acceleration Data, One-Per-Rev values and Poincare Plot for: a) b) 2mm, c) d) 4mm, e) f) 6mm, g) h) 8mm (1400rpm, Feed per Tooth: 0.1 mm/tooth).

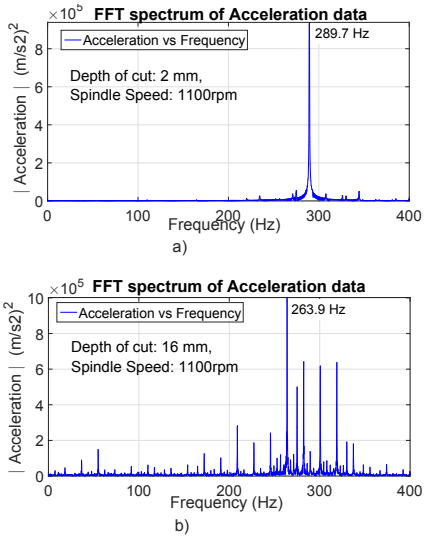

Fig. 7. (a) Acceleration spectrum at 2mm; (b) Acceleration specturm at 16mm.

References

[1] A. Otto, G. Radons, Frequency domain stability analysis of milling processes with variable helix tools, Nineth International Conference on High Speed Machining 1 (0) (2012) 1–6.

[2] D. Bachrathy, G. Stepan, Improved prediction of stability lobes with extended multi frequency solution, CIRP Annals - Manufacturing Technology 62 (1) (2013) 411–414.

[3] N. D. Sims, Fast chatter stability prediction for variable helix milling tools, Proceedings of the Institution of Mechanical Engineers, Part C: Journal of Mechanical Engineering Science 230 (1) (2016) 133–144.

[4] G. Stepan, J. Munoa, T. Insperger, M. Surico, D. Bachrathy, Z. Dombovari, Cylindrical milling tools: Comparative real case study for process stability, CIRP Annals - Manufacturing Technology 63 (1) (2014) 385–388.

[5] A. Otto, S. Rauh, S. Ihlenfeldt, G. Radons, Stability of milling with non-uniform pitch and variable helix Tools, International Journal of Advanced Manufacturing Technology 89 (9-12) (2017) 2613–2625.

[6] T. Insperger, Full-discretization and semi-discretization for milling stability prediction: Some comments, International Journal of Machine Tools and Manufacture 50 (7) (2010) 658–662.

[7] N. D. Sims, B. Mann, S. Huyanan, Analytical prediction of chatter stability for variable pitch and variable helix milling tools, Journal of Sound and Vibration 317 (3-5) (2008) 664–686.

[8] F. Hartung, T. Insperger, G. Stépán, J. Turi, Approximate stability charts for milling processes using semi-discretization, Applied Mathematics and Computation 174 (1) (2006) 51–73.

[9] A. R. Yusoff, N. D. Sims, S. Turner, Experimental Validation of Chatter Stability for Variable Helix Milling Tools, IOP Conference Series: Materials Science and Engineering 26 (2011) 012010.

[10] A. R. Yusoff, Identifying bifurcation behavior during machining process for an irregular milling tool geometry, Measurement: Journal of the International Measurement Confederation 93 (2016) 57–66.

[11] C. A. Harper, Modern Plastics Handbook, McGraw-Hill handbooks, Mcgraw-hill, 2000.

[12] M. Chanda, K. R. Salil, Plastic Technology Handbook, 2006.

[13] T. U. Jagtap, H. A. Mandave, Machining of Plastics: A Review, International Journal of Engineering Research and General Science 3 (2) (2015) 577–581.

[14] R. Keresztes, G. Kalácska, L. Zsidai, Z. Dobrocsi, Machinability of engineering polymers, Sustainable Construction and Design (1) (2011) 106–114.

[15] Y. Altintas, Manufacturing Automation: Metal Cutting Mechanics, Machine Tool Vibrations, and CNC Design, Cambridge University Press, 2012.

[16] G. Stepan, R. Szalai, B. P. Mann, P. V. Bayly, T. Insperger, J. Gradisek, E. Govekar, Nonlinear Dynamics of High-Speed MillingAnalyses, Numerics, and Experiments, Journal of Vibration and Acoustics 127 (2) (2005) 197.

Available online at www.sciencedirect.com

ScienceDirect

Procedia CIRP 82 (2019) 279–284

www.elsevier.com/locate/procedia

17th CIRP Conference on Modelling of Machining Operations

Convergence Analysis of the Multi-Frequency Approach around a Variable-Helix Instability Island

L. Ureña[a,*], E. Ozturk[b], N. Sims[a]

[a]Department of Mechanical Engineering, The University of Sheffield, Mappin Street, Sheffield, S1 3JD, UK
[b]Advanced Manufacturing Research Center with Boeing, Wallis Way, Rotherham, S60 5TZ, UK

Abstract

Variable helix tools are known to have unusual regenerative chatter stability behaviour that can be difficult to predict. This paper explores the convergence and accuracy of a multi-frequency approach (MFA) to stability prediction. An island of instability was identified using the MFA, and the stability boundary was compared to predictions from the semi-discretisation method (SDM) and experimental data. A convergence study for the MFA and SDM showed that the SDM approach was very slow to converge for this specific case, in contrast to its performance at higher spindle speeds. The MFA approach exhibited fast convergence which led to orders of magnitude improvements in the computational speed of the predictions.

Peer-review under responsibility of the scientific committee of The 17th CIRP Conference on Modelling of Machining Operations

Keywords: Convergence; Milling; Variable-Helix Tool; Chatter; Instability Island

1. Introduction

As it is well-known in the scientific community, chatter highly restricts the productivity of machining. Variable helix tools have been proposed as one mechanism to avoid chatter. Here, variation of the helix angles between adjacent teeth, or along the axis of one tooth, can modify the chatter stability, albeit with more complex dynamics and stability of the system. This is because it leads to periodic, piecewise, distributed-time-delayed differential equations with no closed-form solution that requires sophisticated techniques for stability predictions.

Currently, stability predictions of variable-helix-milling processes are broadly performed in the literature using time and frequency domain approaches. The time domain approaches use techniques based on dynamic simulations [1]. One of the most common approaches to stability analysis is the Semi-Discretisation Method (SDM) which was developed by Stepan and his co-workers [2] and extended to consider variable helix tools in [3].

* Corresponding author. Tel.: +44-0114-222-7700.
E-mail address: ueluis1@sheffield.ac.uk (L. Ureña).

Some analysis methods make use of the Fourier transform and series expansion to express the time variable terms of the problem in the frequency domain. For example, the zero-order approach uses the first term of the Fourier expansion of the directional matrix to straightforward predictions of the stability boundaries [4, 5, 6]. Later, enhancements of this method included several harmonics of the directional matrix and frequency response of the system to achieve a more general solution known as the Multi-Frequency Approach (MFA) [7].

Further improvements to the MFA sought to improve the computational load required to determine the stability boundaries and to analyse more complex-tool configurations [7, 8, 9]. In particular, the current project studied the MFA proposed by Sims in [10] for variable-helix-milling tools. This method implemented the Fourier transform, harmonic transfer function approach, and the shift theorems to analyse the system stability. This analysis led to an infinite-size matrix-harmonic-transfer function, that is truncated to a frequency range, taking advantage of the periodicity of this function, and the nature of the receptance. Subsequently, this methodology solved the stability problem by using the general Nyquist-stability criteria, guaranteeing convergence of the solution on the assumption of a maximum frequency at which the frequency response is

2212-8271
Peer-review under responsibility of the scientific committee of The 17th CIRP Conference on Modelling of Machining Operations
10.1016/j.procir.2019.04.054

non-zero.

The present study seeks to extend the work described in [10] by demonstrating the convergence of the method, particularly in the case of an unstable island for a variable helix tool. Furthermore, the stability prediction is compared to experimental data and benchmarked against the semi-discretisation method.

Consequently, at a specific spindle speed and discretisation of the axial depth of cut around an instability island, simulations using both methods estimated the lower and upper stability boundaries. Initially, these simulations used coarse sampling iterations (SDM) or low maximum frequency (MFA) for the estimations. Later, systematic refinements of these parameters gradually caused the estimated boundaries to stabilise at a final solution. Finally, by using the minimum required parameters for convergence, a comparison between the time required to construct the instability island showed the performance of both methods under the defined conditions.

The organisation of the current contribution is as follows. The next section presents the mechanistic force modelling of the variable-helix milling process used by the semi-discretisation and multi-frequency approach to predict stability. Next, section 3 shows the convergence study using both methods around an instability island. Section 4 validates the results obtained from the simulations, while the last section presents the conclusions and further comments about the performed analysis.

2. Milling Dynamic Modelling and Stability

The milling process model implemented in this project firstly assumed that the link formed by the tool-tool holder-spindle was infinitely rigid. Secondly, it assumed that the workpiece behaves as a flexible one-degree-of-freedom workpiece, in which the feed direction (x) is infinitely rigid while the normal one (y) is flexible. Consequently, the primary source of chatter during the milling simulations were the vibrations of the workpiece due to the process forces. These forces can be expressed as follows,

$$F_y = \frac{K_t}{2}\sum_{j=1}^{N}\int_0^b \alpha_j(t,a)\Delta y_j(t,a)da, \tag{1}$$

in which, K_t represents the tangential cutting stiffness, N is the number of flutes of the milling tool, and b is the axial depth of cut along the axial-axis direction a of the tool. Besides, the directional factor $\alpha(t,a)$ and the vibration $\Delta y_j(t,a)$ in the y direction can also be expressed as,

$$\alpha(t,a) = g(\theta_j(t,a))\left[\sin(2\theta_j(t,a)) - K_n\left(1+\cos(2\theta_j(t,a))\right)\right],$$
$$\Delta y_j(t,a) = y(t) - y(t-\tau_j(a)),$$

where $\theta_j(t,a)$ is the angular position of the tooth j, K_n is the ratio of radial to normal cutting stiffness, $\tau_j(a)$ the time delay between the current and previous tooth, and g is a binary function that is 1 when the tooth is engaged in the workpiece and 0 otherwise. Note that in contrast to regular helix tools, the time delay is a function of the axial depth a and the tooth j.

2.1. Semi-Discretization Method

In this section, the semi-discrete method is briefly summarised, following the derivation described in [11] and the modifications described in [3]. Considering the milling process forces from equation 1 in the dynamic system, we obtain,

$$\dot{\mathbf{y}}(t) = \hat{\mathbf{A}}\mathbf{y}(t) + \hat{\mathbf{B}}\sum_{j=1}^{N}\int_0^b \alpha_j(t,a)y(t)da - \hat{\mathbf{B}}\sum_{j=1}^{N}\int_0^b \alpha_j(t,a)y(t-\tau_j(a))da, \tag{2}$$

in which the vector $\mathbf{y}$ and matrices $\mathbf{A}$ and $\mathbf{B}$ represented,

$$\dot{\mathbf{y}}(t) = \begin{pmatrix} y(t) \\ \dot{y}(t)\end{pmatrix}, \hat{\mathbf{A}} = \begin{pmatrix} 0 & 1 \\ -{\omega_{ny}}^2 & -2\zeta_y\omega_{ny}\end{pmatrix}, \hat{\mathbf{B}} = \begin{pmatrix} 0 & 0 \\ \frac{K_t\omega_{ny}^2}{2k_y} & 0\end{pmatrix}, \tag{3}$$

where ω_{ny}, ζ_y and k_y represented modal natural frequency, damping ratio and stiffness of the system, respectively. Additionally, dividing the axial depth of cut b into K elements of height Δa, the equation 2 can be stated as a summation as follows,

$$\dot{\mathbf{y}}(t) = \hat{\mathbf{A}}\mathbf{y}(t) + \hat{\mathbf{B}}\sum_{j=1}^{N}\sum_{k=1}^{K}\alpha_{jk}(t)y(t)\Delta a - \hat{\mathbf{B}}\sum_{j=1}^{N}\sum_{k=1}^{K}\alpha_{jk}(t)\mathbf{y}(t-\tau_{jk})\Delta a. \tag{4}$$

Afterwards, the method required the discretisation of the spindle pass period T into m elements of size Δt, such as $T = m\Delta t$ and $\Delta t = t_i - t_{i-1}$. Therefore, for the discrete time t_i, the time delays can be approximated as,

$$\begin{aligned} y(t_i-\tau_{jk}) &\approx y\left(t_i + \frac{\Delta t}{2} - \tau_{jk}\right) \\ &\approx w_{jk}^a y(t_i - \tau_{jk} + \Delta t) + w_{jk}^b y(t_i - \tau_{jk}) \\ &\approx w_{jk}^a y_{i-m_{jk}+1} + w_{jk}^b y_{i-m_{jk}} \end{aligned} \tag{5}$$

where the delayed index m_{jk} is an integer obtained by,

$$m_{jk} = \text{int}\left(\frac{\tau_{jk}}{\Delta t} + \frac{1}{2}\right),$$

and the weights can be calculated as,

$$w_{jk}^a = \frac{\tau_{jk}}{\Delta t} - \left(m_{jk} + \frac{1}{2}\right)$$
$$w_{jk}^b = 1 - w_{jk}^a.$$

Subsequently, substituting the approximated delay from the equation 5 into the equation 4 and expressing the time interval Δt as $t_{i+1} - t_i$, this then led to a set of equations at discrete time interval as follows,

$$z_{i+1} = [\Phi]z_i,$$

in which $[\Phi]$ represents the transition matrix. Consequently, according to the Floquet theory, a milling process was marginally stable if the modulus of any of the eigenvalues of this matrix is equal to 1, unstable if the modulus were higher than 1, and stable if all the modulus were smaller than 1.

2.2. Multi-Frequency Approach

To summarise the multi-frequency approach proposed by Sims in [10], lets first express the location of the tool flute j respecting to a fixed reference frame as,

$$\phi_j(a) = \phi_{j0} + \beta_j a,$$

in which ϕ_{j0} is the location of this flute at the tip of the tool, which can account for non-equal tooth spacing such as that for a variable pitch tool. Meanwhile, β_j is the pitch gradient related to the helix angle γ_j and the tool radius r as,

$$\beta_j = \frac{\tan \gamma_j}{r},$$

where γ_j is different for every flute j, and when multiplied by the axial depth of cut provides the change in pitch regarding the pitch on the tip of the flute. Once the milling tool started to rotate at a spindle speed Ω, at the instant t, the expression to obtain the angular position of the tooth j is as follows,

$$\theta_j(t, a) = \Omega t + \phi_j(a).$$

Later, expanding the directional factor α into its Fourier series we obtain,

$$\alpha(\theta(t, a)) = \sum_{n=-\infty}^{\infty} e^{jn(\phi_k(a))} A(n) e^{jn\Omega t}, \tag{6}$$

in which,

$$A(n) = \frac{1}{2\pi} \int_{\theta_{st}}^{\theta_{ex}} \alpha(\theta) e^{-jn\theta} d\theta.$$

An important point highlighted by [10] is that, contrary to traditional multi-frequency stability analysis, a depth-of-cut dependent term $e^{jn\phi_j(a)}$ named as the phase-changing term, explicitly appeared in the final Fourier expansion. Subsequently, substituting the equation 6 in the expression 1, and applying the Fourier transform to this equation along with using the first and second shift theorems, gives:

$$F_y(i\omega) = \sum_{n=-\infty}^{\infty} X(i\omega - in\Omega) A(n) \sum_{j=1}^{N} \int_{a=0}^{b} e^{in\phi_j(a)} \left[1 - e^{-\tau_j(a)(i\omega - in\Omega)}\right] da. \tag{7}$$

Later, multiplying both sides of the equation 7 by the frequency response function of the system $G(i\omega)$, the obtained equation is as follows,

$$Y(i\omega) = G(i\omega) \sum_{n=-\infty}^{\infty} Y(i\omega - in\Omega) A(n) \sum_{j=1}^{N} \int_{a=0}^{b} e^{in\phi_j(a)} \left[1 - e^{-\tau_j(a)(i\omega - in\Omega)}\right] da. \tag{8}$$

A more general expression for the frequency response at any harmonic p of the spindle pass frequency can be obtained by rewriting ω as $\omega + p\Omega$. Additionally, by defining q as $p - n$, enables one to rewrite the equation 8 in a matrix form with rows p and columns q ($p = -\infty, \cdots, \infty$; $q = -\infty, \cdots, \infty$) as,

$$\hat{y}_p(i\omega) = \hat{g}_{p,p}(i\omega) \sum_{q=-\infty}^{\infty} \hat{h}_{p,q}(i\omega) \hat{y}_q(i\omega)$$

in which,

$$\begin{aligned}
\hat{y}_p(i\omega) &= Y(i\omega - ip\Omega), \\
\hat{g}_{p,p}(i\omega) &= G(i\omega - ip\Omega), \\
\hat{h}_{p,p}(i\omega) &= A(n) \sum_{j=1}^{N} \int_{a=0}^{b} e^{i(n)\phi_j(a)} \left[1 - e^{-\tau_j(a)(i\omega - iq\Omega)}\right] da, \\
\hat{y}_p(i\omega) &= \hat{g}_{p,p}(i\omega) \sum_{q=-\infty}^{\infty} \hat{h}_{p,q}(i\omega) \hat{y}_q(i\omega).
\end{aligned} \tag{9}$$

For compactness purpose, the expression 9 can be finally expressed as,

$$\hat{\mathbf{Y}}(i\omega) = \mathbf{G}\hat{\mathbf{H}}(i\omega)\hat{\mathbf{Y}}(i\omega).$$

According to the Generalised Nyquist Stability Criterion [12], the system is stable if $\det\left(I - \mathbf{G}\hat{\mathbf{H}}(i\omega)\right)$ (where I is the identity matrix) is non-zero and does not encircle the origin in a clockwise sense. However, because $\mathbf{G}\hat{\mathbf{H}}(i\omega)$ is a doubly-infinite matrix, this seems to be an impossible task. Nevertheless, by taking advantage of the periodicity of $\mathbf{G}\hat{\mathbf{H}}(i\omega)$, and the high-frequency behaviour of $G(i\omega)$, the solutions can be bounded to a frequency region defined as,

$$-\frac{\omega_{max}}{\Omega} - \frac{1}{2} < p < \frac{\omega_{max}}{\Omega} + \frac{1}{2}, \tag{10}$$

in which ω_{max} represents the maximum frequency in which the frequency response function of the system tends towards zero.

3. Comparison of methods

Sections 2.1 and 2.2 have briefly summarised the two stability methods under consideration. From this, it can be seen that both methods begin with the same assumptions regarding the physical system under consideration (for example, linear cutting force coefficients). The SDM method then requires a modal model of the frequency response function, whereas the MFA method operates directly on the numerical frequency response function. The SDM requires a decision on the number of modes to be included in the model, as well as the number of discretisation steps m in the solution. In contrast, the MFA requires an assumption on the maximum frequency of interest in the frequency response function. This differs from previously reported multi-frequency solutions [13] which did not rely on Equation 10 and hence assumed that the number of harmonics must also be manually chosen.

4. Convergence Analysis

To explore the convergence and validity of the stability predictions, a scaled experiment was considered. The machining scenario along with a schematic of the set up are presented in the Table 1 and Figure 1.

Subsequently, numerical simulations resulted in the stability lobes diagram of Figure 2. The blue lines from this plot

represented the stability lobe diagram for the variable helix tool, while the black lines the one for a regular milling tool of 25 degrees of helix angle. Additionally, the value of k in this plot denoted the number of waves per revolution imprinted by the tooth on the workpiece surface. Consequently, milling trials performed below these stability lines represented stable cuts while trials above them unstable ones. For the $k = 3$ of the variable helix stability lobe, the plots revealed the appearance of closed contours or islands, in which milling trials inside this island were unstable trials while outside stable ones.

Parameter	Value
ω_{ny}	285.5 Hz
k_y	3.67 kN/mm
ζ_y	1.54%
$\phi_{10}, \phi_{20}, \phi_{30}$	0°, 120°, 240°
$\gamma_1, \gamma_2, \gamma_3$	25°, 15°, 10°
Radial Immersion	50%
Tool Diameter	16 mm
Material	Copolymer Acetal
Kt	142.2 N/mm^2
Kr	18.9 N/mm^2
Cutting Condition	Up-milling

Table 1: Machining Scenario

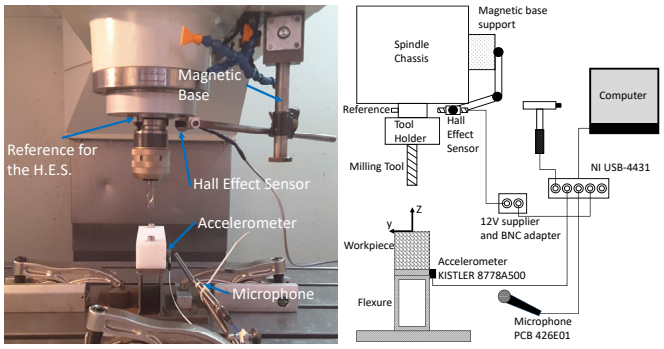

(a) (b)

Fig. 1: (a) Experimental Configuration,(b) Schematic of the Instrumentation

It should be noted that these islands are different from the regular tool islands presented by Insperger in [14] and Patel et al. in [15]. For example, Patel et al showed that a constant regular helix angle introduced a stable region between the so-called flip and Hopf lobes, which could not be predicted with classical stability models. However, the islands of instability illustrated in the present study are a direct consequence of the time delay varying along the axis of the flute: a phenomenon which does not occur with a regular helix tool, even if the constant helix angle is included in the analysis. This behaviour was previously suggested by Sims et al [3] using time domain and semi-discretisation methods, but without experimental validation.

Therefore, the present study pursued to study the convergence of the MFA inside this low-spindle-speed instability island. Additionally, simulations at higher spindle speed aimed

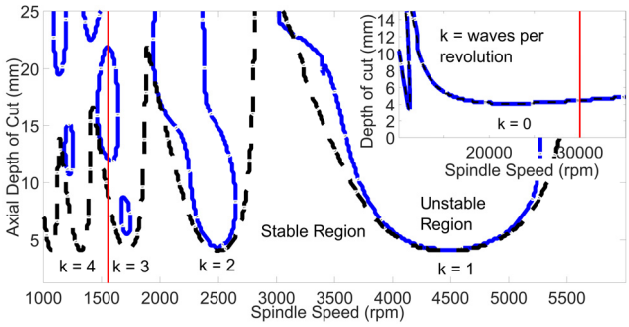

Fig. 2: Stability Lobe Diagram: The blue lines represented the stability boundary for the variable helix tool while the black one for the regular one. For $k = 3$, the stability showed the appearance of an instability island.

to provide a better understanding of the convergence in this region. Therefore, the present study focusses on two regions: one of them being at 30000 rpm, and the second one at 1560 rpm located just inside the instability island. The stability lobes diagram of Figure 2 showed these spindle speeds as vertical red lines.

For the high spindle speed tests, simulations estimated the stability boundary, utilising an axial discretisation of the tool of 0.2 mm. For the frequency value f_{max} (equation 10), it initially used a low-frequency value close to the natural frequency of the system, then it later increased it until 780 Hz at increments of 7.5 Hz. The obtained results are shown in the plot of Figure 3. In this plot, the upper x-axis represents the frequency f_{max}, while the y-axis the axial depth of cut. It is clear that from this plot that at a high spindle speed, even at values of f_{max} close to the natural frequency, the stability boundary converged to the solution that in this case is of 4.4 mm.

Additionally, the same figure shows the results obtained for the SDM approach as a function of multiples of the natural frequency η (lower x-axis). This plot also presented the normalised relationship between η and the number of iterations m per revolutions. From this plot, the stability boundary started at a value of 6.8 mm for a η value of 4. Later, the boundary drastically decreased in magnitude while increasing η until η was equal to 18 when the boundary settled in 4.4 mm as in the MFA. Values of η larger than 18 shown not change in the estimated stability boundary.

It is clear that from this plot that at a high spindle speed, even at values of f_{max} close to the natural frequency, the stability boundary converged to the solution that in this case is of 4.4 mm. On the other hand, for the SDM, the stability boundary started at a value of 6.8 mm for an η value of 4. Later, the boundary drastically decreased in magnitude while increasing η until η was equal to 18 when the boundary settled in 4.4 mm as in the MFA. Values of η larger than 18 shown not change in the estimated stability boundary.

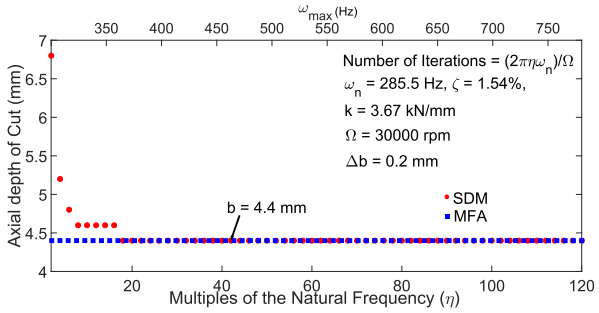

Fig. 3: Convergence Analysis for the MFA and SDM at 30000 rpm.

Later, for the low spindle speed test, simulations estimated the lower and upper stability boundaries of the instability island following a similar procedure for MFA and SDM as in the previous test. The results obtained are shown in Figure 4 a) and b). From the plot in Figure 4 a), it is clear how the upper and lower stability boundaries estimated by MFA initially started at values of 24.1 mm and 11.6 mm for f_{max} = 285 Hz. Later, while increasing the f_{max} value, the upper and lower stability boundaries decreased or increased until they settled at values of 22 and 12 mm. The first boundary to converge was the lower boundary at a frequency f_{max} of 346 Hz, while the upper boundary settled at f_{max} = 368 Hz. This frequency value represented a p harmonic value of approximately 14.

On the other hand, the results for the SDM (Figure 4 b)) showed that the method struggles to converge to the final solutions. For example, the lower stability boundary converged to the same solutions as the MFA at η = 30. Nevertheless, at this value, the upper stability boundary was 2 mm away from the solution estimated by the MFA. At higher sampling frequencies than that, the upper boundary slowly moved toward the value predicted by MFA, but it never achieved this value at the maximum simulated value of η = 70.

As a performance comparison example between MFA and SDM, simulations were performed at 1560 rpm using the minimum convergence parameters for the MFA, and a η = 30 for the SDM. This was implemented on a computer with 16 GB of RAM, and an Intel(R) Core(TM) i7-6700k running at 4 GHz. From these simulations, the MFA could predict the boundaries in 0.55 minutes, while the SDM approximately 32.1 minutes, meaning that the MFA was 58 times faster than the SDM. On the other hand, at the higher spindle speed of 30000 rpm, the MFA proved to be 32 times faster than the SDM.

5. Experimental validation

The validation procedure implemented in the project consisted of four up-milling trials at 1560 rpm aimed to capture the stability boundaries of the island at this spindle speed. Consequently, knowing from the previous section that the stability boundaries at this spindle speed were at approximately 12 and 22 mm, trials at 10, 13, 19, and 23 mm of the axial depth of cut were defined to find the stability transitions from stable to unstable and vice-versa.

The Figure 5 showed instability island obtained by using the MFA diagram with a f_{max} of 368 Hz and axial discretisation of 0.2 mm. The red squares represented the unstable trials while the greed dots the stable ones. Also, Figure 6 a), c), e), and d) showed the acceleration data in blue colour lines as well as the once-per-revolution values as red dots. The green squares in these plots defined the steady state regions of the trials. Using the once-per-revolution values around these regions, the recursive or Poincaré plot of the trials were built and shown in Figure 6 b), d), f), and h).

It is evident from these plots that the trials at 10 and 23 mm were stable because the once-per-revolution values provided the same solution with every revolution, meaning a periodic process. On the other hand, the trials at 13 and 19 mm were subsequently characterised as unstable period doubling and secondary Hopf bifurcations due to the nature of their Poincaré plots. Consequently, these results suggested that the stability boundaries of the island were located between 10 and 13 mm, and 19 and 23 mm, just as the simulations predicted.

6. Conclusions

The current project studied the convergence of the MFA proposed by Sims in [10], around an instability island obtained by using a variable helix milling tool of 16 mm of diameter and helix angles of 25, 15 and 10 degrees. Besides, the dynamic parameters and cutting stiffness from a scaled experiment were used to perform the simulations. Further simulations were executed at a higher spindle speed to have a better understanding of the convergence behaviour of the method and all the results obtained were compared with the SDM.

The results at the high spindle speed showed that the MFA is approximately 32 times faster than the SDM. The MFA proved to converge using values of f_{max} close to the natural frequency. On the other hand, the SDM converged to the final solution at sampling frequencies of 18 times the natural frequency of the system. Afterwards, this performance improvement was also evident while predicting the stabilities boundaries around the low-spindle-speed instability island. The MFA could converge to the stability boundaries using a value of f_{max} of 368 Hz (p = 14 in the equation 10). On the other hand, the SDM struggled to converge to the solutions and even the upper boundaries could not settle in a final solution through the performed simulations. Furthermore, the MFA approach was found to be between 30 and 60 times faster than the SDM and did not require a prior computation of the modal parameters of the system.

The simulations were validated using a scaled experiment in which the results suggested the appearance of the boundaries, and therefore the island in the stability lobe diagram.

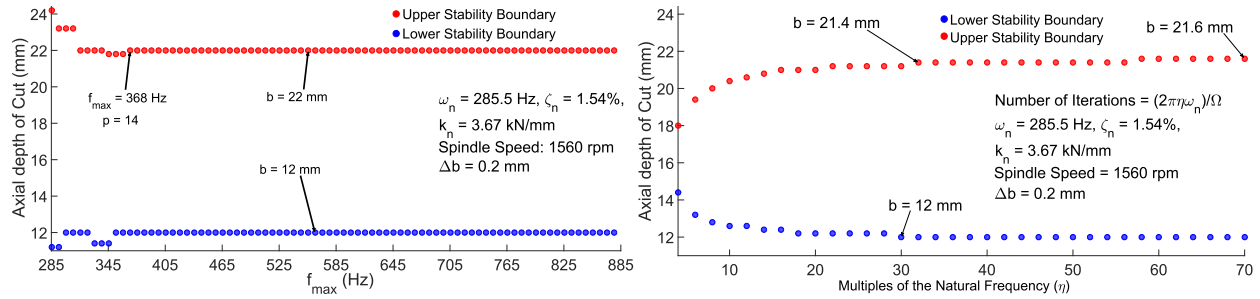

Fig. 4: Convergence Analysis for the MFA (a) and SDM (b).

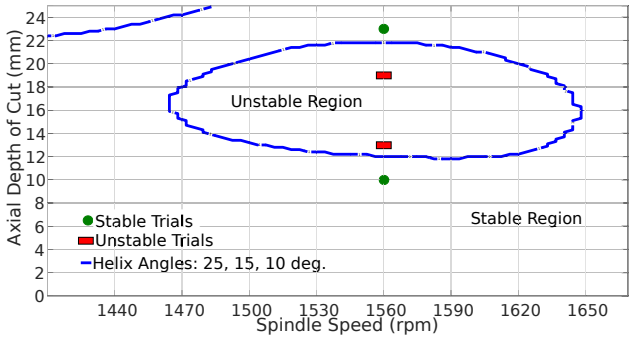

Fig. 5: Instability Island.

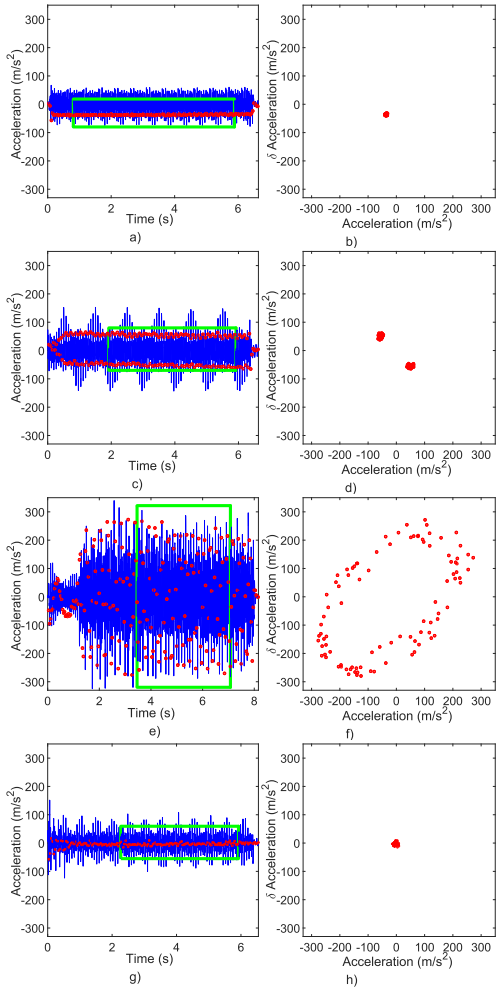

Fig. 6: Acceleration data and once-per-revolution values (y direction) of the milling trials at 1560 rpm, and depth of cuts of a) b) 10 mm, c) d) 13 mm, e) f) 19 mm and e) f) 23 mm.

References

[1] Z. Li, Q. Liu, Solution and analysis of chatter stability for end milling in the time-domain, Chinese Journal of Aeronautics 21 (2) (2008) 169–178.

[2] T. Insperger, G. Stépán, Semi-Discretization for Time-Delay Systems, Vol. 178, 2011.

[3] N. D. Sims, B. Mann, S. Huyanan, Analytical prediction of chatter stability for variable pitch and variable helix milling tools, Journal of Sound and Vibration 317 (3-5) (2008) 664–686.

[4] Y. Altintas, E. Budak, Analytical Prediction of Stability Lobes in Milling, CIRP Annals - Manufacturing Technology 44 (1) (1995) 357–362.

[5] Y. Altintas, Manufacturing Automation, 2011.

[6] G. Jin, Q. Zhang, H. Qi, B. Yan, A frequency-domain solution for efficient stability prediction of variable helix cutters milling, Proceedings of the IMechE, Part C: Journal of Mechanical Engineering Science 228 (15) (2014) 2702–2710.

[7] A. Otto, G. Radons, Frequency domain stability analysis of milling processes with variable helix tools, Nineth International Conference on High Speed Machining 1 (0) (2012) 1–6.

[8] D. Bachrathy, G. Stepan, G. Stépán, G. Stepan, Improved prediction of stability lobes with extended multi frequency solution, CIRP Annals - Manufacturing Technology 62 (1) (2013) 411–414.

[9] G. Stepan, J. Munoa, T. Insperger, M. Surico, D. Bachrathy, Z. Dombovari, Cylindrical milling tools: Comparative real case study for process stability, CIRP Annals - Manufacturing Technology 63 (1) (2014) 385–388.

[10] N. D. Sims, Multi-frequency Chatter Analysis Using the Shift Theorem, IUTAM Symposium on Nonlinear and Delayed Dynamics of Mechatronic Systems 22 (2017) 3–9.

[11] T. Insperger, G. Stépán, Semi-discretization method for delayed systems, International Journal for Numerical Methods in Engineering 55 (5) (2002) 503–518.

[12] M. C. Smith, On the generalized nyquist stability criterion, International Journal of Control 34 (5) (1981) 885–920.

[13] S. D. Merdol, Y. Altintas, Multi Frequency Solution of Chatter Stability for Low Immersion Milling, Journal of Manufacturing Science and Engineering 126 (3) (2004) 459.

[14] T. Insperger, J. Muñoa, J. Munoa, Unstable islands in the stability chart of milling processes due to the helix angle, CIRP - 2nd International Conference on High Performance Cutting (HPC).

[15] B. R. Patel, B. P. Mann, K. A. Young, Uncharted islands of chatter instability in milling, International Journal of Machine Tools and Manufacture 48 (1) (2008) 124–134.